PHENOMENOLOGICAL INVESTIGATION OF A ROUND LIQUID JET INJECTED TRANSVERSELY INTO A SUBSONIC GASEOUS CROSSFLOW

By
MOHSEN BROUMAND

A Thesis submitted to the Faculty of Graduate Studies of
The University of Manitoba
in partial fulfillment of the requirements of the degree of

DOCTOR OF PHILOSOPHY

Department of Mechanical Engineering
University of Manitoba
Winnipeg

Abstract

Inasmuch as power generation systems, in both avionic and stationary applications, are typically powered by liquid fuels, the process of liquid fuel/air mixture preparation plays a key role in combustion (i.e., fuel burning) of these systems. One of the most efficient liquid fuel/air mixture generation techniques in a combustion chamber is by injecting liquid fuel transversely into a gaseous crossflow (JICF). Amongst the various features of this type of flow-field, data describing the trajectory and breakup length of a transverse liquid jet is highly required for combustor design in order to prevent fuel impingement onto the combustor walls. More importantly, it is needed for predicting fuel distribution in a combustor, which directly affects droplets breakup, collision, evaporation, mixing rate with oxidants, and consequently the overall combustion efficiency of an engine.

Due to the complexity associated with the theory behind a transverse liquid jet, a large body of investigations on its features is experimental; however, several experimental challenges such as the limitations in observing the dense spray region hinder the progress in understanding this topic. Moreover, the liquid jet's trajectory and its breakup length vary significantly with changing liquid properties, test/operating conditions and nozzle/injector internal geometries, leading to huge discrepancies between published results/predictions. In this thesis, therefore, a phenomenological investigation, by integrating both theoretical and experimental approaches, has been carried out to gain a more comprehensive understanding of the complex process of a transverse liquid jet in a gaseous crossflow.

A mathematical method was adopted to develop a model for predicting the penetration of a liquid jet in a subsonic gaseous crossflow over a wide range of liquid properties and test/operating conditions. In the near field zone, a force balance was applied to a control-volume, and forces

acting upon the liquid column such as drag, gravitation and surface tension were introduced and then the mass and energy conservation equations were solved using the control-volume or an Eulerian approach, while considering the mass shedding from the liquid column (i.e., surface breakup). In the far field zone, a model for the trajectory of large droplets generated at the column breakup location was developed using a Lagrangian approach, while utilizing the information on the column breakup location obtained from the first zone as the initial conditions for the second zone.

The impact of nozzle internal geometry on the jet exit conditions (i.e., turbulent or non-turbulent liquid jet), and consequently on the liquid jet's trajectory and its breakup length has been examined experimentally in order to reach a more reliable prediction of these features. The experimental data sets were used to validate and extend the applicability of the mathematical models developed in this study. As a result, two modified correlations were proposed to predict the trajectory and breakup length of a round liquid jet injected transversely into a subsonic gaseous crossflow for different liquid properties, test/operating conditions and nozzle internal geometries.

Acknowledgements

First, I have to thank my research supervisor Dr. Madjid Birouk who offered his continuous advice and encouragement throughout the course of this thesis. Without his assistance and dedicated involvement in every step throughout the process, this thesis would have never been accomplished. I really would like to appreciate him for his support and understanding over these past four years.

I also would like to show gratitude to my committee members, Dr. Alidad Amirfazli, Dr. Eric Bibeau, and Dr. Behzad Kordi for their efforts put into reviewing the thesis, and their excellent comments and suggestion.

I would like to express my very sincere gratitude to University of Manitoba for providing me the circumstance to perform my doctoral research and for their financial support. I acknowledge the funding received from the Natural Sciences and Engineering Research Council of Canada (NSERC) and the University of Manitoba Graduate Fellowship (UMGF) to support this research.

Carrying out my thesis demanded more than academic aids, and I have many friends to express my appreciation for their friendship. I would also like to thank the following in the Energy and Combustion Lab of University of Manitoba for their help and discussions: Mohammadreza Farokhi, Graham Rigby, Mahmoud Moussa Abdel Azim, Meng Wang, and Sviatoslaw Karnaoukh and all the other students and staff in the lab.

Finally, and most importantly, none of this was possible without the encouragement and supports that I got from my family who have sacrificed their lives for me and provided unconditional love and care. Finally, I would like to dedicate this thesis to my beloved father, Isa Broumand, who passed away when I was finishing this thesis. He made an untold number of sacrifices for the entire family, and specifically for me to continue my schooling. He has always given me the determination to overcome many trying moments to pursue my dreams. Hence, great appreciation and enormous thanks are due to him.

Table of Contents

List of Figures

List of Tables

List of Abbreviations

Nomenclature

A	liquid column cross sectional area, m2
A_d	frontal area of the droplet, m^2
A_L	lateral surface area of the liquid column, m^2
A_o	nozzle exit area, m^2
Bo	Bond number, $\rho_l g d_j^2/\sigma$
C_D	liquid column average drag coefficient
C_{Dx}	droplet drag coefficient in *x*- direction
C_{Dz}	droplet drag coefficient in *z*- direction
C_d	discharge coefficient of nozzle
D	channel diameter, m
d	liquid column diameter, m
d_d	droplet diameter, m
d_j	liquid jet diameter at the nozzle exit, m
$\boldsymbol{e}_N$	unitary base vector normal to liquid column axis
$\boldsymbol{e}_T$	unitary base vector tangential to liquid column
$\boldsymbol{e}_x$	unitary base vector in horizontal direction
$\boldsymbol{e}_z$	unitary base vector in vertical upwardly direction
g	gravitational acceleration vector, m/s^2
k	local curvature of the jet
L	exit length of nozzle, m
l_c	liquid column perimeter, m

m_d	mass of droplet, kg
$\dot{m}$	rate of mass shedding from the liquid column
$\dot{m}_f$	nozzle mass flowrate, kg/s
Oh	Ohnesorge number, $\mu_l/\sqrt{\rho_l d_j \sigma}$
P	absolute pressure of the crossflow, kPa
q	jet momentum flux ratio, $\rho_l v_j^2/\rho_g u_g^2$
Re_{ch}	channel Reynolds number, $\rho_g u_g D/\mu_g$
Re_j	jet Reynolds number, $\rho_l v_j d_j/\mu_l$
Re_d	droplet Reynolds number
s	arclength of the jet trajectory centerline absolute
T	temperature of the crossflow, K
t_b	column breakup time, s
t_i	onset of surface breakup time, s
t_s	characteristic liquid-phase time, $(\rho_l/\rho_g)^{\frac{1}{2}} d_j/u_g$
t_v^*	characteristics viscous time, $d_j^2/(\mu_l/\rho_l)$
u_g	crossflow velocity, m/s
u_{shed}	droplet velocity after surface breakup
$\boldsymbol{V}$	liquid velocity vector, m/s
V	liquid velocity, m/s
v_j	liquid velocity at the nozzle exit, m/s
We_{aero}	aerodynamic Weber number, $\rho_g v_j^2 d_j/\sigma$
We_g	gas phase Weber number, $\rho_g u_g^2 d_j/\sigma$
We_j	jet Weber number, $\rho_l v_j^2 d_j/\sigma$

x	coordinate in gas crossflow (horizontal) direction , m
x_b	column breakup location, m
z	coordinate in liquid injection (vertical) direction, m

Greek symbol

θ	injection angle
λ_c	column wavelength, m
μ	viscosity, kg/(m.s)
ρ	density, kg/m^3
σ	liquid surface tension, N/m
ψ	liquid column angle
ψ_o	injection angle

Subscripts

b	column breakup
d	droplet
g	gas
j	jet
l	liquid
o	standard conditions
w	water

Declaration the academic achievement

The outline of this thesis follows "sandwich format" whose guidelines are appointed by the Faculty of Graduate Studies, University of Manitoba. It merges four individual papers prepared for publication in peer-reviewed journals. Chapter 1 contains an introduction about the problem statement and the thesis contributions; Chapters 2 to 5 are manuscripts containing an abstract, introduction, methods, results and discussion; Chapter 6 provides the conclusions of the work and recommendations for future research direction.

Chapters 2 to 5 have been published as four journal papers. The contributions of M. Broumand in all the papers are listed as following: developing the research idea, developing the mathematical model, performing experimental examinations, data analysis, drawing the figures, writing all the manuscripts and responding to reviewers' comments. The contribution of my co-author, G. Rigby, in the last paper, chapter 5, consisted of collecting the experimental data.

Copyright Notices

1. With permission from Elsevier:

- **M. Broumand** and M. Birouk, "Liquid Jet in Subsonic Gaseous Crossflow: Recent Progress and Future Challenges", *Progress in Energy and Combustion Science*, Vol. 57 (2016), pp. 1‑29.

2. With permission from Begell House, Inc.:

- **M. Broumand** and M. Birouk, "A Model for Predicting Liquid Jet Trajectory in a Subsonic Gaseous Crossflow", Reprinted from *Atomization and Sprays*, Vol. 25, No. 10, Copyright (2015), pp. 871-893.

3. With permission from American Institute of Aeronautics and Astronautics (AIAA):

- **M. Broumand** and M. Birouk, "A Two-Zone Model for Predicting the Penetration Height of a Liquid Jet in a Subsonic Gaseous Crossflow", *AIAA Journal*, Vol. 54, No. 5 (2016), pp. 1499-1511.

4. With permission from Springer:

- **M. Broumand**, G. Rigby and M. Birouk, "Jet Exit Turbulence Effect on the Column Trajectory and Breakup Location of a Transverse Liquid Jet", *Flow Turbulence and Combustion*, Vol. 99 (2017), pp. 153-171.

Chapter 1

Introduction

1.1. Background and Scope

Both future international aircraft emission regulations introduced by the International Civil Aviation Organization (ICAO), as well as emissions penalties introduced at some airports require the implementation of new clean combustion technologies [1]. Power generation systems (stationary or propulsion) are typically powered by liquid fuels because liquids contain much more energy per unit volume than gaseous fuels. Also, liquids are relatively easy to transport and store using well-established infrastructures. Even if energy supplies move away from petroleum distillates, liquid fuels from other sources (e.g., liquid biofuels) will continue to be important for power generation, especially propulsion. Therefore, novel methods and approaches to be proposed to enhance the mixing of liquid fuel/air in an engine will be definitely result in economical and environmental benefits.

Transverse injection of a liquid fuel jet into a gaseous crossflow (JICF) is one of the most efficient liquid fuel/air mixture generation techniques in a combustion chamber where rapid fuel penetration, vaporization, mixing of vapor/air and ignition, and consequently sustained combustion process are desired. This method of liquid fuel/air mixture preparation enhances flame

stabilization, fuel conversion efficiency, and accordingly emissions reduction [2, 3]. It has various applications, such as low NOx gas turbines, lean premixed prevaporized (LPP) combustors, aircraft engines, high speed direct injection (HSDI) diesel engines, etc.

In order to keep coherent the topic in question; the scope of the present thesis is limited to non-evaporating, non-reacting round (or canonical) liquid jets in subsonic gaseous crossflows with uniform velocity fields and negligible turbulence in near-wall gas boundary layers. Figure 1-1 shows a schematic description of a liquid jet penetrating transversely into a gaseous crossflow where the jet column deforms, waves and finally breaks up into ligaments and droplets [4]. The liquid fragments shedding from the jet undergo subsequent secondary breakup process leading to smaller droplets, and consequently the formation of a spray. From the perspective of hydrodynamic instability analysis, there exists two breakup mechanisms associated with this type of flow field, namely column breakup and surface breakup. In the column breakup process, the unbroken jet begins to ruffle as a result of axial instability which develops along the liquid column and finally breaks up into droplets [5]. As liquid begins to disintegrate from the jet surface (as a result of the instabilities on the jet lateral surface) and the surface breakup process becomes dominant, the jet penetration height decreases [5].

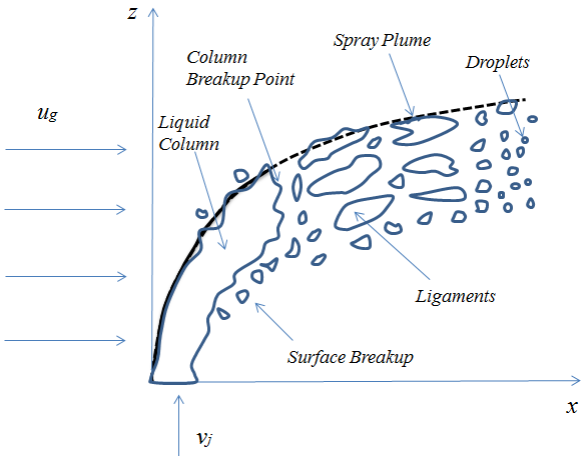

Figure 1-1: Schematic diagram of the breakup of a transverse liquid jet.

1.2. Research Aims

1.2.1. Problem Definition and Motivation

A transverse liquid jet in a gaseous crossflow has several important features which have been extensively investigated during the last two decades [6, 7]. It includes liquid jet's primary breakup regimes, trajectory and its penetration behavior in a crossflow, liquid jet's breakup length, droplets features and their formation mechanisms. Amongst the aforementioned features, the trajectory and breakup length of a transverse liquid jet in a gaseous crossflow are the most important ones as they have direct impact on the distribution of the fuel spray in a combustion chamber, and accordingly its evaporation and mixing rate with the oxidant. This is also important for the design of a combustor as to prevent spray impingement onto its walls. Therefore, the present thesis aims at gaining a more comprehensive understanding of these two features.

Jet trajectory and its penetration refer, respectively, to the trajectory up to the column breakup point (i.e., the solid line in Fig. 1-1, near field region), and to the liquid maximum penetration into

a crossflow (i.e., the dashed line in Fig. 1-1, far field region). Numerous empirical and semi-empirical correlations for predicting the trajectory and penetration of a liquid jet injected into a gaseous crossflow were proposed in the literature. These correlations are expressed in mathematical forms which relate non-dimensional parameters, such as momentum flux ratio $q \equiv \rho_j v_j^2 / \rho_g u_g^2$, jet Reynolds number $Re_j \equiv \rho_j v_j d_j / \mu_j$, gas Reynolds number $Re_g \equiv \rho_g u_g d_j / \mu_g$, gas Weber number $We_g \equiv \rho_g u_g^2 d_j / \sigma$, jet Weber number $We_j \equiv \rho_j v_j^2 d_j / \sigma$, density ratio, ρ_j / ρ_g, viscosity ratio, μ_j / μ_g, Ohnesorge number, $Oh \equiv \mu_j / \sqrt{\rho_j d_j \sigma}$, and Bond number, $Bo \equiv \rho_j g d_j^2 / \sigma$, to the physical characteristics of a transverse liquid jet such as liquid jet trajectory and its breakup location. These correlations, however, show considerable scatters/discrepancies, see, e.g., [6-8]. These discrepancies originate from the complex physics of this two-phase flowfield as liquid jet trajectory and its penetration depend on a number of variables including: a) liquid properties such as density, viscosity and surface tension, b) test conditions at different temperature and pressure of crossflow, c) internal geometry of liquid injector/nozzle whether it is round or sharp edge, and d) measurement methods such as shadowgraphy, Mie scattering, or phase Doppler anemometry (PDPA).

Regarding the second feature of a transverse liquid jet, column breakup length, as discussed earlier in Sub-Section 1.1, there are two modes of liquid jet breakup mechanisms, namely column and surface breakup. The core of a transverse liquid jet/column forms a continuous stream between the jet exit and the location/point of its complete fracture, which is called column breakup point, see Fig. 1-1. Column breakup length of a transverse liquid jet is defined as the streamwise distance it travels into a crossflow before its complete breakup, which is referred to as the column breakup distance in the *x*-axis direction in Fig. 1-1, and column breakup height in the *z*-axis direction, as shown in Fig. 1-1. Knowledge of the location of column breakup point is important for, for

example, modeling a liquid jet in a crossflow. Accurate determination of this location is difficult because of high droplets density around the jet column. That is why there exist discrepancies amongst published predictions of this length [6, 9]. Similar to the trajectory and penetration of a transverse liquid jet, this feature has been reported in the literature using different expressions which correlated the breakup length with different non-dimensional numbers or as a constant.

To narrow down these discrepancies in the predictions of these two features, liquid jet's trajectory and its breakup length would certainly provide invaluable information for both engine researchers and manufacturers in order to design more efficient, less pollutants and higher output combustors.

1.2.2. Research Objectives

The present thesis aims at examining the role of different parameters, such as: liquid properties, test/operating conditions and nozzle internal geometry on the predictions of the trajectory and column breakup length of a liquid jet injected transversely into a subsonic gaseous crossflow by combining theoretical and experimental approaches. Briefly, the general objective of this thesis is summarized in the following research topics.

- Categorizing the correlations available in the literature for predicting the trajectory and column breakup length of a liquid jet in a crossflow based on different factors/conditions which can affect the accuracy of their predictions. This includes the impact of liquid properties, test/operating conditions and nozzle internal geometry.
- Understanding the complex physics of the problem using mathematical modelling, and establishing the contribution of various influencing/controlling non-dimensional parameters.

- Examining experimentally the effect of nozzle internal geometry on the jet flow exit conditions (i.e., turbulent or non-turbulent liquid jet), and its consequent impact on the trajectory and breakup length of a transverse liquid jet.
- Proposing correlations to predict the trajectory and breakup length of a transverse liquid jet valid over an extended range of test conditions. This is achieved by using experimental data with the mathematical models developed in this study to make these correlations as comprehensive as possible.

1.3. Outline of the Thesis

The focus of the thesis is to investigate the role of different prominent parameters including gaseous\liquid properties and liquid injector geometry on the trajectory and breakup length of a transverse liquid jet. Nonetheless, accounting for other characteristics such as the primary breakup regime and the droplets formation mechanisms associated with a transverse jet is also helpful in the overall understanding of the complex physics of the problem. In fact, these characteristics are interconnected and can affect each other. For instance, jet penetration decreases by changing the dominant breakup regime from column breakup to surface breakup. Droplets formation mechanism dictates their size, where the larger the size of a droplet is, the farthest it penetrates into a gaseous crossflow, and thereby longer penetration.

In chapter two of the thesis, therefore, published literature on the characteristics of a liquid jet injected transversally into a subsonic gaseous crossflow is reviewed comprehensively. This covers liquid jet primary breakup regimes and droplets formation mechanisms, in addition to the two main topics of the thesis, that is liquid jet trajectory and its breakup length. In this chapter, published proposed correlations have also been categorized based on relevant test conditions (e.g., liquid

properties, liquid jet and cross airflow characteristics). It is concluded from this chapter that, even when using this categorization, there still exist discrepancies in the predictions between the different correlations. This indicates a lack of comprehensive correlation applicable for a wide range of test conditions. In order to bridge the gap between the predictions of different correlations, in the following chapters of the thesis, two novel correlations were developed to predict the liquid jet trajectory and column breakup location of a transverse liquid jet in a gaseous crossflow.

Chapter three describes a mathematical model developed to predict the trajectory of a liquid jet in a subsonic gaseous crossflow. This model is developed for the jet near-field. Mass and momentum conservation equations are taken into account via using an Eulerian approach, and the tangential and normal components of the governing equations are solved analytically using control-volume analysis. The effect of forces acting on the liquid column, as well as the mass shedding from the liquid column (i.e., surface breakup) are taken into account in developing the model. As a result, an explicit algebraic correlation in a sinusoidal-exponential functional form is expressed as a function of q, Re_j, We_g, We_j, and Bo number. Chapter 3 presents the results of the predictions of the proposed correlation and comparison with published experimental data. The correlation is capable of predicting the trajectory of a transverse jet at different momentum flux ratios, different liquid properties, high temperature and pressure (HTP) test conditions as well as standard temperature and pressure (STP) conditions, and different injection angles. For the range of the test conditions explored in this study, it is found that q plays a predominant role in the predictions of liquid column trajectory, while We_g is also found important as it affects the mass stripping from the liquid column.

Chapter four reports a two zone modelling which is developed using a hybrid Eulerian-Lagrangian approach. The model is capable of predicting liquid jet trajectory and penetration in the far field

jet region, as well as in near field. In the near field zone, similar to chapter three, a force balance is applied to a control volume, and the forces acting upon the liquid column, such as drag, gravitation, and surface tension forces, as well as mass shedding from the liquid column are taken into account. In the far field zone, a logarithmic correlation for predicting the trajectory of large droplets generated at the column breakup location is developed using a Lagrangian approach. Since the behaviour in the near field region establishes the subsequent penetration of a liquid jet in the far field region, the information obtained from the first zone modeling is then used as the initial conditions for the second zone model. In this chapter, the effect of mass shedding from the liquid column and jet Reynolds number, as well as gas to liquid density and viscosity ratio on the liquid jet's trajectory and its penetration height is also studied.

While the impact of different test conditions, such as liquid properties and other jet and crossflow test characteristics, is studied using the mathematical correlations in the chapters 3 and 4, the influence of nozzle internal geometry on the jet exit conditions and consequently on the trajectory and breakup length of a transverse liquid jet required further examination. Chapter 5 is devoted to experimentally examine the role of flow condition at the nozzle exit on the predictions of the trajectory and column breakup location of a transverse liquid jet. In this study, q and other controlling nondimensional parameters (e.g., Re_j, We_g) are kept unchanged. The profiles of the axial mean velocity and their corresponding turbulence intensity at a region very close to the nozzle exit are obtained using particle image velocimetry (PIV) system. Column trajectory and its breakup location are extracted from shadowgraphy images. These experimental data sets are used in the mathematical models developed in this study to account for the effect of the liquid injector/nozzle discharge coefficient. As a result, two previously developed correlations in chapters 3 and 4 are modified in chapter 5; one for predicting the column trajectory of a round liquid jet injected

transversely into a subsonic gaseous crossflow, and the other one for predicting its column breakup length over a wide ranges test conditions of liquid properties, flow characteristics and nozzle internal geometry. In Chapter 5, the correlation for predicting liquid jet column trajectory, which was developed in Chapter 4, with unknown discharge coefficient, was compared with the present experimental data in order to estimate the value of the discharge coefficient for each specific nozzle geometry at different test conditions. It was then used in the correlation to predict the column breakup height of a transverse liquid jet. An in-house MATLAB code is developed in Chapter 5 for determining the jet trajectory and breakup location of a transverse liquid jet (see Appendix A.1).

To summarize, a methodology, which is described schematically in Fig. 1-2, is adopted in the present thesis in order to develop appropriate correlations for predicting the trajectory and breakup length of a transverse liquid jet in a gaseous crossflow while accounting for liquid properties, test/operating conditions and nozzle internal geometry.

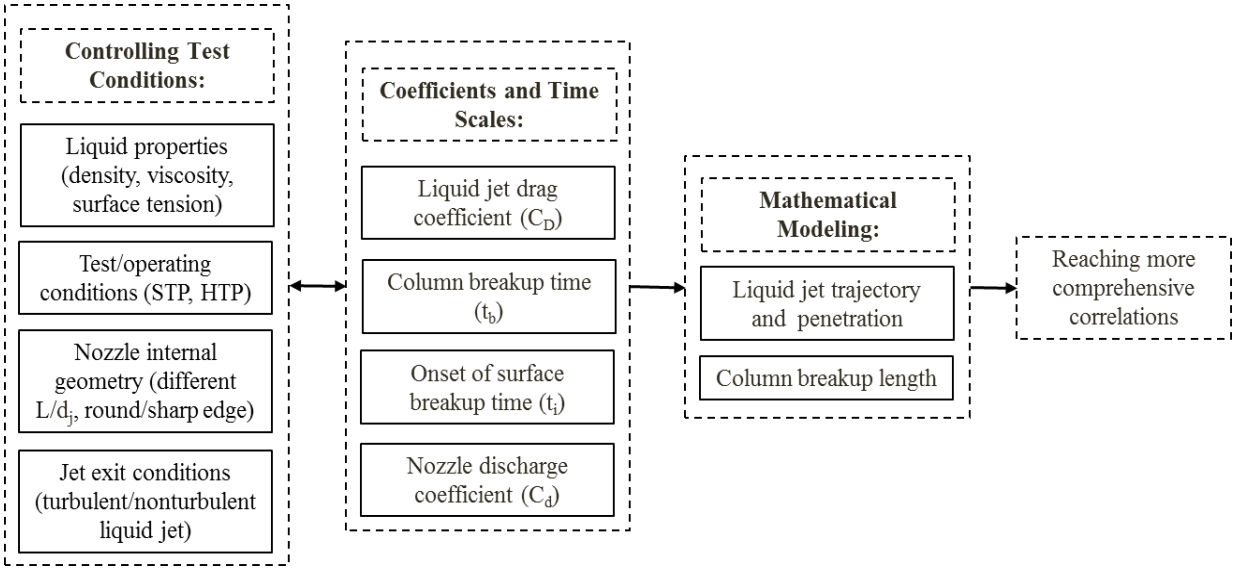

Figure 1-2: A Schematic flow of the adopted methodology.

As is illustrated in Fig. 1-2, in order to achieve the objective of this thesis, that is developing reliable/comprehensive correlations for predicting a transverse liquid jet's trajectory and breakup length, a mathematical approach is employed to derive explicit relationships of these features. These forms of mathematical correlations are a function of several coefficients and time scales, which include liquid jet drag coefficient C_D, column breakup time t_b, onset of surface breakup time t_i, and nozzle discharge coefficient C_d, which are all dependent on the liquid properties, test/operating conditions and nozzle internal geometry. In essence, using appropriate coefficients in these mathematical relationships/correlations is important for the degree of accuracy of their predictions. In order to extend the application and validity of these correlations, the experimental data on the impact of nozzle discharge coefficient (which itself is a function of liquid properties, nozzle internal geometry and jet exit conditions) is employed.

Finally, Chapter six summarizes key findings, limitations and the implications of the results, as well as recommendation for future work.

1.4. References

[1] Rachner M, Becker J, Hassa C, Doerr T. Modelling of the atomization of a plain liquid fuel jet in crossflow at gas turbine conditions. Aerosp Sci Technol 2002;6:495–506.

[2] Wu P-K, Kirkendall KA, Fuller RP, Nejad AS. Breakup processes of liquid jets in subsonic crossflows. J Propuls Power 1997;13:64–73.

[3] Leong, M.Y., McDonell, V.G., and Samuelsen, G.S., "Mixing of an airblast-atomized fuel spray injected into a crossflow of air," NASA Glenn Research Center Report NASA/CR-2000-210467, 2000.

[4] Birouk M, Lekic N. Liquid jet breakup in quiescent atmosphere: A review. At Sprays 2009;19:501–28.

[5] Behzad M, Ashgriz N, Mashayek A. Azimuthal shear instability of a liquid jet injected into a gaseous cross-flow. J Fluid Mech 2015;767:146–72.

[6] M. Broumand and M. Birouk, "Liquid jet in a subsonic gaseous crossflow: Recent progress and remaining challenges," Prog. Energy Combust. Sci., vol. 57, pp. 1–29, Nov. 2016.

[7] M. Wang, M. Broumand, and M. Birouk, "Liquid jet trajectory in a subsonic gaseous cross-flow: an analysis of published correlations," At. Sprays, vol. 26, no. 11, pp. 1083–1110, 2016.

[8] Brown C, McDonell V. Near field behavior of a liquid jet in a crossflow. ILASS Am., Toronto, Canada: 2006.

[9] Osta AR, Sallam KA. Nozzle-geometry effects on upwind-surface properties of turbulent liquid jets in gaseous crossflow. J Propuls Power 2010; 26:936–46.

Chapter 2

Liquid Jet in a Subsonic Gaseous Crossflow: Recent Progress and Remaining Challenges

2.1. Abstract

This article reviews published literature on the characteristics of a liquid jet injected transversally into a subsonic gaseous crossflow. The review covers the following aspects: (i) liquid jet primary breakup regimes, (ii) liquid jet trajectory and penetration, (iii) liquid jet breakup length, and (iv) droplets features and formation mechanisms. The focus is on analyzing the role of different prominent parameters which include gaseous and liquid properties, and liquid injector geometry. The review revealed that gas Weber number plays a crucial role in defining non-turbulent primary breakup regimes, while liquid jet Weber number is of great importance for the transition to turbulent primary breakup. Jet-to-crossflow momentum flux ratio is the most important parameter for predicting the trajectory, penetration, and breakup length of a liquid jet in a crossflow. The characteristics of droplets disintegrated during the primary breakup are mostly influenced by the nozzle exit conditions, whereas the characteristics of droplets produced via the secondary breakup dependent strongly on the velocity of cross airflow. The review revealed that although substantial progress has been made in understanding this complex two-phase flow phenomenon, there still remain several shortcomings which require further research.

2.2. Introduction

The flowfield associated with a jet injected transversely into a crossflow (referred to as JICF), also known as a transverse jet, can be generally classified into two main categories: a gaseous (or liquid) jet in a gaseous (or liquid) crossflow (i.e., single-phase flow), and a liquid (or gaseous) jet in a gaseous (or liquid) crossflow (i.e., multi-phase flow). A transverse jet has numerous applications in industrial, environmental and natural systems, such as air-breathing engines (e.g., dilution air jets, turbine blade film cooling systems, V/STOL aircraft, fuel/air mixers and ramjet/scramjet fuel injectors), rocket engines (e.g., thrust vector control), environmental control systems (e.g., effluent from chimney, smokestack, and flare stacks plumes as well as liquid effluent dispersal in streams), and natural flows (e.g., volcanic plumes in crosswind, bivalve clams and blue crabs, and central venous catheters).

Earliest research of a jet in a crossflow has been motivated by applications related to environmental problems such as plume dispersal from exhaust or pipe stacks or liquid effluent dispersal in streams [1–3]. Thrust vector control in rocket engines by injecting an array of transverse jets into, and deflecting the flow in the nozzle, is another example of the applications of both a liquid and a gaseous transverse jet [1,2]. This jet configuration is also adopted during takeoff, hover, and transition to wing-borne flight in vertical/short takeoff and landing (V/STOL) aircraft for controlling the lift and thrust vectors [1,3]. The superior mixing properties of a transverse jet compared to a jet in quiescent surroundings make this flowfield layout appealing especially for engineering applications when rapid injectant mixing is desired [1,2]. Also, dilution of gaseous jets are introduced downstream of the primary and/or secondary combustion chamber zones in order to decrease the temperature of combustion products before entering the turbine section of a gas turbine engine [1,2,4,5]. Transverse injection of a liquid fuel jet into a gaseous crossflow is an

approach which is often employed in both aviation and stationary power generation systems where rapid fuel penetration, vaporization, mixing of vapor/air and ignition, and consequently sustained combustion process are desired. This method of liquid fuel/air mixture preparation enhances flame stabilization, fuel conversion efficiency, and accordingly emissions reduction [6–9]. The overall performance of a propulsion engine, in terms of thrust and specific impulse, can be enhanced through controlled or actively forced dilution jet injection [1,2,10]. Contrary to film-cooling in gas turbine engines where air jets should penetrate less and adhere to the surface as much as possible, dilution jets require a higher penetration and spread into a crossflow [2]. Transversely injected air jets are also used in the primary zone of gas turbine combustors as a means of controlling the air-fuel mixture ratio and hence the emissions of nitrogen oxides (NOx). Tunable air-fuel mixing allows simultaneous control of NOx and carbon monoxide (CO) emissions [1,2,11]. In the combustion chamber of a direct injection diesel engine, where the air has a strong swirl movement in the cylinder, the interaction between a diesel spray and a crossflow is of importance [6–8].

While the focus of the present review lies on the injection of a liquid jet into a subsonic gaseous crossflow, the main characteristics of a transverse gaseous jet are relevant to the understanding of this topic. In essence, several published studies explored the analogy between a transverse gaseous jet and a transverse liquid jet to overcome the lack of comprehension of the latter [9], even though there exist some distinct differences between their features and controlling parameters which will be discussed later on. For instance, earlier studies (e.g., [12,13]) hypothesized that the occurrence of a progressive flattening of a liquid column, due to the acceleration of the gas flow around the jet, could induce a bow (or kidney) shape deformation of the jet cross-section. Given the similarities between these two flowfields, the general features of a transverse gaseous jet will be

presented first in the following Subsection 1.2.1 followed by the general features of a transverse liquid jet and its corresponding controversial issues introduced in Subsection 1.2.2.

2.2.1. Features of a gaseous jet in a subsonic gaseous crossflow

A gaseous jet in a gaseous crossflow has been widely investigated, and several review papers on this topic are available in the literature [1–3,14,15]. This flowfield typically consists of a jet with a mean velocity v_j injected transversely into a gaseous crossflow with a velocity u_g, and it is usually divided into two main regions: a jet region (near-field region), where the deflection of the jet is still small, and a wake-like region (far-field region), in which the jet is almost aligned with the crossflow. Between these two regions, there exists a region of high jet trajectory curvature. The interaction of a jet and a crossflow creates a complex set of vortex structures as is depicted in Fig. 2-1. The most obvious structure is the counter-rotating vortex pair (CVP). Other coherent structures include horseshoe-shaped vortices, wake vortices, and jet shear layer vortices. The horseshoe and shear layer vortices are best described in the near-field region, whereas the CVP and wake-like characteristics are most evident in the far-field region [15–18].

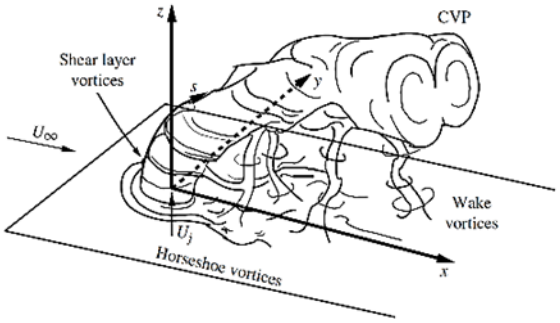

Figure 2-1: Schematic of a transverse gaseous jet, and relevant flow structures (Reprinted from Fric and Roshko [16] with permission from Cambridge University Press).

Among the non-dimensional parameters used to correlate the observed features of this flowfield with fluid properties, test conditions and geometrical parameters are the jet-to-crossflow momentum flux ratio, $q \equiv \rho_j v_j^2 / \rho_g u_g^2 \equiv SR^2$, jet Reynolds number, $Re_j \equiv \rho_j v_j d_j / \mu_j$, and crossflow or gas Reynolds number, $Re_g \equiv \rho_g u_g d_j / \mu_g$; where $S \equiv \left(\rho_j / \rho_g\right)$ is the jet-to-crossflow density ratio, and $R \equiv \left(v_j / u_g\right)$ is the jet-to-crossflow velocity ratio. In the limit of iso-density, $q \equiv R^2$ for a jet in a crossflow.

Another important feature of a transverse gaseous jet is the jet trajectory, which is of fundamental interest and has been widely studied [19–23]. For instance, Karagozian [20] considered a vortex pair issuing from a jet orifice into a crossflow, and by solving the governing equations, a power law correlation for the evolution of jet trajectory was proposed as follows:

$$\frac{z}{d_j} = c_1 r^{n_1} \left(\frac{x}{d_j}\right)^{n_2} \tag{2-1}$$

where $r \equiv \left(\rho_j v_j^2 / \rho_g u_g^2\right)^{1/2} \equiv q^{1/2}$ is called the blowing ratio, constant $c_1 = 0.527$, and power exponents $n_1 = 1.178$ and $n_2 = 0.314$. Hasselbrink and Mungal [21,22] employed similarity analysis and intermediate asymptotic theory to develop scaling laws for velocity, mass-flux and jet trajectory. They proposed two separate correlations for jet trajectory, one for the near-field (or jet region) and the other one for the far-field (or wake-like region), respectively, as follows:

$$\frac{z}{rd_j} = \left(\frac{2}{c_{ej}} \frac{x}{rd_j}\right)^{1/2} \text{ and } \frac{z}{rd_j} = \left(\frac{3}{c_{e\omega}} \frac{x}{rd_j}\right)^{1/3} \tag{2-2}$$

where c_{ej} and $c_{e\omega}$ are the entrainment coefficients in the jet and wake–like region, respectively. Muppidi and Mahesh [23] noted that the scaled trajectories from different experiments showed a considerable scatter even for those having nearly similar velocity ratios. They used direct numerical simulation (DNS) to examine possible reasons of these discrepancies. They mentioned

that jet trajectory can be defined in different ways; for example, based on the local velocity maxima, local scalar maxima, vorticity curves, and time-averaged center streamline, where all of which could affect the prediction of a jet trajectory. The velocity profile at the jet exit (e.g., a top–hat or a fully developed pipe flow profile) has also been mentioned as another reason of the discrepancies in predicting jet's trajectory.

Overall, the non-dimensional parameters used to define the features of a gaseous transverse jet, such as q, Re_j and Re_g, are equally important parameters in analyzing a liquid transverse jet as well. Nonetheless, in the case of a liquid jet injection into a gaseous crossflow, there exists additional physical property, which include surface tension due to the existence of liquid phase discontinuity at the interface between two different fluids (i.e., liquid-gas). This property introduces further non-dimensional parameters, such as gas and jet Weber numbers, Ohnesorge number, and Bond number. Moreover, while jet flow structure and trajectory are common for both transverse gaseous and liquid jet, the breakup process is a unique feature of a liquid jet, which is the result of the interaction between different forces (i.e., kinetic energy of a liquid and gaseous flow, surface tension forces) on the liquid/gas interface. This yields to one of the most challenging aspects of a liquid jet in a subsonic gaseous crossflow, which is named primary breakup. The aforementioned non-dimensional key parameters along with the features relevant to a transverse liquid jet in a gaseous crossflow are discussed in the next sub-section.

2.2.2. Features of a liquid jet in a subsonic gaseous crossflow

A schematic view of a liquid jet penetrating into a subsonic gaseous crossflow is illustrated in Fig. 2-2. From hydrodynamic instability analysis perspective, liquid jet leaves the nozzle as an unbroken column, begins to ruffle as a result of axial instability which develops along the liquid column and finally breaks up into droplets and ligaments, which is named column breakup process

[24–29], as is illustrated in Fig. 2-2. In this mode, the spray trajectory is unsteady or oscillatory [30]. As liquid begins to disintegrate from the jet surface (as a result of hydrodynamic instabilities on the jet lateral surface [25]) and the surface breakup process becomes dominant (see Fig. 2-2), the jet penetration height decreases [31]. An alternative perspective for the surface breakup of a liquid jet is the boundary layer stripping mechanism, in which a viscous boundary layer forms inside the jet due to the outer gas flow [25–28]. In this regard, two major models have been developed to predict the mass shedding due to atomization. The first is the Kelvin-Helmholtz model [32,33], which deduces the mass removal rate from the wavelength and growth rate of the fastest growing surface wave, calculated on the basis of a linearized stability analysis. The second is the Boundary Layer Stripping (BLS) model [34,35]. The basic assumption for this model is that the mass removed from the jet coincides with the flow rate in the liquid boundary layer at the separation point, taken for simplicity as the equatorial plane normal to the airflow. It should be noted that both column and surface breakup mechanisms coexist but with the predominance of one over the other [36]. Overall, the liquid fragments shedding from a jet along its trajectory undergo subsequent secondary breakup process leading to smaller droplets, and consequently the formation of a spray. This mode is favorable for a better atomization and the formation of a steady or non-oscillatory spray [30].

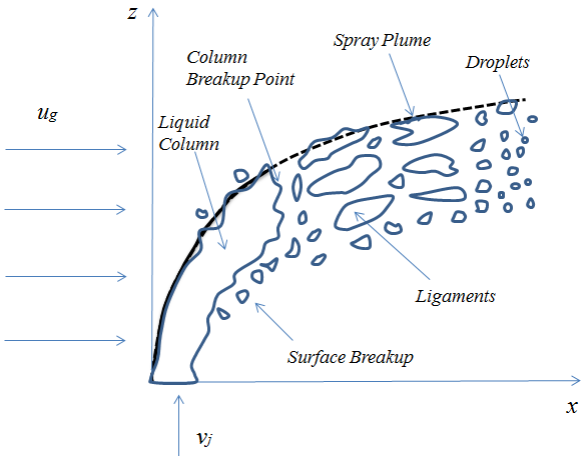

Figure 2-2: Schematic diagram of a jet penetration into a crossflow. Solid and dashed lines show the liquid column and spray plume regions, respectively, Reprinted from Ref. [37] with permission from Begell House.

In order to better understand the physics of a transverse liquid jet, it is preferable to use non-dimensional parameters to express the level dependency of its features (such as jet's breakup regimes, trajectory and penetration, breakup length and droplets formation) on fluid properties, test/operating conditions and geometrical parameters. The important variables relevant to this flowfield can be divided into three groups [38]. The first group contains the liquid-related parameters which includes jet velocity, v_j, liquid density, ρ_j, surface tension, σ, and dynamic viscosity, μ_j. The second group comprises the gaseous phase (i.e., crossflow) parameters which include u_g, ρ_g and μ_g which are the gas density, velocity, and dynamic viscosity, respectively. Finally, the third group consists of the geometrical and surroundings parameters. For example, for a liquid jet injected transversely into a gaseous medium, these parameters consist of the liquid injector/nozzle geometry (i.e., jet diameter, d_j) and the effect of gravity, g. [39]. For an angled injection, one could add another parameter to include the effect of the nozzle tilt. Employing

different approaches like the Buckingham π theorem to evaluate the dimensional relationship between the different terms (e.g., [40]), a particular feature of a liquid jet in a cross flow (e.g., trajectory and penetration) can be written as a function of the jet-to-crossflow momentum flux ratio, q, jet Reynolds number, Re_j, and crossflow Reynolds number, Re_g, similar to a gaseous transverse jet. Moreover, due to the fact that a liquid jet has different properties than a gaseous counterpart, such as liquid surface tension, σ, additional non-dimensional parameters are then needed to completely define its features. It includes gas Weber number $We_g \equiv \rho_g u_g^2 d_j/\sigma$ and jet Weber number $We_j \equiv \rho_j v_j^2 d_j/\sigma$, which are the ratio of gas and liquid inertial forces, respectively, to the liquid surface tension force. There exist also other additional dimensionless parameters for a liquid jet such as density ratio, ρ_j/ρ_g, viscosity ratio, μ_j/μ_g, Ohnesorge number, $Oh \equiv \mu_j/\sqrt{\rho_j d_j \sigma}$, and Bond number, $Bo \equiv \rho_j g d_j^2/\sigma$.

From a practical point of view, the study of a liquid jet in a gaseous crossflow has several challenges. A reason for this is that a transverse jet cannot be reduced to a one-dimensional scheme as the liquid bending in a crossflow induces a greater complexity than the injection of a liquid jet in quiescent or co-flowing surroundings. Furthermore, the core of a transverse liquid jet (i.e., liquid column) forms a continuous stream when leaving the injector/orifice till the first point of its complete fracture, namely column breakup point. This core may be turbulent or non-turbulent at the injector/nozzle exit and will in either case exhibit distinct primary breakup characteristics. The lack of a total understanding of the mechanisms characterizing turbulent regime, as it spans between the extreme cases of Rayleigh breakup and fully developed atomization, is reflected by the lack of models for the atomization in the this regime [9]. Due to the complexity associated with the theory behind this subject, a large body of studies on this topic is experimental; however, different experimental challenges such as the limitations in observing the dense spray region are

slowing down our progress in understanding this topic. Moreover, the features of a transverse liquid jet vary significantly with liquid properties, operating/test conditions and nozzle internal geometry. To date, several attempts have been made to gain a global understanding of the complex process of a transverse liquid jet. For instance, several empirical maps for predicting liquid jet primary breakup regimes, and numerous correlations for predicting trajectory, penetration, breakup length and droplets formation have been reported in the literature (e.g., [26,28,36] to cite only a few). However, as will be shown in the present review, there is still no general consensus about some of these aforementioned concepts. Thus, further research is required in order to gain a better understanding of the features of this important process/phenomenon which in turn will help design more efficient power and propulsion systems that employ a transverse liquid jet.

In this regard, three aspects of a liquid jet in a subsonic gaseous crossflow are reviewed in the present review paper as follows: (i) definition and specifications of a transverse liquid jet's primary breakup regimes, (ii) prediction of a liquid jet trajectory and its penetration behavior in a crossflow, (iii) liquid jet breakup length, and (iv) droplets features and formation mechanisms. The effect of different operating/test conditions, liquid properties, nozzle internal geometry and other effective parameters are considered. These four concepts are of great importance as they have direct influence on the secondary breakup, droplets velocity and size distribution, drops collision and vaporization, mixing rate and finally the efficiency of liquid fuel combustion. In essence, similar to the importance of identifying whether a single-phase flow is laminar or turbulent, specification of the topology, or liquid jet primary breakup regime, is a critical issue in the understanding of a transverse liquid jet. Furthermore, information describing a liquid jet trajectory and its penetration in a crossflow is highly required for the design of combustion chambers as it determine the distribution of fuel, which for instance plays a key role in preventing fuel impingement onto the

walls of a combustor [38]. For example, in some configurations of lean premixed prevaporized (LPP) combustion [41], the range of q should be kept less than 15 in order to avoid fuel impingement on the combustor walls. In addition, similar to the potential core of a single phase jet, or the liquid core of a liquid jet in quiescent gas, liquid jet breakup length is an important feature for modeling a transverse liquid jet.

Motivated by the aforementioned applications along with the features and challenges of a liquid jet injected transversely into a gaseous crossflow, a comprehensive review on this subject seems to be required not only to examine related published literature, but also to shed light on the remaining challenges for future work. Due to space limitations and also to keep coherent the topic in question; the scope of this review is limited to recent results and major findings of non-evaporating, non-reacting round (or canonical) liquid jets in subsonic gaseous crossflows with uniform velocity fields and negligible turbulence in near-wall gas boundary layers. Furthermore, conditions for the appearance of non-turbulent and turbulent round liquid jets are obtained from the primary breakup regime map proposed by Wu et al. [42]. According to this map, liquid jet has smooth surface with no reattachment (i.e., implying a non-turbulent flow) for a nozzle's length/diameter ratio less than 4-6 at high Re_j. On the other hand, a nozzle with a larger length/diameter ratio generates a fully developed turbulent flow at the jet exit for sufficiently high Re_j. In this regard, Section 2.2 is intended to provide a review of the primary breakup of non-turbulent and turbulent liquid jets in a subsonic gaseous crossflow. The two major features of this flowfield, namely trajectory/penetration and breakup length, are examined in sections 2.3 and 2.4, respectively. The outcome of liquid jet breakup which include droplets breakup rate, size and velocity distribution are reviewed in Section 2.5. Finally, concluding remarks along with future research and directions are provided in Section 2.6.

2.3. Liquid jet primary breakup regimes

2.3.1. Non-turbulent liquid jet primary breakup

Numerous empirical maps for predicting the primary breakup regimes of a non-turbulent liquid jet injected into a subsonic gaseous crossflow have been proposed in the literature. For all of these maps, We_g seems to be the most effective non-dimensional parameter for defining the primary breakup regimes. There exist different other types of maps in the literature, such as $We_g - q$ (e.g., [7,36–41]), $We_g - We_j$ (e.g., [47,48]), $Oh - We_g$ (e.g., [27,28]), $We_g - (\lambda_c/d_j)$ (e.g., [27,49]), $We_g - (\lambda_s/d_j)$ (e.g., [27,28]), and $We_g - Re_j$ [50].

The most common map for classifying the primary breakup regimes is $We_g - q$ map. It was first proposed by Wu et al. [26] to classify the observed breakup characteristics of a liquid jet in a gaseous crossflow. Wu et al. [26] asserted that since the breakup process of a liquid jet and a spherical droplet in an airflow are both caused by aerodynamic forces, the general understanding of the aerodynamic secondary breakup of drops could be applicable to the primary breakup of a liquid jet. They classified the observed breakup characteristics of a liquid jet in a crossflow into two main regimes (i.e., column and surface breakup) based on the q and We_g. They concluded that column breakup can be observed at low q and/or low We_g, and the surface breakup regime occurs at high q and/or high We_g. Wu et al. [26] also divided the column breakup region in their breakup map into four sub-regions depending on We_g (i.e., enhanced capillary, bag, multimode and shear breakup). For We_g < 11, the breakup process is caused by capillary forces, which referred to as enhanced capillary breakup. At somewhat higher Weber number (11 < We_g < 30), a transition occurs where both column and bag breakup are observed. At 30 < We_g < 90, the breakup

process is a multimode with bag breakup giving way to surface stripping, and finally shear breakup process for 90 < We_g. The breakup regime map displaying the different regimes of jet breakup, as well as the transition borderline between column and surface breakup based on the visual observation of the work of Wu et al. [26] is depicted in Fig. 2-3. Their column/surface breakup borderline is given by $We_g = 10^{[3.1-\log(q)]/0.81}$. Nonetheless, they mentioned that since this is a gradual transition, identifying a clear threshold for transition between these two regimes is inconclusive and further studies are needed to identify mechanisms for this transition.

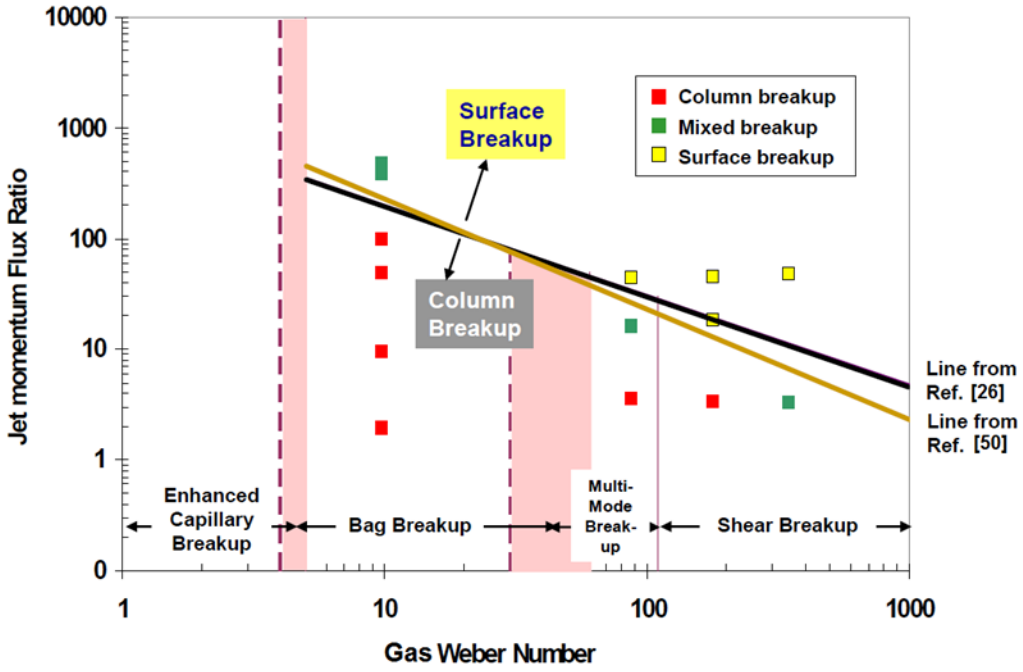

Figure 2-3: $We_g - q$ regime map of primary breakup processes of a nonturbulent liquid jet in a crossflow [50].

Tambe et al. [41] conducted a parametric study of a liquid jet in a gaseous crossflow at standard temperature and pressure (STP) test conditions by focusing on the behavior of jet column and the

produced spray after breakup. They provided a $We_g - q$ primary breakup regime map and observed similar breakup modes (i.e., column and surface breakup) as those reported by Wu et al. [26], and labeled the transition between these two modes as mixed breakup mode. Their transition (mixed) regime, however, occurred at lower q and We_g as compared to that observed by Wu et al. [26]. They plotted the transition borderline between the column and surface breakup mode, and observed a steeper slope of the line, after which they concluded that the effect of We_g on the transition is stronger than that of q. Brown and McDonell [45] also proposed a $We_g - q$ breakup regime map using the test conditions of Wu et al. [26] while considering the effect of nozzle discharge coefficient (examined 3 different nozzle diameters, 0.48, 0.94, and 1.30 mm, having discharge coefficients of 0.88, 0.71 and 0.76, respectively). Similar to earliest studies (Wu et al. [26], and Tambe et al. [41]), they observed two types of breakup regimes: column and surface breakup. They suggested that We_g plays a stronger role and the transition region from column to surface dominated breakup occurred at lower q than that previously suggested by Wu et al. [26], which is consistent with the observations of Tambe et al. [41].

Lakhamraju and Jeng [44] investigated the effect of elevated temperature at atmospheric (standard) pressure (HTSP) on the primary breakup regimes of a liquid jet in an air crossflow. They also varied separately the temperature of both, liquid jet and the air crossflow, up to 363 and 505 K, respectively, in order to test a wide range of test conditions. Consistent with the earlier studies of Wu et al. [26], Tambe et al. [41] and Brown and McDonell [45], they identified two types of breakup regimes: column and surface breakup plotted on a $We_g - q$ primary breakup regime map. Similar to Tambe et al. [41], their transition (or mixed) region occurred at lower q and We_g compared to that of Wu et al. [26]. However, their transition has a steep borderline compared with that of Wu et al. [26], which is different from the observations of Tambe et al. [41].

Becker and Hassa [36] investigated the effect of elevated pressure at room/standard temperature (STHP; that is, up to 15 bar at 290 K) on the primary breakup regimes of a plain jet in an air crossflow. Similar to Wu et al. [26], they confirmed that two basic breakup mechanisms can be discerned (i.e., column breakup and surface breakup). Their data, which were taken at different range of air pressure and velocity (50 – 100 m/s), showed a good agreement with the primary breakup regime map of Wu et al. [26]. Elshamy and Jeng [43] also studied the effect of elevated pressure at room temperature (STHP) on the primary breakup regimes of a water jet in an air crossflow. Air velocity ranged between 39 and 306 m/s, air pressure varied up to 7 bar at room temperature. Similar to Wu et al. [26], Tambe et al. [41], Brown and McDonell [45], Lakhamraju and Jeng [44] and Becker and Hassa [36], they provided a $We_g - q$ primary breakup regime map and observed similar breakup modes; that is, column and surface breakup, and labeled the transition between these two modes as mixed breakup mode. However, their transition (or mixed) region borders were wider (that is; lower q and We_g for the lower limit, and higher q and We_g for the upper limit) compared to those of Wu et al. [26]. Moreover, their transition is somehow steeper than the transition borderline of Wu et al. [26] consistent with the observations of Tambe et al. [41]. Recently, Song et al. [46] studied the breakup, penetration, droplet size, and size distribution of A-1 fuel jet in air crossflow at elevated pressure and room temperature (STHP) test conditions. Song et al. [46] plotted their data on a $We_g - q$ map and proposed a correlation for the boundary between column and surface breakup as a function of q, liquid/gas density and viscosity ratio, and mean drop size. They remarked that the transition borderline between the column and surface breakup shifted towards higher q and We_g numbers when increasing the pressure of air crossflow.

The other type of map used to classify breakup characteristics of a liquid jet in a gaseous crossflow is $We_g - We_j$ map, which was first proposed by Vich and Ledoux [47]. They investigated the

basic disintegration mechanisms of a liquid jet (velocity ranged between 5 and 23 m/s) in a low speed crossflow (velocity ranged between 5 and 45 m/s) at room (STP) test conditions. Several injector diameters of 0.5 mm, 1.0 mm or 1.5 mm were tested. Similar to Wu et al. [26], Vich and Ledoux [47] reported similarities between the breakup properties of a round liquid jet in a gaseous crossflow and the secondary breakup of drops. Vich and Ledoux [47] found several breakup regimes, namely type I (called no crossflow action breakup), arcade breakup named type II (i.e., liquid column breakup at small Weber number), and bag breakup referred to as type III, as depicted in Fig. 2-4. It should be noted that Vich and Ledoux [47] considered We_g up to about 100 which (will be discussed later on) does not cover the shear breakup regime, whereas Wu et al. [26] included a wider range of We_g, close to 1000, in order to cover all breakup regimes in their map.

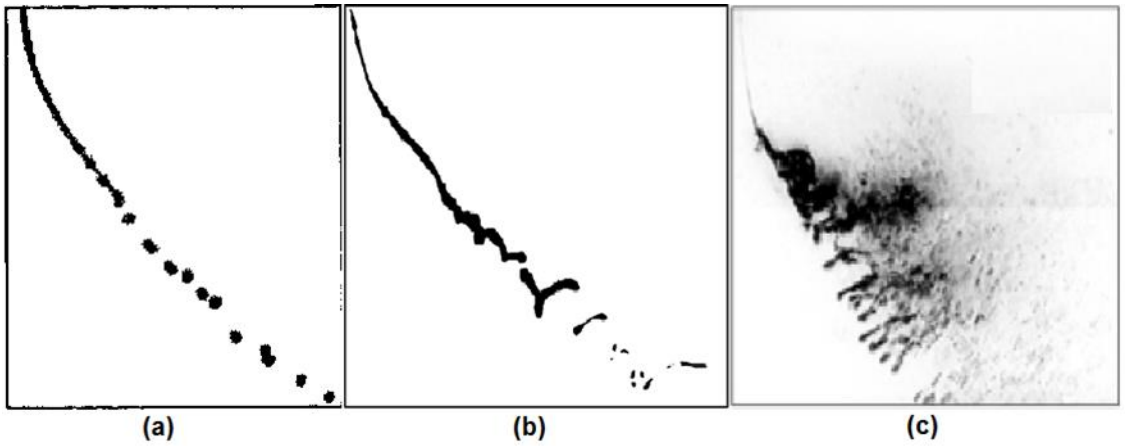

Figure 2-4: Example of a) type I (no crossflow action breakup regime) - reprinted from Vich and Ledoux [47] with permission from Begell House, b) type II (liquid column breakup regime) and c) type III (bag breakup regime) - reprinted from Birouk et al. [48] with permission from Wiley.

Vich and Ledoux [47] provided a breakup regime map based on $We_g - We_j$ by accounting for the influence of We_j in terms of q (i.e., as $We_j = q\, We_g$), and indicated that the type I mode of

breakup, defined as a breakup not modified by the crossflow, is effective up to We_g~1.5. The transition to type II or III appears also to be governed by the gas Weber number, where the same transition criterion ($We_g \sim 8$) from type I to type II or III was found. They pointed out, however, that the transition from I to II was obtained for $We_j < 250$ as is illustrated in Fig. 2-5. They remarked that a We_g ~ 10 has a strong influence on aerodynamic forces. They also provided a breakup regime map based on $(1/q) - We_j$.

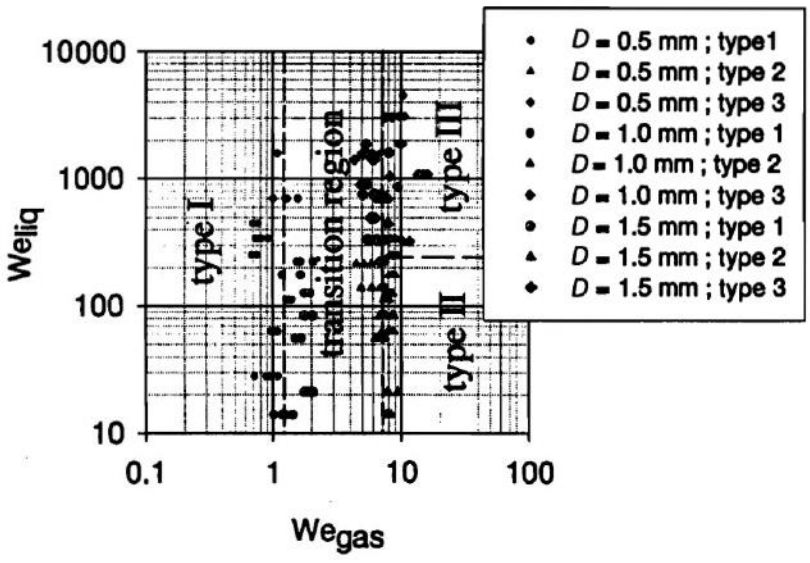

Figure 2-5: $We_g - We_j$ regime map of primary breakup process of a non-turbulent liquid jet in a crossflow. Reprinted from Ref. [47] with permission from Begell House.

Using the same primary breakup regime map as Vich and Ledoux [47], Birouk et al. [48,51] studied the effect of liquid viscosity on the primary breakup of a viscous liquid jet at STP test conditions. They conducted experiments by injecting perpendicularly aero-engine lubrication oil into an air crossflow. Only two types of jet breakup regimes were identified for their explored range of test conditions, which were called column and bag breakup, as suggested by Vich and

Ledoux [47]. In addition to $We_g - We_j$ map, Birouk et al. [48] used a $(1/q) - We_j$ map to show the two identified breakup regimes and the transition region between them. They reported that the transition between these two modes occurred when We_g = 3 – 9 for the range of We_j = 149 – 939. Mazallon et al. [27] extended the investigations of Wu et al. [26] and Vich and Ledoux [47] to quantify the effect of parameters that have influence on the properties of both the primary breakup of a liquid jet in a crossflow and secondary breakup of drops. Inspired by the studies of Hinze [52] on the secondary breakup of drops exposed to shockwave disturbances at large liquid/gas density ratio conditions, Mazallon et al. [27] exploited an analogy between the primary breakup regimes of a round non-turbulent liquid jet in a crossflow and the secondary breakup of drops subjected to shockwave disturbances, and consequently classified the primary breakup regimes in terms of gas Weber number (We_g) and Ohnesorge number (*Oh*). Similar to Wu et al. [26], they found four breakup regimes, though with slightly different transition ranges, namely capillary breakup (We_g < 5), bag breakup (5 < We_g< 60), bag/shear breakup (60 < We_g< 110), and shear breakup (110 < We_g). They considered the ratio of liquid/gas density, ρ_j/ρ_g, of 700 –1100, and the ratio of liquid-viscous/surface-tension forces expressed in terms of Ohnesorge number, *Oh*, in the range of 0.00006 – 0.3. Several different round sharp edged (Borda) nozzles (2, 4, and 16 mm diameter) and a round supercavitating nozzle (1 mm diameter having a sharp-edged inlet and exit with a length/diameter ratio less than 3) were employed in this study in order to generate uniform nonturbulent round liquid jets. Based on the work of Dai et al. [53] and Lienhard [54], Mazallon et al. [27] adopted an actual liquid jet diameter of only 50-70% of the geometric diameter of Borda and supercavitating nozzle. Both a shock tube and a subsonic wind tunnel were used to generate a crossflow. Within the range of their test conditions, Mazallon et al. [27] remarked that the primary breakup regimes were relatively independent of *Oh*. Within the shear breakup regime, however,

they mentioned that the length of the ligament being stripped from the sides of the liquid column increased progressively with increasing *Oh* number. Thus, similar to the secondary breakup of drops in the shear breakup regime [55], a long-ligament breakup regime was defined for $Oh > 0.1$. They mentioned that the long ligament regime presents significant experimental difficulties due to the problem of tracking the flow behavior when ligaments are long. They also reported that, due to the limited dimensions of their crossflow, the transition of a stable liquid jet to the capillary breakup regime at very low crossflow velocity could not be found. Mazallon et al. [27] observed two types of waves from the appearance of waves in the streamwise direction along the liquid column; the wavelengths between nodes - namely column wavelength λ_c which involves the deflection of the entire liquid column at small We_g, and the smaller wavelength, namely surface wavelength λ_s associated with periodic disturbances of the liquid stripping along the sides of the liquid column at larger We_g. They concluded that these wavelengths are mainly function of We_g, and there is a clear relationship between λ_c and λ_s and the properties of bag, bag/shear, and shear breakup of a liquid jet in a crossflow. They, therefore, provided $We_g - (\lambda_c/d_j)$ and $We_g - (\lambda_s/d_j)$ maps with marked We_g that corresponds to the transitions between breakup regimes, as is illustrated in Fig. 2-6

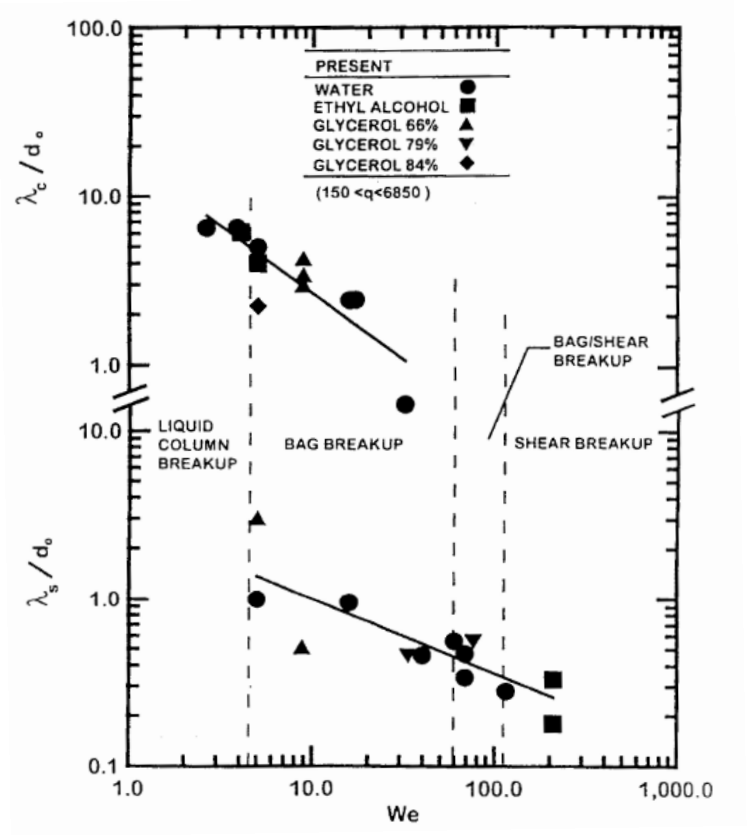

Figure 2-6: $We_g - (\lambda_c/d_j)$ and $We_g - (\lambda_s/d_j)$ regime maps of the primary breakup of a liquid jet in a crossflow. Reprinted from Ref. [27] with permission from Begell House.

Later on, Sallam et al. [28], following the work of Mazallon et al. [27] and using nearly similar liquids and flow properties, reported the following primary breakup regimes of non-turbulent liquid jet in subsonic gaseous crossflow: no breakup ($We_g = 0$), column breakup ($We_g \leq 4$), bag breakup ($4 < We_g < 30$), multimode breakup ($30 < We_g < 110$), and shear breakup ($110 < We_g$) regime. These regimes are nearly similar to those of Mazallon et al. [27]. A sample two-dimensional images of the different modes of jet breakup regimes is shown in Fig. 2-7.

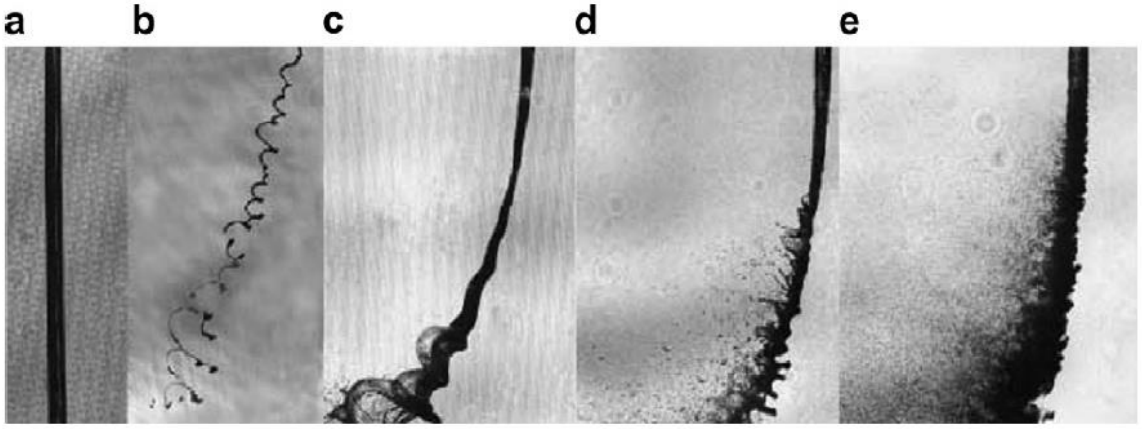

Figure 2-7: Images of the primary breakup process of non-turbulent liquid jet in a gaseous crossflow: a) We_g= 0, no breakup; b) We_g= 3, capillary breakup; c) We_g= 8, bag breakup; d) We_g= 30, multimode breakup; and e) We_g= 220, shear breakup. Reprinted from Ref. [28] with permission from AIAA.

Furthermore, similar to Mazallon et al. [27], Sallam et al. [28] used the similarities between the primary breakup regimes of a round non-turbulent liquid jet in a crossflow and the secondary breakup of drops subjected to shockwave disturbances, and correlated the breakup regimes of a round non-turbulent liquid jet in a crossflow in terms of We_g and *Oh* number. In order to show this relationship, the secondary breakup regime map for drops of Hsiang and Faeth [55] was also depicted in Fig. 2-8 along with the $Oh - We_g$ map of Mazallon et al. [27] and Sallam et al. [28].

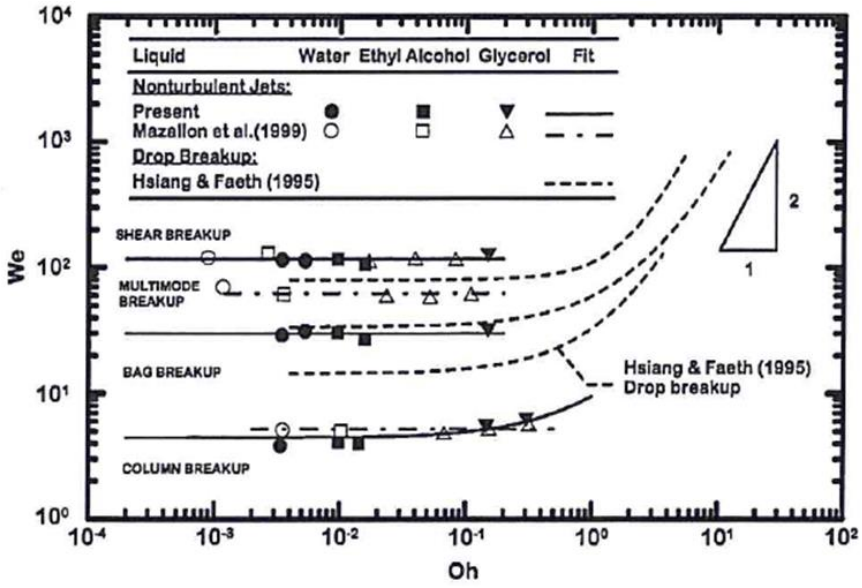

Figure 2-8: $Oh - We_g$ regime map of the primary breakup of a liquid jet in a crossflow. Reprinted from [28] with permission from AIAA.

According to Fig. 2-8, the main difference between the breakup of a drop and that of a liquid jet resides in the fact that the secondary breakup of a drop does not exhibit behavior analogous to enhanced capillary breakup (i.e., named in this figure as column breakup) and it is characterized only by drop deformation regime prior to transition to the bag breakup regime. In addition, the secondary breakup of a drop responds to a greater degree to increasing *Oh* than liquid jet breakup for *Oh* > 0.3. For small *Oh* < 0.3, however, the transition to drop secondary breakup regimes becomes relatively independent of *Oh* number similar to liquid jet primary breakup. As is illustrated in Fig. 2-8, the secondary breakup of a drop has the following transitions: deformation (We_g < 13), bag breakup (13 < We_g < 35), multimode breakup (35 < We_g < 80), and shear breakup (80 < We_g). Overall, while the effect of *Oh* number on breakup regime transition was not considered in the earliest studies (see, e.g., Wu et al. [26], and Vich and Ledoux [47]), Mazallon

et al. [27] and Sallam et al. [28] remarked that the transition between various breakup regimes are not affected significantly by liquid viscosity for low viscous liquids (i.e., $Oh < 0.3$) and by liquid jet exit velocity (i.e., for $q < 8000$). They pointed out that an increased liquid stream velocity would stretch out the breakup process in the liquid jet streamwise and produces higher speed drops.

Following Mazallon et al. [27], Sallam et al. [28] reported a correlation between λ_s/d_j and breakup regimes, where λ_s is the wavelength of the longitudinal waves on the windward side. They observed column breakup for $\lambda_s/d_j > 1$, bag breakup for $\lambda_s/d_j \approx 1$, multimode region featuring surface stripping and column breakup for $0.1 < \lambda_s/d_j < 1$, and shear breakup for $\lambda_s/d_j \approx 0.1$, as shown in Fig. 2-9. This figure contains the data of Mazallon et al. [27] in addition to that of Sallam et al. [28]. Based on these results, Sallam et al. [28] proposed a correlation as follows: $\lambda_s/d_j = 3.4We_g^{-0.45}$; valid for $4 < We_g$, $Oh < 0.12$ and q in the range of 3 – 8000.

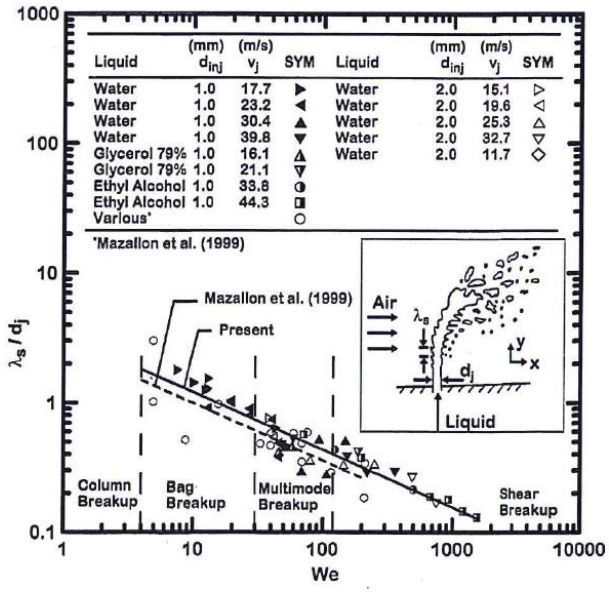

Figure 2-9: $We_g - (\lambda_s/d_j)$ regime map of the primary breakup process of a liquid jet in a crossflow. Reprinted from Ref. [28] with permission from AIAA.

Ng et al. [49] investigated experimentally one of the primary breakup regimes (bag breakup) of a non-turbulent liquid jet in a gaseous crossflow at room temperature and atmospheric pressure (STP). Similar to Mazallon et al. [27], they provided a $We_g - (\lambda_c/d_j)$ primary breakup regime map with specific We_g corresponding to the transition between different breakup regimes, as shown in Fig. 2-10. They, however, reconsidered the map and showed theoretically and experimentally that the wavelength of the column waves observed by Mazallon et al. [27] for the bag breakup regime has somewhat stronger dependence on We_g than in their case.

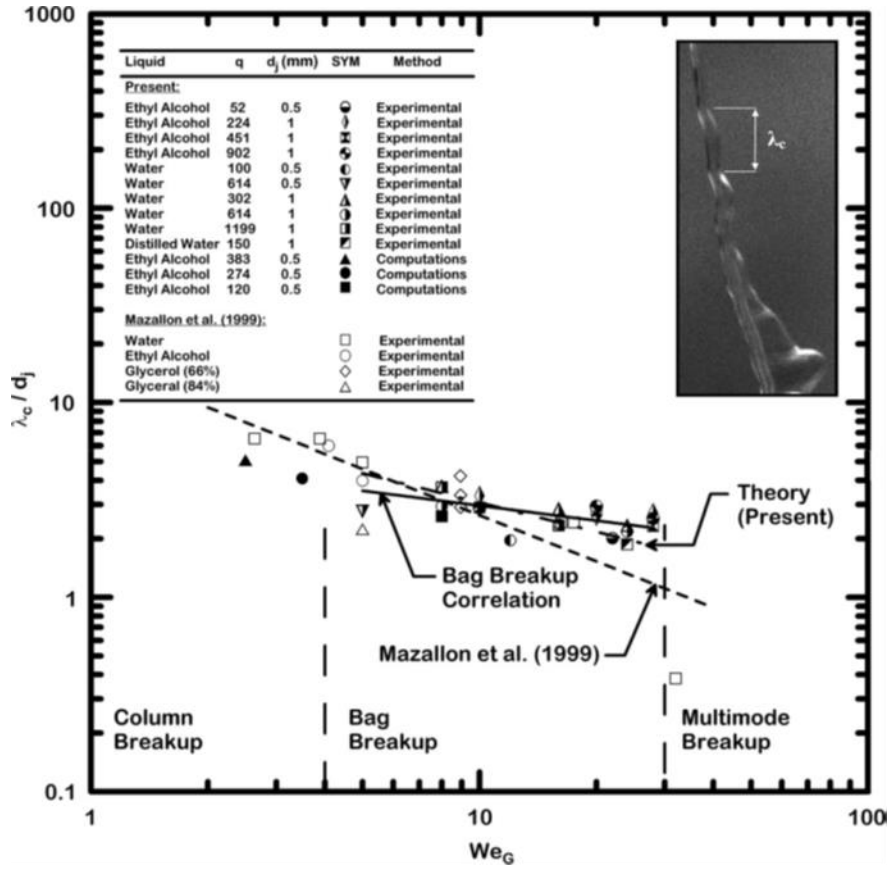

Figure 2-10: Liquid column wavelengths as a function of gas Weber number for non-turbulent liquid jet in a gaseous crossflow. Reprinted from [49] with permission from Elsevier.

At the same time, Madabhushi et al. [50] revisited the $We_g - q$ primary breakup regime map of a liquid jet in a subsonic gaseous crossflow using a number of datasets reported in the earlier studies and provided a $We_g - Re_j$ map. They plotted the breakup data from references [36,45] along with their data in terms of We_g and Re_j, as is illustrated in Fig. 2-11. From their analysis, they concluded that the surface breakup-dominated points have jet Reynolds numbers of approximately 5000 or higher (i.e., beyond the laminar to turbulent flow transition), whereas most of the column breakup dominated points fall below this line. Thus, the $Re_j = 5000$ line was taken as the transition between the surface and column breakup-dominated regimes.

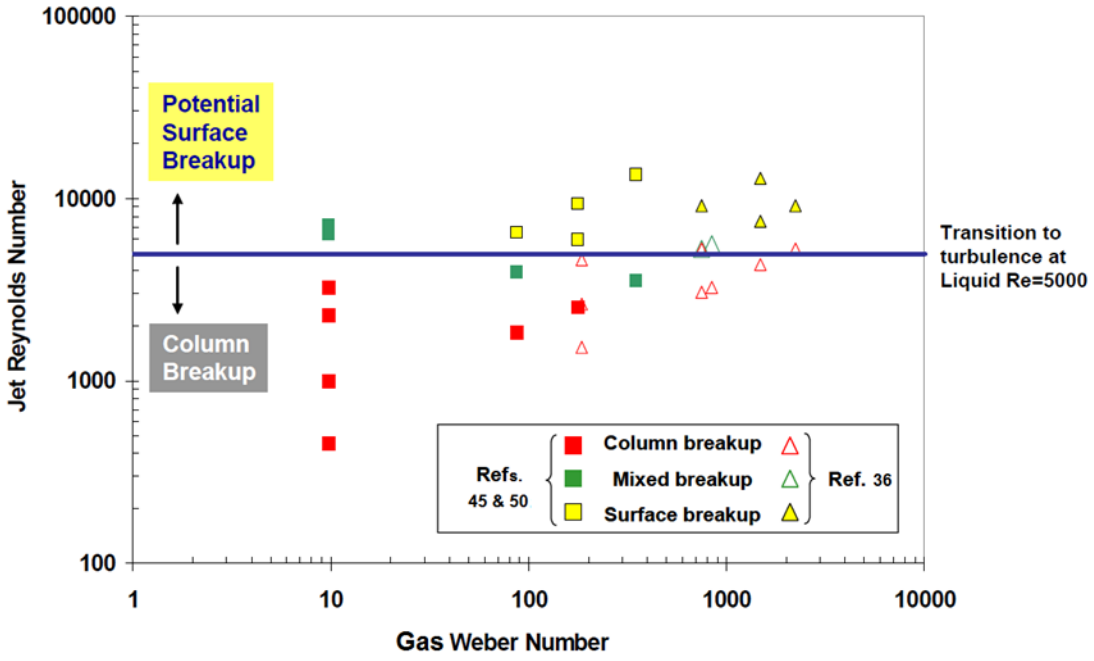

Figure 2-11: $We_g - Re_j$ primary breakup regime map for round liquid jet in gaseous crossflow [50].

To find the deformation and breakup properties of a non-turbulent liquid jet in a gaseous crossflow at conditions that are difficult to address using experiments (i.e., large Ohnesorge number where

liquid viscosity effect is important), Aalburg et al. [56] developed numerical predictions to find these properties. Their computational test conditions were set as follows: Re_g= 12.5 – 200, We_g= 0.1 – 100000, Oh = 0.001 – 100, liquid/gas density ratios of 2 – ∞, and liquid/gas molecular viscosity ratios of 0.001 – 1000. Aalburg et al. [56] suggested that the predicted normalized maximum deformation of 100% provided a reasonable estimate of conditions required for the onset of breakup. Using the classical $Oh - We_g$ coordinates of Hinze [52], they provided a liquid jet breakup regime map. Aalburg et al. [56] remarked that liquid/gas density ratio has a little effect on the deformation and breakup regime boundaries of a non-turbulent liquid jet in a gaseous crossflow for $\rho_j/\rho_g > 30$, and particularly when Oh is small. They also demonstrated that there was a significant increase of the resistance of a liquid jet to deformation when gas Reynolds number approached small values typically of the order of Stokes flow regime. They also found that at large Ohnesorge number, where liquid viscosity effect is more important than that of surface tension, jet deformation is controlled by a new dimensionless number $We_g{}^{1/2}/Oh$. Consequently, they constructed a breakup regime map for large Oh jet using the drag/liquid viscous forces ratio $We_g{}^{1/2}/Oh$ and surface tension force/liquid viscous forces $1/Oh$ as the map coordinates, as shown in Fig. 2-12.

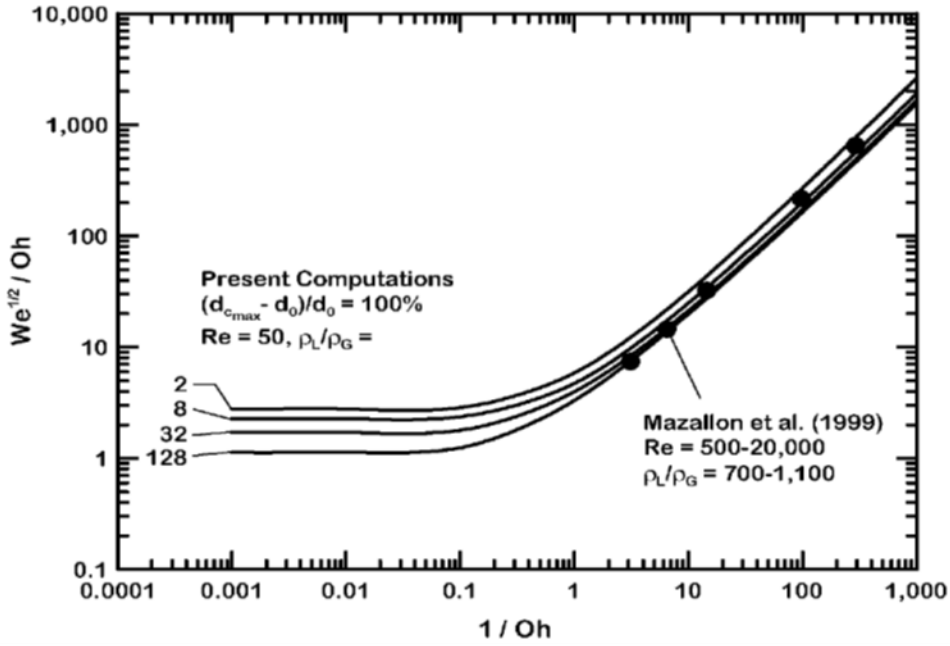

Figure 2-12: Measured and predicted regime map of primary breakup of a non-turbulent liquid jet in a crossflow based on $We_g{}^{1/2}/Oh$ and $1/Oh$ coordinates [56].

As is illustrated in Fig. 2-12, Aalburg et al. [56] remarked that, for $Oh < 1$, the measured and predicted deformation and breakup regime transitions are independent of *Oh* and can be identified through We_g, which is in agreement with previous observations (see, e.g., Wu et al. [26], Mazallon et al. [27], or Sallam et al. [28]). In contrast, for $Oh \gg 1$, their predictions indicated that $We_g \sim Oh^2$.

2.3.2. Primary breakup of turbulent liquid jet

The effect of liquid jet turbulence on the primary breakup regimes of a round liquid jet in a subsonic gaseous crossflow is reviewed in this section. Drops formation along the surface of a turbulent liquid jet, called turbulent primary breakup, is a common mechanism of spray formation

in practical combustion devices. It is worth mentioning that the contraction of a nozzle/injector must be followed by a long orifice length/diameter ratio passage to yield a fully developed turbulent pipe flow for sufficiently large liquid jet Reynolds numbers [42]. There exist several published maps for classifying the primary breakup regimes of a turbulent liquid jet in a subsonic gaseous crossflow, which include $T_b - \theta$ (e.g., [57]), $Re_j - We_{L\Lambda}q^{1/3}$ (e.g., [58]) and $We_g - We_{L\Lambda}q^{1/n}$ map (e.g., [59,60]).

One of the first attempt to classify the primary breakup regimes of a turbulent liquid jet at STP test conditions was conducted by Fuller et al. [57]. They provided a breakup regime map that divided the column breakup process into two distinct regimes: aerodynamic regime (i.e., column fracture as a result of aerodynamic forces associated with the gaseous crossflow) and non-aerodynamic regime (i.e., column fracture resulting from the instability generated by liquid turbulence and liquid inertial forces). The transition criterion between aerodynamic and non-aerodynamic breakup T_b was found equal to unity, where $T_b = 1.52\left[v_j/\left(u_g - v_j cos\theta\right)\right]\left(\rho_j/\rho_g\right)^{0.5} We_j^{-1/3}$ was defined as the ratio of the aerodynamic to non-aerodynamic breakup timescale. As is illustrated in Fig. 2-13, for $T_b < 1$, column breakup is largely dominated by aerodynamic forces; however, surface waves become more complex and the atomization process is enhanced as T_b is decreased. On the other hand, for $T_b > 1$, column breakup is largely dominated by nonaerodynamic forces; however, the liquid column becomes very straight and the atomization process is inhibited as T_b is increased. To consider the effect of injection angle on the breakup process of a turbulent liquid jet in a subsonic gaseous crossflow, Fuller et al. [57] conducted an experimental investigation with water as the test liquid where 30, 45, 60, 75, and 90 degrees injection angles (θ) were tested. Although Fuller et al. [57] considered the effect of the injection angle on the breakup properties of

a turbulent liquid jet, they did not provide much information about the effect of liquid turbulence on the breakup properties of a transverse liquid jet.

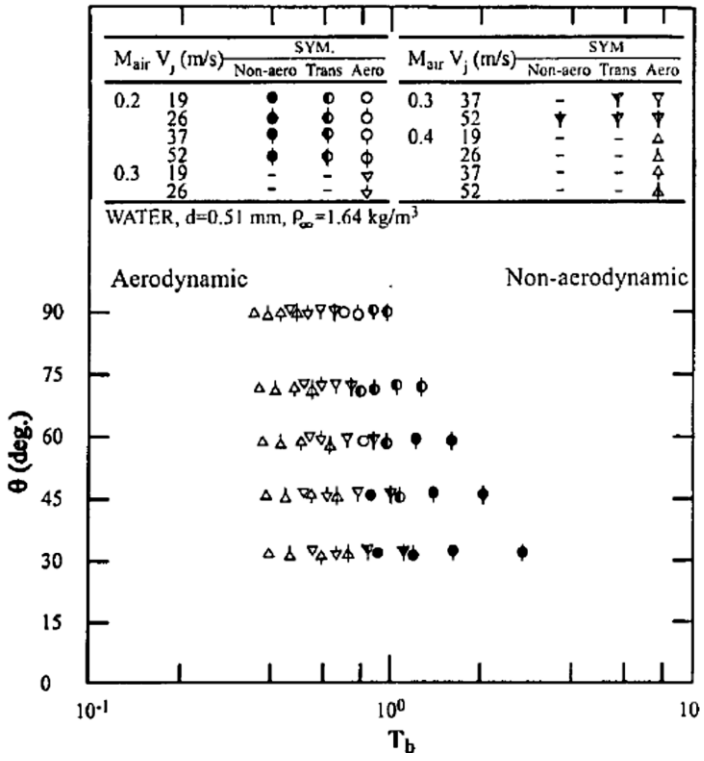

Figure 2-13: Turbulent primary breakup regime map of column breakup properties as a function of T_b and injection angle θ [57].

Aalburg et al. [61] investigated experimentally the deformation and breakup properties of a turbulent liquid jet in a gaseous crossflow at STP test conditions. Following the earlier phenomenological analyses of Wu and Faeth [62], they provided conditions for the aerodynamically-enhanced streamwise location of the onset of turbulent primary breakup along the liquid surface as a function of a new Weber number based on jet exit radial (i.e., crosstream) integral length scale as follows: $We_{L\Lambda} \equiv \rho_j v_j^2 \Lambda/\sigma$, where $\Lambda = d_j/8$. They reported that the onset of turbulent primary breakup always occurred at some distance from the jet exit, and nearing

atomization breakup conditions at large $We_{L\Lambda}$. They also concluded that, within the range of their test conditions, turbulent primary breakup dominated aerodynamic effect so that crossflow did not exert any influence on the ligament properties. They justified this process using the observations of Wu and Faeth [62] who found negligible aerodynamic effect for a density ratio of $\rho_j/\rho_g > 500$ for a liquid jet in quiescent gas. Thus, they suggested larger crossflow velocities and smaller ρ_j/ρ_g ratio should be considered in order to effectively examine the effect of aerodynamic forces. Sankarakrishnan et al. [63] extended the measurements of Aalburg et al. [61] in order to address the effect of the degree of turbulence development in the fluid (i.e., partially or fully developed turbulence) using a pipe having a diameter of 2.0 and 4.0 mm with a length/diameter ratio greater than 40 in order to achieve a fully developed turbulent pipe flow. They reported four regimes of the primary breakup at low jet exit Reynolds number similar to the breakup of non-turbulent breakup regimes. They, therefore, suggested that there is an analogy between the primary breakup of a weakly turbulent round liquid jet in a crossflow and the secondary breakup of a drop. At high jet exit Reynolds number, however, they remarked that turbulent primary breakup dominated the surface breakup mechanism even on the upstream side of a spray, suggesting weak aerodynamic effect on a fully-developed turbulent liquid jet. It should be noted that Sankarakrishnan et al. [63] did not define the transition criterion between a weakly-turbulent and fully turbulent breakup regime. However, they provided the onset of turbulent primary breakup time t_i as a function of viscosity ratio and We_g.

Following the study of Sankarakrishnan et al.[63], Sallam et al. [58] conducted an experimental and computational investigation on the turbulent primary breakup of a round liquid jet in a gaseous crossflow. Round nozzles with longue length/diameter ratio (> 40) were used to generate fully developed turbulent pipe flow at the nozzle exit. Consistent with the observations of

Sankarakrishnan et al. [63], they reported that, at low Re_j when We_g was kept constant, breakup regimes were similar to those of a non-turbulent liquid jet in a crossflow (bag breakup according to images (a) and (b) in Fig. 2-14). At high Re_j, no bags where observed where the breakup was characterized by irregularities on the jet surface which increased downstream of the jet exit and consequently led to the formation of ligaments and drops (i.e., see images (c), (d) and (e) in Fig. 2-14). No difference is observed in the breakup mechanisms among the different liquids shown in Figs. 2-14 (c), (d) and (e). This is because these images are captured at atmospheric/room temperature closer to the nozzle exit. However, at elevated temperature, ethanol evaporates faster than water and consequently would exhibit different jet characteristics particularly in the far-field region [64].

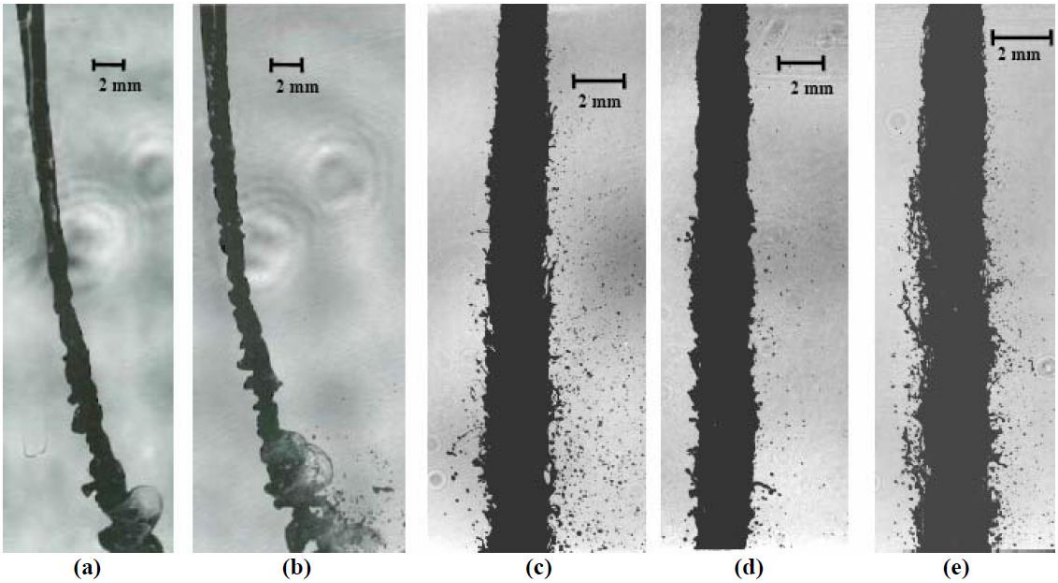

Figure 2-14: Flow visualization showing effect of Re_j on bag breakup regime We_g=16 and d_j=2.0 mm by Sallam et al.[58]. (a) Glycerol, Re_j=3,420, (b) Water, Re_j=19,000, (c) Ethanol, Re_j=40,000, (d) Water, Re_j=90,000, (e) Water, Re_j=140,000.

Sallam et al. [58], therefore, classified the breakup of a fully turbulent liquid jet in a gaseous crossflow into two major regimes known as aerodynamic breakup regime (including column, bag, multimode, and shear breakup, which is similar in appearance to the breakup of a non-turbulent liquid jet in a crossflow), and turbulent breakup regime (which is characterized by the appearance of ligaments and drops at the upwind surface and an increased jet column diameter with increasing distance from the jet exit). These two regimes were separated by Weber number based on jet exit radial (crosstream) integral length scale as follows: $We_{L\Lambda}q^{1/3} = 17000$, as shown in Fig. 2-15.

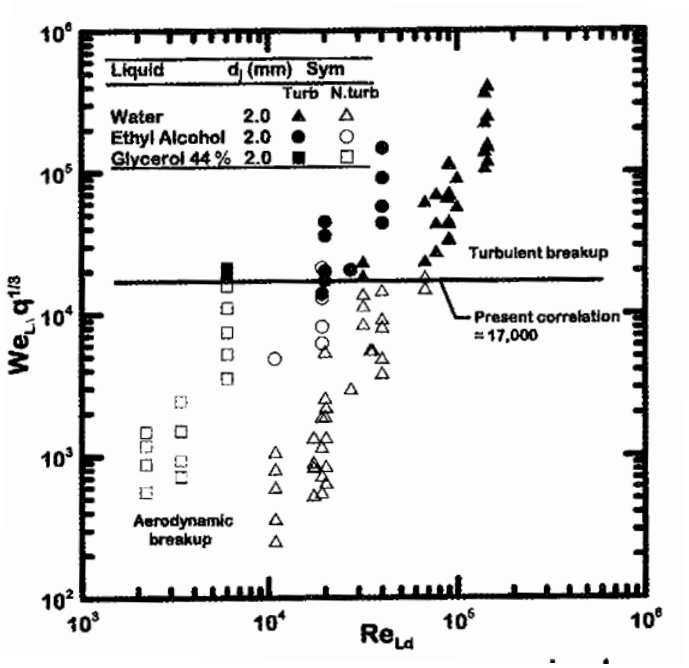

Figure 2-15: Turbulent primary breakup regime map based on Re_j and $We_{L\Lambda}q^{1/3}$ [58].

As is illustrated in Fig. 2-15, both turbulent and aerodynamic breakup occured in the range of jet Reynolds number Re_j = 6,000 – 60,000, with the transition controlled by $We_{L\Lambda}q^{1/3}$. However, only aerodynamic breakup occurred for Re_j < 6000, and only turbulent breakup is observed for $Re_j >$ 60,000.

Lee et al. [65] investigated the deformation and breakup properties of a turbulent liquid jet in a gaseous crossflow. They employed nearly the same test conditions, liquid properties, and injector geometry as those of Aalburg et al. [61]. Lee et al. [65] reported that a turbulent liquid jet did not exhibit the same behavior as a non-turbulent jet, which is in contrast with the observations of Sankarakrishnan et al. [63] especially at low jet exit Reynolds number. For instance, the We_g associated with images (a) and (b) in Fig. 2-16 correspondent to bag or multimode breakup regime for a non-turbulent liquid jet; however, these images reveal that the jet exhibits a behavior like shear breakup regime (i.e., identified by the presence of ligaments and absence of liquid bags). Lee et al. [65] represented liquid turbulence via using liquid Weber number We_j. As is displayed in Fig. 2-16, they observed that the increase in liquid turbulence (Fig. 2-16a to Fig. 2-16b) enhanced the formation of ligaments and subsequently drops which then accelerated the onset of breakup. The effect of crossflow on promoting the formation of ligaments and drops can be noticed in Figs. 2-16b to 2-16d.

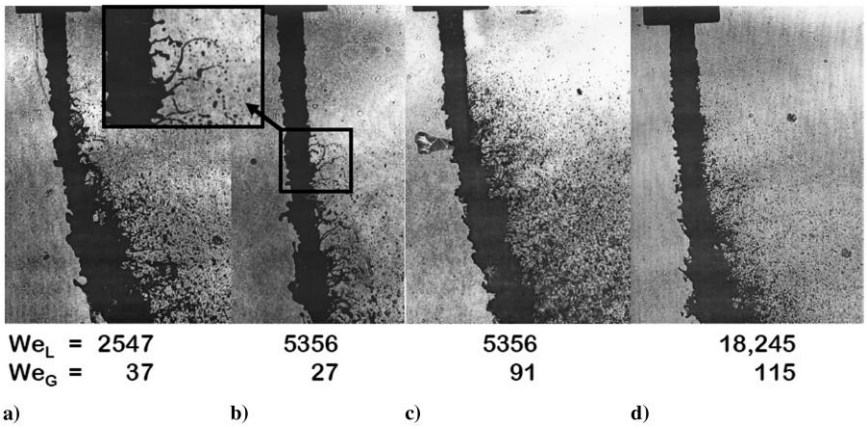

Figure 2-16: Pulsed shadowgraphy images of a-c) round water and d) alcohol jet in air crossflow. The zoomed zone illustrates the formation of ligaments and drops due to Rayleigh breakup. Reprinted from Ref. [65] with permission from AIAA.

Similar to Aalburg et al. [61], Lee et al. [65], following the earlier phenomenological analyses of Wu and Faeth [62], provided conditions for the onset of turbulent primary breakup along the liquid surface as a function of $We_{L\Lambda}$, allowing for aerodynamic enhancement of the breakup process due to the presence of crossflow.

Inspired by earlier studies of the effect of nozzle length/diameter on liquid jet instabilities in quiescent air (see, e.g., [53, 60]), and following the study of Sallam et al. [58] on turbulent primary breakup, Osta et al. [59,60] conducted an experimental study to examine the effect of nozzle length/diameter ratio on the transition criterion of a turbulent liquid jet. Straight nozzles with length/diameter ratios of 10, 20, and 40 were used to generate turbulent liquid jet in a gaseous crossflow at STP test conditions. Similar to Sallam et al. [58], Osta et al. [59,60] used the formation of ligaments on the upstream surface of a turbulent liquid jet in a crossflow to classify the breakup-regime map into two major regimes known as aerodynamic and turbulent breakup regime. They concluded that: i) the breakup length of a turbulent liquid jet in a crossflow decreases with increasing the injector length/diameter ratio which is probably due to increased turbulence level induced by the longer orifice passage, and ii) a liquid jet issued from a longer injector passage tends to have earlier transition to turbulent primary breakup. Osta et al. [60] represented the transition borderline between the aerodynamic and turbulent primary breakup of a liquid jet in a gaseous crossflow using a non-dimensional parameter $We_{L\Lambda}q^{1/n}$ where $n = 2, 3$ and 5. Consistent with the observations of Sallam et al. [58], they concluded that a $We_{L\Lambda}q^{1/3} = 17000$ represents appropriately the boundary between aerodynamic and turbulent breakup regime in We_g-$We_{L\Lambda}q^{1/n}$ map regardless of the injector length/diameter ratio.

Recently, Zheng and Marshall [67] conducted an experimental study to investigate the primary breakup regimes of a round liquid (water) jet in an air crossflow at low ranges of q = 10 - 50

and We_g = 4 - 16 at standard/room temperature and pressure (STP) conditions. They provided a $We_g - q$ regime map and reported two breakup regimes: capillary enhanced breakup (named column breakup) and bag breakup. They concluded that the transition between these two breakup modes occurs for We_g= 8 - 12. They also mentioned that for $q > 40$, this transition happened earlier and was attributed to the fact that liquid jet breakup would be facilitated/promoted at higher q. Nonetheless, they did not explore the transition borderline between the aerodynamic and turbulent breakup regime.

Eslamian et al. [30] experimentally studied the effect of elevated temperature and pressure (HTP; ranged between 298 - 573 K and 207 - 517 kPa, respectively) of a subsonic air crossflow on the primary breakup regimes of a transversally injected water jet. Eslamian et al. [30] employed a $We_g - q$ breakup regime map similar to the map of a non-turbulent liquid jet. They concluded that, at both elevated temperature and pressure (HTP) conditions, the surface breakup mode was initiated at lower q and We_g in comparison with the transition borderline of Becker and Hassa [36], who also examined the effect of crossflow pressure but at room temperature (STP) conditions. Moreover, Eslamian et al. [30] showed that the surface breakup mode was initiated at lower q and We_g, which is in contrast with the findings of Song et al. [46] who studied the breakup of a non-turbulent liquid jet in a crossflow at elevated pressures and stated that the transition borderline between the column and surface breakup shifted towards higher q and We_g when increasing cross airflow pressure.

2.3.3. Concluding remarks on liquid jet primary breakup

Given the results available thus far concerning the primary breakup regimes of a non-turbulent liquid jet in a subsonic gaseous crossflow, the identified regimes seem to be independent of q,

We_j, Oh and other non-dimensional parameters except We_g. Published We_g corresponding to the transition of various breakup regimes are summarized in Table 2-1 below.

Table 2-1: Summary of the We_g corresponding to the primary breakup transition of a non-turbulent liquid jet in a gaseous crossflow

Breakup regime\References	Zheng & Marshall [67]*	Sallam et al. [28]	Birouk et al. [48]	Mazallon et al. [27]	Vich & Ledoux [47]	Wu et al. [26]	Hsiang & Faeth [55]**
Capillary/bag breakup	8-12	4	3-9	5	1.5-8	11	13
Bag/multimode breakup	-	30	-	60	-	30	35
Multimode/shear breakup	-	110	-	110	-	90	80

* Although turbulent jet was studied, the examined range of Re_j = 2000 – 8000 was relatively low

**Secondary breakup regime of drops for comparison

As is shown in Table 1, it is interesting to notice that Wu et al. [26] reported similar liquid jet primary breakup regimes and transition Weber number, We_g, to those reported by Hsiang and Faeth [55] for the secondary breakup of drops. Vich and Ledoux [47] found that We_g for the transition to bag breakup ranges between 1.5 and 8 (that is, an average of $We_g \sim 5$), while Birouk et al. [48] found an average value of We_g = 6, which is in agreement with the finding of Mazallon et al. [27] and Sallam et al. [28]. Zheng and Marshall [67], however, reported larger We_g (with an average value of 10) for the transition to bag breakup, which might be due to the fact that they used a larger length/diameter ratio nozzle (L/d = 20) which generates a fully developed turbulent jet (though their range of Re_j = 2000 – 8000), or could be a result of using a protruding nozzle to inject liquid at 20 mm away from the nozzle-wall in order to eliminate the effect of non-uniform velocity field in the gas boundary layer along the test section. We_g found by Mazallon et al. [27] and Sallam et al. [28] are in excellent agreement for the capillary (column)/bag and multimode/shear breakup regime transitions. There is, however, a great difference in the bag/multimode breakup regime transition between Mazallon et al. [27] and Sallam et al. [28],

whereas those of Sallam et al. [28] and Wu et al. [26] are in excellent agreement. It is worth mentioning that completely different breakup regimes are observed when injecting a liquid jet into a quiescent gaseous medium [24,68]. These regimes can be categorized according to We_j and We_g (where We_g is based on liquid jet velocity) as: (a) Rayleigh breakup (for $We_j > 8$ and $We_g < 0.4$), (b) first wind-induced regime (for $0.4 < We_g < 13$), (c) second wind-induced regime (for $13 < We_g < 40$), and (d) atomization regime (for $We_g > 40$). The capillary and bag breakup mechanisms of a transverse liquid jet resembles the first two (i.e., Rayleigh and first wind-induced) breakup mechanisms of a liquid jet injected into quiescent gaseous medium, where long-wavelength surface disturbances along with large disintegrated droplets are observed. Multimode and shear breakup mechanisms of a transverse liquid jet are also similar to the second wind-induced and atomization regimes of a liquid jet injected into quiescent gas, where short-wavelength waves and smaller droplets are produced.

On the other hand, there is still no consensus about the criterion concerning the other breakup classification of non-turbulent liquid jet (i.e., transition from column to surface breakup regime). Given the fact that this transition is gradual and comprises an overlap region for both breakup mechanisms, several studies (e.g., Wu et al. [26] and Madabhushi et al. [50]) quoted that the exact boundaries of this transition region in a $We_g - q$ regime map is difficult to pinpoint. In fact, some studies defined a region while others gave a borderline between these two breakup regimes (i.e., column and surface breakup regime). Some remarked a stronger dependency [43,45,46,50], and others weaker We_g dependency [41,44] of the transition region compared to the observations of Wu et al. [26]. Some studies, such as [30,41,44], suggested that the transition region from column to surface dominated breakup occurs at lower q and We_g, while some, such as [46], found it to happen at higher q and We_g compared to the observations of Wu et al. [26]. Published data on

these transition regions and borderlines, in a $We_g - q$ map, which indicates the transition between column/surface breakup regime at room and elevated test conditions, is gathered and depicted in Fig. 2-17.

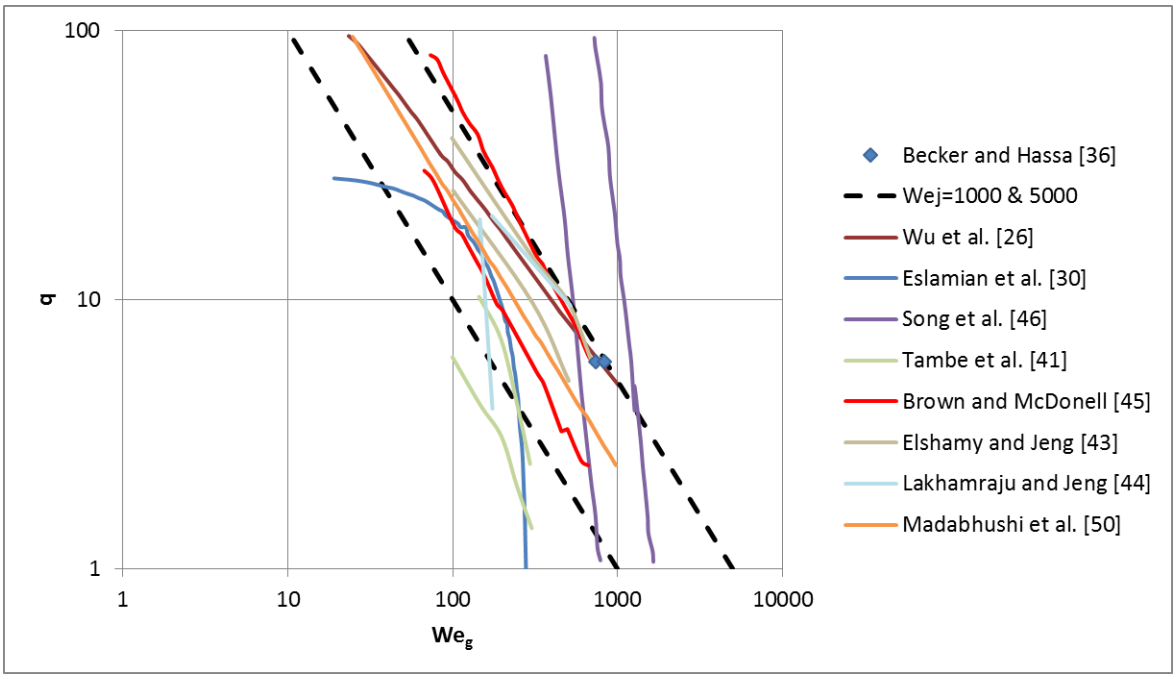

Figure 2-17: Column/surface breakup transition regions and borderlines of a liquid jet in a gaseous crossflow.

As is illustrated in Fig. 2-17, the majority of the predicted transition regions and borderlines can be located between the two dashed lines which correlate We_g with q as follows: $We_g = 10^{[k-\log(q)]}$, where $k \cong 3 - 3.7$. By doing some mathematical manipulations, the following expression can be obtained: $qWe_g \equiv We_j = 10^k$, which suggests that $We_j \cong 1000 - 5000$ (with an average $We_j \cong 3000$) as an appropriate region which describes the column/surface breakup transition region for a liquid jet in a subsonic gaseous crossflow at room (STP) and elevated (HTP) test conditions.

As for the transition criterion for turbulent breakup of a liquid jet in a gaseous crossflow, according to the observations of Sallam et al. [58], and Osta et al. [60], this relationship $We_{L\Lambda}q^{1/3}$ = 17,000 represents the transition borderline between the aerodynamic/turbulent primary breakup regimes. Since $We_{L\Lambda} \equiv (\Lambda/d_j)We_j$ with $\Lambda = d_j/8$ and $We_j \equiv qWe_g$, the criterion can be expressed as $q^{4/3}We_g = 272{,}000$. This correlation can also be rewritten as $We_g = 10^{[5.43-(4/3)\log(q)]}$. The straight/solid line of this correlation is depicted in a $We_g - q$ map in Fig. 2-18 by considering the range of We_g used by Sallam et al. [58] and Osta et al. [60].

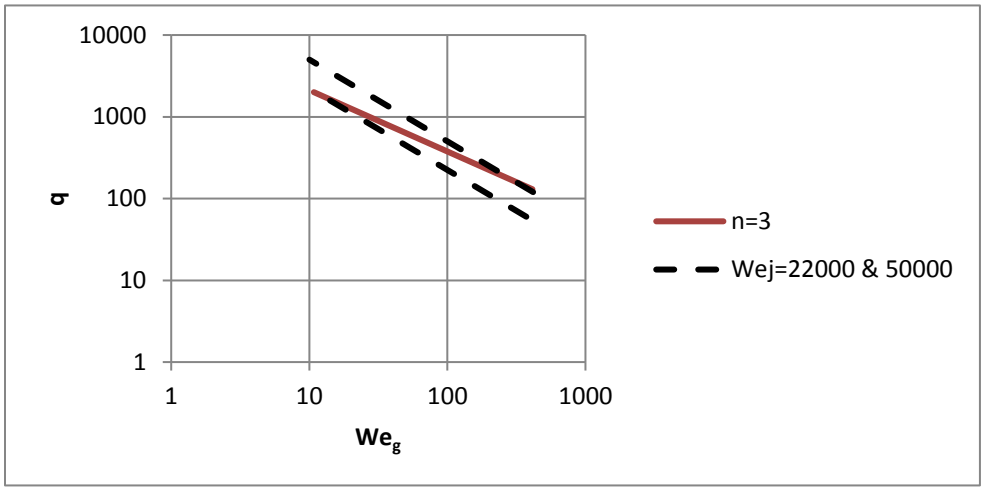

Figure 2-18: Aerodynamic/turbulent breakup transition borderline of a liquid jet in a gaseous crossflow as defined by Sallam et al. [58], and Osta et al. [60].

As is shown in Fig. 2-18, the predicted transition borderline can be located between the two dashed lines which correlate We_g with q as follows: $We_g = 10^{[m-\log(q)]}$, where $m \cong 4.35$ and 4.7. By doing the same mathematical manipulations as for the non-turbulent liquid jet above, the following relationship can obtained: $qWe_g \equiv We_j = 10^k$, which suggests $We_j \cong 22{,}000 - 50{,}000$ (with an average value of $We_j \cong 35{,}000$) as an appropriate boundary to predict the

aerodynamic/turbulent breakup transition region for a liquid jet in a subsonic gaseous crossflow. It should be mentioned that, contrary to the non-turbulent breakup regimes that seem to be well established for different test conditions, all the experiments on the turbulent primary breakup have been conducted at STP test conditions. Hence, more investigations on the effect of high temperature and pressure (HTP) on the primary breakup regimes of a turbulent liquid jet are needed.

The effect of non-dimensional parameters, such as We_j and We_g, on liquid jet instabilities and surface waves along the liquid column seems to be required, as they play a key role on the primary breakup and size of ligaments and drops. On this issue, there is still a controversy amongst published experimental results and the data of high fidelity simulations. As was illustrated in Fig. 2-9, following Mazallon et al. [27], Sallam et al. [28] measured experimentally the characteristic length scale of the KH-like instabilities along the trajectory of a non-turbulent liquid jet and proposed a scaling law of the form $\lambda/d = C_1 {We_g}^{-0.45}$ for $We_g > 4$, where λ is the wavelength of the disturbance and C_1 is a constant. Ng et al. [69] confirmed their experimental observations by using a Volume Of Fluid (VOF) simulation approach. In contrast, for constant We_j, Pai et al. [70] employed a spectrally refined interface tracking technique and predicted a wavelength that is almost constant across their explored range of We_g, which does not appear to agree with the experimental results of Sallam et al. [28] for multimode breakup regime. Sedarsky et al. [71] reported that the correlation of Sallam et al. [28] did not hold for their experimental data. Li and Soteriou [72] used a Coupled Level Set and Volume Of Fluid (CLSVOF) simulation technique and indicated that while their predictions of the surface wavelengths matched well with the empirical correlation of Sallam et al. [28] for low gas Weber numbers, their predictions could not be compared with the empirical correlation at high gas Weber number due to the fact that two-

dimensional traveling waves were not accounted for in their simulation. On the other hand, Xiao et al. [73] adopted the same approach (i.e., CLSVOF) and indicated that their simulated surface wavelengths at different gas Weber numbers agreed well with the experimental measurements of Sallam et al. [28]. Farvardin et al. [74] conducted a series of experimental tests using biodiesel and diesel as well as their blends and confirmed the trend of the changes of surface wavelength observed by Sallam et al. [28]. Wang et al. [75] theoretically investigated the surface waves of a round liquid jet in a gaseous crossflow utilizing linear stability analysis, and reported the same trend of wavelength changes as Mazallon et al. [27] and Sallam et al. [58]. Hence, more investigations on the wavelength of the disturbances and their connections to the primary breakup regimes of both turbulent and non-turbulent liquid jets at different test conditions (standard and high test conditions) are required.

2.4. Liquid jet trajectory and penetration

Liquid jet trajectory and its penetration in a gaseous crossflow are among the most important features of a transverse liquid jet as they have direct impact on the distribution of the fuel spray in a combustion chamber, and accordingly its evaporation and mixing rate with oxidant. This is also important for the design of a combustor as to prevent spray impingement onto its walls. Jet trajectory and its penetration refer, respectively, to the trajectory up to the column breakup point (i.e., the solid line in Fig. 2-2), and to the liquid maximum penetration into a crossflow (i.e., the dashed line in Fig. 2-2). Numerous empirical and phenomenological correlations for predicting the trajectory and penetration of a liquid jet injected into a gaseous crossflow were proposed in the literature. These correlations were expressed in terms of non-dimensional parameters; such as q, Re_j, Re_g, We_g, We_j, viscosity ratio and density ratio. These correlations, however, show

considerable scatter (see, e.g., [37,45,76]). These discrepancies originate from the complex physics of this two-phase flowfield as liquid jet trajectory and its penetration dependent on a number of variables including liquid properties (e.g., density, viscosity, surface tension), test conditions (e.g., temperature and pressure of crossflow), internal geometry of the nozzle (e.g., discharge coefficient of nozzle and cavitation), and measurement methods (e.g., shadowgraphy, Mie scattering, or phase Doppler anemometry (PDPA)). Inconsistencies in the definition of spray boundaries is another reason of these differences, as Herrmann et al. [77] stated that the commonly reported liquid jet penetration correlations for the windward side trajectory dependent strongly on the threshold being used to identify the leading edge. Given the variety of the aforementioned factors it may not be possible to resolve these discrepancies completely. However, it might be possible to narrow the gap provided that these correlations are categorized based on proper test conditions (e.g., liquid properties, liquid jet and cross airflow characteristics). These correlations may also be classified according to their mathematical functional form such as power-law, logarithmic or exponential form. They could also be further categorized based on whether they are applicable just to a specific region, near- or far-field, or cover both regions such as multi zone correlations, or whether they predict the upper or lower boundaries of a spray. Liquid jet trajectory can also be grouped according to the primary breakup regimes (bag, multimode and shear breakup regimes), as the deformation of a liquid jet depends on the breakup regime [28]. While most of published studies were carried out at standard temperature and pressure (STP) conditions, still several studies were conducted at elevated crossflow temperature and pressure (HTP). In fact, a change in test conditions can lead to a change in both liquid and gas properties, which in turn affect the trajectory and penetration of a transverse liquid jet in a crossflow.

2.4.1. Standard temperature and pressure (STP) conditions

There were numerous published studies which investigated the injection of a liquid jet into a subsonic gaseous crossflow at standard temperature and pressure (STP) test conditions [26,31,41,43,45,67,74,78–88]. These studies correlated liquid jet trajectory mostly in terms of x/d_j and q. However, a few studies which used other liquids in addition to water included the viscosity ratio and We_g to take into account liquid properties in order to make their correlations comprehensive. These published correlations along with their range of test conditions are summarized in Table 2-2.

Table 2-2: Correlations of liquid jet trajectory in a subsonic gaseous crossflow at STP test conditions

Correlations	q	We_g	x/d_j	Reference
$z/d_j = 1.37q^{0.5}(x/d_j)^{0.5}$	3.4-185	57-1180	0-12	Wu et al. [26]
$z/d_j = 4.3q^{0.33}(x/d_j)^{0.33}$	4.9-48.8	55-647	50-500	Wu et al. [78]
$z/d_j = 3.17q^{0.33}(x/d_j)^{0.4}$	0.5-12	40-475	0-200	Lin et al. (PDPA) [79]
$z/d_j = 2.42q^{0.48}(x/d_j)^{0.24}$	2-40	40-475	0-90	Lin et al. (Shadowgraph) [79]
$z/d_j = 2.898q^{0.43}(x/d_j)^{0.384}We_g^{-0.11}(\mu_j/\mu_w)^{-0.108}$	18-36	1.3-106.2	0-100	Stenzler et al. [80]
$z/d_j = 5.38q^{0.467}(x/d_j)^{0.281}We_g^{-0.119}$	1.95-71.23	97.83-905.34	0-45	Elshamy and Jeng [43]
$z/d_j = 1.55\ln(1.66(x/d_j)+1)q^{0.53}$	0.7-10.2	50.5-1725.1	0-30	Tambe et al. [41]
$z/d_j = 1.297q^{0.491}(x/d_j)^{0.509}$	23	<60	0-12	Ahn et al. [81]
$z/d_j = 2.45q^{0.5}(x/d_j)^{0.33}We_g^{-0.061}$	0.8-22	97-573	0-30	Brown and McDonell [45]
$z/d_j = 1.997q^{0.444}(x/d_j)^{0.444}$	8.3-726	9.3-159	0-63.5	Iyogun et al. [82]
$z/d_j = 3.688q^{0.43}(x/d_j)^{0.384}We_g^{-0.11}(\mu_j/\mu_w)^{-0.108}$	9-18	0.9-164.3	0-100	Stenzler et al. [83]
$z/d_j = 1.627q^{0.47}(x/d_j)^{0.46}(\mu_j/\mu_w)^{0.079}$	8.3-726	9.3-159	0-40	Birouk et al. [84]
$z/d_j = 1.52\left(\frac{q}{(0.84)^2}\right)^{0.5}(x/d_j)^{0.33}$	11-37	84.7-665	0-50	Brown et al. [85]
$z/d_j = (1.46ln(x/d_j) + 3.3)q^{0.5}We_g^{-0.05}$	1-54	9-345	0-10	Thawley et al. [86]
$z/d_j = (1.46ln(x/d_j) + 1.5)q^{0.5}We_g^{-0.05}$	1-54	9-345	0-10	Wang et al. [87]
$z/d_j = 2.39q^{0.46}(x/d_j)^{0.6}We_g^{-0.2}$	10-50	4-16	0-20	Zheng and Marshall [67]
$z/d_j = 2.291q^{0.417}(x/d_j)^{0.429}$	2.0-29.1	5.3-47.9	0-27	Yoon et al. [88]
$z/d_j = 3.688q^{0.43}(x/d_j)^{0.384}We_g^{-0.085}(\mu_j/\mu_w)^{-0.222}$	10-135	28-82	0-50	Farvardin et al. [74]
$z/d_j = 1.48q^{0.43}(x/d_j)^{0.43}$	38, 136	17, 145	0-70	Bolszo et al. [31]

These correlations are also plotted in Fig. 2-19 for typical $q = 20$ and $We_g = 100$, and water as liquid. Correlations used liquids other than water were not plotted in this figure because they did not include liquid viscosity in their expressions which is why their correlations [31,86,87] underpredict the trend shown in this figure. The correlation of Zheng and Marshall [67] is excluded as it was proposed for a narrow range of low We_g limited to the column and bag breakup regimes. Since Stenzler et al. [80,83] reported two correlations for nearly the same liquids and test conditions, only the recent one is plotted in this figure. Finally, only the correlation of Lin et al. [79] based on data obtained using PDPA technique was considered in this figure as the one found with shadowgraph technique showed significant departure from this general trend.

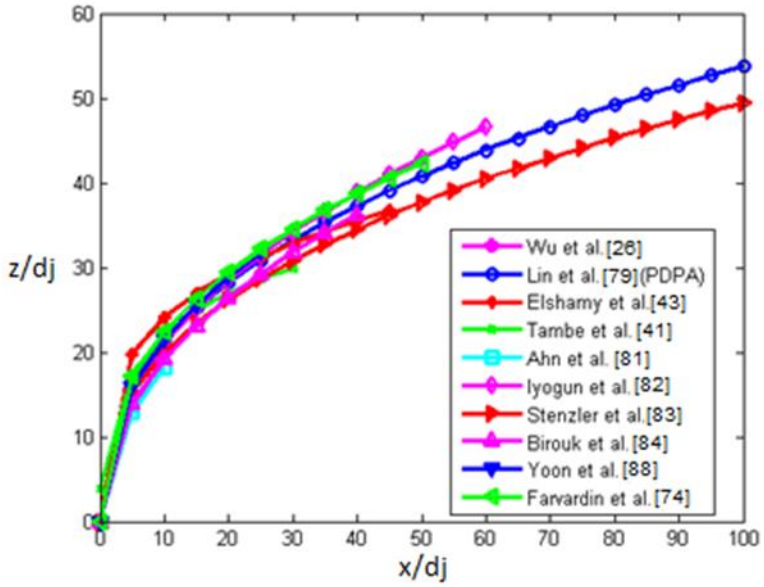

Figure 2-19: Water jet trajectory and penetration in a subsonic gaseous crossflow at STP test conditions for typical q = 20 and $We_g = 100$.

These correlations plotted in Fig. 2-19, using water as the liquid at STP test conditions, exhibit excellent agreement with an average difference of around $5d_j$ at different jet locations from the nozzle exit up to $x/d_j = 100$. The agreement among the predictions of these correlations remains rather similar at different q and We_g.

2.4.2. High temperature and pressure (HTP) conditions

There exist several studies specifically focused on liquid jet trajectory and penetration at high temperature and pressure (HTP) test conditions. To account for the effect of HTP test conditions, the proposed correlations included parameters such as temperature ratio, pressure ratio and density ratio in addition to x/d_j and q which were used for STP conditions as presented above. It would be useful to categorize published correlations at HTP test conditions into three subgroups: i) high temperature and standard pressure (HTSP); ii) standard temperature and high pressure (STHP); and iii) high temperature and high pressure test conditions (HTP). This is to facilitate understanding the effect of changing each parameter independently.

HTSP studies [44,80,83,88] examined the impact of increasing cross airflow temperature on liquid jet trajectory and its penetration. The correlations proposed along with their range of test conditions are summarized in Table 2-3.

Table 2-3: Correlations of a liquid jet trajectory in a subsonic gaseous crossflow at HTSP test conditions

Correlations	q	We_g	x/d_j	T(K)	Reference
$z/d_j = 2.630q^{0.442}(x/d_j)^{0.390}We_g{}^{-0.088}(\mu_j/\mu_w)^{-0.027}$	18-36	1.3-106.2	0-100	291-573	Stenzler et al. [80]
$z/d_j = 1.844\ln(1.324(x/d_j) + 1)q^{0.456}(T/T_o)^{-0.117}$	1-49.5	50.3-967.5	1-30	366.5-505.4	Lakhamraju and Jeng [44]
$z/d_j = 3.354q^{0.442}(x/d_j)^{0.391}We_g{}^{-0.088}(\mu_j/\mu_w)^{-0.027}$	9-18	0.9-164.3	0-100	291-573	Stenzler et al. [83]
$z/d_j = 2.241q^{0.402}(x/d_j)^{0.41}$	2-29.1	5.3-47.9	0-27	293, 500	Yoon et al. [88]

Stenzler et al. [80,83] reported that, at constant q and u_g, increasing temperature led to an increase in jet penetration. In fact, increasing temperature reduces gas density and thereby decreases We_g. This is why Stenzler et al. [80,83] adopted a negative exponent of We_g to reflect on this inverse relationship. At constant q, if We_g (or the gas inertial force $\rho_g u_g^2$) decreases then We_j (or the liquid jet inertial force $\rho_l v_j^2$) must also decrease proportionally. Thus, there must be another reason for the increase in jet penetration when the gas and liquid inertial forces are equally changed. The rate of mass shedding from droplets is directly proportional to ρ_g and u_g [89,90]. Thus, at constant u_g, the rate of mass shedding from droplets decreases with decreasing ρ_g leading to larger droplets. These larger droplets, which still possess greater momentum, penetrate farther into a crossflow. This is consistent with the numerical analysis of Herrmann et al. [77] who reported that the post-primary atomization spray penetrates farther in both directions of jet and transverse when increasing ρ_j/ρ_g (or decreasing ρ_g). Lakhamraju and Jeng [44] stated that, at constant q and We_g (and accordingly constant We_j), jet penetration decreases with increasing crossflow temperature. This is why their exponent of the temperature ratio is negative, which is an indication of the inverse relationship between jet penetration and temperature change. In fact, at constant q

and We_g, the gas inertial force $\rho_g u_g^2$ and the liquid jet inertial force $\rho_l v_j^2$ must be constant where an increase in temperature will lead to a decrease in ρ_g and hence increase in u_g. Since the exponent of ρ_g is smaller than that of u_g in the correlation of the rate of mass shedding [89,90], a decrease in ρ_g and an increase in u_g will lead to an increase in mass shedding, which results in smaller droplets and thereby less jet penetration. Yoon et al. [88] reported that increasing temperature had led to an increased jet penetration due to reduced gas density, which is consistent with Stenzler et al. [80,83]; however, increased crossflow velocity, u_g, led to decreased jet penetration, which is consistent with the findings of Lakhamraju and Jeng [44]. These correlations are plotted in Fig. 2-20 for typical $q = 20$, We_g= 50 and $T = 500$ K with water as the liquid.

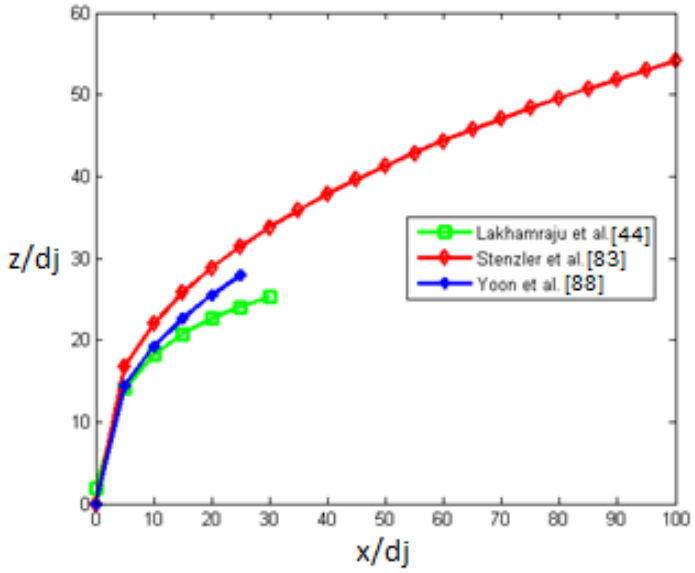

Figure 2-20: Water jet trajectory and penetration in a subsonic gaseous crossflow at HTSP test conditions for q = 20, We_g=50 and $T = 500$ K.

As is illustrated in Fig. 2-20, similar to the STP test conditions, the predicted trends for high temperature and standard pressure (HTSP) at these typical test conditions differ by an average of around $5d_j$ from the nozzle exit up to $x/d_j = 30$.

There exist some studies which investigated the effect of increasing the pressure at room temperature of a cross airflow on liquid jet trajectory and penetration [36,43,46,91–93]. The proposed correlations along with their range of test conditions are tabulated in Table 2-4 and plotted in Fig. 2-21.

Table 2-4: Correlations of a liquid jet trajectory in a subsonic gaseous crossflow at HTSP test conditions

Correlations	q	We_g	x/d_j	P(bar)	Reference
$z/d_j = 1.48\ln(3.56(x/d_j)+1)q^{0.42}$	1-40	90-2120	0-22	1.5-15	Becker and Hassa [36]
$z/d_j = 4.95q^{0.424}(x/d_j)^{0.279}We_g{}^{-0.076}(P/P_o)^{-0.05}$	2-71	98-905	0-45	1,5,7	Elshamy and Jeng [43]
$z/d_j = 2.698q^{0.441}(x/d_j)^{0.367}We_{aero}{}^{-0.069}$	5-200	We_{aero}= 8.1-444.8	0-12	10,20	Ragucci et al. [91]
$z/d_j = 1.6\ln(3.81(x/d_j)+1)q^{0.4}$	3-24	(1.2E+06) d_j- (2.3E+06) d_j	1.4-50	2-8	Freitag and Hassa [92]
$z/d_j = 1.8641\sqrt{q}\left[\frac{1}{(1+0.7403\,x/d_j)} + \ln(1+0.7403\,x/d_j)\right]$	5-100	400-1600	0-60	5	Lubarsky et al. [93]
$z/d_j = 1.163q^{0.557}(x/d_j)^{0.463}We_g{}^{0.111}(\rho_j/\rho_g)^{-0.0}(\mu_j/\mu_g)^{-0.086}$	5-25	250-1000	0-8	2.07-9.65	Song et al. [46]
$z/d_j = 4.391q^{0.556}(x/d_j)^{0.214}We_g{}^{-0.011}(\rho_j/\rho_g)^{-0.082}(\mu_j/\mu_g)^{-0.053}$			8-55		

Becker and Hassa [36] stated that small droplets were generated at high ambient pressure, which have little inertia, especially in a high gas density, and thus cannot penetrate very far as they were swept away by the air stream. Freitag and Hassa [92], consistent with Becker and Hassa [36], reported that the stepwise rise of static air pressure caused finer drops to form. Elshamy and Jeng [43] observed that, at constant q and We_g, jet penetration slightly decreased with increased crossflow pressure. In contrast, Song et al. [46] showed that, at constant q and We_g, spray penetrated farther when increasing ambient pressure. In fact, at constant q and We_g, both the airflow and liquid jet inertial force $\rho_g u_g^2$ and $\rho_l v_j^2$ must remain constant so that an increase in ρ_g caused by increasing pressure will lead to a decrease in u_g. Since the exponent of ρ_g is smaller than that of u_g in the correlation of the rate of mass shedding [89,90], an increase in ρ_g and a decrease in u_g will lead to a decrease in mass shedding which results in an increase in liquid jet penetration.

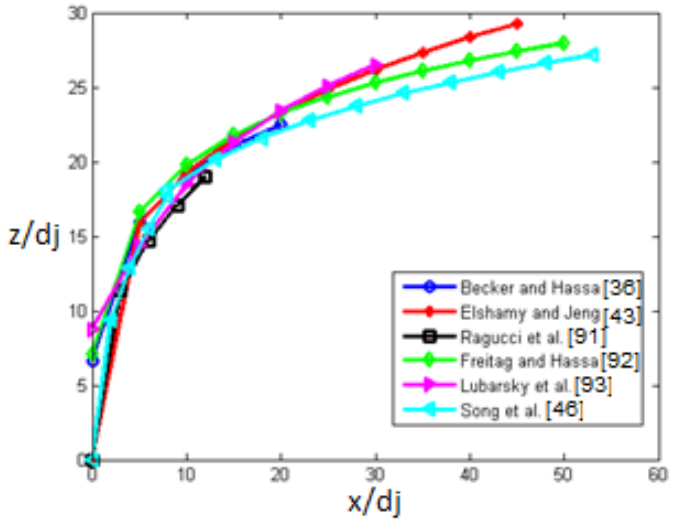

Figure 2-21: Water jet trajectory and penetration in a subsonic gaseous crossflow at STHP test conditions for q = 20, We_g=500 and P = 5 bar.

As is illustrated in Fig. 2-21, similar to STP and HTSP test conditions, the predicted trends at STHP test conditions (at typical $q = 20$ and $We_g = 500$, $P = 5$ bar with water as the test liquid) exhibit a difference of around $5d_j$ at different distances from nozzle exit up to $x/d_j = 50$.

The effect of both high temperature and high pressure (HTP) of crossflow on liquid jet trajectory and penetration was also studied [9,30,94–96]. The proposed correlations along with their range of test conditions are summarized in Table 2-5 and plotted in Fig. 2-22.

Table 2-5: Correlations of liquid jet trajectory in a subsonic gaseous crossflow at HTP test conditions

Correlations	q	We_g	x/d_j	P (bar)	T (K)	Reference
$z/d_j = 15q^{0.5}(x/d_j)^{0.33} We_g{}^{-0.41}(\mu_j/\mu_W)^{-0.027}$	2.2-75	700-1580	0-12	3.8-6.5	350-475	Masuda and McDonell [94]
$z/d_j = 0.909q^{0.476}(x/d_j)^{0.35} We_{aero}{}^{-0.128} Re_g^{0.135}$	12.2-71.4	We_{aero} = 10.4-410.5	0-12	10,20	300&600	Bellofiore et al. [9]
$z/d_j = 2.28q^{0.422}(x/d_j)^{0.367} We_{aero}{}^{-0.015} (\mu_g/\mu_{air,300K})^{0.186}$	5-280	We_{aero} = 7-340	0-12	20	600	Ragucci et al. [95]
$z/d_j = 1.44\ln(1.06(x/d_j)+1)q^{0.4356} We_g{}^{0.01147}(T/T_o)^{0.295}$	16-76	399-1630	0-40	5-20	280-650	Li et al. [96]
$z/d_j = 0.191q^{0.3}(x/d_j)^{0.43} Re_{ch}^{0.12} Re_j^{0.14}$	10-80	20-487	0-17	2.1-5.2	298-573	Eslamian et al. [30]

Bellofiore et al. [9] stated that high temperature and pressure crossflow affected the atomization level due to the change in air density. They also mentioned that, even at T = 600 K, the evaporation of water drops was not significant within 100 times the jet diameter downstream of the injection

point. Li et al. [96] varied the crossflow density by changing the air pressure in order to examine the effect of gas Weber number on liquid jet penetration. They reported that gas Weber number did not have a significant effect on jet penetration at both room and high temperature conditions. They, however, mentioned that the crossflow temperature ratio has a significant effect on jet penetration where it was greater at higher temperature. Eslamian et al. [30] reported that an increase in crossflow air temperature led to an increase in the rate of mass shedding and consequently smaller droplets which resulted in a slight decrease in jet penetration particularly in the far-field. On the other hand, they asserted that, at constant q and v_j (or constant We_j), an increased ambient pressure (and hence the density while the crossflow velocity decreased so that We_g remained unchanged) decreased the rate of mass shedding and consequently the formation of larger droplets, which resulted in an increased jet penetration height.

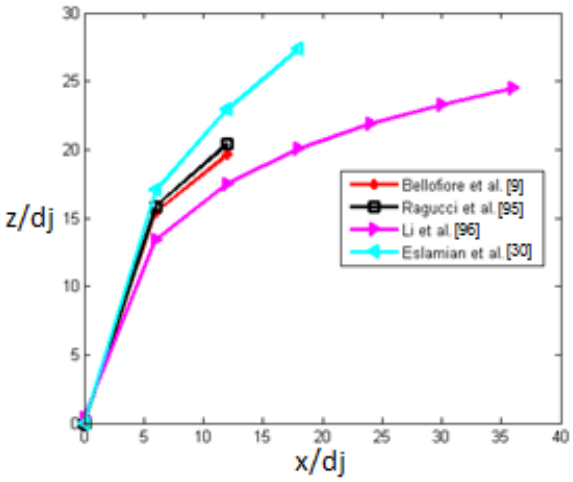

Figure 2-22: Water jet trajectory and penetration in a subsonic gaseous crossflow at HTP test conditions for q = 20, We_g= 500, T = 500 K, P = 5 bar.

As is illustrated in Fig. 2-22, the predictions of the proposed correlations at HTP test conditions differ by about $5d_j$ up to x/d_j = 10, however, for larger x/d_j in the far-field, Eslamian et al. [30] correlation over predicts the general trend. The correlation of Masuda and McDonell [94] is excluded in this figure as it underpredictes largely the general trends, which is believed to be due mainly to the fact that their injector was mounted recessed instead of flush. In fact, Masuda and McDonell [94] asserted that their results approached the prediction of the correlations proposed for flush type nozzle at high values of q (but not at low q), when a recess of about $10d_j$ is added to the measured jet penetration (which is equivalent to placing the nozzle flush). Several computational modeling and theoretical analysis have been carried out to predict the trajectory and penetration of a liquid jet injected into a cross airflow over a wide range of test conditions. In general, numerical studies of a liquid jet in a cross airflow can be categorized based on the used approach; that is, Eulerian or Lagrangian framework. Regarding the Eulerian approach, for instance, Spyrou et al. [97], and Farvardin and Dolatabadi [98] employed a Volume Of Fluid (VOF) simulation as a surface capturing model to predict the liquid jet trajectory. Pai et al. [70] employed a spectrally refined interface tracking technique to track liquid-gas interface. They compared their predictions of the liquid jet trajectory at different values of q and We_g with the experimental results of Lee et al. [65]. Herrmann [99,100], and Herrmann et al. [77] employed a Refined Level Set Grid (RLSG) method coupled with Lagrangian method for small drops to perform a detailed simulation of the primary atomization region. They studied the effect of liquid/gas density ratio on liquid jet trajectory [77], and compared their predictions with the empirical correlations of Wu et al. [26], and Stenzler et al. [83]. Li and Soteriou [72,101] used a Coupled Level Set and Volume Of Fluid (CLSVOF) simulation integrated with Lagrangian method for small drops. They compared liquid jet trajectory with the empirical correlations of Wu

et al. [26], but with an adjusted drag coefficient based on the breakup regimes from the measurement of Sallam et al. [28]. Xiao et al. [73] employed the same approach (i.e., CLSVOF) to predict the trajectory of a liquid jet in a cross airflow. There exist some studies which employed a Lagrangian approach (or particle tracking method) to predict liquid jet trajectory based on modeling the breakup of droplets (instead of a liquid column) injected into a cross airflow [34,35,102–104], following the study of Liu et al. [105], who studied the injection of droplets into a cross airflow. Several theoretical analysis are performed in order to predict liquid jet trajectory by taking into account the forces exerted on a liquid jet [13,76,106–112]. Wang et al. [37], in a recent publication, carried out a statistical analysis of published correlations to determine the minimum average standard deviations of their predictions of a transverse liquid jet trajectory. As a result, optimum values of the coefficients/exponents of a more general form of correlation are suggested for predicting the trajectory of a transverse liquid jet over wide range of test conditions.

2.4.3. Concluding remarks on liquid jet trajectory and penetration

The correlations presented above exhibited discrepancies in the prediction of the trajectory and penetration of a liquid jet in a crossflow. This is attributed to a variety of different factors such as errors and uncertainties in experiments and measurement methods as well as other factors. However, these differences can be narrowed down if correlations are categorized/regrouped based on factors pertaining to the problem and its own test conditions. For instance, different approaches (experimental [30], statistical [37], and analytical [112]) showed that the inadequacy of using solely q for predicting the trajectory of a liquid jet in a crossflow particularly at elevated pressure and/or temperature conditions. That is why the effect of other dimensionless group numbers, such as jet Weber number $We_j = qWe_g$, jet Reynolds number Re_j, gas (crossflow) Reynolds number Re_g, Ohnesorge number, Oh, Bond number Bo, gas to liquid density ratio ρ_j/ρ_g, and gas to liquid

viscosity ratio μ_j/μ_g, should be accounted for depending on the degree of their contributions and interdependency. For instance, changing temperature will change air crossflow properties. Therefore, choosing simultaneously both temperature ratio and a non-dimensional number based on air properties may not represent the independent effect of each parameter. This is the reason why, for example, the exponent of temperature ratio is negative in Lakhamraju and Jeng [44] (at constant q and We_g), while it is positive in Li et al. [96] (at constant q and variable We_g). This interdependency is one of the most important reasons contributing to the discrepancies between published correlations. Ragucci et al. [95] reported that, since the heat-up time of liquid jet is longer than the lifetime of the continuous liquid column, the density of liquid jet can be used as a reference density for examining the impact of elevated temperature cross airflow (gas flow). Nonetheless, the surface tension depends on the temperature at the interface between the two phases, which is not easy to estimate. Hence, while most of the studies used a reference temperature, Ragucci et al. [95] employed the lowest interfacial temperature by following the classical approach of the vaporization of a single-component drop in quiescent gas. Overall, q is necessary to predict the trajectory of a jet as it represents the ratio between the gas and liquid inertial forces. The properties of liquid jet can be accounted for using the following non-dimensional parameters; μ_g/μ_l, Re_j, or Oh. Parameters such as We_g, ρ_j/ρ_g, or Re_g can be used to represent the properties of gaseous crossflow. We_g and ρ_j/ρ_g are important for predicting the extent of the penetration of a liquid jet into a subsonic gaseous crossflow as they define/dictate the size of droplets in the far-field region. On the other hand, in the near-field region, We_g plays a key role in defining the primary breakup regimes, and also in predicting the onset time of surface breakup along the jet column [28]. Altering the primary breakup regime of a liquid jet affects its deformation, and consequently its penetration [28]. An increase in ρ_j/ρ_g results in a noticeable

increase in liquid core penetration with reduced bending and spreading in the transverse directions [77]. It should be mentioned that out of the three dimensionless numbers q, We_j and We_g, only two are independent. Furthermore, We_j and Re_j can be related using Ohnesorge number as $Oh = \left(We_j\right)^{0.5}/Re_j$. Although Lee et al. [65] asserted that the presence of turbulence in a liquid jet has little effect on liquid column trajectory, Re_j affects the primary breakup regimes (see Section 2) of a transverse liquid jet, as it plays a crucial role relative to the presence of instabilities on the surface of a liquid jet where transition from laminar to turbulent behavior occurs. Bo number becomes important only when jet nozzle diameter exceeds the capillary length of liquid (e.g., 2.7 mm for water) [39]. The initial injection angle [57] and nozzle geometry (i.e., discharge coefficient) [45] are also key parameters for describing liquid jet trajectory and penetration in a crossflow. As Brown et al. [45] mentioned, it appears that most published jet penetration correlations assumed a liquid jet velocity based on the volume flow rate divided by the injector cross sectional area. However, since the actual jet velocity is inversely promotional to the discharge coefficient of a nozzle, and because the discharge coefficient is a function of jet Reynolds number Re_j and its internal geometry, difference in the nozzle internal geometry could be one of the reasons of the discrepancies in the predictions of these correlations. Brown et al. [45,85,113] reported that the value of the discharge coefficient depends on both internal geometry and diameter of a nozzle which can change the value of the momentum flux ratio, q, up to 50% for a nozzle with a length to diameter ratio of 4. Ahn et al. [81,114] reported that liquid column trajectory of non-cavitating and cavitating jets have similar trend, but different to liquid column trajectory of hydraulic flip jets because the surface of hydraulic flip liquid jet flow detaches from the inner wall of the orifice hole. Lubarsky et al. [93] investigated spray trajectories formed by Jet-A fuel injected into a cross airflow using different injector geometries (sharp edge with $L/d_j = 10$, and round

edge with $L/d_j \sim 1$). They reported that the discharge coefficient of the sharp edge orifice is relatively constant, $C_d \sim 0.75$, within their tested range of Re_j number, while the discharge coefficient of a round edge orifice is $C_d \sim 0.96$ for Reynolds numbers exceeding $Re_j = 10{,}000$. They indicated higher spray penetration into a cross airflow (~12%) for a sharp edge orifice comparing with a round edged orifice. They attributed this observation to a larger droplet size generated by a sharp injector and, possibly by the higher velocity of some droplets. Therefore, the jet velocity, calculated based on the metered nozzle flowrate divided by a nozzle exit area (i.e., discharge coefficient $= 1$), should be normalized by an actual nozzle's discharge coefficient (i.e., discharge coefficient < 1) in order to render the injection velocity independent of nozzle's geometry and determine the jet actual velocity required for calculating q, Re_j, We_j. While the focus of the present review paper is on non-evaporating liquid jets, it is worth mentioning that Prakash et al. [64] studied the penetration of a highly volatile liquid fuel (ethanol) jet at elevated temperature test conditions and observed a higher trajectory than that at standard conditions, which they attributed to the effect of liquid vaporization.

2.5. Liquid jet breakup (fracture) length

As discussed earlier (Sub-Section 2.2.2), there are two modes of liquid jet breakup processes, namely column and surface breakup. The core of a transverse liquid jet (i.e., liquid column) forms a continuous stream between the jet exit and the location (point) of its complete fracture (i.e., column breakup point). Knowledge of the location of column breakup point is important for, for example, modeling a liquid jet in a crossflow. Accurate determination of this location is difficult because of high droplets density around the jet column. That is why there exist discrepancies among the predictions of this length in published literature. Similar to the trajectory and penetration of transverse liquid jet (presented in Section 2.4), this feature has been presented in

published literature using different expressions which correlated the breakup length with different non-dimensional numbers or a constant. Column breakup length of a transverse liquid jet is defined as the streamwise distance it travels into a crossflow before its complete breakup, which is referred to as the column breakup distance (i.e., *x*-axis direction in Fig. 2-2), and column breakup height (i.e., *z*-axis direction, as shown in Fig. 2-2), respectively. Published correlations of liquid jet breakup length are categorized and discussed below.

2.5.1. Column breakup (fracture) distance

The majority of published correlations for predicting the column breakup distance related the non-dimensional form of this distance (i.e., normalized by the jet diameter, x_b/d_j) to a constant. This suggests that the column breakup distance is insensitive to gaseous or liquid phase properties. For instance, Inamura et al. [115] found x_b/d_j to be in the range of 3.0 - 3.5. However, Wu et al. [26] proposed a larger value for a transverse liquid jet as $x_b/d_j = 8.06 \pm 1.46$. Becker and Hassa [36], who investigated the effect of elevated pressure on a transverse liquid jet, reported $x_b/d_j \approx 8$. Sallam et al. [28] experimentally investigated this distance for a non-turbulent round liquid jet and found $x_b/d_j = 8$. Tambe et al. [41] defined this distance as the mean location of the formation of the first ligament, with a mean value of 14.97 and a standard deviation of 1.37. Ahn et al. [81] measured this distance for noncavitating flows as $x_b/d_j = 8.02 \pm 1.43$, while they asserted that, in cavitating flows, as the injection differential pressure increases, cavitation develops and liquid jet becomes turbulent, which leads to a shorter column breakup distance. Iyogun et al. [82], and Birouk et al. [84], reported this distance as $x_b/d_j \approx 12$. The measurements of Lee et al. [65] yielded $x_b/d_j = 5.20$ and $x_b/d_j = 8.64$ for, respectively, turbulent and nonturbulent liquid jet in

a crossflow. Xiao et al. [73] adopted a Coupled Level Set and Volume Of Fluid (CLSVOF) simulation approach for both turbulent and nonturbulent liquid jets. In agreement with the experiment results of Lee et al. [65], they reported a shorter breakup distance of a turbulent liquid jet than that of a nonturbulent jet at the same gas Weber number. Gopala et al. [116] reported a shorter distance compared to Wu et al. [26], and Sallam et al. [28], and attributed this discrepancy to the technique that they used in comparison with the shadowgraphy or Mie scattering techniques commonly employed. Osta et al. [60] measured the column breakup distance of a turbulent liquid jet considering nozzles with different length/diameter ratio. They showed that the column breakup distance of a turbulent liquid jet with different length/diameter ratio ranges between the two constant values reported by Lee et al. [65] for turbulent liquid jet, and by Sallam et al. [28] for nonturbulent liquid jets; i.e., $x_b/d_j = 5.20 - 8$. Thawley et al. [86] and Wang et al. [87] used a larger data set compared to Wu et al. [26] and Becker and Hassa [36] and reported that $x_b/d_j = 6.9$. Zheng and Marshall [67] used a nozzle with a length/diameter ratio larger than 20 to obtain a fully developed turbulent velocity profile. They reported two different constant values for the liquid breakup distance with respect to gas Weber number, which are as follows: $x_b/d_j = 15.1$ for $We_g \leq 8$, and $x_b/d_j = 5.9$ for $We_g \geq 12$.

Birouk et al. [48] experimentally showed that at lower liquid viscosity, up to approximately 0.029 Pa.s, the liquid breakup distance exhibited a tendency to be almost constant corroborating earlier published findings. However, at higher liquid viscosity, up to 0.058 Pa.s, they reported that liquid jet breakup distance increased with increasing q, and become dependent on the liquid viscosity where its effect was accounted for using Oh. They, therefore, proposed two empirical correlations for the liquid breakup distance as follows: $x_b/d_j = 0.00368q + 14.095$ for $\mu_l < 0.029$ Pa. s, and $x_b/d_j = 542.64q^{0.87}Oh^{25}$ for $\mu_l > 0.029$ Pa. s.

Bellofiore et al. [9] carried out experiments at high temperature and pressure (HTP) conditions, and claimed that the liquid breakup distance depends on the test/operating conditions, as follows: $x_b/d_j = 3.794{We_{aero}}^{0.366}$. The same group, Ragucci et al. [91], reported that the liquid breakup distance at high pressure test conditions is a function of both q and $\mathrm{We_{aero}}$ and was expressed as follows: $x_b/d_j = 3.687q^{-0.068}{We_{aero}}^{0.420}$. Raguccie et al. [95] also suggested that in addition to these two nondimensional parameters, air viscosity might also play a role (though quite negligible) in defining the liquid breakup distance at HTP test conditions, and proposed the following relationship: $x_b/d_j = 4.17q^{-0.095}{We_{aero}}^{0.382}\left(\mu_g/\mu_{air,\ 300\,K}\right)^{0.046}$. Li and Soteriou [101], in a numerical simulation, indicated that a reduced liquid/gas density ratio can cause a reduction of the height of the liquid column breakup location. Xiao et al. [73] showed numerically that the breakup distance decreases as the gas Weber number increases for a nonturbulent liquid jet. The aforementioned numerical and experimental studies demonstrated the importance of test conditions and their consequent effects on liquid and gas properties (or in other words, on non-dimensional parameters) and hence on the prediction of the column breakup location.

There are several studies which investigated the effect of injection angle on the liquid breakup distance. Fuller et al. [57], suggested two empirical correlations to predict liquid breakup distance with respect to T_b which are expressed as follows: $x_b/d_j = 9.3 + 2.6\left[v_j cos\theta/\left(u_g - v_j cos\theta\right)\right]\left(\rho_j/\rho_g\right)^{0.5}$ for $T_b < 1$, and $x_b/d_j = (9.3/T_b^2) + 1.7{We_j}^{1/3}cos\theta$ for $T_b > 1$, where θ is the injection angle, and T_b is the ratio of the aerodynamic to nonaerodynamic breakup timescale (as defined in Sub-section 2.2). Costa et al. [117], however, stated that the liquid breakup distance for angled injection cases cannot be independent of q, and they proposed that $x_b/d_j = \left(z_b/d_j\right)cotan\theta$, where $z_b/d_j = 8.05q^{0.5}$ is the nondimensional liquid breakup height.

Kim et al. [118] studied the effect of injection angle on both forward and reverse injection cases, and proposed two empirical correlations to predict liquid breakup distance with respect to θ as follows: $x_b/d_j = 6.34q^{0.07}/sin^2\,\theta$ for $\theta \leq$ 90-degree, and $x_b/d_j = 1.14q^{0.39}/sin^2\,\theta$ for $\theta >$ 90-degree.

As summarized in Table (2-6), the average jet column breakup distance x_b/d_j is a constant value ranging between 8 and 12. However, x_b/d_j becomes even smaller (< 8) when i) instabilities are present on the liquid jet surface caused by cavitation or ii) the transition from laminar to turbulent jet flow regime occurs earlier. On the other hand, this distance can increase with viscosity for viscous liquids. Furthermore, different parameters, such as the change of gas properties at high temperature and pressure test conditions, injection angle and measurement methods can all affect this distance, and make it dependent on different nondimentional parameters.

Table 2-6: Correlations of column breakup distance of a liquid jet in a subsonic gaseous crossflow

Column breakup distance correlations	q	$\mathbf{We_g}$	Reference
$x_b/d_j = 3.0 - 3.5$	v_j=7-26 m/s	u_g=55-140 m/s	Inamura et al. [115]
$x_b/d_j = 8.06 \pm 1.46$	3.4-185	57-1180	Wu et al. [26]
$x_b/d_j \approx 8$	1-40	90-2120	Becker and hassa [36]
$x_b/d_j = 8$	3-450	0.5-260	Sallam et al. [28]
$x_b/d_j = 14.97$	0.7-10.2	50.5-1725.1	Tambe et al. [41]
$x_b/d_j = 8.02 \pm 1.43$	-	-	Ahn et al. [81]
$x_b/d_j \approx 12$	8.3-726	9.3-159	Iyogun et al. [82] and Birouk et al. [84]
$x_b/d_j \approx 8.64$ (nonturbulent)	3-200	0-282	Lee et al. [65]
$x_b/d_j \approx 5.20$ (turbulent)			

$x_b/d_j = 5.20 - 8$	v_j=10-46 m/s	166, 332, 376	Osta et al. [60]
$x_b/d_j = 6.9$	1-54	9-345	Thawley et al. [86] and Wang et al. [87]
$x_b/d_j = 15.1\ (We_g \leq 8)$	10-50	4-16	Zheng and Marshall [67]
$x_b/d_j = 5.9\ (We_g \geq 12)$			
$x_b/d_j = 0.00368q + 14.095$ ($\mu_l <$ 0.029 Pa s)	12-284	1.6-13.8	Birouk et al. [48]
$x_b/d_j = 542.64q^{0.87}Oh^{25}$ ($\mu_l > 0.029$ Pa s)			
$x_b/d_j = 3.794{We_{aero}}^{0.366}$	12.2-71.4	We_{aero}=10.4-410.5	Bellofiore et al. [9]
$x_b/d_j = 3.687q^{-0.068}{We_{aero}}^{0.420}$	5-200	We_{aero}=8.1-444.8	Ragucci et al. [91]
$x_b/d_j = 4.17q^{-0.095}{We_{aero}}^{0.382}\left(\mu_g/\mu_{air,\ 300\,K}\right)^{0.046}$	5-280	We_{aero}=7-340	Raguccie et al. [95]
$x_b/d_j = 9.3 + 2.6\left[v_j cos\theta/\left(u_g - v_j cos\theta\right)\right]\left(\rho_j/\rho_g\right)^{0.5}$ ($T_b < 1$)	12-3777	5.5-223	Fuller et al. [57]
$x_b/d_j = (9.3/T_b^2) + 1.7{We_j}^{1/3}cos\theta$ ($T_b > 1$)			
$x_b/d_j = (8.05q^{0.5})cotan\theta$	22.9-637.4	0.07-52	Costa et al. [117]
$x_b/d_j = 6.34q^{0.07}/sin^2\,\theta$ ($\theta \leq 90$)	21-105	u_g=60 m/s	Kim et al. [118]
$x_b/d_j = 1.14q^{0.39}/sin^2\,\theta$ ($\theta > 90$)			

2.5.2. Column breakup (fracture) height

While the majority of correlations of the column breakup distance predict a constant value, the correlations of the column breakup height are mostly expressed in a nondimensional form. For instance, Inamura et al. [115] found that the liquid breakup height depends on q, but did not propose a correlation. Wu et al. [26] used a phenomenological approach to propose two correlations for the column breakup height; one theoretical as $z_b/d_j = 3.44q^{0.5}$, and another empirical as $z_b/d_j = 3.07q^{0.53}$. Similar to Inamura et al. [115] and Wu et al. [26], Tambe et al

[41] reported that the liquid breakup height increased with q, but no correlation was proposed. Ahn et al. [81] asserted that for noncavitating flows, the breakup length of a liquid jet followed well the results of Wu et al. [26]. However, for cavitating flows, the liquid breakup height had a smaller value, similar to the x-directional breakup distance discussed previously (Sub-section 4.1). Osta et al. [60] measured the column breakup height of a turbulent liquid jet by considering nozzles with different length/diameter ratios, and proposed an empirical correlation for each specific length/diameter ratio, expressed as follows: $z_b/d_j = 3.3q^{0.5}$ for length/diameter ratio of 10 and $d_j = 4$ mm, $z_b/d_j = 3.1q^{0.5}$ for length/diameter ratio of 20 and $d_j = 2$ mm, $z_b/d_j = 2.7q^{0.5}$ for length/diameter ratio of 40 and $d_j = 4$ mm. Osta et al. [60], in an experimental study using a wind tunnel, reported that when a liquid is injected into a wind tunnel's crossflow, liquid jet must cross the wall boundary layer. This consequently causes a delay in its breakup time, and hence yields a shorter liquid column in comparison with that of a jet injected into a shock-tube test facility which has a much thinner boundary layer. Thawley et al. [86] and Wang et al. [87] reported the following correlation for the liquid breakup height $z_b/d_j = 2.5q^{0.53}$. Zheng and Marshall [67] used a nozzle with a length/diameter ratio larger than 20 to achieve a fully developed turbulent velocity profile, and reported two different correlations for the liquid breakup height with respect to gas Weber number as follows: $z_b/d_j = 10.7q^{0.40}$ for $We_g \leq 8$, and $z_b/d_j = 4.46q^{0.40}$ for $We_g \geq 12$. They, therefore, concluded that the effect of q on the liquid breakup height for both groups have the same behavior but different coefficient.

Birouk et al. [48] demonstrated that, for high liquid viscosity, similar to the breakup distance, the liquid breakup height depends on liquid viscosity in addition to q. However, their criterion for defining the low and high viscosity regions changed from 0.029 to 0.019 Pa s. They provided two

correlations for the liquid breakup height as follows: $z_b/d_j = 3.13q^{0.53}$ for $\mu_l < 0.019$ Pa s, and $z_b/d_j = 8.60q^{0.87}Oh^2$ for $\mu_l > 0.019$ Pa s.

Bellofiore et al. [9] examined high temperature and pressure (HTP) test conditions and proposed a correlation for the liquid breakup height as a function of q and Re_g, which accounted for both air density and viscosity effect on jet penetration, as follows: $z_b/d_j = 1.449q^{0.476}{Re_g}^{0.135}$. Ragucci et al. [91] stated that the liquid breakup height of a transverse liquid jet at high pressure test conditions, similar to their correlation for liquid breakup distance, is a function of q and We_{aero} and expressed as $z_b/d_j = 4.355q^{0.416}{We_{aero}}^{0.085}$. However, liquid breakup height is more sensitive to q and less sensitive to We_{aero} in comparison with the liquid breakup distance correlation. Raguccie et al. [95], then, included air viscosity effect to predict the liquid breakup height at HTP test conditions with their correlation expressed as $z_b/d_j = 3.85q^{0.387}{We_{aero}}^{0.126}\left(\mu_g/\mu_{air,\ 300\,K}\right)^{0.202}$, where the breakup height is more sensitive to air viscosity compared to the breakup distance.

Fuller et al. [57], similar to the liquid breakup distance, suggested two empirical correlations to predict liquid breakup height for angled injection cases with respect to T_b., which are expressed as follows: $z_b/d_j = 2.6\left[v_j sin\theta/\left(u_g - v_j cos\theta\right)\right]\left(\rho_j/\rho_g\right)^{0.5}$ for $T_b < 1$, and $z_b/d_j = 1.7{We_j}^{1/3}sin\theta$ for $T_b > 1$. Kim et al. [118], proposed two empirical correlations to predict liquid breakup height for both forward and reverse injection cases, and two empirical correlations to predict liquid breakup distance with respect to θ as follows: $z_b/d_j = 6.33q^{0.314}sin^2\theta$ for $\theta \leq 90$ degree, and $z_b/d_j = 4.64q^{0.317}sin^{0.5}\theta$ for $\theta > 90$ degree.

Table 2-7 illustrates that the column breakup height is directly proportional to q; which can be expressed in the following form: $z_b/d_j = cq^n$ where $c = 2.5 - 4.4$ and $n = 0.4 - 0.53$. Similar to the column breakup distance (Subsection 2.5.1), the height may decrease as a result of the presence of instabilities on the jet surface due to cavitation and turbulent effect, while it may increase with viscosity for viscous liquids.

Table 2-7: Correlations of the column breakup height of a liquid jet in a subsonic gaseous crossflow

Column breakup height correlations	q	We_g	Reference
$z_b/d_j = 3.44q^{0.5}$ (theoretically)	3.4-185	57-1180	Wu et al. [26]
$z_b/d_j = 3.07q^{0.53}$ (empirically)			
$z_b/d_j = 3.3q^{0.5}\left(L/d_j = 10, \text{and } d_j = 4 \text{ mm}\right)$	v_j=10-46 m/s	166, 332, 376	Osta et al. [60]
$z_b/d_j = 3.1q^{0.5}\left(L/d_j = 20, \text{and } d_j = 2 \text{ mm}\right)$			
$z_b/d_j = 2.7q^{0.5}\left(L/d_j = 40, \text{and } d_j = 4 \text{ mm}\right)$			
$z_b/d_j = 2.5q^{0.53}$	1-54	9-345	Thawley et al. [86] and Wang et al. [87]
$z_b/d_j = 10.7q^{0.40}\left(We_g \leq 8\right)$	10-50	4-16	Zheng and Marshall [67]
$z_b/d_j = 4.46q^{0.40}\left(We_g \geq 12\right)$			
$z_b/d_j = 3.13q^{0.53}$ ($\mu_l < 0.019$ Pa s)	12-284	1.6-13.8	Birouk et al. [48]
$z_b/d_j = 8.60q^{0.87}Oh^2$ ($\mu_l > 0.019$ Pa s)			
$z_b/d_j = 1.449q^{0.476}{Re_g}^{0.135}$	12.2-71.4	We_{aero}=10.4-40.5	Bellofiore et al. [9]
$z_b/d_j = 4.355q^{0.416}{We_{aero}}^{0.085}$	5-200	We_{aero}=8.1-444.8	Ragucci et al. [91]
$z_b/d_j = 3.85q^{0.387}{We_{aero}}^{0.126}\left(\mu_g/\mu_{air,\ 300\,K}\right)^{0.202}$	5-280	We_{aero}=7-340	Raguccie et al. [95]
$z_b/d_j = 2.6\left[v_j sin\theta/\left(u_g - v_j cos\theta\right)\right]\left(\rho_j/\rho_g\right)^{0.5}$ $(T_b < 1)$	12-377	5.5-223	Fuller et al. [57]
$z_b/d_j = 1.7{We_j}^{1/3} sin\theta$ $(T_b > 1)$			
$z_b/d_j = 8.05q^{0.5}$	22.9-637.4	0.07-52	Costa et al. [117]
$z_b/d_j = 6.33q^{0.314}sin^2\theta$ $(\theta \leq 90)$	21-105	u_g=60 m/s	Kim et al. [118]
$z_b/d_j = 4.64q^{0.317}sin^{0.5}\theta$ $(\theta > 90)$			

2.5.3. Concluding remarks on liquid jet breakup (fracture) length

Based on published literature, it appears that liquid breakup distance can mostly be predicted by a constant value, and the liquid breakup height is correlated with q. However, these correlations show some degree of discrepancies in predicting the breakup length, similar to the trajectory and penetration correlations discussed in Section 2.4, due to different reasons such as difficulties in observing the breakup location obstructed by the high droplet density around the jet column, errors and uncertainties associated with experiments and measurement methods, etc. Similar to the trajectory and penetration correlations (see Section 2.4), these differences can be narrowed down and the correlations can be employed appropriately provided that one considers the prevailing parameters. For instance, Ahn et al. [81], Lee et al. [65], Osta et al. [60] and Birouk et al. [119] stated that the presence of cavitation and turbulence enhances the process of liquid column breakup as a whole, and consequently shortens the column breakup time and length of a turbulent liquid jet in a crossflow when compared with a nonturbulent liquid jet. Moreover, Birouk et al. [48] stated that, for high viscous liquids, the breakup length should be correlated to Oh in addition to q. Bellofiore et al. [9] and Raguccie et al. [91,95] also showed that, for high temperature and pressure test conditions, in addition to q, nondimensional parameters such as We_{aero} should be taken into account for correlating liquid breakup length. According to Fuller et al. [57], Costa et al. [117] and Kim et al. [118], for angled jet injections, the breakup length can be predicted by accounting for the effect of different nondimentional numbers which include q and We_j in addition to the injection angle θ. Overall, column breakup distance can be approximated by a constant ranging as $x_b/d_j = 8 - 12$, whereas column breakup height can be correlated as $z_b/d_j = cq^n$; where $c = 2.5 - 4.4$ and $n = 0.4 - 0.53$. Li and Soteriou [72,101], who employed a Coupled Level Set and Volume Of Fluid (CLSVOF) simulation integrated with Lagrangian method, revealed that the calculated

breakup location is slightly smaller than that reported experimentally [26,28]. They attributed this difference to the fact that experimental studies used only one view (a single plane) for determining the breakup location, which can be affected by the obtrusion of neighboring liquid structures. Further studies are required in order to develop comprehensive correlations capable of predicting liquid jet breakup length over a wider range of test conditions of liquid properties, liquid and gaseous jet test conditions and nozzle geometry.

2.6. Droplets features and formation mechanisms

The breakup of a liquid jet involves two sequential processes: primary and secondary breakup [120]. For a liquid jet injected into a subsonic cross airflow, as is depicted in Fig. 2-2, the primary breakup is governed by two mechanisms: column and surface breakup. Ligaments and droplets disintegrating from liquid column, via the primary breakup, undergo secondary breakup mechanism leading to smaller droplets, and consequently the formation of a spray in the far-field region. Since the features of droplets and their formation mechanisms are different in the near- and far-field regions of a liquid jet in a subsonic crossflow, they will be discussed separately in the following sections.

2.6.1. Liquid jet's near-field region

Formation of droplets in the near-field region as a result of the primary breakup of a liquid jet is the process which determines the initial properties of the spray dispersed phase in the far-field region and consequently plays a key role in defining the secondary breakup, droplets interactions and fuel/air mixing rate. On the other hand, factors such as secondary breakup and droplets interactions in the far-field may overrule the outcome of the primary breakup. The focus of this

section, therefore, is on the size and velocity distribution, as well as the formation rate of droplets generated along the liquid column surface. This is important in order to achieve better understating of the underlying physics of liquid jet primary breakup. As was explained earlier in section 2.2.2 (features of a liquid jet in a subsonic gaseous crossflow), two mechanisms have been proposed for droplets formation along a liquid column jet injected into a cross airflow; namely: hydrodynamic instability and boundary layer stripping (BLS) mechanism in the near-nozzle's cross-section of a liquid jet, as illustrated schematically in Fig. 2-23.

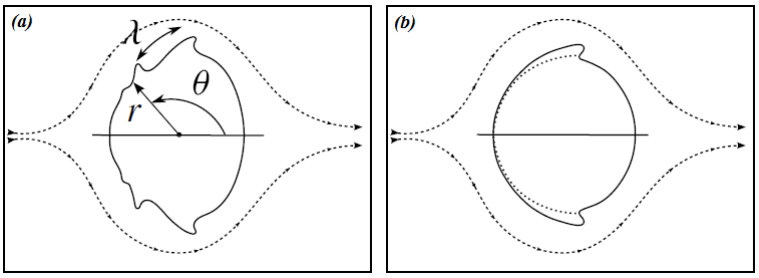

Figure 2-23: Near-nozzle cross-section of liquid jet. a) hydrodynamic instability mechanism, and b) boundary layer stripping mechanism. Reprinted from Ref. [25] with permission from Cambridge University Press.

As is shown in Fig. 2-23(a), hydrodynamic instability analysis postulates that the temporal growth of azimuthal instabilities (shear instabilities) is responsible of the formation of interface corrugations, which are eventually shears off the jet surface [25,121–123]. The analysis is based on a continuous formulation of the momentum equations in which the jet and cross-flow are considered to be slightly miscible at the vicinity of the interface. This method supports an inviscid breakup mechanism which is opposed to the boundary layer stripping analysis where the liquid viscosity plays a key role. During the injection of a liquid jet into a cross airflow, there exists another form of instability (axial instability) that develops on the jet windward surface farther away

from the nozzle, which is responsible for the column breakup process [25,121–123]. The reader can find more detail about the application of the stability analysis for a jet injected into a quiescent atmosphere or crossflow in Refs. [14,15,75,124–126].

As for the boundary layer stripping perspective, as is illustrated in Fig. 2-23(b), a viscous boundary layer is assumed to form at the jet periphery due to the existence of shear forces between the gaseous and liquid phase. Eventually, liquid droplets disintegrate off the boundary layer which is formed inside the liquid jet due to the influence of the outer airflow. The diameter of the formed droplets is comparable to the thickness of the liquid boundary layer [28,127]. While the former analysis has only been recently proposed [25,123], the latter has been widely employed in order to develop semi-empirical correlations for the size, velocity and formation rate of droplets produced from the surface breakup of a nonturbulent [28,49,58,127], and a turbulent [58,60,61,65] liquid jet in a cross airflow. Therefore, they will be discussed in details for both non-turbulent and turbulent liquid jet in the following subsections.

2.6.1.1. *Droplets formation from nonturbulent liquid jet*

The formation of ligaments and droplets along a liquid surface of a nonturbulent liquid jet in a cross airflow has been studied in the literature [28,49,58,127]. Sallam et al. [28] asserted that, within the shear breakup regime, the appearance of drops always precedes by the appearance of ligaments protruding downstream from the region near the sides of liquid jet towards the wake region. In order to find the size of droplets along the liquid jet surface, they proposed a correlation for the size of ligaments, and then predicted the size of droplets by taking into account Rayleigh breakup of drops at the end of ligaments. Sallam et al. [28] exploited an analogy between the primary breakup of a liquid jet in a cross airflow, and the primary breakup of a liquid jet in a still gas [128] for ligaments and drops formation. By equating the momentum flux (relative to the bulk

of liquid jet) of a ligament with a given size, d_{li}, to the maximum surface tension force required to start the formation of a ligament with such a size, they proposed two semi-empirical correlations for the ligaments diameter at the onset of ligament formation as follows:

$$\frac{d_{li}}{d_j} = 0.07\left[\frac{(\mu_j/\mu_g)}{We_g}\right]^{\frac{1}{2}}, \qquad for\ (\mu_j/\mu_g)/We_g < 2.0 \tag{2-3}$$

$$\frac{d_{li}}{d_j} = 0.095, \qquad for\ (\mu_j/\mu_g)/We_g > 2.0 \tag{2-4}$$

They suggested a constant ratio of drops diameter, d_{pi}, to ligaments diameter, d_{li}, at the onset of ligaments formation based on Rayleigh breakup mechanism, as follows:

$$\frac{d_{pi}}{d_{li}} = 1.2 \tag{2-5}$$

Sallam et al. [28] associated the diameter of ligaments along the liquid jet surface, d_l, to the thickness of the liquid jet boundary layer caused by the cross airflow. Proceeding in the same manner as Chou et al. [129], Sallam et al. [28] identified two regimes for ligaments formation along the liquid jet surface and the variation of their diameter as a function of liquid jet streamwise distance, z; namely: transient and quasi-steady regime. The transient regime is associated with the progressive growth of the boundary layer as a function of time (or with increasing z) which supplies liquid to the base of ligaments. They proposed a semi-empirical correlation for the ligaments diameter as follows [28]:

$$\frac{d_l}{d_j} = 3.6\left[\frac{(\mu_j/\rho_j)z}{v_j d_j^2}\right]^{\frac{1}{2}}, \qquad for\ (\mu_j/\rho_j)z/v_j d_j^2 < 0.001 \tag{2-6}$$

For the quasi-steady regime, Sallam et al. [28] assumed that the boundary layer reaches its maximum possible growth of a thickness which is a fixed fraction of the liquid jet diameter. They proposed the following correlation for this regime:

$$\frac{d_l}{d_j} = 0.11, \qquad for\ \left(\mu_j/\rho_j\right)z/v_j d_j^2 > 0.001 \tag{2-7}$$

In both regimes of ligaments growth, the diameter of drops, d_p, formed at the tip of ligaments is considered to be a fixed value of ligaments diameter based on the Rayleigh breakup mechanism, which is expressed as follows:

$$\frac{d_p}{d_l} = 1.2 \tag{2-8}$$

The velocity of droplets, disintegrated from the surface of non-turbulent liquid jet in a cross airflow within the conditions of shear breakup regime, has also been measured in the dense spray region [28]. Sallam et al. [28] performed measurements close to the tip of ligaments to minimize the effect of drops velocity relaxation to the ambient velocity, and proposed two correlations for the components of drops velocity in the liquid jet streamwise direction, v_p, and cross airflow direction, u_p, as follows [28]:

$$\frac{v_p}{v_j} = 0.7 \tag{2-9}$$

$$\frac{u_p\left(\rho_j/\rho_g\right)^{\frac{1}{2}}}{u_g} = 6.7 \tag{2-10}$$

They revealed that drops velocity after breakup is nearly independent of drops diameter. They, however, indicated that the gas-phase drag during the breakup process affected drops velocity [28]. This consequently caused v_p component to become slightly smaller than the jet velocity (see Eq.

2-9), and u_p component to significalty grow higher than that of crossflow velocity (Eq. 2-10) [28]. It is worth noticing that Li et al. [130], and Li and Soteriou [72] employed an Eulerian approach to carry out a high fidelity Coupled Level Set and Volume Of Fluid (CLSVOF) simulation in order to directly capture liquid-gas interface involving topological changes. Following the study of Herrmann [99,100], Li and Soteriou [72] integrated their simulation with Lagrangian method for small drops, and compared their results concerning the size and velocity of droplets as well as other characteristics of a liquid jet in a cross airflow with their counterparts' experimental data of Sallam et al. [28]. Li and Soteriou [72] reported a similar u_p component probability distribution, though with a peak value around 12, which is larger than that in Eq. (2-10). This discrepancy was attributed to the large uncertainties in determining droplets velocity using two-dimensional images. Li and Soteriou [72] also calculated that the peak value of v_p distribution and found it to range between 0.5 and 0.6, which is in reasonable agreement with the value of 0.7 in Eq. (2-9). They revealed that the jet transverse velocity (i.e., the third component of droplets velocity in y-direction according to Fig. 2-1) is very small, suggesting that the majority of droplets travel transversally.

Ng et al. [49] measured droplets size distribution disintegrated from a non-turbulent liquid jet in a cross airflow at the conditions of bag breakup regime. They revealed that the bag breakup resulted in three distinctive droplets sizes as follows: (a) very small droplets due to the breakup of the bag membrane, (b) small droplets due to the breakup of the two strings of the ring, and (c) large droplets associated with the nodes. They observed that the size of bag-droplets, defined by Sauter Mean Diameter (SMD or d_{32}), is independent of the gas Weber number, We_g, and represented by the following relation:

$$\frac{SMD_{\text{bag}}}{d_j} \approx 0.14 \tag{2-11}$$

Nonetheless, they reported that the size of the node- and the ring-droplets decrease with increasing We_g, and proposed two correlations for these two types of droplets as follows:

$$\frac{SMD_{\text{ring}}}{d_j} = 4.8We_g^{-1.0} \tag{2-12}$$

$$\frac{SMD_{\text{node}}}{d_j} = 11.4We_g^{-1.0} \tag{2-13}$$

Ng et al. [49] measured also droplets velocity right after the bag breakup of a non-turbulent liquid jet in a cross airflow, and revealed that droplets velocity is independent of their size. They proposed two correlations for the components of node-droplets velocity in the liquid jet streamwise direction, v_{node}, and cross airflow direction, u_{node}, as follows:

$$\frac{v_{node}}{v_j} \approx 0.9 \tag{2-14}$$

$$\frac{u_{node}}{u_g} \approx 0.28 \tag{2-15}$$

and two correlations for the components of ring-droplets velocity in the liquid jet streamwise direction, v_{ring}, and cross airflow direction, u_{ring}, as follows:

$$\frac{v_{ring}}{v_j} \approx 0.87 \tag{2-16}$$

$$\frac{u_{ring}}{u_g} \approx 0.27 \tag{2-17}$$

as well as two correlations for the components of bag-droplets velocity in the liquid jet streamwise direction, v_{bag}, and cross airflow direction, u_{bag}, as follows:

$$\frac{v_{bag}}{v_j} \approx 0.56 \tag{2-18}$$

$$\frac{u_{bag}}{u_g} \approx 0.34 \tag{2-19}$$

Ng et al. [49] observed that the bag-droplets, immediately after breakup, travel with a higher cross-stream velocity but with a lower jet streamwise velocity than the node- and the ring-droplets due to the high pressure produced by the stagnating gas on the upwind side of the bags that upon bursting propels the bag-droplets in the direction of cross airflow. The bag-droplets then travel into a separate trajectory than the relatively larger node-and ring-droplets.

In addition to droplets size and velocity, droplet formation rate has also been studied in order to completely describe the process of droplets formation. For instance, Sallam et al. [28], inspired by their earlier studies on turbulent primary breakup of a liquid jet in still gas [128], determined the mass flux of droplets leaving the liquid column by measuring the volume (and hence the mass) of the generated droplets per unit of jet-projected area and unit time for shear breakup regime using double-pulse holograms. They considered only the downstream half of the liquid column as opposed to the entire periphery of a turbulent liquid jet in still gas. They defined a liquid surface breakup efficiency factor, ε, as follows:

$$\varepsilon = \dot{m}_f^{"}/(\rho_j u_p) \tag{2-20}$$

where $\dot{m}_f^{"}$ is the average mass flux of liquid drops leaving the liquid column, and u_p is obtained from Eq. (2-10). They mentioned that although the limits of ε is between 0 for the onset of drop formation, and 1 for conditions where liquid drops form in a continuous manner over all the downstream liquid projected area, the actual appearance of liquid surface during a non-turbulent primary shear breakup, and particularly as the result of Rayleigh breakup at the tip of the growing

ligaments along the surface, suggests that ε is generally less than unity. Employing the dimensionless liquid jet streamwise length z/z_b between the jet exit and conditions where the liquid column breaks up as a whole, Sallam et al. [28] proposed a correlation for, ε, as follows:

$$\varepsilon = 6.89 \times 10^{-4} \exp\left(\frac{5.43z}{z_b}\right) \tag{2-21}$$

Li and Soteriou [72] numerically investigated the drops formation rate of a liquid jet injected into a crossflow for different We_g and reported a similar ε profile to that experimentally found by Sallam et al. [28]. However, they observed a shift in the profile when varying We_g, which is attributed to the difference in the definition of the projected area compared with that of Sallam et al. [28]. It is worth mentioning that Li and Soteriou [72] reported that, in contrast to the case of $We_g = 40$ and $We_g = 160$, the case of $We_g = 10$ has lower breakup efficiency due to the dominant role of column breakup compared to surface breakup at $We_g = 10$. However, this numerical finding needs to be confirmed experimentally.

Overall, based on published studies reviewed in this section, it is shown that, in the shear breakup regime, the ratio of drops diameter to ligaments diameter is a fixed value under on Rayleigh breakup mechanism (Eqs. 2-5 and 2-8). The ligaments diameter at the onset of ligaments formation is a function of We_g (Eq. 2-3), whereas the ligaments diameter along the column surface depends on v_j (Eq. 2-6). In both cases, liquid and gas properties and jet diameter are of importance in defining the ligaments diameter. The ligaments diameter along the column surface (Eq. 2-6) depends also on z, which shows that larger size ligaments, and consequently larger drops are formed in the liquid jet streamwise direction. Furthermore, droplets formation rate can be correlated by a dimensionless length along the liquid column (Eq. 2-21). In the bag breakup regime, the size distribution of drops shows different trend. The size of bag-droplets diameter is

independent of We_g and is a fixed fraction of jet exit diameter (Eq. 2-11), whereas the size of the node- and the ring-droplets decrease with increasing We_g (Eqs. 2-12 and 2-13). Droplets velocity after breakup is independent of its diameter for both breakup (bag and shear breakup) regimes. Features of droplets disintegrated along a nonturbulent liquid column in a cross airflow have been obtained experimentally by Sallam and co-workers [28,49,58,127] for the both breakup regimes, and numerically by Li et al. [130], and Li and Soteriou [72] for just the shear breakup regime. In addition, Sallam and co-workers [28,49,58,127] examined the effect of a supercavitating nozzle with a sharp-edged inlet and exit on liquid jet exit conditions (cavitation and hydraulic flip). However, the effect of round-edged nozzles on the features of droplets generated during the primary breakup over the surface of liquid column is still lacking and needs to be investigated. Therefore, more numerical and experimental studies are needed to shed more light on the features of droplets of a nonturbulent liquid jet.

2.6.1.2. *Droplets formation from a turbulent liquid jet*

Semi-empirical correlations are proposed for the variation of ligaments diameter, d_l, as a function of the distance from the jet exit, z, [58,60,61,65]. The effect of turbulent primary breakup on a liquid jet injected into a cross airflow is accounted for by following the approach of Sallam and Faeth [128] for a liquid injected into a still gas, as follows [65]:

$$\frac{d_l}{\Lambda} = 0.73\left[\frac{z}{\left(\Lambda We_{L\Lambda}^{1/2}\right)}\right]^{0.5} \tag{2-22}$$

where $We_{L\Lambda} \equiv \rho_j v_j^2 \Lambda/\sigma$ is Weber number based on the jet exit radial (i.e., crosstream) integral length scale Λ. Lee et al. [65] demonstrated that ligaments properties are clearly dominated by liquid turbulence, while cross airflow have no noticeable effect for $We_g < 300$.

Based on Rayleigh breakup of ligaments (similar to a non-turbulent liquid jet injected into a cross airflow), Lee et al. [65] assumed that the SMD of drops formed by ligaments breakup is proportional to the corresponding ligaments diameter, and proposed the following correlation for the size of droplets after the turbulent primary breakup.

$$\frac{SMD}{\Lambda} = 0.56\left[\frac{z}{\left(\Lambda We_{L\Lambda}^{1/2}\right)}\right]^{0.5} \tag{2-23}$$

Following the aforementioned studies of turbulent liquid jet, Osta and Sallam [60] studied the effect of nozzle geometry (length/diameter ratio, L/d_j, and the inlet curvature, R/d_j) on the ligaments diameter along the upwind surface of a liquid jet and reported that longer L/d_j nozzle produces larger-sized ligaments. They proposed a correlation which has the following form:

$$\frac{d_l}{\Lambda} \sim \left(\frac{1}{C_1}\right)\left[\frac{z}{\left(\Lambda We_{L\Lambda}^{1/2}\right)}\right]^{\frac{1}{C_2}} \tag{2-24}$$

where C_1 and C_2 are obtained experimentally and found to depend on L/d_j and R/d_j.

The velocity of droplets disintegrated from liquid jet surface as a result of the turbulent primary breakup is reported in several published studies [58,60,61,65]. Similar to Sallam et al. [28], Lee et al. [65] performed measurements closer to the ligaments tip in order to minimize the effect of droplet velocity relaxation to the ambient velocity. Two correlations for the components of drops velocity in the liquid jet streamwise direction, v_p, and cross airflow direction, u_p, are proposed [65] as follows:

$$\frac{v_p}{v_j} = 0.75 \tag{2-25}$$

$$\frac{u_p(\rho_j/\rho_g)^{\frac{1}{2}}}{u_g} = 4.82 \quad (2\text{-}26)$$

Lee et al. [65] asserted that, similar to the findings of Sallam et al. [28] for a non-turbulent liquid jet, the effect of cross airflow causes v_p component to decrease below of the jet velocity (see Eq. 2-25), and u_p component to increase significantly above crossflow velocity (see Eq. 2-26). Following the approach of Sallam et al. [28] for finding droplets formation rate of a non-turbulent liquid jet in a cross airflow, Lee et al. [65] measured the flux of liquid drops due to turbulent primary breakup along the liquid surface and proposed a correlation for surface efficiency factor, ε, as follows:

$$\varepsilon = 7.76 \times 10^{-4} \exp\left(\frac{5.5z}{z_b}\right) \quad (2\text{-}27)$$

It should be noted that in order for Lee et al. [65] to compare their results with those of Sallam et al. [28], they employed (Eq. (2-27)) a non-turbulent breakup length (z_b similar to Eq. (2-21)) instead of the turbulent breakup length which is shorter [65]. They reported that their measured ε for a round liquid jet agrees well with earlier results of non-turbulent liquid jet [28], with a smaller value of ε at the onset of breakup but approaches unity towards the end of the liquid column. However, they demonstrated that ε started at a smaller z/z_b for a turbulent liquid jet compared to a non-turbulent jet. This is because turbulence precipitates the onset of breakup of a turbulent liquid jet closer to the jet exit.

The literature reviewed above revealed that the diameter of ligaments and droplets generated along the liquid column is a function of v_j, liquid properties, integral length scale of the flow field and jet diameter (Eqs. 2-22 and 2-23). It also depends on z where for a turbulent liquid jet in a cross airflow, similar to a nonturbulent jet, larger size ligaments and drops form as the distance from the

nozzle exit increases in the liquid jet streamwise direction. Furthermore, similar to a nonturbulent jet, droplets velocity after breakup is independent of diameter for turbulent breakup regime (Eqs. 2-25 and 2-26). Similarly, droplets formation rate can be correlated with the dimensionless length along the liquid column (Eq. 2-27), but with a higher rate compared to that of nonturbulent breakup owing to the effect of turbulence. Similar to a nonturbulent jet, details about the features of droplets disintegrated along a turbulent liquid column in a cross airflow have been obtained experimentally by Sallam and co-workers [58,60,61,65]. Finally, although features of droplets from a turbulent liquid jet have been documented experimentally using two-dimensional images, three-dimensional high-fidelity simulations are still required.

2.6.2. Liquid jet's far-field region

Droplets generated via secondary breakup are of great importance to the process of liquid fuel atomization. It is important to mention that although a well distributed and finely dispersed spray in the far-field region is often desired in the majority of engineering applications (e.g., [131]), a non-uniform droplets distribution is also advantageous in some other applications (e.g., [132]).

Experimental measurements of droplets size distribution downstream of the liquid column showed its dependency on the velocity of cross airflow, u_g [34,36,40,41,46,74,131,133–138]. Gas Weber number, We_g, is used in different studies [40,136–138] to account for the effect of both gas inertia and liquid surface tension. Several studies examined the distribution of droplets as a function of the jet downstream location in addition to gas Weber number. These studies [40,136–138] asserted that, in general, at low We_g (i.e., where the dominant primary breakup mode is column breakup), droplets size reaches its maximum at the outer periphery of spray plume where larger droplets prevail. This is attributed to their higher momentum and longer velocity relaxation time which

consequently make them penetrate farther into cross airflow. At high We_g (i.e., where the surface breakup tends to dominant), however, droplets size reaches its maximum in the core region as even larger droplets cannot penetrate farther down due to greater aerodynamic force of cross airflow. In essence, surface breakup produces smaller droplets during the primary breakup, as opposed to droplets generated by column breakup process which easily follow cross airflow. Nonetheless, Lubarsky et al. [138] showed a double peak distribution of droplets size downstream of a liquid jet at low We_g ($We_g \sim 33$), which suggeste the existence of a multimode breakup process.

Ingebo and Foster [133], and Ingebo [134] are the first to describe the effect of column wavelength on droplets features. They observed that short wave-length disturbances near the nozzle exit produce relatively small droplets, whereas long wave-length disturbances farther down in cross airflow produce relatively large droplets. Ingebo [133,134] correlated drops mean size, defined by Sauter Mean Diameter (SMD or d_{32}), with gas Weber, Reynolds number, and a pressure sensitive dimensionless group gl/c^2 (where g is the acceleration due to gravity, l is the mean free molecular path, and c stands for root-mean-square molecular velocity). Nonetheless, Less and Schetz [135] asserted that since Ingebo and Foster [133] tested only high momentum flux ratio, q, conditions, droplets' mean diameter is determined independently of q and v_j. Consequently, Less and Schetz [135] included v_j in their proposed relation of SMD (see Table 8). Similarly, Tambe et al. [41] reported that surface breakup intensifies with increasing q, which in turn results in smaller SMD. Becker and Hassa [36] reported that the influence of cross airflow velocity is much weaker at high pressure than at atmospheric test conditions, which implies a lack of a strong correlation between droplets size and We_g at high pressure test conditions. Farvardin et al. [74] studied the effect of liquid viscosity on droplets size downstream of a nozzle with a diameter of 0.5 mm and reported that droplets size distribution attained similarity at 50 mm, which is attributed to the fact that

droplets become very fine at this flow location and hence not subjected to further secondary breakup. Song et al. [46] employed We_g, the ratio of Re_j/Re_g (or q), and liquid/gas density and viscosity ratio to account for the surroundings air pressure and liquid properties in order to develop a relation for predicting the mean size of drops/spray. Published correlations of the mean diameter of droplets in the far-field region for a liquid jet injected into a subsonic cross airflow are summarized in Table 2-8.

Table 2-8: Correlations of the mean diameter of droplets in the far-field region for a liquid jet injected into a subsonic cross airflow.

Column breakup height correlations	Reference
$d_{30} = 3.9\, d_j \left(We_g/Re_g\right)^{0.25}$	Ingebo and Foster [133]
$d_j/d_{32} = 1.4\left(We_g Re_g\right)^{0.4} (gl/\bar{c}^2)^{0.15} \;\; for\; We_g Re_g > 10^6$	Ingebo [134]
$d_{32}(microns) = 3500\left(\mu_j \sigma/u_g\, v_j\right)^{0.2}\left(1/\rho_j\right)^{1.4}\; (cgs\; units)$	Less and Schetz [135]
$d_{32}/\, d_j$ $= 1.015$ $\times 10^{19} {Re_g}^{-3.5998} {Re_j}^{-1.8094} {We_g}^{2.2474}\left(x/\, d_j\right)^{-0.6867}\left(y/\, d_j\right)^{1.9718}$	Kihm at al. [40]
$d_j/d_{32} = 0.267 {We_g}^{0.44} q^{0.08}\left(\rho_j/\rho_g\right)^{0.30}\left(\mu_j/\mu_g\right)^{-0.16}$	Song et al. [46]

There exists two factors which affect droplets velocity distribution downstream of a liquid jet injected into a cross airflow. The first one is the flow wake region caused by the presence of liquid column, and the second is the droplets size. The interplay between these two factors defines the distribution of droplets velocity [103]. Regarding the first factor, several studies reported a lower-velocity region in the spray wake behind the liquid jet but peaks at the outer and inner periphery of the jet [41,74,136,137,139]. The wake region, hence, is used as an indication of the level of momentum exchange between liquid column and cross airflow [137]. Mashayek et al. [103] stated

that the effect of liquid column on the flow diminishes with increasing liquid jet streamwise distance, z, due to the column breakup. This, therefore, leads to a more direct momentum exchange between droplets and the cross airflow, and thus the acceleration of droplets. As for the second factor (droplets size), the size and velocity profiles generally show that (see, e.g., [103]) the larger are the droplets, the slower they move downstream. For instance, Pontus et al. [131] depicted a relationship between droplets size and velocity at several planes downstream of the nozzle exit into cross airflow. They reported that larger droplets exhibited slower velocity, and the velocity-size relationship seemed to be fully established farther downstream into cross airflow. Similar to size distribution, droplets velocity downstream of a liquid jet in a cross airflow is a function of u_g (or We_g) [41,136–138]. Elshamy et al. [139] attributed the variation in the velocity distribution of droplets to the change of We_g. In fact, liquid jet breakup regime shifts from column to surface breakup as We_g increases. This results in the variation of the size and velocity distribution of droplets. Lubarsky et al. [138] studied droplets velocity components at different We_g. They reported that the velocity of droplets in the cross airflow streamwise direction showed a considerable lag with respect to the incoming airflow's mean velocity, especially within the core of spray. They noted that the absolute value of the velocity lag is directly proportional to We_g. This observation is confirmed by Mashayek et al. [103] who asserted that it takes longer distance for droplets to merge into the gas stream velocity for larger u_g. The findings of Lubarsky et al. [138] also corroborate previous studies, in that larger droplets form at low We_g and penetrate farther away from the nozzle exit with a higher liquid jet streamwise velocity; while smaller droplets form at high We_g and closely follow the jet flow within the core of spray and then shifts back towards the nozzle exit as spray bends due to vortex flow.

The momentum flux, q, plays a key role on the velocity distribution of the secondary droplets downstream of a liquid jet where it is a dominant factor in defining the deflection, penetration and disintegration height of a liquid jet in a cross airflow [103]. Inamura et al. [136] asserted that the minimum droplets velocity decreases with increasing q. This might be due to the increase of the level of momentum exchange between liquid column and cross airflow (larger wake region), as Inamura et al. [136] mentioned that the location where droplets velocity reaches its minimum resides farther away from the nozzle exit in the liquid jet streamwise direction. Inamura et al. [136] indicated that the minimum droplets velocity increases rapidly downstream of the nozzle exit which consequently leads to a more uniform distribution of droplets velocity; whereas it is less uniform in the vicinity of the liquid nozzle exit. Mashayek et al. [103] also observed the same behavior and noted that the velocity profile of droplets velocity becomes more uniform farther down into the cross airflow streamwise direction. Elshamy et al. [139] examined the effect of the pressure of cross airflow and reported that, for lower Stokes number (this number determines how quickly droplets can respond to the change in the surroundings air velocity), droplets follow airstream more quickly and more closely. Elshamy et al. [139] found that the Stokes number of a droplet is inversely proportional to the square root of the air density (pressure), and thus the droplets normalized velocity has more uniform distribution at higher ambient pressures. Farverdin et al. [74] examined experimentally the effect of liquid viscosity on droplets velocity and reported an increased jet bending in the near-field region (liquid column) due to an increase in liquid viscosity which results in less momentum residue for carrying droplets, and hence a decrease in the velocity of droplets. Farvardin and Dolatabadi [98], via an Eulerian approach, coupled Large Eddy Simulation (LES) with a Volume Of Fluid (VOF) simulation and reported the same downward trends of droplets velocity with increasing liquid viscosity.

Several numerical simulations studies are performed to gain knowledge on droplets' features in the far-field region. For instance, Khosla et al. [140] used an Eulerian approach to develop an atomization model for liquid jet in a crossflow using a high fidelity Volume Of Fluid (VOF) simulation. They developed several expressions of size, velocity and mass flux of droplets generated via the primary breakup, and also size and mass shedding of droplets due to the secondary breakup. They validated their numerical simulation of volume flux and SMD of droplets in the far-field region using the experimental data reported in [36,137]. Liu et al. [105] employed a Lagrangian approach to model the breakup of the injection of a single droplet in a cross airflow. In another investigation, Liu et al. [141] employed a Lagrangian approach to examine the effect of cross airflow on the behavior of a liquid jet where they considered the injection of successive droplets into a cross airflow and employed a modified drop drag coefficient. Their numerical drops size distribution showed a qualitative agreement with the experimental results of Kihm et al. [40]. Similar approach has been adopted in the literature to predict droplets features in the far-field region (e.g., [33–35,102,103,142]). These numerical studies were able to qualitatively capture the main spray features such as droplets size and velocity distribution by employing submodels for droplets stripping including Taylor analogy breakup (TAB), boundary layer stripping (BLS), Rayleigh-Taylor, and Kelvin-Helmholtz (K-H) wave model. A summary of the models developed in these studies is available in Ref. [103].

Overall, these reviewed studies above showed that We_g, q, and liquid/gas properties are important for predicting droplets features/characteristics in the far-field region. Liquid jet breakup regime can change with We_g, and hence droplets size and velocity. Increasing q has two distinct effects on the size of droplets; it can change the breakup regime (see Fig. 2-3), or increase the column breakup height (see section 2.5.2). This consequently results in an increased length of the liquid

column and hence the generation of finer drops via surface breakup. q affects droplets velocity, as it has direct effect on the mode of breakup regime and also the wake region and hence the momentum exchange between the cross airflow and droplets. Clearly additional high fidelity simulations are needed to shed more light on the effect of, for example, gas and liquid properties on droplets' features/characteristics in the far-field.

2.6.3. Concluding remarks on droplets features and formation mechanisms

It is concluded that the characteristics of droplets disintegrated during the primary breakup are not significantly affected by the velocity of cross airflow. However, they are influenced by the nozzle exit conditions such as turbulence. On the hand, further studies are needed to unravel the role of cavitation (nozzle internal geometry). The size of ligaments and droplets formed by both nonturbulent and turbulent primary breakup increases along a liquid jet streamwise direction. Droplets velocity is independent of the size. However, the characteristics/features of droplets produced via the secondary breakup dependent strongly on the velocity of cross airflow, and there is a clear relationship between droplets size and their velocity.

There is a reasonable literature on ligaments diameter and droplets size and velocity generated by the primary breakup for both non-turbulent [28,49,58,127] and turbulent [58,60,61,65] liquid jet injected into a cross airflow at STP test conditions. On the other hand, studies on the effect of HTP on the properties of liquid jet surface and accordingly the characteristics of disintegrated droplets are still lacking. Due to the discrepancies between the experimental data [28] and numerical results [72] for the velocity distribution of such droplets and their formation rate, three-dimensional high-fidelity simulations and high resolution images are required.

The characteristics of droplets formed by the secondary breakup have been investigated quite extensively at STP test conditions. There exist also a few studies at standard temperature and high pressure (STHP) test conditions [36,46]. Heat transfer between the liquid and gaseous phase at high temperature test conditions (which involves evaporation) certainly affects droplets size and consequently their velocity in the far-field region [143]. This, in turn, would influence the mixing characteristics between spray droplets and cross airflow. Thus, further studies are needed to understand the mechanism of two-phase interaction under more practical (HTP) test conditions.

2.7. Final concluding remarks and recommendations for future research

This review paper seeks to provide an overview as well as detailed analysis of the physical phenomena that dominate the primary breakup regimes, trajectory and penetration, column breakup (fracture) length, and droplets formation of a liquid jet injected transversely into a subsonic gaseous crossflow. Owing to the importance of this complex two-phase flow-field, numerous investigations have been reported in recent decades. Although, a wealth of knowledge has been acquired, there still exist discrepancies among the predictions/findings due to several factors, such as flow-field status (e.g., cavitation, turbulence), liquid properties (e.g., role of density, viscosity and surface tension), test/operating conditions (temperature and pressure conditions), liquid injector/nozzle internal geometry (e.g., discharge coefficient effect), injection angle (forward or reverse), experimental errors and uncertainties involved in developing correlations. This overview, therefore, classified published results and findings based on their pertaining conditions using non-dimensional numbers. Overall, the literature revealed that gas Weber number, We_g, plays a crucial role in defining non-turbulent primary breakup regimes, while liquid jet Weber number, We_j, is of great importance for the transition to turbulent primary

breakup. Jet-to-crossflow momentum flux ratio, q, is the most important/dominant parameter for predicting the trajectory, penetration, and breakup length of a liquid jet in a crossflow. While the characteristics of droplets disintegrated during the primary breakup are influenced by nozzle exit conditions, the features of droplets produced via the secondary breakup dependent strongly on the velocity of cross airflow. However, in order to develop comprehensive understanding of the physical features of a liquid jet in a gaseous crossflow with respect to different liquid properties at different test conditions and nozzle/injector geometry, other controlling non-dimensional parameters, such as jet Reynolds number, Re_j, gas Reynolds number, Re_g, density ratio, ρ_j/ρ_g, viscosity ratio, μ_j/μ_g, Ohnesorge number, Oh, and Bond number, Bo, as well as the effect of initial injection angle and nozzle geometry should not be overlooked. The degree of the importance of each of these parameters depends on the specific conditions of the problem at hand.

Although substantial progress has been made, several challenges and shortcomings remain unresolved. For instance, Mazallon et al. [27] quoted the long ligaments regime presents significant experimental difficulties due to the problem of tracking flow behavior when ligaments are long. Moreover, the effect of viscous forces on the characteristics of a transverse liquid jet and the role of Ohnesorge number and/or jet Reynold number of viscous fluids on the primary breakup regime, turbulent structures, and jet trajectories all still require further investigations. For example, Farvardin et al. [74] reported that increasing liquid viscosity causes jet trajectory to bend more, while Birouk et al. [84], who tested relatively more viscous liquids, reported the opposite scenario, that is an increase in liquid jet trajectory with viscosity. It is worth mentioning that investigating viscous liquids is of great importance, as liquid biofuels such as vegetable oils, which have relatively high viscosity, are gaining more ground as an important source of energy for power generation. Another application of viscous liquids concerns the injection of lubricating oil into a

rotating annular airflow in the cavity of aero-engine bearing chamber [48,51]. Several atomization methods can be used to improve spray properties of viscous liquid jets in order to produce a more uniform distribution of finer droplets, which includ preheating liquid jet [144], employing electrostatic injection method [145], using swirl atomizers [146], effervescent atomizers and flow-blurring injectors [147]. Furthermore, knowledge on the effect of test conditions (e.g., injecting liquid jet into a high temperature and pressure crossflow, which is practically more relevant) on the primary breakup regimes, turbulent structures, trajectory and penetration, and breakup length of a transverse liquid jet is still less established. For instance, there is lack of experimental investigations on the effect of high pressure and temperature on turbulent primary breakup and its corresponding aerodynamic/turbulent transition criterion of a liquid jet in a gaseous crossflow. In fact, all published experimental studies on this phenomenon are limited to room test conditions [57–59,62,63]. In addition, as is depicted in Fig. 2-19, Eslamian et al. [30] reported that surface breakup regime is initiated at lower q and We_g under both high temperature and high pressure test conditions, while Song et al. [46] stated that column/surface breakup transition borderline shifts towards higher q and We_g when increasing cross airflow pressure. The effect of density and viscosity ratios on liquid jet trajectory in the near- and/or far-field regions or both together would be helpful to reach a comprehensive understanding, even though studying the near-field region is experimentally challenging due to high drops density around jet column. Several studies used different imaging diagnostics such as shadowgraph, Mie scattering, PIV, and PDA techniques to examine some features of a transverse liquid jet. These imaging methods are useful for determining the primary breakup regimes, trajectory and penetration depth, column breakup length, and droplet features in the dilute region (see, e.g., [36,139,148]). Imaging sensor (e.g., high speed camera), however, has limited spatial resolution particularly in optically dense regions due to noise from

multiply-scattered light [71]. Nonetheless, only a few studies used pulsed holography [28,65] and ballistic imaging [149,150] techniques to acquire more details of the evolution of liquid column surface and droplets formation as a result of surface breakup in the primary breakup region (dense region). More information about experimental imaging techniques employed in the optically dense regions of a spray can be found in a recent review paper by Linne [151]. Because of the limitations of experiments in resolving the spatiotemporal evolution of the near-field region, numerical studies such as direct numerical simulations based on interface tracking/capturing methods would be invaluable in this case. Nonetheless, it should be mentioned that, computationally, it remains challenging to resolve the wide range of spatial and temporal scales involved and to properly account for the large variation of density across a liquid-gas interface [72]. Furthermore, while there exist several studies which examined the effect of the thickness of non-uniform velocity field in the gas boundary layer on a test section walls on the features of a transverse liquid jet by employing recessed [94], or protruded [67] jets instead of flush type, and also by using a shock tube facility [28] instead of a wind tunnel, the effect of gas boundary layer on the features of a transverse liquid jet still require further investigations. In addition, while there exist a large body of studies available in the literature which used a uniform velocity of a cross airflow with a weak turbulence intensity in the near-wall boundary layer region of a test section, and also there exist investigations on the effect of a liquid jet injected transversely into a swirling crossflow [152,153], more studies are required to examine the effect of the characteristics of a turbulent cross airflow (e.g., turbulence intensity and turbulent length scales) on the features of a transverse liquid jet.

2.8. References

[1] Karagozian AR. Transverse jets and their control. Prog Energy Combust Sci 2010;36:531–53.

[2] Mahesh K. The interaction of jets with crossflow. Annu Rev Fluid Mech 2013;45:379–407.

[3] Margason R. Fifty years of jet in crossflow research. AGARD-CP 534, 1993.

[4] Ekkad S V, Ou S, Rivir RB. Effect of jet pulsation and duty cycle on film cooling from a single jet on a leading edge model. J Turbomach 2006;128:564.

[5] Cerri G, Giovannelli A, Battisti L, Fedrizzi R. Advances in effusive cooling techniques of gas turbines. Appl Therm Eng 2007;27:692–8.

[6] Desantes JM, Arrègle J, López JJ, García JM. Turbulent gas jets and diesel-like sprays in a crossflow: A study on axis deflection and air entrainment. Fuel 2006;85:2120–32.

[7] Padala S, Le MK, Kook S, Hawkes ER. Imaging diagnostics of ethanol port fuel injection sprays for automobile engine applications. Appl Therm Eng 2013;52:24–37.

[8] Guo M, Kishi R, Shi B, Ogata Y, Nishida K. Effects of cross-flow on fuel spray injected by hole-type injector for direct injection gasoline engine. At Sprays 2015;25:81–98.

[9] Bellofiore A, Cavaliere A, Ragucci R. Air density effect on the atomization of liquid jets in crossflow. Combust Sci Technol 2007.

[10] Vermeulen PJ, Grabinski P, Ramesh V. Mixing of an acoustically excited air jet with a confined hot crossflow. J Eng Gas Turbines Power 1992;114:46.

[11] Bowman CT. Control of combustion-generated nitrogen oxide emissions: Technology driven by regulation. Symp Combust 1992;24:859–78.

[12] Heister SD, Nguyen T, Karagozian AR. Modeling of liquid jets injected transversely into a supersonic crossflow. AIAA J 1989;27:1727–34.

[13] Nguyen T, Karagozian AR. Liquid fuel jet in subsonic crossflow. J Propuls Power 1992;8:21–9.

[14] Karagozian AR. The jet in crossflow. Phys Fluids 2014;26:101303.

[15] Getsinger DR, Gevorkyan L, Smith OI, Karagozian AR. Structural and stability characteristics of jets in crossflow. J Fluid Mech 2014;760:342–67.

[16] Fric TF, Roshko A. Vortical structure in the wake of a transverse jet. J Fluid Mech 1994;279:1–47.

[17] Kelso RM, Lim TT, Perry AE. An experimental study of round jets in cross-flow. J Fluid Mech 1996;306:111–44.

[18] Muppidi S, Mahesh K. Direct numerical simulation of round turbulent jets in crossflow. J Fluid Mech 2007;574:59–84.

[19] Broadwell JE, Breidenthal RE. Structure and mixing of a transverse jet in incompressible flow. J Fluid Mech 1984;148:405–12.

[20] Karagozian AR. An analytical model for the vorticity associated with a transverse jet. AIAA J 1986;24:429–36.

[21] Hasselbrink EF, Mungal MG. Transverse jets and jet flames. Part 1. Scaling laws for strong transverse jets. J Fluid Mech 2001;443:1–25.

[22] Hasselbrink EF, Mungal MG. Transverse jets and jet flames. Part 2. Velocity and OH field imaging. J Fluid Mech 2001;443:27–68.

[23] Muppidi S, Mahesh K. Study of trajectories of jets in crossflow using direct numerical simulations. J Fluid Mech 2005;530:81–100.

[24] Birouk M, Lekic N. Liquid jet breakup in quiescent atmosphere: A review. At Sprays 2009;19:501–28.

[25] Behzad M, Ashgriz N, Mashayek A. Azimuthal shear instability of a liquid jet injected into a gaseous cross-flow. J Fluid Mech 2015;767:146–72.

[26] Wu P-K, Kirkendall KA, Fuller RP, Nejad AS. Breakup processes of liquid jets in subsonic crossflows. J Propuls Power 1997;13:64–73.

[27] Mazallon J, Dai Z, Faeth GM. Primary breakup of nonturbulent round liquid jets in gas crossflows. At Sprays 1999;9:291–312.

[28] Sallam KA, Aalburg C, Faeth GM. Breakup of round nonturbulent liquid jets in gaseous crossflow. AIAA J 2004;42:2529–40.

[29] Schetz JA, Padhye A. Penetration and breakup of liquids in subsonic airstreams. AIAA J 1977;15:1385–90.

[30] Eslamian M, Amighi A, Ashgriz N. Atomization of liquid jet in high-pressure and high-temperature subsonic crossflow. AIAA J 2014;52:1374–85.

[31] Bolszo CD, McDonell VG, Gomez GA, Samuelsen GS. Injection of water-in-oil emulsion jets into a subsonic crossflow: An experimental study. At Sprays 2014;24:303–48.

[32] Liu AB, Reitz RD. Mechanisms of air-assisted liquid atomization. At Sprays 1993;3:55–75.

[33] Madabhushi RK. A model for numerical simulation of breakup of a liquid jet in crossflow. At Sprays 2003;13:413–24.

[34] Rachner M, Becker J, Hassa C, Doerr T. Modelling of the atomization of a plain liquid fuel jet in crossflow at gas turbine conditions. Aerosp Sci Technol 2002;6:495–506.

[35] Khosla S, Crocker DS. CFD modeling of the atomization of plain liquid jets in cross flow for gas turbine applications. Vol. 1 Turbo Expo 2004, ASME; 2004, p. 797–806.

[36] Becker J, Hassa C. Breakup and atomization of a kerosene jet in crossflow at elevated pressure. At Sprays 2002;12:49–68.

[37] Wang M, Broumand M, Birouk M. Liquid jet trajectory in a subsonic gaseous cross-flow: an analysis of published correlations. At Sprays 2016:accepted for publication.

[38] Mashayek A, Ashgriz N. Atomization of a liquid jet in a crossflow. Handb. At., Springer ScienceþBusiness Media, LLC; 2011, p. 657–83.

[39] Scharfman BE, Bush JWM, Techet, H. A. Hydrodynamic instabilities in round liquid jets in gaseous crossow. ILASS Am. 25th Annu. Conf. Liq. At. Spray Syst., Pittsburgh, PA: 2013.

[40] Kihm KD, Lyn GM, Sun SY. Atomization of cross-injecting sprays into convective air stream. At Sprays 1995;5:417–33.

[41] Tambe S, Jeng S, Mongia H, Hsiao G. Liquid Jets in Subsonic Crossflow. 43rd AIAA Aerosp. Sci. Meet. Exhib. - Meet. Pap., Reno, Nevada: 2005.

[42] Wu P-K, Miranda RF, Faeth GM. Effects of initial flow conditions on primary breakup of nonturbulent and turbulent liquid jets. At Sprays 1995;5:175–96.

[43] Elshamy O, Jeng SM. Study of liquid jet in crossflow at elevated ambient pressures. ILASS Am., Irvine, CA: 2005.

[44] Lakhamraju R, Jeng SM. Liquid jet breakup in subsonic air stream at elevated temperatures. ILASS Am., Irvine, CA: 2005.

[45] Brown C, McDonell V. Near field behavior of a liquid jet in a crossflow. ILASS Am., Toronto, Canada: 2006.

[46] Song J, Cary Cain C, Guen Lee J. Liquid jets in subsonic air crossflow at elevated pressure. J Eng Gas Turbines Power 2014;137:041502.

[47] Vich G, Ledoux M. Investigation of a liquid jet in a subsonic cross-flow. Int J Fluid Mech Res 1997;24:1–12.

[48] Birouk M, Azzopardi BJ, Stäbler T. Primary break-up of a viscous liquid jet in a cross airflow. Part Part Syst Charact 2003;20:283–9.

[49] Ng C-L, Sankarakrishnan R, Sallam KA. Bag breakup of nonturbulent liquid jets in crossflow. Int J Multiph Flow 2008;34:241–59.

[50] Madabhushi RK, Leong MY, Arienti M, Brown CT, McDonell VG. On the breakup regime map of liquid jet in crossflow. ILASS Am. 19th Annu. Conf. Liq. At. Spray Syst., Toronto, Canada: 2006.

[51] Birouk M, Stäbler T, Azzopardi BJ. An experimental study of liquid jets interacting with cross airflows. Part Part Syst Charact 2003;20:39–46.

[52] Hinze JO. Fundamentals of the hydrodynamic mechanism of splitting in dispersion processes. AIChE J 1955;1:289–95.

[53] Dai Z, Chou W-H, Faeth GM. Drop formation due to turbulent primary breakup at the free surface of plane liquid wall jets. Phys Fluids 1998;10:1147.

[54] Lienhard JH. Velocity Coefficients For Free Jets From Sharp-Edged Orifices. J Fluids Eng 1984;106:13.

[55] Hsiang L-P, Faeth GM. Drop deformation and breakup due to shock wave and steady disturbances. Int J Multiph Flow 1995;21:545–60.

[56] Aalburg C, van Leer B, Faeth GM, Sallam KA. Properties of nonturbulent round liquid jets in uniform gaseous cross flows. At Sprays 2005;15:271–94.

[57] Fuller RP, Wu P-K, Kirkendall KA, Nejad AS. Effects of injection angle on atomization of liquid jets in transverse airflow. AIAA J 2000;38:64–72.

[58] Sallam K, Ng C, Sankarakrishnan R, Aalburg C, Lee K. Breakup of turbulent and non-turbulent liquid jets in gaseous crossflows. 44th AIAA Aerosp. Sci. Meet. Exhib., American Institute of Aeronautics and Astronautics; 2006.

[59] Osta A, Sallam K. Effect of nozzle length/diameter ratio on the breakup of round liquid jets in crossflow. 46th AIAA Aerosp. Sci. Meet. Exhib., American Institute of Aeronautics and

Astronautics; 2008.

[60] Osta AR, Sallam KA. Nozzle-geometry effects on upwind-surface properties of turbulent liquid jets in gaseous crossflow. J Propuls Power 2010;26:936–46.

[61] Aalburg C, Faeth GM, Sallam K. Primary breakup of round turbulent liquid jets in uniform gaseous crossflows. 43rd AIAA Aerosp. Sci. Meet. Exhib., Reno, Nevada: American Institute of Aeronautics and Astronautics; 2005.

[62] Wu P-K, Faeth GM. Aerodynamic effects on primary breakup of turbulent liquids. At Sprays 1993;3:265–89.

[63] Sankarakrishnan R, Sallam KA, Chambers FW. Effects of turbulence on the breakup of round liquid jets in gaseous crossflow. Vol. 2 Fora, vol. 2005, ASME; 2005, p. 281–5.

[64] Prakash RS, Sinha A, Raghunandan BN, Tomar G, Ravikrishna R V. Challenges and opportunities breakup of volatile liquid jet in hot cross flow. Procedia IUTAM 2015;15:18–25.

[65] Lee K, Aalburg C, Diez FJ, Faeth GM, Sallam KA. Primary breakup of turbulent round liquid jets in uniform crossflows. AIAA J 2007;45:1907–16.

[66] McCarthy MJ, Molloy NA. Review of stability of liquid jets and the influence of nozzle design. Chem Eng J 1974;7:1–20.

[67] Zheng Y, Marshall AW. Charactrization of the initial spray from low-Weber-number jets in crossflow. At Sprays 2011;21:575–89.

[68] Lin SP, Reitz RD. Drop and spray formation from a liquid jet. Annu Rev Fluid Mech 1998;30:85–105.

[69] Ng C-L, Sallam KA, Metwally HM, Aalburg C. Deformation and surface waves properties of round nonturbulent liquid jets in gaseous crossflow. ASME 2005 Fluids Eng. Div. Summer Meet., Houston, Texas, USA: 2005, p. 293–7.

[70] Pai MG, Pitsch H, Desjardins O. Detailed numerical simulations of primary atomization of liquid jets in crossflow. 47th AIAA Aerosp. Sci. Meet. Incl. New Horizons Forum Aerosp. Expo., Orlando, Florida: 2009.

[71] Sedarsky D, Paciaroni M, Berrocal E, Petterson P, Zelina J, Gord J, et al. Model validation image data for breakup of a liquid jet in crossflow: part I. Exp Fluids 2010;49:391–408.

[72] Li X, Soteriou MC. High-fidelity Simulation of high density-ratio liquid jet atomization in crossflow with experimental validation. ILASS Am. 26th Annu. Conf. Liq. At. Spray Syst., Portland, OR: 2014.

[73] Xiao F, Dianat M, McGuirk JJ. Large eddy simulation of liquid-jet primary breakup in air crossflow. AIAA J 2013;51:2878–93.

[74] Farvardin E, Johnson M, Alaee H, Martinez A, Dolatabadi A. Comparative study of biodiesel and diesel jets in gaseous crossflow. J Propuls Power 2013;29:1292–302.

[75] Wang S, Huang Y, Liu ZL. Theoretical analysis of surface waves on a round liquid jet in gaseous crossflow. At Sprays 2014;24:23–40.

[76] Broumand M, Birouk M. A model for predicting the trajectory of a liquid jet in a subsonic gaseous crossflow. At Sprays 2015;25:871–93.

[77] Herrmann M, Arienti M, Soteriou M. The impact of density ratio on the liquid core dynamics of a turbulent liquid jet injected into a crossflow. J Eng Gas Turbines Power 2011;133:061501.

[78] Wu P-K, Kirkendall KA, Fuller RP, Gruber MR, Nejad AS. Spray trajectories of liquid fuel jets in subsonic crossflows. Int J Fluid Mech Res 1997;24:128–37.

[79] Lin CK, Kennedy JP, Jackson TA. A review on penetration heights of transverse liquid jets in high-speed flows. 15th Annu. Conf. Liq. At. Spray Syst., n.d., p. 345–9.

[80] Stenzler J, Lee J, Santavicca D. Penetration of liquid jets in a crossflow. 41st Aerosp. Sci. Meet. Exhib., American Institute of Aeronautics and Astronautics; 2003.

[81] Ahn K, Kim J, Yoon Y. Effects of orifice internal flow on transverse injection into subsonic crossflows: Cavitation and hydraulic flip. At Sprays 2006;16:15–34.

[82] Iyogun CO, Birouk M, Popplewell N. Trajectory of water jet exposed to low subsonic cross-flow. At Sprays 2006;16:963–80.

[83] Stenzler JN, Lee JG, Santavicca DA, Lee W. Penetration of liquid jets in a cross-flow. At Sprays 2006;16:887–906.

[84] Birouk M, Iyogun CO, Popplewell N. Role of viscosity on trajectory of liquid jets in a cross-airflow. At Sprays 2007;17:267–87.

[85] Brown CT, Mondragon MU, McDonell G V. Investigation of the effect of injector discharge coefficient on penetration of a plain liquid jet into a subsonic crossflow. ILASS Am. 20th Annu. Conf. Liq. At. Spray Syst., 2007, p. 15–8.

[86] Thawley SM, Mondragon UM, Brown CT, Mcdonell VG. Evaluation of column breakpoint and trajectory for a plain liquid jet injected into a crossflow, 2008, p. 1–11.

[87] Wang Q, Mondragon UM, Brown CT, McDonell VG. Charactrization of trajectory, break point, and break point dynamics of a plain liquid jet in a crossflow. At Sprays 2011;21:203–19.

[88] Yoon HJ, Hong JG, Lee C-W. Correlations for penetration height of single and double liquid jets in cross flow under high-temperature conditions. At Sprays 2011;21:673–86.

[89] Ranger AA, Nicholls JA. Aerodynamic shattering of liquid drops. AIAA J 1969;7:285–90.

[90] Chryssakis C, Assanis D. A secondary atomization model for liquid droplet deformation and breakup under high weber number conditions. 18th Annu. Conf. Liq. At. Spray Syst., 2005.

[91] Ragucci R, Bellofiore A, Cavaliere A. Trajectory and momentum coherence breakdown of a liquid jet in high-density air cross-flow. At Sprays 2007;17:47–70.

[92] Freitag S, Hassa C. Spray Characterization of a kerosene jet in cross flow of air at elevated pressure. ILASS, Cologne, Germany: 2008.

[93] Lubarsky E, Shcherbik D, Bibik O, Gopala Y, Bennewitz JW, Zinn BT. Fuel jet in cross flow- experimental study of spray characteristics. 23rd Annu. Conf. Liq. At. Spray Syst., Ventura, Canada: 2011.

[94] Masuda BJ, Mcdonell VG. Penetration of a recessed distillate liquid jet into a crossflow at elevated pressure and temperature. Test, Kyto, Japan: 2006.

[95] Ragucci R, Bellofiore A, Cavaliere A. Breakup and breakdown of bent kerosene jets in gas turbine conditions. Proc Combust Inst 2007;31:2231–8.

[96] Li L, Lin Y, Xue X. Injection of liquid kerosene into a high-pressure subsonic air crossflow from normal temperature to elevated temperature. Proc. ASME Turbo Expo, Copenhagen, Denmark: 2012.

[97] Spyrou N, Choi D, Sadiki A, Janicka J. Large eddy simulation of the breakup of a kerosene jet in crossflow. 7th Int. Conf. Multiph. Flow, Tampa, Fl., USA: 2010.

[98] Farvardin E, Dolatabadi A. Simulation of biodiesel jet in cross flow. ICLASS 2012, 12th Trienn. Int. Conf. Liq. At. Spray Syst., Heidelberg, Germany: 2012.

[99] Herrmann M. Detailed numerical simulations of the primary atomization of a turbulent liquid jet in crossflow. Proc. ASME Turbo Expo 2009 Power Land, Sea Air, Orlando, USA: 2009.

[100] Herrmann M. Detailed numerical simulations of the primary atomization of a turbulent liquid jet in crossflow. ASME J Eng Gas Turbines Power 2010;132.

[101] Li X, Soteriou M. Prediction of high density-ratio liquid jet atomization in crossflow using high fidelity simulations on HPC. 50th AIAA Aerosp. Sci. Meet. Incl. New Horizons Forum Aerosp. Expo., American Institute of Aeronautics and Astronautics; 2012.

[102] Behzad M, Mashayek A, Ashgriz N. A KIVA-based model for liquid jet in cross flow. ILASS-Americas 22nd Annu. Conf. Liq. At. Spray Syst., Cincinnati, OH: 2010.

[103] Mashayek A, Behzad M, Ashgriz N. Multiple injector model for primary breakup of a liquid jet in crossflow. AIAA J 2011;49:2407–20.

[104] Broumand M, Farokhi M, Birouk M. Penetration height of a circular liquid jet in a subsonic gaseous crossflow: An Eulerian-Lagrangian approach. 54th AIAA Aerosp. Sci. Meet., American Institute of Aeronautics and Astronautics; 2016.

[105] Liu AB, Mather D, Reitz RD. Modeling the effects of drop drag and breakup on fuel sprays. SAE Pap 930072 1993.

[106] Mashayek A, Jafari A, Ashgriz N. A Model for the penetration of a liquid jet in crossflow. ILASS Am. 19th Annu. Conf. Liq. At. Spray Syst., Toronto, Canada: 2006.

[107] Mashayek A, Jafari A, N. Ashgriz. On the jet trajectory of a liquid jet in crossflow. ICLASS-2006, Kyoto, Japan: 2006.

[108] Mashayek A, Jafari A, Ashgriz N. A model for deformation of liquid jets and droplets subjected to gaseous flows. ILASS Am. 20th Annu. Conf. Liq. At. Spray Syst., Chicago, IL: 2007.

[109] Mashayek A, Jafari A, Ashgriz N. Improved model for the penetration of liquid jets in subsonic crossflows. AIAA J 2008;46:2674–86.

[110] Mashayek A, Ashgriz N. Model for deformation of drops and liquid jets in gaseous crossflows. AIAA J 2009;47:303–13.

[111] Marzbali SN, Dolatabadi A. Near-field trajectory of circular liquid jets injected into subsonic gaseous crossflow. 49th AIAA Aerosp. Sci. Meet. Incl. New Horizons Forum Aerosp. Expo., American Institute of Aeronautics and Astronautics; 2011.

[112] Broumand M, Birouk M. Two-zone model for predicting the trajectory of liquid jet in gaseous crossflow. AIAA J 2016;54:1499–511.

[113] Brown CT, Mondragon UM, McDonell VG. Liquid jet in crossflow: consideration of injector geometry and liquid physical properties. ILASS Am. 25th Annu. Conf. Liq. At. Spray Syst., Pittsburgh, PA: 2013.

[114] Ahn K, Kim J, Yoon Y. Effect of cavitation on transverse injection into subsonic crossflows. 39th AIAA/ASME/SAE/ASEE Jt. Propuls. Conf. Exhib., American Institute of Aeronautics and Astronautics; 2003.

[115] Inamura T, Nagai N, Hirai T, Asano H. Disintegration phenomena of metalized slurry fuel jets in high speed air stream. Proc. 5th Int. Conf. Liq. At. Spray Syst., Gaithersberg, MD, USA: 1991.

[116] Gopala Y, Lubarsky E, Zinn B. Liquid jet in crossflow-A novel method to locate the column breakup point. 46th AIAA Aerosp. Sci. Meet. Exhib., American Institute of Aeronautics and Astronautics; 2008.

[117] Costa M, Melo MJ, M. Sousa JM, Levy Y. Spray characteristics of angled liquid injection into subsonic crossflows. AIAA J 2006;44:646–53.

[118] Kim M-K, Song J, Hwang J, Yoon Y. Effects of canted injection angles on the spray characteristics of liquid jets in subsonic crossflows. At Sprays 2010;20:749–62.

[119] Birouk M, Nyantekyi-Kwakye B, Popplewell N. Effect of nozzle geometry on breakup length and trajectory of liquid jet in subsonic crossflow. At Sprays 2011;21:847–65.

[120] Lefebvre AH, Ballal DR. Gas Turbine Combustion - Aternative Fuels and Emissions. 3rd ed. FL, USA: CRC Press (Taylor Frances Group); 2010.

[121] Behzad M, Ashgriz N. An analysis of the surface breakup mechanism of a liquid jet in cross-flow. ICLASS 2012, 12th Trienn. Int. Conf. Liq. At. Spray Syst., Heidelberg, Germany: 2012.

[122] Behzad M, Ashgriz N, Mashayek A. Azimuthal shear instability of a liquid jet in gas crossflow. ILASS-Americas 25th Annu. Conf. Liq. At. Spray Syst., Pittsburgh, PA: 2013.

[123] Behzad M, Ashgriz N, Karney BW. Surface breakup of a non-turbulent liquid jet injected into a high pressure gaseous crossflow. Int J Multiph Flow 2016;80:100–17.

[124] Amini G, Dolatabadi A. Axis-switching and breakup of low-speed elliptic liquid jets. Int J Multiph Flow 2012;42:96–103.

[125] Amini G, Ihme M, Dolatabadi A. Effect of gravity on capillary instability of liquid jets. Phys Rev E 2013;87:53017.

[126] Amini G, Lv Y, Dolatabadi A, Ihme M. Instability of elliptic liquid jets: Temporal linear stability theory and experimental analysis. Phys Fluids 2014;26.

[127] Sallam K, Aalburg C, Faeth G. Primary breakup of round nonturbulent liquid jets in gaseous crossflows. 41st Aerosp. Sci. Meet. Exhib., American Institute of Aeronautics and Astronautics; 2003.

[128] Sallam KA, Faeth GM. Surface properties during primary breakup of turbulent liquid jets in still air. AIAA J 2003;41:1514–24.

[129] Chou W-H, Hsiang L-P, Faeth GM. Temporal properties of drop breakup in the shear breakup regime. Int J Multiph Flow 1997;23:651–69.

[130] Li X, Arienti M, Soteriou M, Sussman M. Towards an Efficient, High-Fidelity Methodology for Liquid Jet Atomization Computations. 48th AIAA Aerosp. Sci. Meet. Incl. New Horizons Forum Aerosp. Expo., American Institute of Aeronautics and Astronautics; 2010.

[131] Eriksson P, Orbay R, Klingmann J. Experimental investigations of a low Weber liquid spray in air cross flow. ICLASS-2006, Kyoto, Japan: 2006.

[132] Lefebvre AH. Atomization and Sprays. Hemisphere, New York: 1989.

[133] Ingebo RD, Foster H. Drop size distribution for cross-current break-up of liquid jets in air streams. 1957.

[134] Ingebo RD. Aerodynamic effect of combustor inlet air pressure on fuel jet atomization. J Propuls Power 1985;1:137–42.

[135] Less DM, Schetz JA. Transient behavior of liquid jets injected normal to a high-velocitygas stream. AIAA J 1986;24:1979–86.

[136] Inamura T, Nagai N. Spray characteristics of liquid jet traversing subsonic airstreams. J Propuls Power 1997;13:250–6.

[137] Wu P-K, Kirkendall KA, Fuller RP, Nejad AS. Spray structures of liquid jets atomized in subsonic crossflows. J Propuls Power 1998;14:173–82.

[138] Lubarsky E, Reichel JR, Zinn BT, McAmis R. Spray in crossflow: dependence on Weber number. J Eng Gas Turbines Power 2009;132:21501.

[139] Elshamy O, Tambe S, Cai J, Jeng S-M. PIV and LDV measurements for liquid jets in crossflow. 45th AIAA Aerosp. Sci. Meet. Exhib., American Institute of Aeronautics and Astronautics; 2007.

[140] Khosla S, Conley A, Smith CE. Towards a robust phenomenological turbulent jet-in-crossflow atomization model. ILASS Am. 20th Annu. Conf. Liq. At. Spray Syst., Chicago, IL: 2007.

[141] Liu F, Smallwood GJ, Gulder OL. Numerical study of breakup processes of water jet injected into a cross air flow. ICLASS 2000 Proc. Eighth Int. Conf. Liq. At. Spray Syst., Pasadena, CA: 2000.

[142] Madabhushi KR, Leong MY, Hautman DJ. Simulation of the break-up of a liquid jet in crossflow at atmospheric conditions. ASME Turbo Expo 2004 Power Land, Sea, Air, Vienna, Austria: 2004.

[143] Li X, Soteriou M, Arienti M, Sussman M. High-fidelity simulation of atomization and evaporation in a liquid jet in cross-flow. 49th AIAA Aerosp. Sci. Meet. Incl. New Horizons Forum Aerosp. Expo., American Institute of Aeronautics and Astronautics; 2011.

[144] Wiest HK, Heister SD. Experimental study of a heated liquid jet in a crossflow. 51st AIAA/SAE/ASEE Jt. Propuls. Conf., American Institute of Aeronautics and Astronautics; 2015.

[145] Malkawi G, Yarin AL, Mashayek F. Breakup mechanisms of electrostatic atomization of corn oil and diesel fuel. J Appl Phys 2010;108.

[146] Surya Prakash R, Gadgil H, Raghunandan BN. Breakup processes of pressure swirl spray in gaseous cross-flow. Int J Multiph Flow 2014;66:79–91.

[147] Jiang L, Agrawal AK. Investigation of glycerol atomization in the near-field of a flow-blurring injector using time-resolved PIV and high-speed visualization. Flow, Turbul Combust 2015;94:323–38.

[148] Bellofiore A, Cavaliere A, Ragucci R. PIV charactrization of sprays generated by crossflow injection in high-density airflow. 22nd Annu. Conf. Liq. At. Spray Syst. (ILASS-Europe), 2008, Como Lake, Italy: 2008.

[149] Linne MA, Paciaroni M, Gord JR, Meyer TR. Ballistic imaging of the liquid core for a steady jet in crossflow. Appl Opt 2005;44:6627–34.

[150] Sedarsky D, Paciaroni M, Zelina J, Linne M. Near field fluid structure analysis for jets in crossflow with ballistic imaging. ILASS Am. 20th Annu. Conf. Liq. At. Spray Syst., Chicago, IL: 2007.

[151] Linne M. Imaging in the optically dense regions of a spray: A review of developing techniques. Prog Energy Combust Sci 2013;39:403–40.

[152] Masuda BJ, McDonell VG, Oskam GW. Mixing of a plain jet into a swirling crossflow. ILASS Am. 21st Annu. Conf. Liq. At. Spray Syst., Orlando, Florida: 2008.

[153] Tambe SB, Jeng S-M. A study of liquid jets injected transversely into a swirling crossflow. ILASS Am. 21st Annu. Conf. Liq. At. Spray Syst., Orlando, Florida: 2008.

Chapter 3

A Model for Predicting the Trajectory of a Liquid Jet in a Subsonic Gaseous Crossflow

3.1. Abstract

This paper presents an approach for modeling a liquid jet trajectory in a subsonic gaseous crossflow. Forces acting on the liquid column including drag, gravitation, surface tension and viscous are all accounted for along with the mass and energy conservation equations which are employed to model the liquid jet trajectory. The tangential and normal components of the governing equations are solved analytically using control-volume analysis. A novel correlation in a sinusoidal-exponential functional form is developed as a function of the momentum flux ratio, gas and jet Weber number, jet Reynolds number and Bond number. This correlation is capable of predicting jet trajectory of different liquids in a subsonic crossflow at different operating conditions and injection angles. The predictions showed reasonable agreement with published experimental data and empirical correlations.

Nomenclature		***Greek symbol***	
A	liquid jet cross sectional area, m^2	θ	injection angle
A_L	lateral surface area of the liquid jet,	μ	liquid viscosity, kg/(m.s)
Bo	m^2Bond number, $\rho g d_j^2/\sigma$	μ_g	gas viscosity, kg/(m.s)
C_D	average drag coefficient	ρ	density, kg/m^3
D	channel diameter, m	σ	liquid surface tension, N/m
d	liquid jet diameter, m	ψ	liquid jet angle
d_j	liquid jet diameter at the nozzle exit, m		
g	gravitational acceleration vector, m/s^2		
l_c	liquid jet perimeter, m		
Oh	Ohnesorge number, $\mu_j/\sqrt{\rho_j d_j \sigma}$		
P	absolute pressure of the crossflow, kPa		
q	jet momentum flux ratio, $\rho v_j^2/\rho_g u_g^2$		
Re_{ch}	channel Reynolds number, $\rho_g u_g D/\mu_g$		
Re_j	jet Reynolds number, $\rho v_j d_j/\mu$		
s	curve-abscissa		
T	absolute temperature of the crossflow, K		
u	crossflow velocity, m/s		
$\boldsymbol{V}$	fluid velocity vector, m/s		
V	fluid velocity, m/s		
v_j	fluid velocity at the nozzle exit, m/s		
We_{aero}	aerodynamic Weber number, $\rho_g v_j^2 d_j/\sigma$		
We_g	gas phase Weber number, $\rho_g u_g^2 d_j/\sigma$		
We_j	liquid phase Weber number, $\rho v_j^2 d_j/\sigma$		
x	crossflow streamwise, m		
z	liquid injection sreamwise, m		

3.2. Introduction

The transformation of a liquid column into a spray when injected into a gaseous crossflow is of great importance in several industrial processes, transportation systems, agriculture, meteorology and medicine (e.g., [1-2]). One of the most efficient spray generation techniques in a combustion chamber is by injecting the liquid fuel perpendicularly into a gaseous crossflow. The process of liquid jet breakup and fuel/oxidant mixing plays a crucial role in the flame stabilization and emission control (e.g., [3-4]). However, the design of such combustion chambers requires

knowledge about spray penetration/trajectory in order, for example, to prevent fuel impingement onto the combustors' walls (e.g., [2]).

Liquid breakup occurs through the interaction of two fluid streams when a liquid jet discharges into a gaseous crossflow [5]. A liquid jet generally leaves a nozzle as an unbroken column, is perturbed, and then torn into small ligaments and drops as a result of aerodynamic effect of the gaseous crossflow [5]. This process in the near-field of a liquid jet is referred to as the primary breakup [5]. Afterwards, ligaments and drops resulting from the primary breakup further break down into finer droplets [5]. This process is known as a secondary breakup [5,6].

Numerous empirical and theoretical correlations for predicting the trajectory of a liquid jet injected perpendicularly into a crossflow have been proposed in the literature. For instance, there exist three popular forms of correlations: power-law equation (e.g., [6-17]), logarithmic equation (e.g., [18-23]) and exponential equation (e.g., [24-25]). Some studies proposed two separate correlations for the liquid jet trajectory, one for the near-field or column region and another for the far-field zone or spray plume region (e.g., [11,15]); and others proposed one single correlation to predict the entire region of the liquid jet trajectory (e.g., [9,16]). Some of these correlations were developed under standard temperature and pressure (STP) conditions (e.g., [6-7, 10-11, 14-16, 19, 22]), and others considered high temperature and pressure (HTP) conditions (e.g., [8-9, 12-13, 17-18, 20-21, 23]). These correlations might also be categorized according to whether they predict the centerline or the windward boundary of the liquid jet.

The power-law correlation, presented below in a generalized form Eq. (3-1), is the earliest, simplest and most common functional form that has been used by several investigators to predict a liquid jet trajectory in a subsonic gaseous crossflow.

$$\frac{z}{d_j} = c_1 q^{n_1} \left(\frac{x}{d_j}\right)^{n_2} We_g^{n_3} \left(\frac{\mu}{\mu_w}\right)^{n_4} Re_{ch}^{n_5} Re_j^{n_6} \left(\frac{P}{P_o}\right)^{n_7} \quad (3\text{-}1)$$

where x, z are the crossflow and the liquid injection sreamwise, respectively, and dj is the nozzle (or jet) diameter. The non-dimensional parameters such as $q = \rho_j v_j^2 / \rho_g u_g^2$ is the ratio of jet to gas momentum flux; gas phase Weber number which is defined as a ratio between forces that act to break apart a liquid structure (due to air shearing by the crossflow) and the surface tension acting to hold it together (i.e., $We_g = \rho_g u_g^2 d_j / \sigma$); $Re_{ch} = \rho_g u_g D / \mu_g$ and $Re_j = \rho v_j d_j / \mu$ are the channel/crossflow and the liquid phase Reynolds number, respectively. The coefficients (c_1 and n_1 to n_7) proposed by different researchers are tabulated in Table 3-1. The parameters P and μ are, respectively, the crossflow pressure and liquid viscosity; and the subscripts w and o stand for water and standard conditions, respectively.

Table 3-1: Coefficients of power-law correlations (Eq. (3-1)).

Reference	c_1	n_1	n_2	n_3	n_4	n_5	n_6	n_7	q	We_g
Wu et al. [6]	1.37	0.5	0.5	0	0	0	0	0	3.38-185	57-1179
Lin et al. [7][1]	2.42	0.48	0.24	0	0	0	0	0	0.5-18.5	-
	3.17	0.33	0.4	0	0	0	0	0		
Elshamy et al. [8]	4.95	0.424	0.279	-0.076	0	0	0	-0.051	1.95-71.23	98-906
Stenzler et al. [9]	3.354	0.442	0.391	-0.088	-0.027	0	0	0	9,14,18	0.9-164.3
Brown et al. [10]	2.45	0.33	0.5	-0.061	0	0	0	0	0.8-22	97-573
Birouk et al. [11]	1.627	0.47	0.46	0	0.079	0	0	0	5.5-726	9.3-175.4
Ragucci et al. [12][2]	2.28	0.422	0.367	0.015	0.186	0	0	0	5-280	7-340
Bellofiore et al. [13][3]	0.909	0.476	0.35	-0.128	0	0.135	0	0	12.2-71.4	18-266
Yoon et al. [14]	2.291	0.417	0.42	0	0	0	0	0	2.0-29.1	5.3-47.9
Zheng et al. [15]	2.39	0.46	0.6	-0.2	0	0	0	0	10-50	4-16
Farvardin et al. [16]	3.68	0.43	0.384	-0.085	-0.222	0	0	0	10-135	28-82
Eslamian et al. [17]	0.167	0.31	0.37	0	0	0.11	0.15	0.15	10-80	20-487

[1] Coefficients in the first row were obtained using shadowgraph method and those in the second row were obtained using PDPA measurements.

[2]Used an aerodynamic Weber number $We_{aero} = \rho_g v_j^2 d_j / \sigma$ instead of gas Weber number and used air viscosity in the viscosity ratio term instead of water viscosity in Eq. (3-1).

[3]Similar to [12] who used aerodynamic Weber number instead of gas Weber number in Eq. (3-1).

The logarithmic correlation, which is presented in a generalized form in Eq. (3-2), is the second most popular functional form that has been used to predict liquid jet trajectory in a subsonic gaseous crossflow.

$$\frac{z}{d_j} = q^{n_1}\left\{c_1 \ln\left[c_2\left(\frac{x}{d_j}\right)^{n_2} + c_3\right] + c_4\right\} We_g^{n_3}\left(\frac{T}{T_\circ}\right)^{n_4} \quad (3\text{-}2)$$

where T and T_o are the operating and atmospheric/standard temperatures, respectively. The coefficients (c_1 to c_4 and n_1 to n_4) proposed by different researchers are given in Table 3-2.

Table 3-2: Coefficients of logarithmic correlations (Eq. (3-2)).

Reference	c_1	c_2	c_3	c_4	n_1	n_2	n_3	n_4	q	We_g
Becker et al. [18]	1.48	3.56	1	0	0.42	1	0	0	1-40	90-2120
Tambe et al. [19]	1.55	1.66	1	0	0.53	1	0	0	0.7-10.2	50.5-1725.1
Lakhamraju et al. [20]	1.844	1.324	1	0	0.456	1	0	-0.117	1-49.5	50.3-262.4
Freitag et al. [21]	1.6	3.81	1	0	0.4	1	0	0	3-24	-
Wang et al. [22]	1.46	1	0	1.5	0.5	1	-0.05	0	1-54	9-345
Li et al. [23]	1.44	1.06	1	0	0.4356	1	0.001147	0.295	16-76	212-1630

The exponential (multi-zone) correlation, Eq. (3-3), has been first utilized by Chen et al. [24] in 1993 for $5 < q < 45$ and $We_g > 100$, and then by Elshamy et al. [25] in 2007 who proposed some exponential correlations for unforced conditions and excited jet conditions.

$$\frac{z}{d_j} = 9.91q^{0.44}\left[1 - exp\left(\frac{-x/d_j}{13.1}\right)\right]\left[1 + 1.67exp\left(\frac{-x/d_j}{4.77}\right)\right]\left[1 + 1.06exp\left(\frac{-x/d_j}{0.86}\right)\right] \quad (3\text{-}3)$$

Considering the effect of the injection angle on the liquid jet trajectory, Baranovsky and Schetz [26] proposed one of the earliest correlations in which they considered the effect of injection angle, θ, on the penetration and break-up of a liquid jet in a supersonic crossflow. They modeled the liquid column as a cylindrical fluid element having the diameter of the nozzle exit orifice which can be accelerated by aerodynamic drag forces of the gaseous crossflow. Afterwards, Fuller et al.

[27] correlated a liquid column trajectory in a subsonic gaseous crossflow with the momentum flux ratio q, transverse injection angle θ and empirically determined drag coefficient C_D by applying a force balance and momentum analysis. Their correlation, which was explicit according to x as function of z, has the following form

$$\frac{x}{d_j} = \frac{1}{\pi}\frac{C_D}{q sin^2\theta}\left(1 - \frac{v_j cos\theta}{u_g}\right)\left(\frac{z}{d_j}\right)^2 + \frac{cos\theta}{sin\theta}\left(\frac{z}{d_j}\right) \quad (3\text{-}4)$$

From the correlations related to the both perpendicular and canted injection angle, it is seen that coefficients and power exponents related to one specific term (e.g., x/d_j, q or other parameters) differed from one study to another as there is no consensus on the role of each term. Even the coefficients presented by the same investigators differed when changing the method of measurement [7].

These discrepancies could be attributed to different factors such as operating conditions and measurement techniques, inconsistencies in the definition of spray boundary, different internal geometry of liquid injectors, liquids with different properties, assumptions made in developing these correlations, etc (e.g., [10, 28]). In addition, due to the complex physics of two-phase flows, the complete numerical simulation of such flows seems economically unfeasible [29]. The present paper, therefore, aims at understanding better the complex physics of the problem as well as presenting a simple and reliable model capable of predicting a liquid jet trajectory in a subsonic crossflow at different operating conditions and injection angles for different liquids.

3.3. Model description

3.3.1. Introduction

The interaction of two fluid streams (i.e., a liquid jet discharged into a gaseous crossflow) is treated by adopting a new approach which uses control-volume analysis. In general, there are three basic

approaches to the analysis of arbitrary flow problems: a) Control-volume or large-scale analysis, b) Differential or small scale analysis, and c) Experimental, or dimensional analysis. The control volume is the newest and most common method which gives engineers a valuable tool for flow analysis without the need for expensive and time consuming numerical simulations and experimental tests [30].

Early studies (e.g., [6, 27, 31]) developed a theoretical model for predicting the trajectory of a liquid jet where the liquid jet was assumed as a stack of thin cylindrical elements piled on top of each other. By considering the linear-momentum relation (or Newton's law) and performing a force balance on the element, the motion of the system along the jet trajectory was calculated. In the present analysis, however, a force balance is applied to a control-volume form suitable for arbitrary region instead of the fluid element [30]. First, forces acting upon the liquid jet column such as drag, gravitation, surface tension and viscous forces are introduced and then the mass and energy conservation equations are developed using the control-volume approach. The tangential and normal components of the governing equations are then solved analytically taking into account relevant boundary conditions. As a result, an explicit algebraic correlation in a sinusoidal-exponential functional form to predict the trajectory of a liquid jet in a subsonic gaseous crossflow is obtained as a function of the physical parameters that play a role in the liquid jet breakup process.

3.3.2. Physical problem, governing equations and model

In order to predict the trajectory of a liquid jet in a subsonic gaseous crossflow, a theoretical model is developed taking into account the mass and energy conservation equations and using control-volume analysis. The conservation laws are applied through the cylindrical control volume associated with a reference coordinate system (x, z), as illustrated in Fig. 3-1.

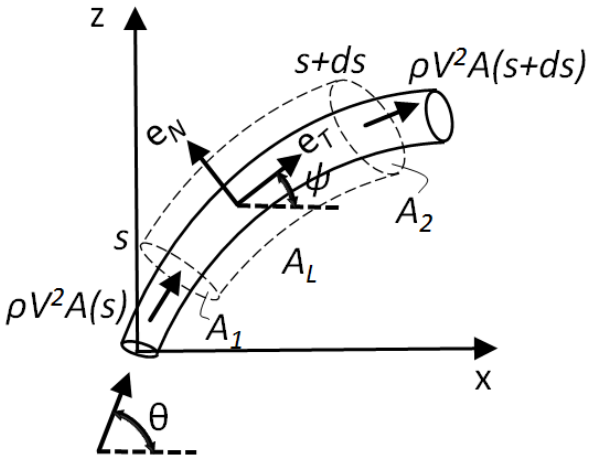

Figure 3-1: A control volume defined for local momentum conservation due to mass exchange.

The control volume is bounded by two disks A_1 and A_2 at the curve-abscissa s and s+ds, respectively, and by A_L, which is the lateral surface of the cylinder intercepting A_1 and A_2, as shown in Fig. 3-1. In this figure, the x axis origin is located at the center of the injection point (centreline at the nozzle's exit orifice), and z axis has the same origin as x but it is directed in the same direction of the jet injection angle (that is, perpendicular to x). This choice has been made to derive the trajectory equations for the centerline of the liquid jet which can be easily changed to its windward boundary by moving the initial coordinate system to the left corner of the nozzle outlet. Furthermore, in the present model, a convenient local framework with the normal and tangent unitary vectors ($\boldsymbol{e}_N, \boldsymbol{e}_T$) is defined where ψ is the angle between the vertical and the tangent axis. The following geometrical parameters and relations are also defined as

- $\boldsymbol{V}$ $(= V\boldsymbol{e}_T)$ is the fluid velocity vector relative to the reference coordinate system, where V is the fluid velocity.

- d, l_c and A are the liquid jet diameter, perimeter and cross sectional area, respectively, which are all dependent on s.
- the local curvature of the jet trajectory can be defined as $k = \frac{d\boldsymbol{e}_T}{ds} = \frac{d\psi}{ds}\boldsymbol{e}_N = \cos\psi\frac{d\psi}{dx}\boldsymbol{e}_N = \frac{d\sin\psi}{dx}\boldsymbol{e}_N$ when using $\frac{d}{ds} = \frac{dx}{ds}\cdot\frac{d}{dx} = \cos\psi\frac{d}{dx}$
- $\boldsymbol{e}_{\mathrm{z}} = \sin\psi\,\boldsymbol{e}_T + \cos\psi\boldsymbol{e}_N$ and $\boldsymbol{e}_{\mathrm{x}} = \cos\psi\,\boldsymbol{e}_T - \sin\psi\,\boldsymbol{e}_N$

Given the steady flow within the control volume, the integral form of the mass-conservation law can be written as follows:

$$\int_{cs}\rho(\boldsymbol{V}\bullet\boldsymbol{n})dA = 0 \tag{3-5}$$

where $\boldsymbol{n}$ is the outward normal unit vector. The linear-momentum relation applied to the control volume can be expressed as

$$\sum\boldsymbol{F} = \int_{cs}\boldsymbol{V}\rho(\boldsymbol{V}\bullet\boldsymbol{n})dA \tag{3-6}$$

In essence, the entire equation is a vector relation due to the term $\boldsymbol{V}$ in the integral term which holds for the momentum flux through the control volume, and the term $\sum\boldsymbol{F}$ is the vector sum of all forces acting on the control volume.

As shown in Fig. 3-2, there are, in general, four different forces acting on a liquid jet in a crossflow, which are

- the weight of the column: $-\rho gAds\boldsymbol{e}_{\mathrm{z}}$, submitted to gravitation force;
- the surface tension force acting along the column: $\sigma l_c\boldsymbol{e}_T|_{s+ds} - \sigma l_c\boldsymbol{e}_T|_s = \sigma(dl_c\boldsymbol{e}_T/ds)ds = \sigma(dl_c/ds\;\boldsymbol{e}_T + l_c\,d\boldsymbol{e}_T/ds)ds$;
- the viscous force: $\mu A_L(dV\boldsymbol{e}_T/ds) = \mu l_c(dV/ds\;\boldsymbol{e}_T + V\,d\boldsymbol{e}_T/ds)ds$;

- the drag (aerodynamic) force due to the gaseous crossflow: $^1/_2\, C_D \rho_g u_g^2 d \times ds \boldsymbol{e}_x$;

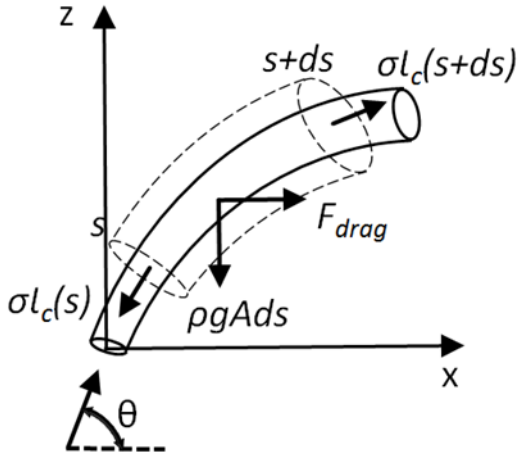

Figure 3-2: Local equilibrium of forces on a control volume.

From the geometrical relations, these forces can be projected on the framework axis ($\boldsymbol{e}_N$, $\boldsymbol{e}_T$) as follows:

$$\sum \boldsymbol{F} \bullet \boldsymbol{e}_T \frac{1}{ds} = -\rho g A \sin\psi + \sigma \frac{dl_c}{dx} \cos\psi + \mu l_c \frac{dV}{dx} \cos\psi + \frac{1}{2} C_D \rho_g u_g^2 d \cos\psi \qquad (3\text{-}7)$$

$$\sum \boldsymbol{F} \bullet \boldsymbol{e}_N \frac{1}{ds} = -\rho g A \cos\psi + \sigma l_c \frac{d \sin\psi}{dx} + \mu V l_c \frac{d \sin\psi}{dx} - \frac{1}{2} C_D \rho_g u_g^2 d \sin\psi \qquad (3\text{-}8)$$

According to Fig. 3-1, the variation of the momentum flux due to mass exchange through the jet control surface can be also defined as

$$\rho V^2 A \boldsymbol{e}_T|_{s+ds} - \rho V^2 A \boldsymbol{e}_T|_s = \rho (dV^2 A \boldsymbol{e}_T/ds) ds = \rho (dV^2 A/ds\ \boldsymbol{e}_T + V^2 A\, d\boldsymbol{e}_T/ds) ds.$$

Therefore, the tangential and normal components of the momentum flux through the control surface can be expressed as follows:

$$\int_{cs} \boldsymbol{V}\rho(\boldsymbol{V}\bullet\boldsymbol{n})dA\bullet\boldsymbol{e}_T \frac{1}{ds} = \rho\frac{dV^2A}{dx}\cos\psi \tag{3-9}$$

$$\int_{cs} \boldsymbol{V}\rho(\boldsymbol{V}\bullet\boldsymbol{n})dA\bullet\boldsymbol{e}_N \frac{1}{ds} = \rho V^2A\frac{d\sin\psi}{dx} \tag{3-10}$$

Substituting Eqs. (3-7) through (3-10) in Eq. (3-6), the governing equations of the trajectory of a liquid jet in a gaseous crossflow can finally be expressed as

$$\rho\cos\psi\left(-gA\tan\psi + \frac{\sigma}{\rho}\frac{dl_c}{dx} + l_c\frac{\mu}{\rho}\frac{dV}{dx} + \frac{1}{2\rho}C_D\rho_g u_g^2 d - \frac{dV^2A}{dx}\right) = 0 \tag{3-11}$$

$$\rho\sin\psi\left(-gA\cot\psi + \frac{\sigma}{\rho}\frac{l_c}{\sin\psi}\frac{d\sin\psi}{dx} + \frac{\mu}{\rho}\frac{Vl_c}{\sin\psi}\frac{d\sin\psi}{dx} - \frac{1}{2\rho}C_D\rho_g u_g^2 d - \frac{V^2A}{\sin\psi}\frac{d\sin\psi}{dx}\right) = 0 \tag{3-12}$$

3.3.3. Calculation of the liquid jet trajectory

In the present model, in order to highlight the underlying atomization physics and to propose an explicit algebraic correlation for the liquid jet trajectory without the need for numerical solutions of the complicated governing equations, it is assumed that the liquid column can be approximated as a cylindrical fluid element having a diameter equal to that of the liquid jet at the nozzle exit, d_j. This assumption has been widely adopted in the literature (e.g., [6, 26-27]). In fact, considering the jet liquid column as a cylinder with a constant diameter leads to neglect the mass stripping along the liquid column and also mass losses induced by liquid evaporation, as well as the deformation and flattening of the liquid column. To make this assumption rational, Wu et al. [6] considered $C_D = 1.696$ as an average value of the drag coefficients along the entire length of the jet liquid column, which includes the effects of liquid column deformation, flattening and mass

stripping. They reported that the averaged drag coefficient increases as the liquid viscosity μ increases, which hence leads to a less penetration of the liquid jet into the airstream. They also proposed a correlation for the prediction of C_D of different liquids as $C_D/C_{Dw} = 0.984(\mu/\mu_w)^{0.364}$, where $C_{Dw} = 1.51$ and μ_w are the drag coefficient of water and water viscosity, respectively. Mashayek et al. [31] proposed a theoretical model for the penetration of a liquid jet in a subsonic gaseous crossflow by considering the deformation of the jet cross sectional area from a circular to an elliptic shape along its path. Mass stripping has been considered in their model in the form of a decrease in the jet cross sectional area. Their predicted liquid jet trajectory, which was obtained by calculating numericallyC_D, was in good agreement with the trajectory obtained using the empirical C_D suggested by Wu et al. [6]. They also developed a series of equations, as a function of Reynolds number, to calculate drag coefficient for different cross sectional shapes through two-dimensional simulations. Recently, Kim et al. [32] proposed an empirical average drag coefficient of 1.3 for different forward injection angles including: 30, 45, 60, 75, and 90 degrees, and 0.2 for reverse injection angles.

Given the aforementioned assumption, the mass-conservation law for incompressible flow, Eq. (3-5), can be simplified as $A\times V = \left(\pi d_j^2/4\right)v_j$, where V and v_j are, respectively, the liquid velocity in the control volume along the jet column and at the jet exit. Hence, Eq. (3-11) becomes

$$tan\,\psi = \frac{1}{2\rho} C_D \rho_g u_g^2 d/gA \tag{3-13}$$

Substituting Eq. (3-13) into Eq. (3-12), and rewriting it in non-dimensional form, it becomes

$$\frac{\alpha}{d_j}\sin\psi = \beta\frac{d\sin\psi}{dx} \tag{3-14}$$

where α and β are

$$\alpha = \frac{1}{q}\left(\frac{2C_D}{\pi} + \frac{\pi}{2C_D}\frac{Bo^2}{We_g^2}\right) \tag{3-15}$$

$$\beta = 4\left(\frac{1}{We_j} + \frac{1}{Re_j}\right) - 1 \tag{3-16}$$

where Bond number, $Bo = \rho g d_j^2/\sigma$, prescribes the ratio of the gravitational to surface tension forces acting on the liquid jet, and liquid phase Weber number, $We_j = \rho v_j^2 d_j/\sigma$, is the ratio of liquid inertia to surface tension.

Considering $\frac{d\sin\psi}{dx} = \cos\psi\frac{d\psi}{dx}$ and $\tan\psi = \frac{dz}{dx}$, and substituting them into Eq. (3-14), the variation of z as a function of ψ is found by integrating this equation with respect to x, and considering the boundary condition $\psi = \theta$ at $z = 0$ so that

$$z = \frac{\beta}{\left(\alpha/d_j\right)}(\psi - \theta) \tag{3-17}$$

In addition, to calculating ψ as a function of x, Eq. (3-14) can be rewritten as $\left(\frac{\alpha}{d_j}\right)/\beta = \frac{1}{G}\frac{dG}{dx}$, where $G = \sin\psi$. By integrating this equation with respect to x, and taking the boundary condition that $G = \sin\theta$ at $x = 0$, we obtain

$$\psi = \sin^{-1}\left[\sin\theta.exp\left(\frac{\left(\alpha/d_j\right)}{\beta}x\right)\right] \tag{3-18}$$

Finally, by eliminating ψ from Eqs. (3-17) and (3-18), an explicit correlation in a sinusoidal-exponential functional form for a liquid jet trajectory in a gaseous crossflow is obtained as follows:

$$z^* = \frac{\beta}{\alpha}\left(\sin^{-1}\left[\sin\theta.exp\left(\frac{\alpha}{\beta}x^*\right)\right] - \theta\right) \tag{3-19}$$

where $z^* = z/d_j$ and $x^* = x/d_j$ are, respectively, the non-dimensional liquid injection and gas streamwise distance from the nozzle.

3.4. Results and discussion

Equation (3-19) shows that, in addition to the ratio of jet momentum flux to gas momentum flux, q, the effect of other parameters such as gas Weber number (We_g), jet Weber number $(We_j = qWe_g)$, jet Reynolds number (Re_j), and Bond number (Bo) is also considered in order to predict the extent of the penetration of a liquid jet into a subsonic gaseous crossflow. It is worth noticing that the square root of the Bond number prescribes the ratio of the liquid jet diameter d_j to the capillary length (2.7 mm for water). This number plays an important role in liquid jet breakup when the jet nozzle diameter exceeds the capillary length [33].

Figure 3-3a compares the calculated trajectories using the present model with the experimental data of Wu et al. [6] for water at different momentum flux ratios (q = 4.7, 18.4 and 70.4 where the liquid jet velocity increases as $v_j = 9.8, 19.4, 37.9$ m/s). As expected, from Wu et al. [6], the liquid jet penetrates farther into the crossflow and bends less as v_j increases. The operating conditions for the predictions in Fig. 3-3 are exactly those of Wu et al. [6] (P = 140 kPa, T = 306 K, $d_j = 0.5 \times 10^{-3}$m). Despite the fact that there is a good agreement between the present predictions and published experimental results, the present model slightly underestimates and overestimates the experimental data for the weakest and strongest q, respectively. This might be due to the fact that a constant drag coefficient (the average drag coefficient proposed by Wu et al. [6]) is used in the present model for different q. This coefficient may change noticeably when the breakup regime of the liquid jet changes from column breakup to surface breakup mode. This is

because a change to surface breakup mode affects the rate of mass stripping from the liquid column [31]. In fact, at a fixed gas Weber number We_g, the liquid jet undergoes column breakup without surface breakup when q is small, as surface breakup occurs before the liquid column instability at high q [6].

Figure 3-3b compares the calculated trajectory for one of the cases in Fig. 3-3a with the experimental results of Wu et al. [6] and the empirical correlations proposed by Tambe et al. [19], Brown et al. [10], and Yoon et al. [14], which all were proposed at standard temperature and pressure (STP) conditions. This figure shows that the agreement of the prediction of the present model with the experimental results of Wu et al. [6] is better than the other empirical correlations displayed in Fig. 3-3b. This could be attributed to the fact that the drag coefficient used in the present model is the one proposed by Wu et al. [6].

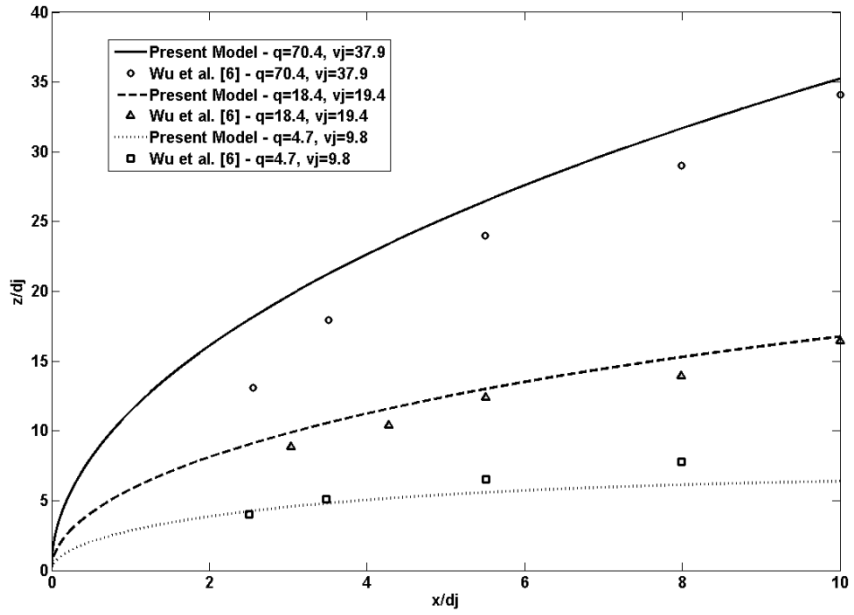

(a)

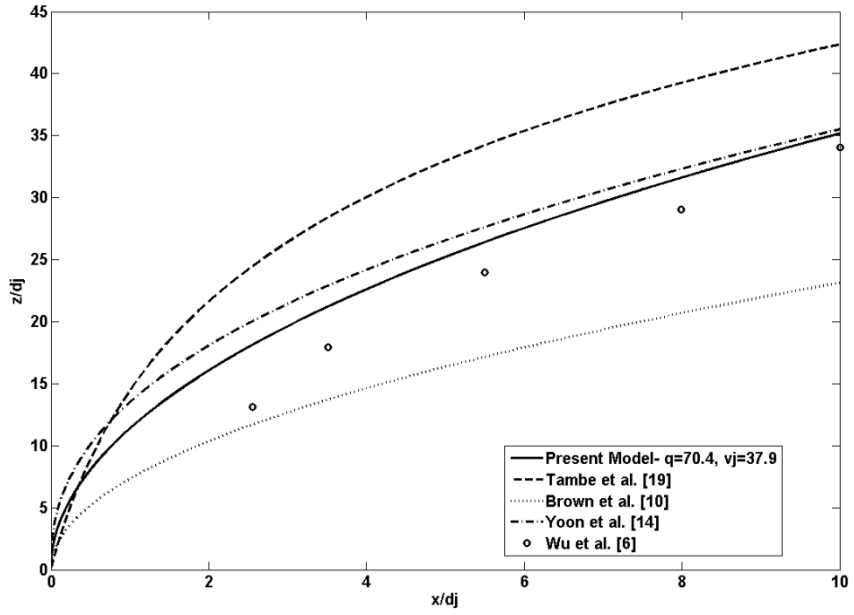

(b)

Figure 3-3: Comparison of the present model calculated water jet trajectory with the a) experimental data of Wu et al. [6] at different momentum flux ratios, b) experimental data of Wu et al. [6] and other empirical correlations proposed by [10, 14, 19] for a fixed momentum flux ratio.

In order to examine the effect of liquid properties on the present model capabilities for predicting a jet trajectory in a crossflow, diesel fuel is used instead of water as a working fluid. Figure 3-4 shows a compariosn of the calculated trajectories of the present model with the experimental data of Farvardin et al. [16] for diesel (the operating conditions for calculating the trajectories are exactly those of Farvardin et al. [16] (P = 101.325 kPa, T = 293.15 K, $d_j = 0.5 \times 10^{-3}$ m)). As Farvardin et al. [16] used the correlation of Stenzler et al. [9] to compare with their experimental results, the correlation of Stenzler et al. [9] is also illustrated in this figure.

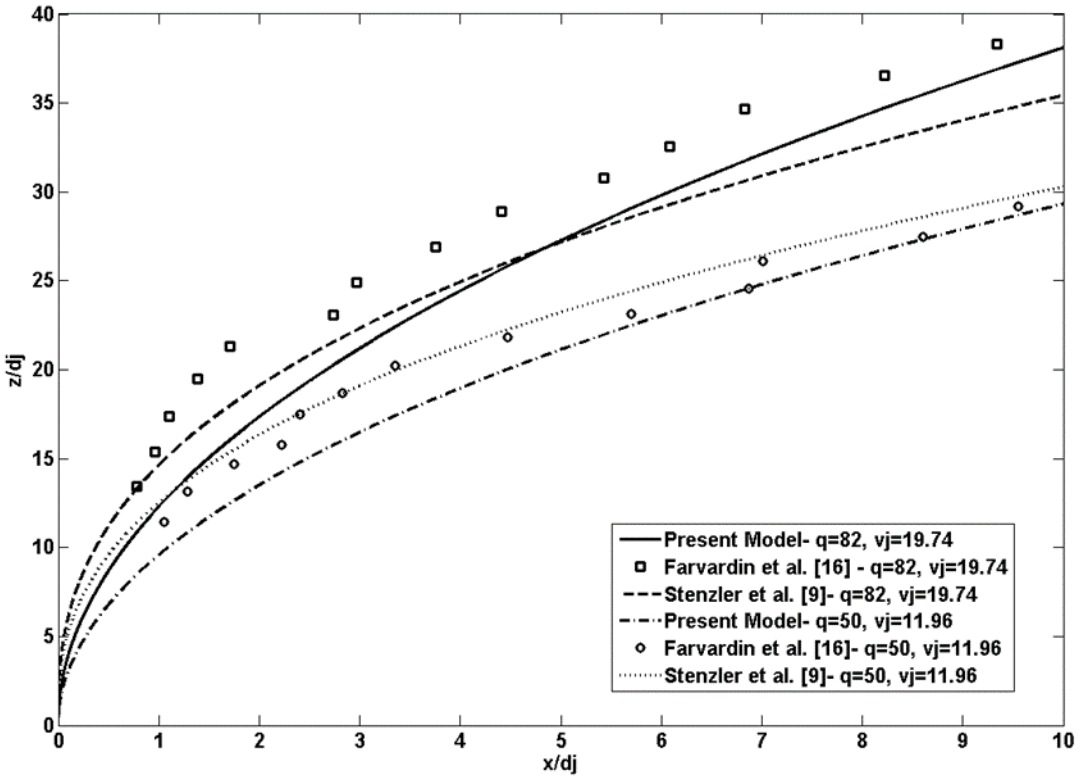

Figure 3-4: Comparison of the present model calculated diesel jet trajectory with the experimental data of Farvardin et al. [16] and the correlation of Stenzler et al. [9] for different momentum flux ratios.

This figure shows that apart in the very near-field of the jet, the present model shows reasonable agreement with the experimental data of Farvardin et al. [16]. The present model's calculated jet trajectory is slightly underpredicted in comparsion with their experimental counterpart. This might be due to the difference in the liquid properties (density, viscosity and surface tension) bewteen diesel (ρ = 850 kg/m3, μ = 1.190 × 10^{-3} kg/(m.s) and σ = 0.0252 N/m) and water (ρ = 996 kg/m3, μ = 0.865 × 10^{-3} kg/(m.s) and σ = 0.0635 N/m) where in the present model, the average drag coefficient for diesel was estimated using the emperical correlation proposed by Wu et al. [6], which relates the drag coefficient of a liquid to its viscosity. In particular, the surface tension of diesel, which plays an effective role in gas Weber number, $We_g = \rho_g u_g^2 d_j/\sigma$, is approximately one third of that of water, which has direct effect on mass stripping from the liquid column and consequently on the averge drag coefficient. In fact, high gas Weber number governs the onset and the rate of mass stripping from the column surface owing to the increased contribution to air shearing forces [31].

Liquid jet trajectory in a subsonic gaseous crossflow has also been investigated at high temperature and pressure (HTP) conditions (e.g., [8-9, 12-13, 17-18, 20-21, 23]). High pressure and temperature conditions could affect the liquid jet behavior through the crossflow gas density, which yields better atomization [13]. On the other hand, Eslamian et al. [17] argued that a decrease in crossflow velocity with an increase in pressure could have an adverse effect on atomization, and consequently larger droplet might form. They also showed that the jet penetration height slightly decreases, particularly at far distances from the nozzle outlet, when increasing the crossflow gas temperature and velocity.

Figure 3-5 compares the calculated trajectory of the present model with the experimental data of Eslamian et al. [17] for water at a fixed momentum flux ratio, q = 50. The operating conditions for

the trajectory in Fig. 3-5 are exactly those of Eslamian et al. [17] (P = 379 and 517 kPa, T = 573 K, $d_j = 0.57 \times 10^{-3}$m).

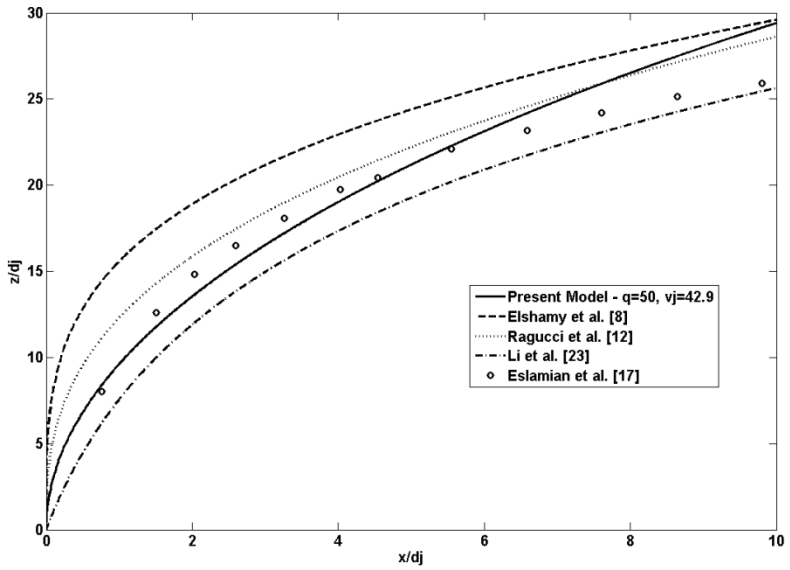

(a)

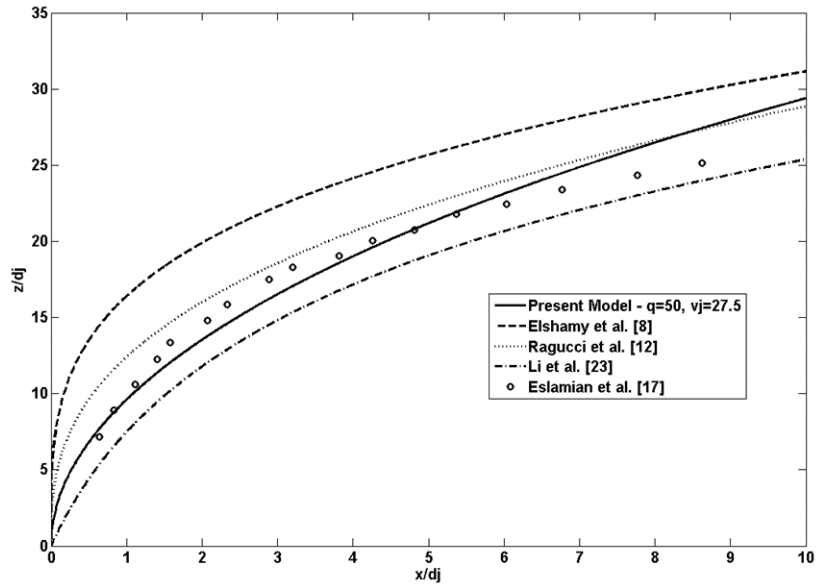

(b)

Figure 3-5: Comparison of the present model calculated water jet trajectory with the experimental data of Eslamian et al. [17], and published empirical correlations for a fixed momentum flux ratio at a) *P* = 379 kPa, *T* = 573 K, and b) *P* = 517 kPa, *T* = 573 K.

In addition, Fig. 3-5 illustrates a comparison with the trajectory obtained by the empirical correlations proposed by Elshamy et al. [8], Ragucci et al. [12], and Li et al. [23], which all are proposed at the elevated pressure and temperature conditions. As shown in Fig. 3-5, the liquid jet trajectory predicted by the correlations proposed by Elshamy et al. [8], and Li et al. [23] overestimates and underestimates the experimental data, respectively. However, the present model predictions and that of the correlation of Ragucci et al. [12] show a better agreement with the experimental results, particularly in the near-field region (prior to the column break up location). The present model capability in predicting jet trajectory at elevated crossflow pressure and temperature conditions was also testd using other liquids where kerosene fuel was used instead of water. Figure 3-6 shows a comparison of the calculated trajectoriy using the present model with the experimental data of Rachner et al. [4]. Note that the operating conditions for calculating the trajectory are those of Rachner et al. [4] (P = 580 kPa, T = 280 K, $d_j = 0.45 \times 10^{-3}\ m$). A numerical and experimental study on the atomization of kerosene at elevated coditions was done by Rachner et al. [4], but no correlation for the trajectory of liquid jet was provided. Figure 3-6 shows also a comparison with the empirical correlations proposed by Elshamy et al. [8], Ragucci et al. [12], and Li et al. [23].

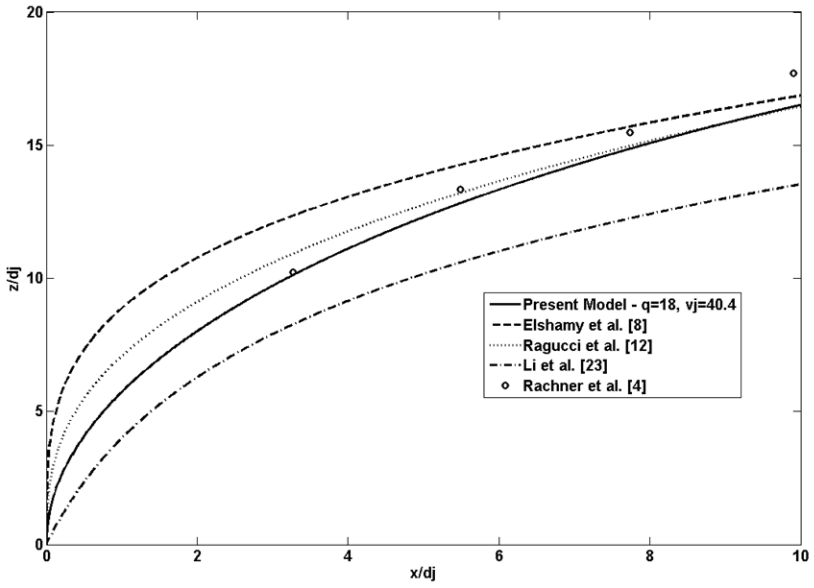

Figure 3-6: Comparison of the present model calculated kerosene liquid jet trajectory with the experimental data of Rachner et al. [4] and published empirical correlations for a fixed momentum flux ratio, at P = 580 kPa and T = 280 K.

Similar to the observations in Fig. 3-5, the comparison in Fig. 3-6 shows a better agreement between the calculated trajectory of the present model and the experimental data of Rachner et al. [4]. However, both the present model and the numerical predictions (not shown in Fig. 3-6) of Rachner et al. [4] slightly underestimate the trajectory of the experimental data closer to the column breakup point. This might be attributed to the fact that an average drag coefficient was used in the present model. This is because, high-pressure of the crossflow could affect the mass stripping from the liquid column by changing the surface tension of the liquid, and consequently gas Weber number. This may lead to a change in the liquid column surface roughness, and hence the drag coefficient of the liquid jet column in a crossflow [31].

In order to improve the atomization of a liquid jet in a gaseous crossflow, some studies investigated the effect of the injection angle (both forward and reverse injections [26-27, 32]). The injection angle was found to have a greater effect on the jet characteristics compared to other parameters such as the momentum flux ratio, particularly the jet trajectory and atomization quality of the liquid jet (droplet size and veocity) [34-35]. For instance, it was reported that, when decreasing the injection angle, the liquid column straightens, the column penetration decreases, and the atomization process is inhibited [27]. Figure 3-7 compares the calculated trajectories of the present model with the experimental data of Kim et al. [32] for different forward injection angles ($\theta = 30$ and 60 degrees).

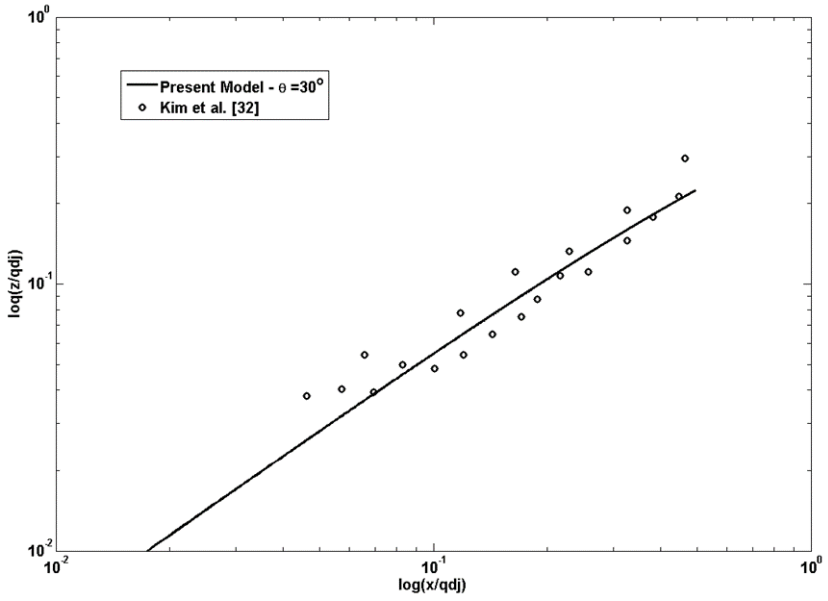

(a)

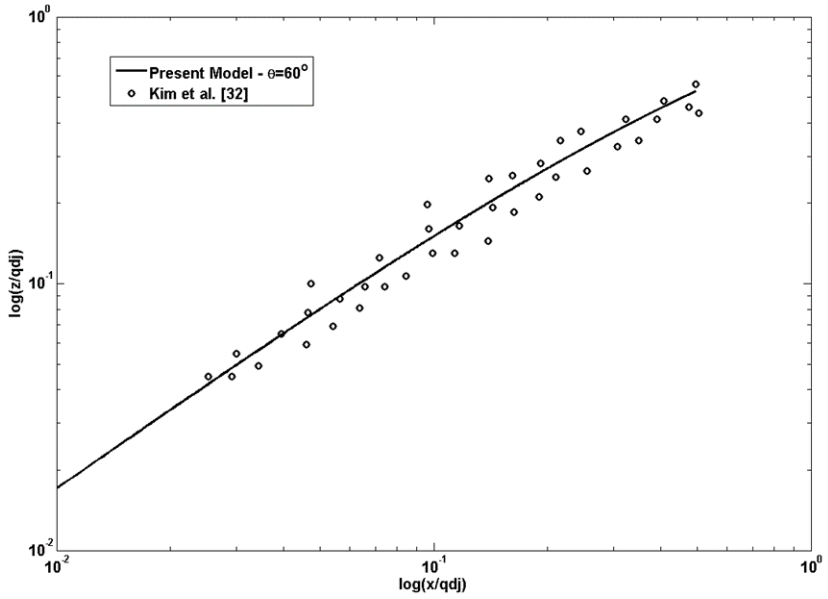

(b)

Figure 3-7: Comparison of the present model calculated water jet trajectory with the experimental data of Kim et al. [32] for different forward injection angles a) $\theta = 30$ and b) $\theta = 60$ degrees.

This figure shows a good agreement, which might be due to fact that the present model used the same average drag coefficient (CD = 1.3) as Kim et al. [32] for different forward injection angles. Figure 3-8 compares the present model calculated trajectory with the experimental data of Kim et al. [32] for different reverse injection angles ($\theta = 105, 120, 135, 150$ degrees).

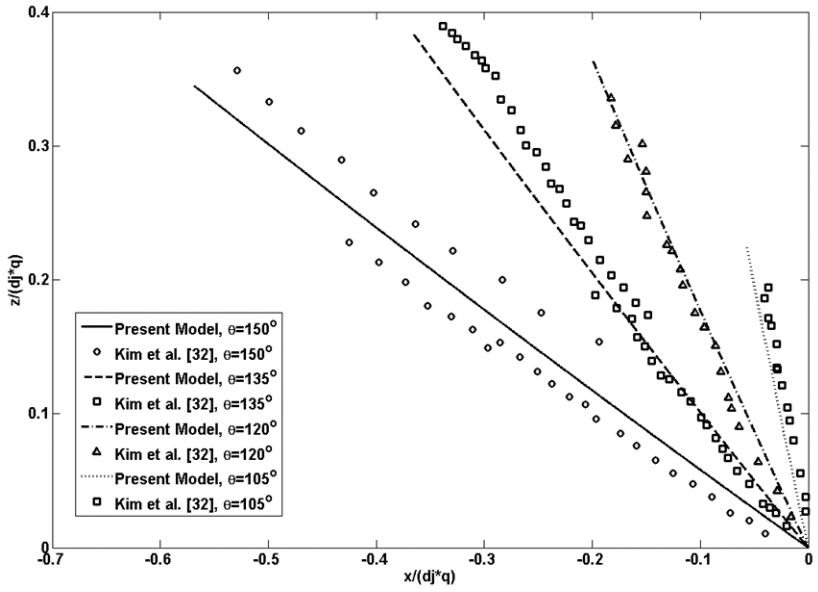

Figure 3-8: Comparison of the present model calculated water jet trajectory with the experimental data of Kim et al. [32] for different reverse injection angles ($\theta = 105, 120, 135, 150$ degrees).

Again, this figure shows a reasonable agreement between the present model predictions and published experimental data. In the calculations of the present model, the same average drag coefficient (CD = 0.2) as Kim et al. [32] was used. For $\theta = 105$ degree, however, the trajectory of the present model slightly underpredicts the experimental data. This might be due to the fact that its angle is close to the 90 degrees whose drag coefficient would be close to the coefficient of the perpendicular injection (CD = 1.3) instead of that for the reverse injection (CD = 0.2).

Figure 3-9 shows the present model calculated trajectories of water for perpendicular injection, different forward and reverse injection angles ($\theta = 30, 45, 60, 90, 105, 120, 135, 150$ degrees), at atmospheric standard conditions for $q = 70.4$ and $v_j = 37.9$ m/s. The breakup points were calculated according to the empirical correlations of Kim et al. [32] for the breakup distances of forward and reverse injections.

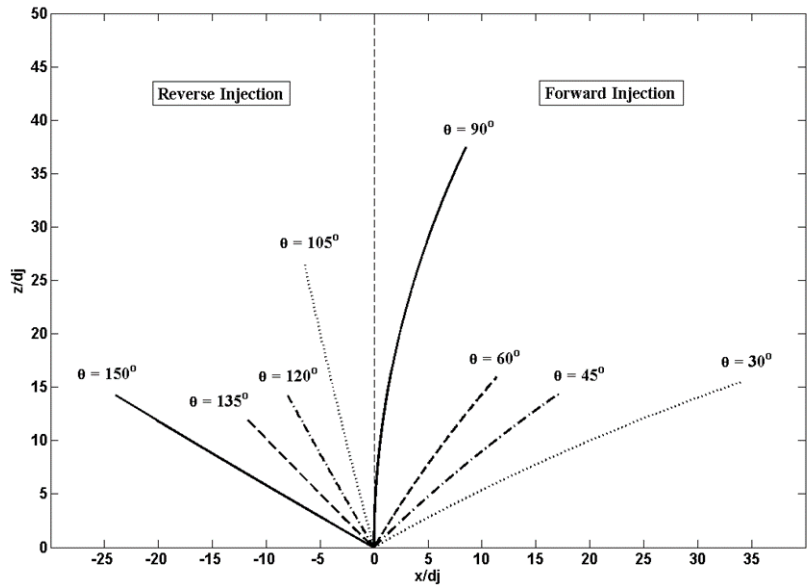

Figure 3-9: Present model ccalculated trajectories of water jet for different injection angles, (the gas crossflow flows from left to right for $q = 70.4$ and $v_j = 37.9$ m/s at atmospheric standard conditions).

As revealed in this figure, the breakup length of the liquid jet decreases with increasing the injection angle from the horizontal axis for the forward and reverse injections, and also increases close to the perpendicular angle in the both cases. This is in line with the findings of Costa et al. [34] who reported that the breakup length decreases with increasing the injection angle from 15 to 45 degrees.

3.5. Conclusion

A model is developed to predict the trajectory of a liquid jet in a subsonic gaseous crossflow at different operating conditions and liquid injection angles. The present model has been developed by taking into account all the physics governing the breakup/atomization process of a liquid jet injected into a crossflow. That is, in addition to the momentum flux ratio q, other parameters such as gas Weber number, We_g, jet Weber number, $We_j = qWe_g$, jet Reynolds number, Re_j, and Bond number, Bo, are all considered in the formulation of the model. However, for the range of the test conditions explored in the present study (i.e., low viscosity and small nozzle diameters), q is found to play a predominant role in the prediction of liquid column trajectory. In addition, We_g is also found important, as it affects the average drag coefficient due to mass stripping from the liquid column. However, Bo number becomes only important when the jet nozzle diameter exceeds the capillary length of the liquid [33], and Re_j plays an important role for high viscose liquids (Ohnesorge number $Oh = \mu_j/\sqrt{\rho_j d_j \sigma}$ more than 0.1 [36]). It is believed that the present formulation of the model, which resulted in the development of an equation in a sinusoidal-exponential functional form, provides a reliable prediction of a liquid jet trajectory over a wide range of operating conditions including the injection angle with minimal computational costs.

Although the present model calculations exhibited overall a good agreement with published experimental results, there still show slight discrepancies. This is believed to originate from the definition of the average drag coefficient at different test conditions. In fact, most of the information about the drag coefficient available in the literature is either an estimation based on averaging limited experimental test data or obtained using two-dimensional numerical simulation of the jet cross-sectional area. Two-dimensional simulation has several limitations in that it fails

to capture surface waves properties and also the interaction between the cross sections along the liquid jet axis [37, 38]. Therefore, further understanding of the break up process to develop reliable information about the drag coefficient is necessary which might be accomplished via three-dimensional treatments of a liquid jet in a gaseous crossflow combined with comprehensive experiments over extended test conditions.

3.6. References

[1] G.G. Nasr, A.J. Yule, L. Bendig, Industrial Sprays and Atomization: Design, Analysis and Applications, springer-verlag London, 2002.

[2] N. Ashgriz, Handbook of Atomization and Sprays, Springer Science Business Media LLC, 2011.

[3] M.Y. Leong, V.G. McDonell, G.S. Samuelsen, Mixing of an airblast-atomized fuel spray injected into a crossflow of air. NASA Glenn Research Center Report NASA/CR-2000-210467, 2000.

[4] M. Rachner, J. Becker, C. Hassa, T. Doerr, Modelling of the atomization of a plain liquid fuel jet in crossflow at gas turbine conditions, Aerospace Science and Technology 6, 495–506, 2002.

[5] M. Birouk and N. Lekic, Liquid jet breakup in quiescent atmosphere: a review, Atomization and Sprays, 19 (6), 501–528, 2009.

[6] P.K. Wu, K.A. Kirkendall, R. P. Fuller, and A. S. Nejad, Breakup processes of liquid jets in subsonic crossflows, Journal of Propulsion and Power, Vol. 13, No. 1, pp. 64-73, 1997.

[7] K.C. Lin, P. J. Kennedy, T.A. Jackson, Penetration heights of liquid jets in high-speed crossflows, AIAA 2002-0873, 40th AIAA Aerospace Sciences Meeting and Exhibit, Reno, Nevada, 2002.

[8] O.M. Elshamy, and S.M. Jeng, A study of liquid jet in crossflow at elevated ambient pressures, Proceedings of the 18th International Conference on Liquid Atomization and Spray System, Madison, Irvine, CA, May 2005.

[9] J. N. Stenzler, J. G. Lee, and D. A. Santavicca, Penetration of liquid jets in a crossflow, atomization and sprays, vol. 16, pp. 1–20, 2006.

[10] C.T. Brown, and V.G. McDonell, Near field behavior of a liquid jet in a crossflow, Proceedings of the ILASS Americas, 19th Annual Conference on Liquid Atomization and Spray Systems, ILASS-2006, Toronto, Canada, May 2006.

[11] M. Birouk, C.O. Iyogun, and N. Popplewell, Role of viscosity on trajectory of liquid jets in a cross-airflow, Atomization and Sprays, 17(3), pp. 267–287, 2007.

[12] R. Ragucci, A. Bellofiore, A. Cavaliere, Breakup and breakdown of bent kerosene jets in gas turbine conditions, Proceedings of the Combustion Institute 31, 2231–2238, 2007.

[13] A. Bellofiore, A. Cavaliere, R. Ragucci, Air density effect on the atomization of liquid jets in crossflow, Combust. Sci. and Tech., 179, 319–342, 2007.

[14] H.J. Yoon , J.G. Hong , C.W. Lee , Correlations for penetration height of single and double liquid jets in crssflow under high temperature conditions, Atomization and Sprays, vol. 21 (8), pp. 673-686, 2011.

[15] Y. Zheng , and A.W. Marshall, Characterization of the initial spray form low-Weber-number jets in crossflow, Atomization and Sprays, vol. 21 (7), pp. 575-589, 2011.

[16] E. Farvardin, M. Johnson, H. Alaee, A. Martinez, A. Dolatabadi, Comparative study of biodiesel and diesel jets in gaseous crossflow, Journal of Propulsion and Power, Vol. 29, No. 6, pp. 1292-1302, 2013.

[17] M. Eslamian, A. Amighi, N. Ashgriz, Atomization of liquid jet in high-pressure and high-temperature subsonic crossflow, AIAA Journal, Vol. 52, No. 7, pp. 1374-1385, 2014.

[18] J. Becker, and C. Hassa, Breakup and atomization of a kerosene jet in crossflow at elevated pressure. Atomization Sprays, 11, 49–67, 2002.

[19] S.B. Tambe, S.M. Jeng, H.C. Mongia, G. Hsiao, Liquid jets in subsonic crossflow, Paper AIAA 2005-731, 43rd AIAA Aerospace Sciences Meeting and Exhibit, Reno, NV, January 2005.

[20] R.R Lakhamraju, and S. M. Jeng, Liquid jet breakup studies in subsonic air stream at elevated temperatures, ILASS Americas. I8thAnnual Conference on Liquid Atomization and Spray Systems. Irvine. CA. May 2005.

[21] S. Freitag, and C. Hassa, Spray characteristics of a kerosene jet in crossflow of air at elevated pressure. In: Proceedings ILASS- Europe 2008.

[22] Q. Wang, U.M. Mondragon, C.T. Brow, V.G. McDonell, Characterization of trajectory, break point, and break point dynamics of a plain liquid jet in a crossflow, Atomization and Sprays, Vol 21(3), pp 203-219, 2011.

[23] L. Li, Y. Lin, X. Xue, W. Gao, C.J. Sung, Injection of liquid kerosene into a high-pressure subsonic air crossflow from normal temperature to elevated temperature, ASME Turbo Expo 2012: Turbine Technical Conference and Exposition, Copenhagen, Denmark, June 11–15, 2012.

[24] T.H. Chen, C.R. Smith, D.G. Schommer, A.S. Nejad, Multi-zone behavior of transverse liquid jet in high-speed flow, AIAA paper 93- 0453, 1993.

[25] O.M. Elshamy, S. B. Tambe, J. Cai, S. M. Jeng, Excited liquid jets in subsonic crossflow, 45th AIAA Aerospace Sciences Meeting and Exhibit 8-11 January 2007, Reno, Nevada.

[26] S. I. Baranovsky, and J. A. Schetz, Effect of injection angle on liquid injection in supersonic flow, AIAA Journal, Vol.18, No. 6, pp. 625-629, 1980.

[27] R. P. Fuller, P.K. Wu, K. A. Kirkendall, A. S. Nejad, Effects of injection angle on atomization of liquid jets in transverse airflow, AIAA Journal, Vol. 38, No. 1, pp. 64-72, 2000.

[28] E. Lubarsky, D. Shcherbik, O. Bibik, Y. Gopala, J. W. Bennewitz, B. T. Zinn, Fuel jet in crossflow, experimental study of spray characteristics, ILASS Americas, 23rd Annual Conference on Liquid Atomization and Spray Systems, Ventura, CA, May 2011.

[29] A. Mashayek, M. Behzad, N. Ashgriz, Multiple injector model for primary breakup of a liquid jet in crossflow,AIAA Journal, Vol. 49, No. 11, pp. 2407-2420, 2011.

[30] F. M. White, Fluid Mechanics, Forth Edition, Mcgraw-Hill Series in Mechanical Engineering, 1998.

[31] A. Mashayek, A. Jafari, N. Ashgriz, Improved model for the penetration of liquid jets in subsonic crossflows, AIAA Journal, Vol. 46, No. 11, pp. 2674-2686, 2008.

[32] M.K. Kim, J. Song., J. Hwang, Y. Yoon, Effects of canted injection angles on the spray characteristics of liquid jets in subsonic crossflows, Atomization and Sprays, Vol. 20, No.9, pp. 749762, 2010.

[33] B. E. Scharfman, J. W. M. Bush, A. H. Techet, Hydrodynamic instabilities in round liquid

jets in gaseous crossow, ILASS-Americas 25th Annual Conference on Liquid Atomization and Spray Systems, Pittsburgh, PA, May 2013.

[34] M. Costa, M. J. Melo, J. M. M. Sousa, Y. Levy, Spray characteristics of angled liquid injection into subsonic crossflows, AIAA Journal, Vol. 44, No. 3, pp. 646-653, 2006.

[35] H. Almeida, J. M. M. Sousa, M. Costa, Effect of the liquid injection angle on the atomization of liquid jets in subsonic crossflows, Atomization and Sprays, Vol 24(1), pp 81-96, 2014.

[36] J. Mazallon, Z. Dai, G.M. Faeth, Primary breakup of nonturbulent round liquid jets in gas crossflows, Atomization and Sprays, Vol. 9, pp. 291-311, 1999.

[37] C.L. Ng, Deformation, wave phenomena, and breakup outcomes of round nonturbulent liquid jets in uniform gaseous crossflow, PhD, Oklahoma State University, 2006.

[38] C.L. Ng, K.A. Sallam, H.M. Metwally, and C. Aalburg, Deformation and surface waves properties of round nonturbulent liquid jets in gaseous crossflow, ASME Fluids Engineering Summer Conference, Paper No. FEDSM2005-77469, 2005.

Chapter 4

A Two-Zone Model for Predicting the Trajectory and Penetration Height of a Liquid Jet in a Subsonic Gaseous Crossflow

4.1. Abstract

A hybrid Eulerian-Lagrangian approach was utilized to develop a model for predicting the penetration of a liquid jet in a subsonic gaseous crossflow. This was achieved by taking into account the effect of all forces acting on the jet including drag, gravitation and surface tension, as well as the mass shedding from the liquid column. The effect of mass shedding from the liquid column and jet Reynolds number on the spray penetration height was also studied. It was found that, although the momentum flux ratio q plays a predominant role in the prediction of a liquid jet column, the liquid jet penetration can be affected when changing the ambient temperature and pressure (or gas to liquid density and viscosity ratio) especially when holding constant q and jet velocity v_j. Two correlations were developed in the form of sinusoidal-exponential and logarithmic function for the prediction of liquid column and droplets plume regions, respectively. The proposed correlations are capable of predicting jet penetration of different liquids in a subsonic crossflow at different operating conditions and injection angles. The predictions showed reasonable agreement with published experimental data and empirical correlations.

Nomenclature

A	liquid column cross sectional area, m^2
A_d	frontal area of the droplet, m^2
A_L	lateral surface area of the liquid column, m^2
Bo	Bond number, $\rho_l g d_j^2/\sigma$
C_D	liquid column average drag coefficient
C_{Dx}	droplet drag coefficient in *x*- direction
C_{Dz}	droplet drag coefficient in *z*- direction
D	channel diameter, m
d	liquid column diameter, m
d_d	droplet diameter, m
d_j	liquid jet diameter at the nozzle exit, m
$\boldsymbol{e}_N$,	unitary base vector normal to liquid column axis
$\boldsymbol{e}_T$	unitary base vector tangential to liquid column
$\boldsymbol{e}_x$	unitary base vector in horizontal direction
$\boldsymbol{e}_z$	unitary base vector in vertical upwardly direction
g	gravitational acceleration vector, m/s^2
k	local curvature of the jet
l_c	liquid column perimeter, m
m_d	mass of droplet, kg
$\dot{m}$	rate of mass shedding from the liquid column
Oh	Ohnesorge number, $\mu_l/\sqrt{\rho_l d_j \sigma}$
P	absolute pressure of the crossflow, kPa
q	jet momentum flux ratio, $\rho_l v_j^2/\rho_g u_g^2$
Re_{ch}	channel Reynolds number, $\rho_g u_g D/\mu_g$
Re_j	jet Reynolds number, $\rho_l v_j d_j/\mu_l$
Re_d	droplet Reynolds number
s	arclength of the jet trajectory centerline absolute
T	temperature of the crossflow, K
t_b	column breakup time, s
t_i	onset of surface breakup time, s
t_s	characteristic liquid-phase time, $(\rho_l/\rho_g)^{\frac{1}{2}} d_j/u_g$
t_v^*	characteristics viscous time, $d_j^2/(\mu_l/\rho_l)$
u_g	crossflow velocity, m/s
u_{shed}	droplet velocity after surface breakup
$\boldsymbol{V}$	liquid velocity vector, m/s
V	liquid velocity, m/s
v_j	liquid velocity at the nozzle exit, m/s
We_g	gas phase Weber number, $\rho_g u_g^2 d_j/\sigma$
We_j	jet Weber number, $\rho_l v_j^2 d_j/\sigma$
x	coordinate in gas crossflow (horizontal) direction, m
x_b	column breakup location, m
z	coordinate in liquid injection (vertical) direction, m

Greek symbol

λ_c	column wavelength, m
μ	viscosity, kg/(m.s)
ρ	density, kg/m^3
σ	liquid surface tension, N/m
ψ	liquid column angle
ψ_o	injection angle

Subscripts

b	column breakup
d	droplet
g	gas
j	jet
l	liquid
o	standard conditions
w	water

4.2. Introduction

In the last decades, transverse injection of a liquid jet into an elevated temperature and pressure gaseous crossflow is an approach which is often employed in both avionic and stationary power generation systems where fast vaporization and mixing rate are desired. This method of liquid fuel/air mixture preparation enhances flame stabilization, fuel conversion efficiency, and accordingly emission reduction [1-4]. In such systems, data describing a liquid jet trajectory and its penetration in a crossflow is highly required for combustor design as it determines the distribution of the fuel in a combustor and plays a crucial role in preventing fuel impingement onto the walls of a combustor [5].

Numerous empirical and theoretical correlations for predicting the trajectory of a liquid jet injected into a gaseous crossflow were proposed in the literature. Given the avionic applications, earlier studies were allocated to supersonic and hypersonic crossflows (see, e.g., [6-8]). Published studies on the transverse injection of a liquid jet into a subsonic crossflow can generally be categorized based on the operating/test conditions used in extracting the results such as i) room conditions; ii) elevated temperature and room pressure; iii) room temperature and elevated pressure; iv) elevated temperature and pressure conditions. There were numerous published studies which investigated the injection of a liquid jet into a subsonic gaseous crossflow at room test conditions (e.g., [1, 9-19]). These studies mostly correlated the liquid jet trajectory with x/d_j and q. For instance, Wu et al. [1] experimentally studied the breakup process of a liquid jet injected into a subsonic gaseous crossflow (at Mach number of 0.2, 0.3 and 0.4) at test conditions close to the room conditions (T = 306 K and P = 140 kPa). They correlated the liquid column trajectory with q (see Eq. (4-1) below) based on force analysis of a cylindrical liquid element subjected to an aerodynamic drag force. They predicted the height of the column breakup locations utilizing the time required for an

analogous droplet to complete an aerodynamic secondary breakup process, and concluded that the aerodynamic forces acting on a droplet and those acting on a liquid column have similar effect.

$$\frac{z}{d_j} = 1.37\left(q\frac{x}{d_j}\right)^{0.5} \tag{4-1}$$

Published studies at elevated temperature and room pressure conditions reported additional parameters in addition to those of Eq. (4-1) [20-23]. For instance, temperature ratio [21] or gas Weber number and viscosity ratio [20, 22] were included. Stenzler et al. [22] experimentally studied the trajectory of a jet injected into a subsonic gaseous crossflow using different liquid properties (e.g., water, acetone and 4-heptanone) at different air crossflow temperatures, up to 573.15 K. They indicated that We_g and liquid viscosity, through their respective effect on droplet size and the trajectory of liquid column, affect the liquid jet penetration. They proposed different correlations for unheated and heated air crossflow. For example, their correlation for all cases was expressed as

$$\frac{z}{d_j} = 3.688q^{0.430}\left(\frac{x}{d_j}\right)^{0.384} We_g^{-0.110}\left(\frac{\mu_l}{\mu_w}\right)^{-0.108} \tag{4-2}$$

There also exist some studies which specifically focused on liquid jet penetration at room temperature and elevated pressure conditions (e.g., [24-28]). For instance, Elshamy and Jeng [25] experimentally investigated the breakup and penetration of a plain liquid jet injected into a high-pressure air crossflow, up to 700 kPa. They added gas Weber number and pressure ratio to their correlation, Eq. (4-3), in order to consider the impact of cross airflow pressure on the jet trajectory.

$$\frac{z}{d_j} = 4.95q^{0.424}\left(\frac{x}{d_j}\right)^{0.279} We_g^{-0.076}\left(\frac{P}{P_o}\right)^{-0.051} \quad (4\text{-}3)$$

To test the conditions relevant to real combustors, some researchers investigated the effect of both elevated temperature and pressure of cross airflow on liquid jet penetration (e.g., [29-36]). Eslamian et al. [36], for instance, examined the breakup and penetration of a water jet injected into a subsonic gaseous crossflow under elevated temperature up to 573 K and pressure up to 517 kPa. They also studied the effect of these parameters on the shape and the streamwise area of the spray plume, and noted that at a given pressure, temperature, and air crossflow velocity, there exists an optimum liquid jet velocity that corresponds to a maximum spray area and optimum atomization process. They concluded that correlating solely the jet trajectory with x/d_j and q oversimplify the flow dynamics, especially at elevated conditions. Therefore, they added channel and jet Reynolds numbers in Eq. (4-4) to consider the impact of elevated conditions on the properties of both air and liquid, and accordingly on the jet trajectory.

$$\frac{z}{d_j} = 0.191q^{0.3}\left(\frac{z}{d_j}\right)^{0.43} Re_{ch}^{0.12} Re_j^{0.14} \quad (4\text{-}4)$$

From the reviewed correlations above, it appears that as the test conditions change from room to elevated conditions (e.g., approaching real gas turbine conditions), the momentum flux ratio q alone becomes inadequate to predict the trajectory of a liquid jet; and hence other parameters such as gas to liquid density and viscosity ratio should be taken into account. It is also seen that coefficients and power exponents related to one specific term (e.g., x/d_j, q or other parameters) differ from one study to another as there is a wide range of variation in the penetration predictions of a liquid jet. There are various parameters contributing to these discrepancies such as different

liquid properties, test conditions, injector/nozzle geometries, measurement techniques, assumptions and uncertainties made in developing these correlations. For instance, most data on jet penetration were determined employing a simple thresholding technique which depends on a specific value used in each study to identify the boundaries of a liquid jet in a crossflow. Moreover, as Brown et al. [16] mentioned, it appears that most published jet penetration correlations assumed a liquid jet velocity based on the volume flow rate divided by the injector cross sectional area (i.e., a discharge coefficient of 1.0). However, since the discharge coefficient of a nozzle is a function of jet Reynolds number Re_j and its internal geometry, this could be one more reason of these discrepancies. Furthermore, the contributing parameters may have some level of interdependency. For instance, changing temperature would change air crossflow properties, which in turn could affect liquid jet trajectory in a gaseous crossflow. This interdependency could also be one of the reasons contributing to these discrepancies; as one study showed that viscosity leads to a higher jet penetration [22], whereas another reported the opposite scenario [10].

Chen et al. [37] stated that several zones of a liquid jet (i.e., liquid column region adjacent to the injector and spray plume region in the far-field) exhibit different characteristics and a combined functional form is required to describe their penetration profile. The liquid column region, corresponding to jet bending region before column breakup location, is highly affected by aerodynamic drag force. On the other hand, the spray plume region, corresponding to droplets plume region after secondary breakup, depends on droplets size. Hence, the present study aims examining the complex physics of the problem and hence establishing the contribution of the various influencing parameters. In this study, a two-zone model was adopted where a wide range of liquid properties and crossflow test conditions were considered. The ultimate objective was to develop reliable prediction of a liquid jet penetration into a subsonic gaseous crossflow.

4.3. Model Description

The interaction of two fluid streams (i.e., a liquid jet discharged into a gaseous crossflow) is treated by adopting a new method which uses a hybrid Eulerian-Lagrangian approach. A schematic view of a liquid jet penetrating into a subsonic gaseous crossflow is illustrated in Figure 4-1. In general, the liquid jet leaves the nozzle as an unbroken column, begins to ruffle as a result of Kelvin-Helmholtz instability which develops along the liquid column and finally breaks up into droplets due to column breakup process [38], as is illustrated in Fig. 4-1a. As the liquid begins to disintegrate from the column and the surface breakup becomes dominant due to the increased air crossflow shear force (see Fig. 4-1b), the jet penetration height decreases [19].

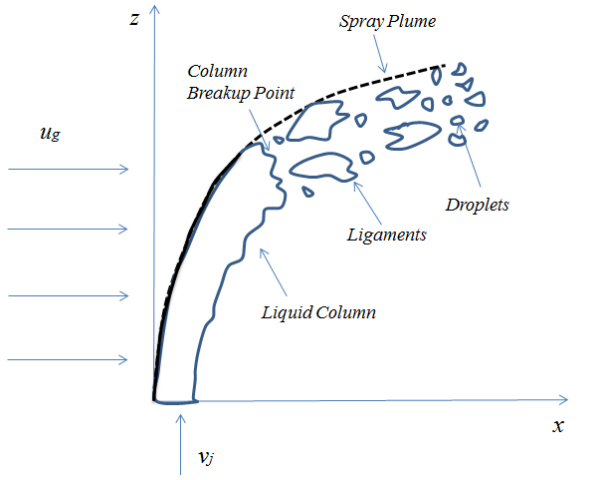

(a)

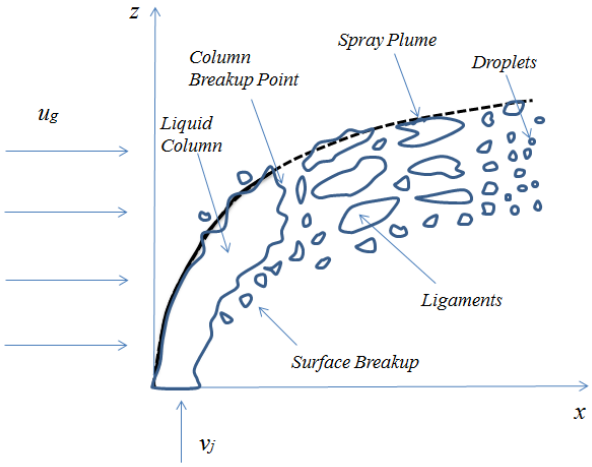

(b)

Figure 4-1: Jet penetration into crossflow a) column breakup, and b) surface breakup; solid and dashed lines show the liquid column and spray plume regions respectively.

Early studies [1, 39-41] developed a theoretical model for predicting the trajectory of a liquid jet where the liquid jet was assumed as a stack of thin cylindrical elements piled on top of each other. A force analysis was then performed on the element, and the motion of the system along the jet trajectory was calculated. In the present analysis, however, two approaches have been combined concerning the physics of two different zones of the liquid jet. In the first or near field zone, a force

balance was applied to a control-volume, and forces acting upon the liquid column such as drag, gravitation and surface tension forces were introduced and then the mass and energy conservation equations were developed using the control-volume or an Eulerian approach, while considering the mass shedding from the liquid column (i.e., surface breakup). This led to develop an explicit algebraic correlation in a sinusoidal-exponential functional form to predict the trajectory of a liquid jet in a subsonic gaseous crossflow. In the second or far field zone, a logarithmic functional form for the trajectory of large droplets generated at the column breakup location was developed using a Lagrangian approach, while utilizing the information on the column breakup location obtained from the first zone as the initial conditions for the second zone. In other words, the behavior in the near field region establishes the subsequent penetration of the liquid jet in the far field region, where the column breakup location, x_b, determines the boundaries of these zones.

4.3.1. First Zone – Eulerian Approach

An Eulerian approach was utilized to predict the trajectory of a transverse liquid jet in the near field ($x \leq x_b$), that is the liquid column. A mathematical model was developed which takes into account the mass and energy conservation equations and also consider mass shedding from the liquid column. The conservation laws were applied through the cylindrical control volume associated with a reference coordinate system (x, z), as illustrated in Fig. 4-2.

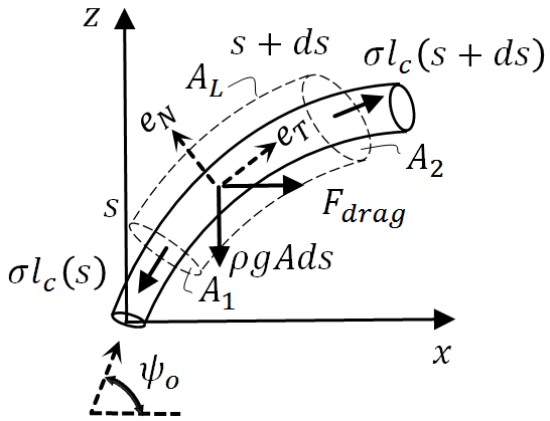

(a)

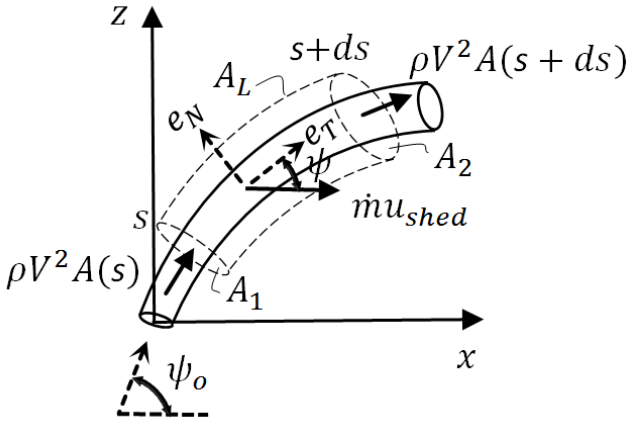

(b)

Figure 4-2: A control volume defined for *a*) local equilibrium of forces on a control volume, *b*) local momentum conservation due to mass exchange.

The control volume is bounded by two disks A_1 and A_2 at the arclength of the jet trajectory centerline s and s+ds, respectively, and by A_L, which is the lateral surface of the cylinder intercepting A_1 and A_2. In this figure, the x axis origin is located at the center of the injection point (centreline at the nozzle's exit orifice), and z axis has the same origin as x but it is perpendicular to x.

In the present model, a convenient local framework with the normal and tangent unitary vectors ($\boldsymbol{e}_N, \boldsymbol{e}_T$) is defined where ψ is the angle between the horizontal (e_x) and the tangential (e_T) axes. The following geometrical parameters and relations are also defined as

- $\boldsymbol{V}$ ($= V\boldsymbol{e}_T$) is the liquid velocity vector relative to the reference coordinate system, where V is the liquid velocity.
- d_j, l_c and A are the liquid jet diameter, perimeter and cross sectional area, respectively, which are all dependent on s.
- the local curvature of the jet trajectory can be defined as $k = \frac{d\boldsymbol{e}_T}{ds} = \frac{d\psi}{ds}\boldsymbol{e}_N = \cos\psi\frac{d\psi}{dx}\boldsymbol{e}_N = \frac{d\sin\psi}{dx}\boldsymbol{e}_N$ when using $\frac{d}{ds} = \frac{dx}{ds}\cdot\frac{d}{dx} = \cos\psi\frac{d}{dx}$

The unitary base vectors ($\boldsymbol{e}_x, \boldsymbol{e}_z$) in the horizontal and vertical direction are related to the unitary base vectors ($\boldsymbol{e}_N, \boldsymbol{e}_T$) in normal and tangential direction as

- $\boldsymbol{e}_{\mathrm{z}} = \sin\psi\,\boldsymbol{e}_T + \cos\psi\boldsymbol{e}_N$ and $\boldsymbol{e}_{\mathrm{x}} = \cos\psi\,\boldsymbol{e}_T - \sin\psi\,\boldsymbol{e}_N$

Given the steady flow within the control surface, the integral form of the mass-conservation law can be written as follows:

$$\int_{cs}\rho_l(\boldsymbol{V}\bullet\boldsymbol{n})dA = 0 \tag{4-5}$$

where n is the outward normal unit vector. The linear-momentum relation applied to the control surface can be expressed as

$$\sum\boldsymbol{F} = \int_{cs}\boldsymbol{V}\rho_l(\boldsymbol{V}\bullet\boldsymbol{n})dA \tag{4-6}$$

In essence, the entire equation is a vector relation due to the term $\boldsymbol{V}$ in the integral term which holds for the momentum flux through the control volume, and the term $\sum \boldsymbol{F}$ is the vector sum of all forces acting on the control volume.

As shown in Fig. 4-2a, there are, in general, four different forces acting on a liquid jet in a crossflow namely

- the weight of the column: $-\rho_l g A ds \boldsymbol{e}_z = -\rho_l g A ds(\sin\psi\, \boldsymbol{e}_T + \cos\psi \boldsymbol{e}_N)$, submitted to gravitation force;
- the surface tension force acting along the column: $^1/_2\, \sigma_l l_c \boldsymbol{e}_T\big|_{s+ds} - {}^1/_2\, \sigma_l l_c \boldsymbol{e}_T\big|_s = {}^1/_2\, \sigma_l (dl_c \boldsymbol{e}_T/ds) ds = {}^1/_2\, \sigma_l (dl_c/ds\, \boldsymbol{e}_T + l_c\, d\boldsymbol{e}_T/ds) ds$;
- the drag (aerodynamic) force due to the gaseous crossflow: $^1/_2\, C_D \rho_g \left(u_g - V cos\psi\right)^2 d_j ds \boldsymbol{e}_x = {}^1/_2\, C_D \rho_g \left(u_g - V cos\psi\right)^2 d_j ds(\cos\psi\, \boldsymbol{e}_T - \sin\psi\, \boldsymbol{e}_N)$;

Regarding the drag force, it is worth mentioning that Wu et al. [1] reported that the jet velocity in x direction ($V cos\psi$) is less than 16% of the crossflow air velocity u_g, and hence they assumed that the velocity difference can be represented by a constant, u_g, when the variation of $\left(u_g - V cos\psi\right)$ is accounted for in C_D. Since the drag coefficient C_D proposed by Wu et al. [1] is adopted in the present study (as will be discussed later on), the drag force considered in the present model is expressed as $^1/_2\, C_D \rho_g u_g^2 d_j ds(\cos\psi\, \boldsymbol{e}_T - \sin\psi\, \boldsymbol{e}_N)$. From the geometrical relations, these forces can be projected on the framework axis ($\boldsymbol{e}_N$, $\boldsymbol{e}_T$) as follows:

$$\sum \boldsymbol{F} \bullet \boldsymbol{e}_T \frac{1}{ds} = -\rho_l g A \sin\psi + \frac{1}{2}\sigma_l \frac{dl_c}{dx}\cos\psi + \frac{1}{2} C_D \rho_g u_g^2 d_j \cos\psi \qquad (4\text{-}7)$$

$$\sum \boldsymbol{F}\bullet\boldsymbol{e}_N \frac{1}{ds} = -\rho_l g A\cos\psi + \frac{1}{2}\sigma_l l_c \frac{d\sin\psi}{dx} - \frac{1}{2}C_D\rho_g u_g^2 d_j \sin\psi \tag{4-8}$$

According to Fig. 4-2b, the variation of the momentum flux due to mass exchange through the jet control surface A can be defined as

through A_1 and A_2 as

$$\begin{aligned}\rho_l V^2 A\boldsymbol{e}_T|_{s+ds} - \rho_l V^2 A\boldsymbol{e}_T|_s &= \rho_l(dV^2 A\boldsymbol{e}_T/ds)ds \\ &= \rho_l(dV^2 A/ds\ \boldsymbol{e}_T + V^2 A\, d\boldsymbol{e}_T/ds)ds\end{aligned} \tag{4-9}$$

through $A_L$as

$$\dot{m}u_{shed}e_x = \dot{m}u_{shed}(\cos\psi\,\boldsymbol{e}_T - \sin\psi\,\boldsymbol{e}_N) \tag{4-10}$$

where $\dot{m}$ is the rate of mass shedding from the liquid column as the jet moving along its trajectory, and u_{shed} is the droplet velocity after breakup along the direction of the crossflow. In the present model, the equation of mass shedding rate, Eq. (4-11), is based on the aerodynamic shattering of liquid drops, which was first introduced and applied for liquid droplets shattering [42, 43], and then was used for the column shedding of a liquid jet with some modifications [40, 44-45].

$$\dot{m} = \frac{3}{4}(\pi d_j)^{\frac{3}{2}} G\left(\frac{8\mu_l}{3G\rho_l u_g}\right)^{\frac{1}{2}} \rho_l u_g \frac{(t_b - t_i)}{t_b} R_M \tag{4-11}$$

where $G = \left(\frac{\rho_g}{\rho_l}\right)^{\frac{1}{3}}\left(\frac{\mu_g}{\mu_l}\right)^{\frac{1}{3}}$.

In the present model, two modifications were used. First, as the mass shedding from the liquid column (surface breakup) is highly dependent on the gas Weber number We_g and accordingly breakup modes (i.e., bag, multimode, and shear breakup regimes) of the jet, the term $(t_b - t_i)/t_b$ was added to make the equation applicable for all breakup modes based on t_i. It is assumed that

the mass shedding associated with each of these breakup modes is averaged along the liquid column from the jet exit to the column breakup location. Where t_b is the time of penetration of a liquid jet into a crossflow (i.e., its column breakup time), which was reported by Sallam et al. [46] for $We_g < 300$ as $t_b = 2.5t_s$, where $t_s = \left(\rho_l/\rho_g\right)^{\frac{1}{2}} d_j/u_g$ is the characteristic liquid-phase time of Ranger and Nicholls [42]. Gopala et al. [33] then showed that the breakup time is smaller for the range of $We_g > 300$. The parameter $t_i = 0.0004\left[\left(\mu_l/\mu_g\right)/\, We_g\right] t_v^*$ is the time of the onset of surface breakup, where $t_v^* = d_j^2/(\mu_l/\rho_l)$ is the characteristic viscous time [46]. The second modification was achieved by adding mass ratio $R_M = \left((3/2) \times 1/d_j\right) ds$ to Eq. (4-11) in order to make it compatible for a cylindrical liquid jet [40, 45]. Furthermore, $u_{shed} = 6.7u_g/\left(\rho_l/\rho_g\right)^{\frac{1}{2}}$ is defined according to the velocity correlation of the measurements of Sallam et al. [46].

Finally, the tangential and normal components of the momentum flux through the control surface can be expressed as follows:

$$\int_{cs} \boldsymbol{V}\rho_l(\boldsymbol{V}\bullet\boldsymbol{n})dA\bullet\boldsymbol{e}_T \frac{1}{ds} = \rho_l \frac{dV^2 A}{dx}\cos\psi + \rho_l \left[\frac{9(\pi)^{\frac{3}{2}}}{8} G \left(\frac{8\mu_l d_j}{3G\rho_l u_g}\right)^{\frac{1}{2}} \frac{(t_b - t_i)}{t_b}\right] \frac{6.7u_g^2}{\left(\rho_l/\rho_g\right)^{\frac{1}{2}}}\cos\psi \tag{4-12}$$

$$\int_{cs} \boldsymbol{V}\rho_l(\boldsymbol{V}\bullet\boldsymbol{n})dA\bullet\boldsymbol{e}_N \frac{1}{ds} = \rho_l V^2 A \frac{d\sin\psi}{dx} - \rho_l \left[\frac{9(\pi)^{\frac{3}{2}}}{8} G \left(\frac{8\mu_l d_j}{3G\rho_l u_g}\right)^{\frac{1}{2}} \frac{(t_b - t_i)}{t_b}\right] \frac{6.7u_g^2}{\left(\rho_l/\rho_g\right)^{\frac{1}{2}}}\sin\psi \tag{4-13}$$

Substituting Eqs. (4-7 & 4-8) and (4-12 &4-13) in Eq. (4-6), the governing equations of the trajectory of a liquid jet in a gaseous crossflow can finally be expressed as

$$\rho_l \cos\psi \left(-gA\tan\psi + \frac{1}{2}\frac{\sigma_l}{\rho_l}\frac{dl_c}{dx} + \frac{1}{2}C_D\frac{\rho_g}{\rho_l}u_g^2 d_j - \frac{dV^2A}{dx} - \left[\frac{9(\pi)^{\frac{3}{2}}}{8}G\left(\frac{8\mu_l d_j}{3G\rho_l u_g}\right)^{\frac{1}{2}}\frac{(t_b - t_i)}{t_b}\right]\frac{6.7u_g^2}{(\rho_l/\rho_g)^{\frac{1}{2}}}\right) = 0 \quad (4\text{-}14)$$

$$\rho_l \sin\psi \left(-gA\cot\psi + \frac{1}{2}\frac{\sigma_l}{\rho_l}\frac{l_c}{\sin\psi}\frac{d\sin\psi}{dx} - \frac{1}{2}C_D\frac{\rho_g}{\rho_l}u_g^2 d_j - \frac{V^2A}{\sin\psi}\frac{d\sin\psi}{dx} + \left[\frac{9(\pi)^{\frac{3}{2}}}{8}G\left(\frac{8\mu_l d_j}{3G\rho_l u_g}\right)^{\frac{1}{2}}\frac{(t_b - t_i)}{t_b}\right]\frac{6.7u_g^2}{(\rho_l/\rho_g)^{\frac{1}{2}}}\right) = 0 \quad (4\text{-}15)$$

Although, in reality, the jet cross section changes slightly into a kidney shape [47], it is assumed in this model that the liquid column can be approximated as a cylindrical liquid element having a diameter equal to that of the liquid jet at the nozzle exit, d_j. This assumption has been widely adopted in the literature (e.g., [1, 39, 48]). To make this assumption rational and to include the liquid column deformation and turbulence effect, Wu et al. [1] proposed a correlation for the prediction of an average value of the drag coefficient along the entire length of the liquid column (C_D) for different liquids as $C_D/C_{Dw} = 0.984(\mu_l/\mu_w)^{0.364}$, where $C_{Dw} = 1.51$ and μ_w are the water drag coefficient and viscosity, respectively. This correlation was then confirmed by a numerical study of Mashayek et al. [40], who accounted for the change in the jet cross sectional area from a circular to an elliptic shape. For more information on the effect of drag coefficient on the trajectory of a liquid jet, one can refer to Mashayek et al. [40]. With this assumption, the terms dl_c/dx, dV/dx, dV^2A/dx in Eq. (4-14) become zero, and hence Eqs. (4-14) and (4-15) become

$$\tan\psi = \left(\frac{1}{2}C_D\rho_g u_g^2 d_j - \rho_l\left[\frac{9(\pi)^{\frac{3}{2}}}{8}G\left(\frac{8\mu_l d_j}{3G\rho_l u_g}\right)^{\frac{1}{2}}\frac{(t_b - t_i)}{t_b}\right]\frac{6.7u_g^2}{\left(\rho_l/\rho_g\right)^{\frac{1}{2}}}\right)\Big/\rho_l gA \tag{4-16}$$

$$\begin{aligned}\frac{1}{2}C_D\frac{\rho_g}{\rho_l}u_g^2 d_j - \left[\frac{9(\pi)^{\frac{3}{2}}}{8}G\left(\frac{8\mu_l d_j}{3G\rho_l u_g}\right)^{\frac{1}{2}}\frac{(t_b - t_i)}{t_b}\right]\frac{6.7u_g^2}{\left(\rho_l/\rho_g\right)^{\frac{1}{2}}} \\ = -gA\cot\psi + \left(\frac{1}{2}\frac{\sigma_l}{\rho_l}\frac{l_c}{\sin\psi} - \frac{V^2 A}{\sin\psi}\right)\frac{d\sin\psi}{dx}\end{aligned} \tag{4-17}$$

Substituting Eq. (4-16) into Eq. (4-17) to cancel $\cot\psi$, and multiplying both sides of the resulting equation by $\rho_l \sin\psi$, the following relation can be obtained

$$\begin{aligned}\left\{\left(\frac{1}{2}C_D\rho_g u_g^2 d_j - \rho_l\left[\frac{9(\pi)^{\frac{3}{2}}}{8}G\left(\frac{8\mu_l d_j}{3G\rho_l u_g}\right)^{\frac{1}{2}}\frac{(t_b - t_i)}{t_b}\right]\frac{6.7u_g^2}{\left(\rho_l/\rho_g\right)^{\frac{1}{2}}}\right)\right. \\ \left. + \left[(\rho_l gA)^2\Big/\left(\frac{1}{2}C_D\rho_g u_g^2 d_j - \rho_l\left[\frac{9(\pi)^{\frac{3}{2}}}{8}G\left(\frac{8\mu_l d_j}{3G\rho_l u_g}\right)^{\frac{1}{2}}\frac{(t_b - t_i)}{t_b}\right]\frac{6.7u_g^2}{\left(\rho_l/\rho_g\right)^{\frac{1}{2}}}\right)\right]\right\}\sin\psi \\ = \left(\frac{1}{2}\sigma_l l_c - \rho_l V^2 A\right)\frac{d\sin\psi}{dx}\end{aligned} \tag{4-18}$$

Dividing both sides of Eq. (4-18) by $\rho_l V^2 A$, and rewriting it in a non-dimensional form, it becomes

$$\frac{\alpha}{d_j}\sin\psi = \beta\frac{d\sin\psi}{dx} \tag{4-19}$$

where the coefficients α and β are expressed as

$$\alpha = \gamma + \left(\frac{Bo}{We_j}\right)^2\frac{1}{\gamma} \tag{4-20}$$

$$\gamma = \frac{2C_D}{\pi q} + \left(\frac{410}{q}\right)^{\frac{3}{4}}\left(\frac{\rho_g}{\rho_l}\right)^{-\frac{1}{12}}\left(\frac{\mu_g}{\mu_l}\right)^{\frac{1}{6}}\left(\frac{t_b - t_i}{t_b}\right)Re_j^{-\frac{1}{2}}$$

$$\beta = \frac{2}{We_j} - 1$$

where Bond number, $Bo = \rho_l g d_j^2/\sigma_l$, prescribes the ratio of the gravitational to surface tension forces acting on a liquid jet; liquid phase Weber number, $We_j = \rho_l v_j^2 d_j/\sigma_l$, is the ratio of liquid inertia to surface tension, and $Re_j = \rho_l v_j d_j/\mu_l$ is the liquid phase Reynolds number.

Considering $\frac{d \sin\psi}{dx} = \cos\psi \frac{d\psi}{dx}$ and $\tan\psi = \frac{dz}{dx}$, and substituting them into Eq. (4-19), the variation of z as a function of ψ can be found by integrating this equation with respect to x, and considering the boundary condition $\psi = \psi_o$ at $z = 0$ so that

$$z = \frac{\beta}{\left(\alpha/d_j\right)}(\psi - \psi_o) \tag{4-21}$$

In addition, to calculating ψ as a function of x, Eq. (4-19) can be rewritten as $\left(\frac{\alpha}{d_j}\right)/\beta = \frac{1}{Q}\frac{Q}{dx}$, where $Q = \sin\psi$. By integrating this equation with respect to x, and taking the boundary conditions as $Q = \sin\psi_o$ at $x = 0$, we obtain

$$\psi = \sin^{-1}\left[\sin\psi_o . exp\left(\frac{\left(\alpha/d_j\right)}{\beta}x\right)\right] \tag{4-22}$$

Finally, by eliminating ψ in Eqs. (4-21) and (4-22), an explicit correlation in a sinusoidal-exponential functional form for a liquid jet trajectory in a gaseous crossflow is obtained as follows:

$$z^* = \frac{\beta}{\alpha}\left(\sin^{-1}\left[\sin\psi_o . exp\left(\frac{\alpha}{\beta}x^*\right)\right] - \psi_o\right) \tag{4-23}$$

where $z^* = z/d_j$ and $x^* = x/d_j$ are, respectively, the non-dimensional liquid injection and gas streamwise distance from the nozzle. Finally, since equation (4-23) was derived for the centerline (or core) of the jet and in order to find the jet penetration, the coordinates must be transferred from

the center of the control surface to the upper boundary of the liquid jet [40]. Consequently, considering Fig. 4-2, two transformations were applied as $\left(x-(d/2)sin\psi+(d/2)\right)$ in the x-direction, and $(z+(d/2)cos\psi)$ in z-direction.

4.3.2. Second Zone – Lagrangian Approach

In this section, in order to find the penetration into a crossflow of a liquid jet after column breakup (that is in the droplets region which is named here as second zone), a functional form for the trajectory of large droplets created at the column breakup location$(x=x_b)$ were developed using a Lagrangian approach. Because of the fact that droplets, after column breakup are no longer connected to the liquid column and only exposed to the crossflow, do not necessarily follow the liquid column trajectory Eq. (4-23). To solve the equations governing the motion of droplets in x and z directions, two initial conditions were required. Concerning the initial positon of droplet, it was considered to be at the column breakup location $x=x_b$ and its corresponding $z=z_b$. In addition, the initial velocity of droplets at $x=x_b$ was assumed to be equal to the liquid column velocity, and its x- and z- components were found by projecting the velocity vector in these two directions using Eq. (4-22). In addition, the size of droplets generated in the column breakup location is given as [49],

$$d_d=d_j(1.5\lambda_c)^{1/3} \tag{4-24}$$

where $\lambda_c=16.3d_jWe_g^{-0.79}$ is the wavelengths between nodes [50].

Since the main objective of the present model was to develop correlations for predicting the penetration (or the upper boundary) of a liquid jet, it is assumed that the effect of the interaction between droplets and their secondary breakup on the jet penetration is negligible. The evaporation

was also neglected, as experiments on the jet trajectory at elevated temperature and pressure test conditions [30, 36] revealed that the droplet evaporation has negligible effect on jet trajectory up to $x/d_j = 100$, which is the range considered in the present study. Furthermore, the gravity force in z-direction was not considered in the present modeling, as the mass of droplet and accordingly the resulting gravity force is insignificant when compared with the drag force effect (e.g., Refs. [5] and [9]). With these assumptions, and presuming a decoupled approach of the droplet momentum equations; where the influence of $\left(v_g - v_j sin\psi\right)$ and $\left(u_g - v_j cos\psi\right)$ term in, respectively, the momentum equation in x- and z-direction (with v_g as the crossflow velocity in z-direction is taken zero in this study) is neglected. The equations governing the motion of a droplet using Lagrangian approach take the following form in x- and z-direction [5]

In x-direction:

$$m_d \frac{dx^2}{dt^2} = A_d \rho_g \left(u_g - \frac{dx}{dt}\right)^2 C_{Dx} \tag{4-25}$$

where $m_d = \rho_l (1/6)\pi d_d^3$ is the mass of the droplet, in which d_d is the diameter of the droplet at the column breakup location, and $A_d = (1/4)\pi d_d^2$ is the droplet frontal area. C_{Dx} is the drag coefficient of droplet in the x-direction, and its average value for a smooth sphere is 0.47 [51]. In the present model, however, in order to find a more accurate value of C_{Dx}, the formula of Putnam [5] is adopted as follows:

$$C_{Dx} = \begin{cases} \dfrac{24}{Re_d}\left(1 + \dfrac{Re_d^{2/3}}{6}\right) & \text{if } Re_d \leq 1000 \\ 0.424 & \text{if } Re_d > 1000 \end{cases} \tag{4-26}$$

where $Re_d = \rho_l \left(u_g - v_j cos\psi_b\right) d_d / \mu_l$ is the droplet Reynolds number in the x-direction at the column breakup location.

Integrating Eq. (4-25) twice according to time (t), and considering the initial conditions where $x = x_b$ and $\frac{dx}{dt} = v_j \cos\psi_b$ at $t = 0$, with ψ_b is the the angle between e_x and e_T axes at $x = x_b$ from Eq. (4-22), we reach

$$x = u_g t - \frac{1}{K_1} ln\left[1 + K_1\left(u_g - v_j \cos\psi_b\right)t\right] + x_b \tag{4-27}$$

where $K_1 = \left(A_d \rho_g C_{Dx}\right)/m_d$.

In z-direction:

$$m_d \frac{dz^2}{dt^2} = -A_d \rho_g \left(\frac{dz}{dt}\right)^2 C_{Dz} \tag{4-28}$$

where C_{Dz} is the drag coefficient of the droplet in the z- direction, which is calculated uing Eq. (4-26), where $Re_d = \rho_l\left(v_j sin\psi_b\right)d_d/\mu_l$ is the droplet Reynolds number in the z-direction at the column breakup location. Integrating Eq. (4-28) twice according to time (t), and considering the initial conditions where $z = z_b$ and $\frac{dz}{dt} = v_j \sin\psi_b$ at $t = 0$, we reach

$$z = \frac{1}{K_2} ln\left[1 + K_2\left(v_j \sin\psi_b\right)t\right] + z_b \tag{4-29}$$

where $K_2 = \left(A_d \rho_g C_{Dz}\right)/m_d$. Eliminating the time (t) from Eqs. (4-27) and (4-29), we obtain x as a function of z as follows:

$$x' = u_g \left\{\frac{1}{K_2\left(v_j \sin\psi_b\right)}\left[exp(K_2 z') - 1\right]\right\} - \frac{1}{K_1} ln\left[1 + \left\{\frac{K_1\left(u_g - v_j \cos\psi_b\right)}{K_2\left(v_j \sin\psi_b\right)}\left[exp(K_2 z') - 1\right]\right\}\right] \tag{4-30}$$

where $x' = x - x_b$ and $z' = z - z_b$.

4.4. Results and Discussions

Equation (4-23) shows that in addition to the ratio of jet momentum flux to gas momentum flux (q), the effect of other dimensionless group numbers such as jet Weber number $(We_j = qWe_g)$, jet Reynolds number (Re_j), Bond number (Bo), gas to liquid density ratio $\left(\frac{\rho_g}{\rho_l}\right)$, and gas to liquid viscosity ratio $\left(\frac{\mu_g}{\mu_l}\right)$ are relevant to the trajectory of a liquid jet in a crossflow. In the second zone, Eq. (4-30) shows that in addition to the aforementioned group numbers, the size of droplets at the column breakup location d_d is also crucial in order to predict the extent of the penetration of a liquid jet into a subsonic gaseous crossflow; and accordingly, gas Weber number $(We_g = We_j/q)$ is also important, as it defines d_d. We_g also plays a role in predicting the onset time of surface breakup t_i. It is worth noticing that out of the three dimensionless numbers q, We_j and We_g, only two are independent. Furthermore, We_j and Re_j can be related using Ohnesorge number as $Oh = \left(We_j\right)^{0.5}/Re_j$. The injection angle ψ_o is also found to have a crucial effect on the characteristics of a liquid jet [39, 52-54]. The present model is capable of predicting the penetration of a liquid jet with different injection angles ψ_o. In this section, however, the perpendicularly injection, $\psi_o = \pi/2$, of a liquid jet into a gaseous crossflow was adopted, as it leads to a maximum penetration height into a crossflow and is more practical in comparison with other jet angles. Fuller et al. [39] reported that the column penetration decreases with decreasing the injection angle, and the atomization process is inhibited. Brown et al. [12, 16, 55] also showed that the mode of breakup of a liquid jet has a weaker dependency upon the momentum flux ratio in comparison with the nozzle geometry (i.e., discharge coefficient of the nozzle). Thus, this parameter is taken into account in calculating the velocity of a liquid jet in the present modeling.

The effect of the aforementioned parameters on the jet penetration is discussed in the following sub-sections.

4.4.1. Effect of Momentum Flux Ratio

Figure 4-3a compares the calculated liquid jet trajectory using the present model (i.e., Eq. (4-23) for the near field, and Eq. (4-30) for the far field) with the experimental data of Rachner et al. [3] for kerosene with different momentum flux ratios (q = 2, 6 and 18 with the corresponding crossflow velocity u_g=75 ,75 and 100 m/s, respectively). The test conditions for the predictions of the different cases were those of Rachner et al. [3] (P = 580 - 590 kPa and T = 280 K). Moreover, the column breakup location was considered to be $x_b/d_j = 5.2$ for a turbulent liquid jet according to Lee et al. [56]. The orifice diameter of the nozzle was $d_j = 0.45$ mm, with a fixed discharge coefficient of about 0.6 [3].

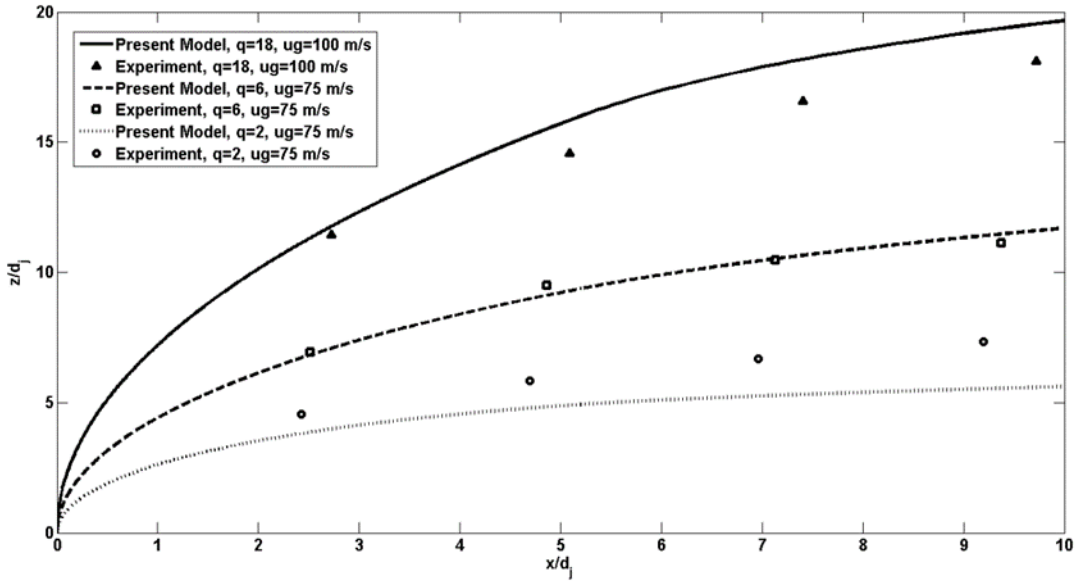

(a)

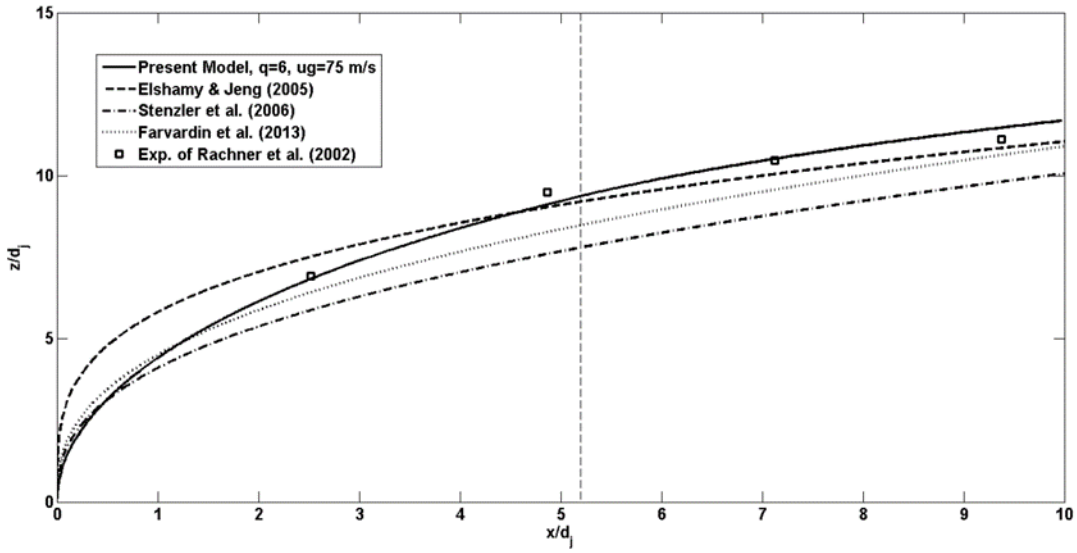

(b)

Figure 4-3: Comparison of the present model calculated kerosene jet trajectory with the a) experimental data of Rachner et al. [3] at different momentum flux ratios, b) experimental data of Rachner et al. [3] and other empirical correlations proposed by Elshamy and Jeng [25], Stenzler [22], and Farvardin et al. [18] for a fixed momentum flux ratio.

It should be noted that in order to compare the predictions of the present model, the raw data in the literature were used, rather than using the published correlations. In doing so, the actual value of q, and accordingly the actual value of v_j existed in the experiments were used in plotting the predicted trajectories, with considering the impact of the nozzle's discharge coefficient on the actual nozzle exit area, v_j and accordingly q based on the formula of Lefebvre [57] for discharge coefficient of a plain-orifice atomizer. Therefore, for the cases in which the actual v_j was not available in the literature and was calculated based on the metered nozzle flowrate divided by the nozzle exit area, an average value of discharge coefficient suggested by Brown et al. [12, 16, 55] was used. For instance, Brown et al. [12, 16, 55] reported that the value of the discharge coefficient depends on both the internal geometry and the diameter of the nozzle (e.g. for tapered nozzles with $d_j = 0.48,\ 0.95$ and 1.30 mm the discharge coefficients are considered to be 0.88 ± 0.08, 0.71 ± 0.08 and 0.76 ± 0.05, respectively [12]).

As expected (e.g., see [1]), q plays a key role in the prediction of the liquid column trajectory, and the liquid jet penetrates farther into the crossflow as q increases. Despite the fact that there is a good agreement between the present predictions and its counterpart published experimental results, the present model slightly underestimates and overestimates the experimental data for the weakest and strongest q, respectively. This slight difference might be due to the fact that a constant drag coefficient of the liquid jet column C_D (the average drag coefficient proposed by Wu et al. [1]) was used in the present model for different q. Wu et al. [1] correlated this coefficient with only the viscosity of the liquid used in their tests; however, it may change noticeably when the breakup regime of the liquid jet changes from column breakup to surface breakup. The breakup regime can change when either varying q at a constant We_g or varying We_g at a constant q [1]. In the column breakup regime, the aerodynamic force due to a gaseous crossflow plays a key role in

deforming the cross section of a liquid column [40]. This deformation would in turn affect the drag coefficient of a liquid jet. However, in the surface breakup regime, where liquid droplets and ligaments disintegrate from the column, the shape of the liquid column is controlled by the rate of mass shedding. This process decreases the aerodynamic effect of a gaseous crossflow on the deformation of the column and its corresponding drag coefficient in comparison with the column breakup regime. For instance, in the numerical work of Rachner et al. [3], C_D-correlation for a circular cylinder in a yawed crossflow was first used and then corrected by an empirical factor to meet the measured jet penetration of their baseline case (q = 6).

Figure 4-3b compares the calculated trajectory for one of the cases in Fig. 4-3a (q = 6 and u_g=75 m/s) with the experimental results of Rachner et al. [3] and the empirical correlations proposed by Elshamy and Jeng [25], Stenzler et al. [22], and Farvardin et al. [18]. This figure shows a good agreement of the present model predictions with the experimental results of Rachner et al. [3]. Moreover, the empirical correlation proposed by Elshamy and Jeng [25] has better agreement with the experimental results of Eslamian et al. [36] and also the present predictions than the other empirical correlations displayed in Fig. 4-3b. The reasons behind this discrepancy could be attributed to the difference in the test conditions where those of Elshamy and Jeng's [25] are nearly similar to those of Rachner et al. [3] (i.e., room temperature and elevated pressure); whereas Stenzler et al. [22] included room and elevated temperature at standard pressure conditions, and Farvardin et al. [18] tested only room temperature and pressure conditions.

In order to examine the present model for the region far from the nozzle; that is for $x_b \ll x$ as shown in Fig. 4-4, the calculated trajectory using the present model is compared with the experimental data of Stenzler et al. [22] for water at different momentum flux ratio (q = 14 and

18, with the corresponding crossflow velocity of u_g=75.5 and 54.5 m/s, respectively) up to $x/d_j = 100$. The test conditions used for the present predictions were chosen from one of the test cases of Stenzler et al. [22] (i.e., T = 291.15 K and P = 100 kPa).

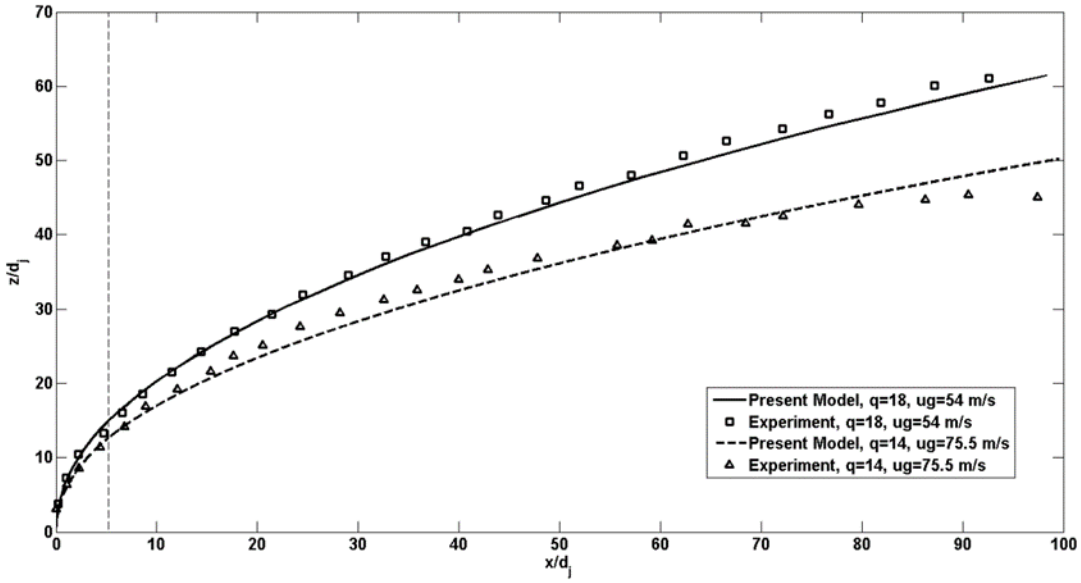

Figure 4-4: Comparison of the present model calculated water jet trajectory with the experimental data of Stenzler et al. [22] for different momentum flux ratios.

This figure shows that the present model shows reasonable agreement with the experimental data of Stenzler et al. [22], which were presented for the upper boundary of the liquid jet. This confirms what was stated earlier that the behavior in the near field region establishes the subsequent penetration of a liquid jet in the far field region. Therefore, since the prediction of the present model in the region near the nozzle was reliable as was shown in Fig. 4-3, this agreement in the region far from the nozzle was expected.

4.4.2. Effect of Mass Shedding

Figure 4-5 compares the calculated trajectory using the present model with the experimental results of Eslamian et al. [36] for water (at q = 50, v_j=42.9 m/s, T = 573 K and P = 379.2 kPa), and the empirical correlations proposed by Elshamy and Jeng [25], Stenzler et al. [22], and Farvardin et al. [18]. This figure shows that, although the present predictions fairly agree with the experimental results of Eslamian et al. [36], there is still a noticeable difference especially in the far-field (less than about 17%). However, this difference is believed to be within the experimental error involved in the collection of data reported in [36]. Figure 4-5 reveals also that the agreement of the empirical correlation proposed by Stenzler et al. [22] with the experimental results of Eslamian et al. [36] and present predictions is better than the other empirical correlations. This could be attributed to the fact that the test conditions of Stenzler et al. [22] are nearly similar to those of Eslamian et al. [36], i.e., at elevated temperature conditions which means that it can properly capture the effect of varying ambient temperature.

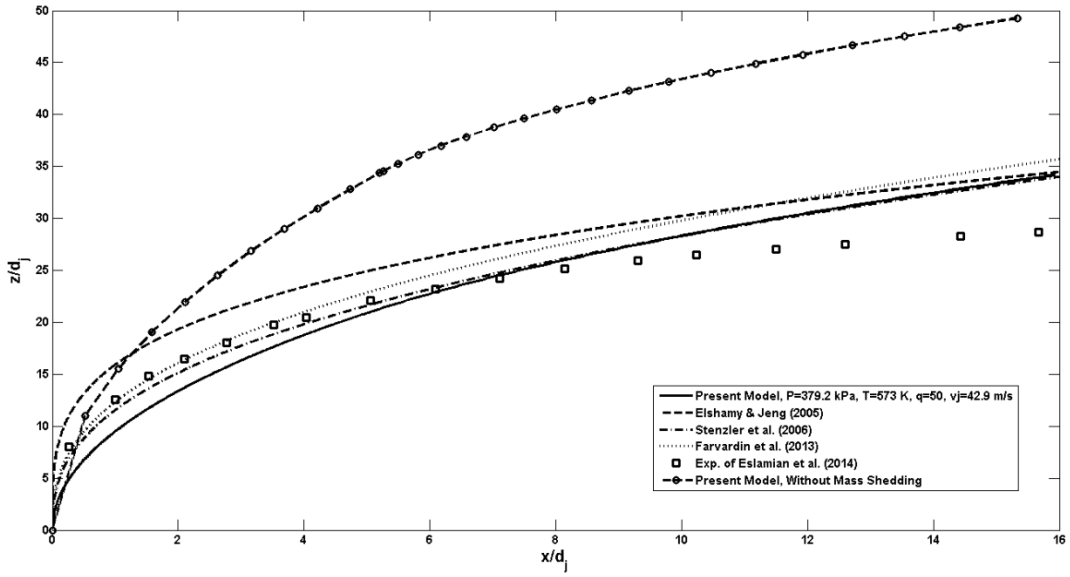

Figure 4-5: Comparison of the present model calculated water jet trajectory with the a) experimental data of Eslamian et al. [36] and other empirical correlations proposed by Elshamy and Jeng [25], Stenzler et al. [22], and Farvardin et al. [18] for a fixed momentum flux ratio, and showing the effect of mass shedding on liquid jet trajectory at constant q, v_j, T and P.

To study the effect of the mass shedding on the liquid jet trajectory, the predicted trajectory of the liquid jet using the present model without considering mass shedding is also included in Fig. 4-5. This figure reveals the importance of mass reduction due to the surface breakup mechanism (i.e., mass shedding) as liquid jet loses a large portion of its initial mass by the time it reaches the column breakup location [5]. As a result, the ratio of its momentum to the momentum of the gas stream decreases, which in turn causes the liquid jet to bend earlier. Neglecting this process, therefore, leads to overpredicting the jet trajectory, which can be as large as around $20d_j$ at $x = 16d_j$ for the case in Fig. 4-5.

4.4.3. Effect of Ambient Temperature and Pressure

Eslamian et al. [36], in their experimental study, stated that due to several parameters involved in the physical problem, there is no straightforward procedure to examine the effect of temperature and pressure, unless some of the parameters can be kept constant. Therefore, to investigate the impact of air crossflow temperature, the calculated liquid jet trajectory using the present model is compared in Fig. 4-6a with the experimental data of Eslamian et al. [36] for water at typical constant momentum flux ratio q = 50, crossflow air pressure P = 206.8 kPa, liquid injection velocity v_j = 19.2 m/s, nozzle diameter d_j = 0.46 mm, and different air crossflow temperatures (T = 298, 473 and 573 K where the corresponding crossflow velocities are u_g = 55.2, 69.7 and 76.5 m/s, respectively). As is illustrated in Fig. 4-6a, the jet penetration height slightly decreases with increasing the air crossflow temperature. It should be noted that at constant q, v_j and P, with increasing temperature (from 298 to 573 K), the air density decreases (from 2.422 to 1.255 Kg/m3), and accordingly the crossflow air velocity increases (from 55.2 to 76.5 m/s). In addition, the viscosity of the air crossflow increases (from 18.483×10-6 to 29.86×10-6 Kg/m.s) with increasing temperature. Considering the coefficients of the present model, i.e., Eq. (4-20), if the density ratio $\left(\frac{\rho_g}{\rho_l}\right)^{-\frac{1}{12}}$ and the viscosity ratio $\left(\frac{\mu_g}{\mu_l}\right)^{\frac{1}{6}}$ change (while keeping constant q, v_j and P), the mass shedding term will be affected. Since the power exponents of the density and viscosity ratio are negative $(-1/12)$ and positive $(1/6)$, respectively, a decrease in the density ratio and an increase in the viscosity ratio will lead to an increase in the mass shedding from the liquid column, which in turn causes the liquid jet to bend more. Although there is a good agreement between the present predictions and the experiment results, the proposed model does not completely reproduce the experimental data especially in the far-field. This could be partly due to the error involved in the experimental data, as Eslamian et al. [36] stated that very small droplets may not be detected by

the camera due to insufficient reflected laser light. They also reported that, at elevated temperature test conditions, evaporation may eliminate very small droplets or become invisible for the camera. This might be another reason for the overestimation of the trajectory in the far-field, as the effect of evaporation was assumed to be insignificant up to the spray length considered here $x/d_j = 100$ [30].

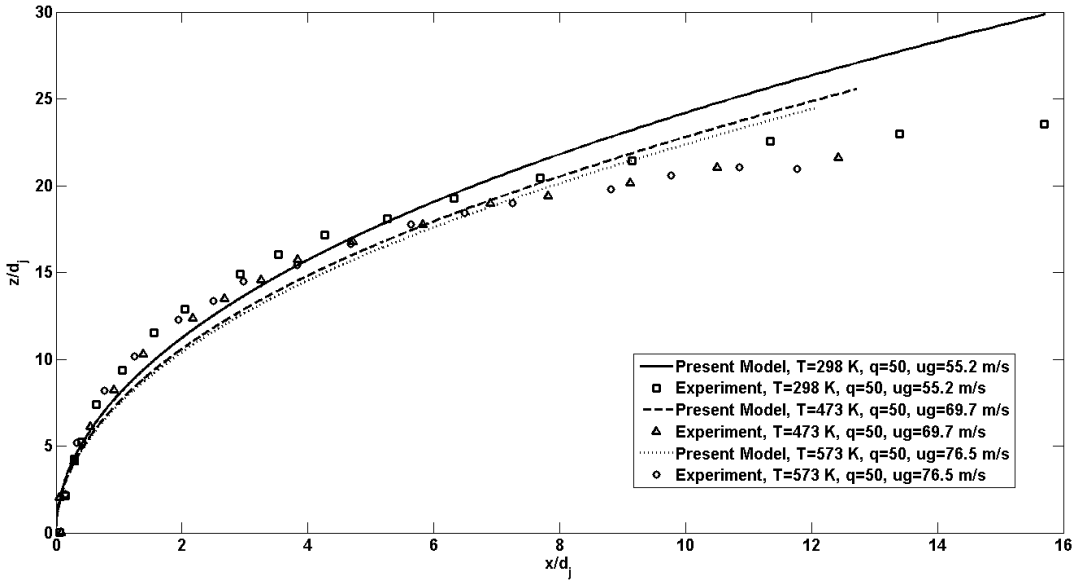

(a)

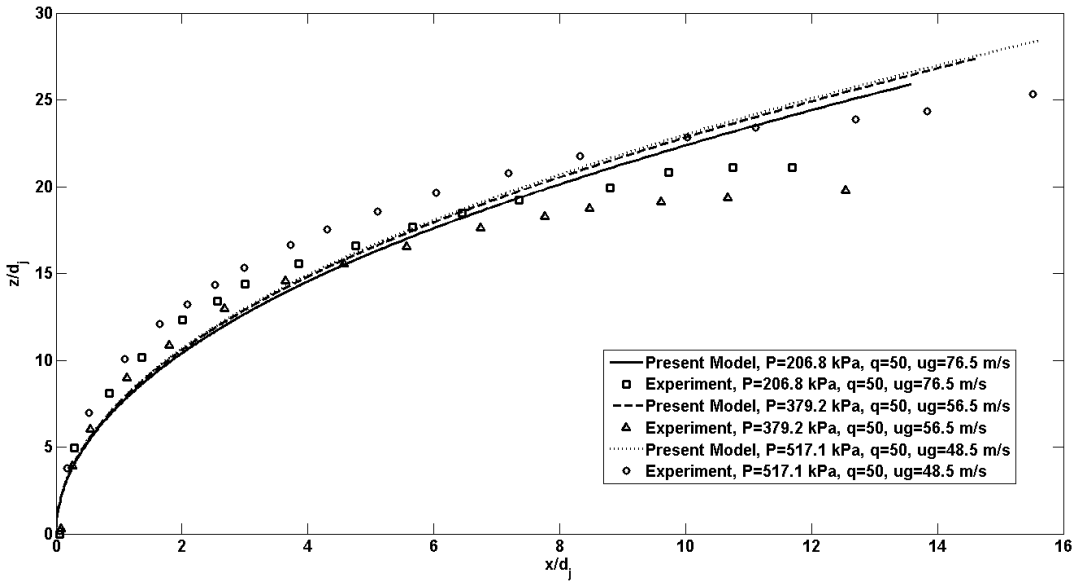

(b)

Figure 4-6: Effect of air crossflow a) temperature, and b) pressure on liquid jet trajectories at constant q and v_j.

To show the effect of cross airflow pressure on a liquid jet trajectory, the calculated trajectory using the present model is compared in Fig. 4-6b with the experimental data of Eslamian et al. [36] for water at typical momentum flux ratio q = 50, crossflow air temperature T = 573 K, liquid injection velocity v_j = 19.2 m/s, nozzle diameter d_j = 0.46 mm, and different cross airflow pressures (P = 206.8, 379.2 and 517.1 kPa where the corresponding crossflow velocities are u_g = 76.5, 56.5 and 48.5 m/s, respectively). As illustrated in Fig. 4-6b, the jet penetration height slightly increases with increasing the cross airflow pressure, though Eslamian et al. [36] observed no consistent behavior when pressure changes from 206.8 to 379.2 kPa. It should be noted that at constant q, v_j and T, with an increase in air pressure (from 206.8 to 517.1 kPa), the air density increases (from 1.255 to 3.136 Kg/m3), and accordingly the cross airflow velocity decreases (from 76.5 to 48.5 m/s). In addition, the cross airflow viscosity remains fairly constant with increasing pressure. Given the coefficients of the present model, i.e. Eq. (4-20), if the density ratio $\left(\frac{\rho_g}{\rho_l}\right)^{-\frac{1}{12}}$ changes (while keeping constant q, v_j and P), the mass shedding term will be affected. Since the power exponents of the density ratio is negative $(-1/12)$, an increase in the density ratio leads to a decrease in the mass shedding from the liquid column, which in turn causes the liquid jet to bend less. It should be noted that no consistent behavior was observed by Eslamian et al. [36] as is illustrated in Fig. 4-6b. They attributed this inconsistency to the influence of varying crossflow pressure on the atomization characteristics. They argued that a decrease in the crossflow velocity with an increase in pressure may have an adverse effect on atomization, as large droplets may form which last longer and consequently make the liquid spray to penetration farther into the crossflow. It is worth mentioning that the trend of the present model's predictions also shows an agreement with the experimental results of Song et al. [28], who reported that as ambient pressure increases, the spray penetrates farther in the near- and far-field.

To examine the effect of the density ratio $\left(\frac{\rho_g}{\rho_l}\right)$ and the viscosity ratio $\left(\frac{\mu_g}{\mu_l}\right)$ on the liquid jet trajectory at constant q and v_j, a parametric study was performed and the results are shown in Fig. 4-7. The jet trajectory is calculated by the present model using the test conditions of the experiment of Eslamian et al. [36] for water (i.e., q = 50, v_j=42.9 m/s, T = 573 K, P = 379.2 kPa, ρ_g/ρ_l= 2.4×10-3 and μ_g/μ_l= 2.14×10-2).

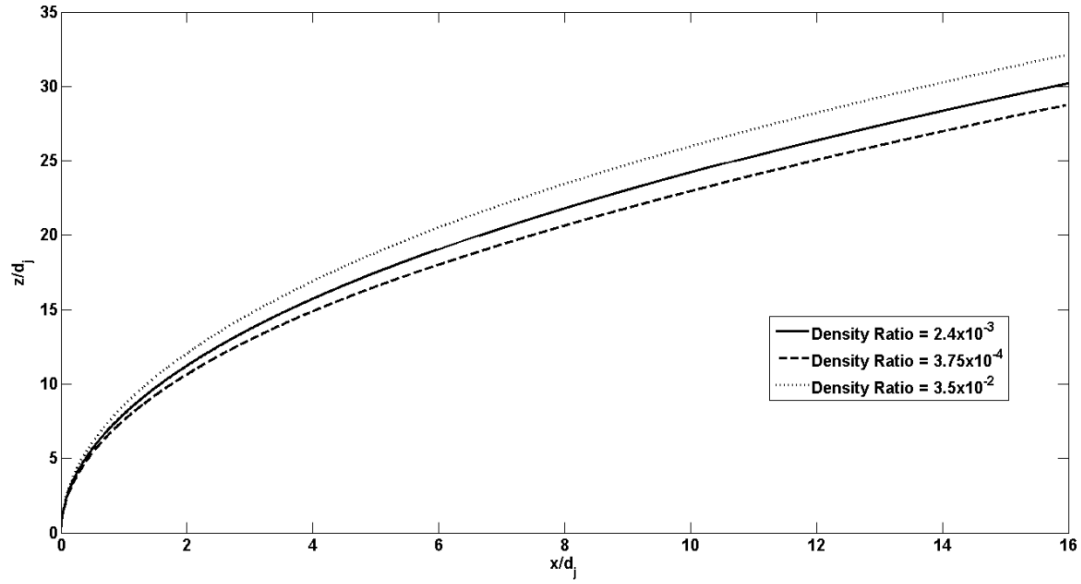

(a)

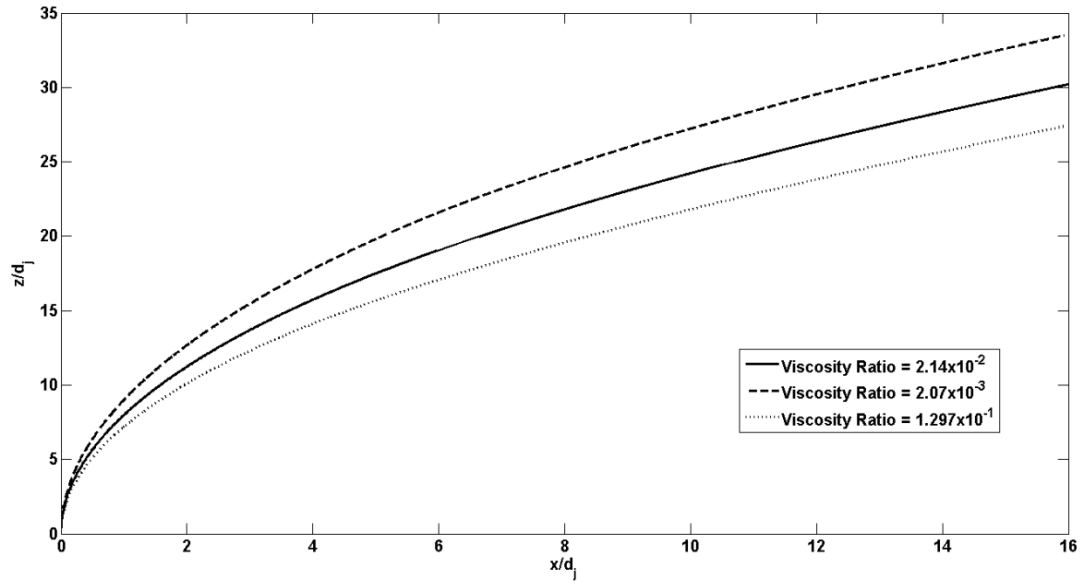

(b)

Figure 4-7: Effect of a) density ratio, and b) viscosity ratio on liquid jet trajectories at constant q and v_j.

As shown in Fig 4-7a, at constant q and v_j, the liquid jet penetrates farther into the crossflow as the density ratio increases (from 3.75×10-4 to 3.5×10-2) where for example it is around $4d_j$ at $x = 16d_j$ for this case. Note that, this range of density ratio is chosen according to the maximum and minimum range of the density ratio available in the literature. Fig 4-7b shows that at constant q and v_j, the liquid jet penetrates less into the crossflow with increasing the viscosity ratio (from 2.07×10-3 to 1.297×10-1), which is around $6d_j$ at $x = 16d_j$ for this case. Similarly to the density ratio, this range of viscosity ratio is chosen according to the maximum and minimum range of the viscosity ratio available in the literature. It can be concluded from Fig. 4-6 and Fig.4-7 that the effect of temperature and pressure of the cross airflow on the jet trajectory can be accurately captured by the present model when using the density and viscosity ratio instead of direct use of the temperature and pressure ratio.

4.4.4. Effect of Jet Reynolds Number

To assess the effect of jet Reynolds number, the calculated trajectory using the present model is compared in Fig. 4-8a with the experimental data of Eslamian et al. [36] for water at typical momentum flux ratio q = 50, crossflow air pressure P = 206.8 kPa, crossflow air temperature T = 473 K, nozzle diameter d_j = 0.46 mm, and different liquid injection velocities (v_j = 19.2, 30.3 and 42.9 m/s where the corresponding cross airflow velocities are u_g = 69.7, 109.6 and 155.3 m/s, respectively). This figure shows that although there is a reasonable agreement between the present predictions and experimental data of Eslamian et al. [36], there still a slight discrepancy between the model predictions and the experiments (for instance, the model predictions overpredict the experimental data by about 20% at x/D = 12). Nonetheless, as is illustrated in Fig. 4-8a, both the

present predictions and their counterparts published experimental data reveal that the jet penetration height increases with increasing liquid jet velocity. It should be noted that at constant q, T and P, an increase in the liquid jet injection velocity (from 19.2 to 42.9 m/s) leads to an increase in both jet Reynolds number Re_j (from 1.017×104 to 2.27×104) and jet Weber number We_j (from 2.66×103 to 13.28×103). Given the coefficients of the present model, if the jet Weber number changes (while keeping constant q, T and P), both the terms α and β in Eq. (4-20) will be affected. However, Bo number in α term is divided by We_j, and since Bo number is much smaller than unity and becomes only important when the jet nozzle diameter exceeds the capillary length of the liquid (e.g., 2.7 mm for water) [58], the effect of this term is insignificant. Moreover, since the parameters $We_j \sim 10^3$ and $Re_j \sim 10^4$ in β term are taken as the inverse of 1, their effect on the liquid jet trajectory is insignificant. On the other hand, $Re_j^{-\frac{1}{2}}$ in γ term has an effect on the liquid trajectory. Since its power exponents is negative $(-1/2)$, increasing the jet Reynolds number leads to a decrease in the mass shedding from the liquid column, which in turn causes the liquid jet to bend less, as is illustrated in Fig. 4-8a.

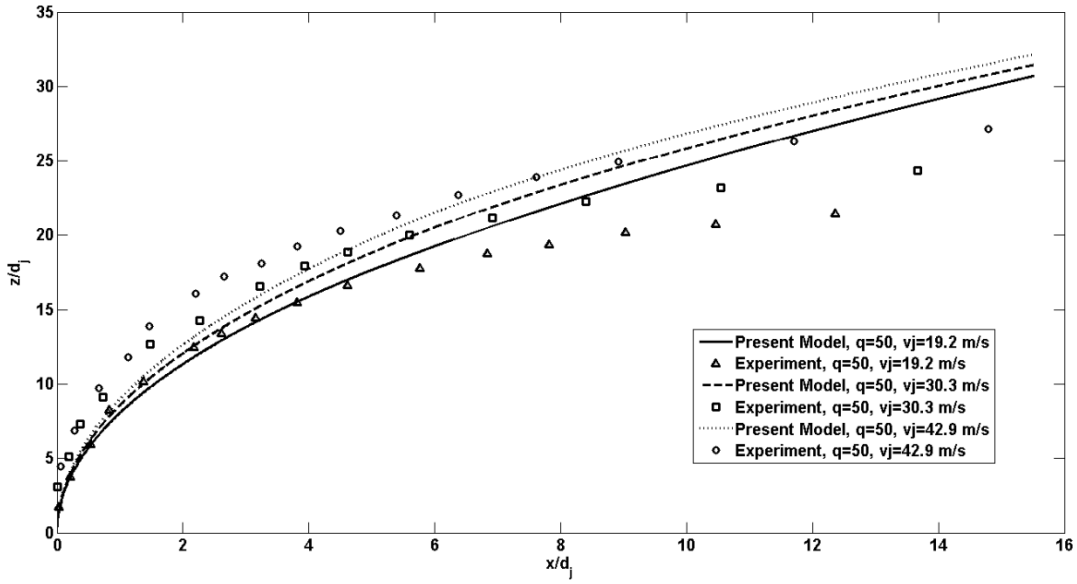

(a)

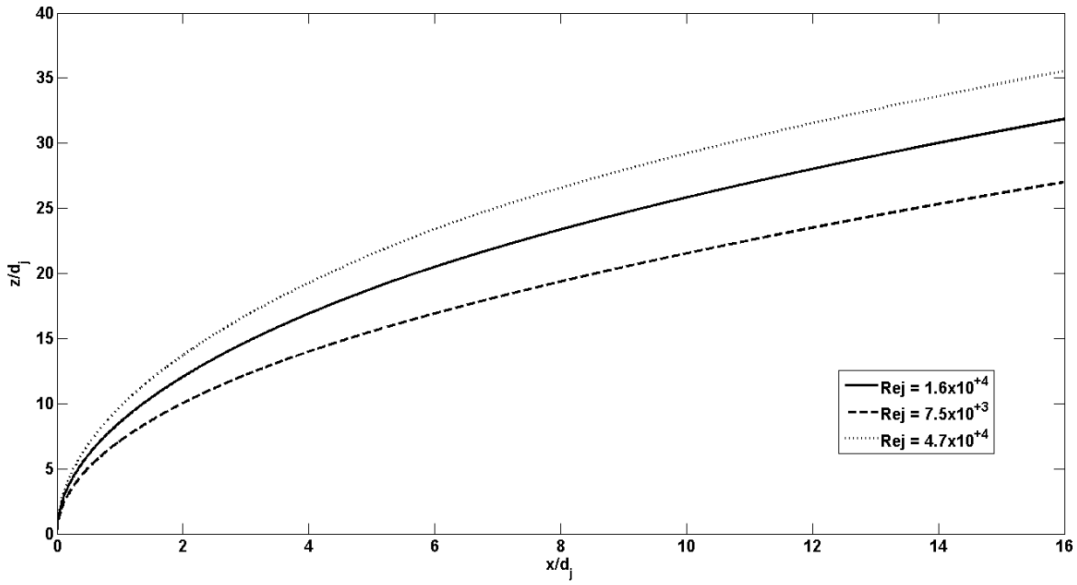

(b)

Figure 4-8: Effect of a) liquid injection velocity, and b) jet Reynolds number on liquid jet trajectories at constant *q*, *T* and *P*.

To shed more light on the effect of Re_j on the liquid jet trajectory at constant q, a parametric study was performed using the present model and the findings are reported in Fig. 4-8b. In calculating jet trajectory, the test conditions of the experiment of Eslamian et al. [36] for water (at q = 50, v_j=30.3 m/s, T = 473 K, P = 206.8 kPa) were used. As is depicted in Fig 4-8b, at constant q, the liquid jet penetrates farther into the crossflow when increasing Re_j from 7.5×103 to 4.7×104 (with increasing v_j from about 14 to 88 m/s); where for instance it increases by around $8d_j$ at $x = 16d_j$. Note that, this range of jet Reynolds number is chosen according to the maximum and minimum range of jet Reynolds number available in the literature.

4.5. Conclusion

A two-zone model is developed by adopting a hybrid Eulerian-Lagrangian approach to predict the penetration of a liquid jet into a subsonic gaseous cross airflow at different operating conditions. The present model has been developed by taking into account all the physics governing the breakup/atomization process of a liquid jet injected into a cross airflow. That is, in addition to the forces acting on the liquid jet including drag, gravitation and surface tension, the effect of the mass shedding from the liquid column, internal geometry of the nozzles and injection angle are all considered in the present model. As a result, two correlations were obtained in a sinusoidal-exponential functional form for the liquid column region (i.e., first zone), and a logarithmic functional form for the droplets plume region (i.e., second zone).

For the range of liquid properties and the test conditions explored in the present study, which is low viscous liquids (i.e., Ohnesorge number $Oh = \mu_j/\sqrt{\rho_j d_j \sigma}$ less than 0.1 [50]) and small diameter nozzle, the finding of the present model, which is in accordance with published literature,

shows that the contribution of the two forces (i.e., gravity, and surface tension) is negligible in comparison with the drag force and mass shedding effect. In that, it suggests that the momentum flux ratio, q, plays a predominant role in the prediction of a liquid column trajectory. However, the liquid jet penetration changes with the temperature and pressure of the cross airflow when keeping constant q and v_j. Their effect on the jet trajectory was accurately captured in the predictions of the present model by employing density ratio $\left(\frac{\rho_g}{\rho_l}\right)$ and viscosity ratio $\left(\frac{\mu_g}{\mu_l}\right)$. For instance, the predictions of the present model showed that, at a constant q and v_j, the liquid jet penetrates farther when increasing the density ratio or decreasing the viscosity ratio. It also showed that, at constant q, P and T, the jet penetrates farther when increasing the jet Reynolds number $\left(Re_j\right)$ which is a consequence of a drop in the mass shedding from the liquid column. Considering solely the momentum flux ratio, therefore, can lead to an oversimplification of the problem, and consequently yields uncertainties in the predictions. As a result, the present model suggests that in addition to the momentum flux ratio, other dimensionless group numbers such as jet Reynolds number, gas to liquid density ratio, gas to liquid viscosity ratio and gas or jet Weber number, are all relevant to the penetration of a liquid jet in a subsonic gaseous crossflow, and thus should be considered in order to establish a comprehensive formulation/correlation for the prediction of a liquid jet penetration in a subsonic gaseous crossflow. It is worth mentioning that some published empirical correlations such as Eqs. (4-2) to (4-4) included some of these controlling parameters. However, there is no consensus on the role of each term/parameter. For instance, despite the fact that Stenzler et al. [22] considered the role of gas Weber number in liquid jet trajectory, Eslamian et al. [36] stated that liquid surface tension significantly increased the standard deviation of their correlation, and therefore gas Weber number was not considered in their analysis. Even other published correlations which included a similar non-dimentional parameter exhibited different

power exponents. For instance, in Eq. 4-2, gas Weber number has a power exponent of -0.110, whereas it is -0.076 in Eq. 4-3. Hence, the present modelling is a step towards developping more comprehensive form of correlations by examining independently the importance of all parameters and accounting for their contributions in predicting the trajectory of a liquid jet in a subsonic gaseous crossflow for different liquid properties at different test conditions.

Since most of published correlations for predicting the penetration height of a liquid jet were empirical with their own source of uncertainties, and the fact that simulation studies were not able to propose an explicit trajectory correlation for design purposes, it is believed that the use of the present approach provides a valuable tool to derive a reliable trajectory correlation with minimal experimental and computational costs. The correlation presented for the first zone, Eq. (4-23), can also be implemented into numerical models where a prediction of the jet trajectory in the second zone is required (see e.g. [3, 44, 45, 49]). In fact, the aforementioned studies rely on trajectory correlations of the liquid column region in order to calculate the locations of droplets shedding from the jet, and accordingly to determine droplet size distribution and other flow parameters in the spray far field region. Some of these numerical studies modified the droplet drag coefficient to force droplets follow a path similar to a liquid jet injected into a crossflow [44, 49], while some others theoretical analysis used their own assumptions to find jet trajectories but with no proposed correlations [3, 45]. Therefore, the present model can be used as an input sub-model in all of the aforementioned references, as well as, in future numerical models as to provid a reliable explicit correlation for the jet trajectory applicable at different test conditions (e.g. room and elevated test conditions).

Finally, although the present model calculations exhibited an overall good agreement with published experimental results, there still show slight discrepancies. This is believed to originate

either from the assumptions and average values used in the present model including drag coefficient of the liquid column and droplets or discharge coefficients of the nozzles, or from the experimental uncertainties (such as the threshold value considered to identify the boundary of a liquid jet, errors associated with the measurements tools, and manufacturing process of liquid injectors). Therefore, more physical insight into the break up/atomization process in order to develop reliable database is necessary. This might be accomplished via three-dimensional treatments of a liquid jet in a gaseous crossflow combined with comprehensive experiments over extended test conditions.

4.6. References

[1] Wu, P.K., Kirkendall, K.A., Fuller, R. P., and Nejad, A. S., "Breakup processes of liquid jets in subsonic crossflows," Journal of Propulsion and Power, Vol. 13, No. 1, 1997, pp. 64-73.

[2] Leong, M.Y., McDonell, V.G., and Samuelsen, G.S., "Mixing of an airblast-atomized fuel spray injected into a crossflow of air," NASA Glenn Research Center Report NASA/CR-2000-210467, 2000.

[3] Rachner, M., Becker, J., Hassa, C., and Doerr, T., "Modelling of the atomization of a plain liquid fuel jet in crossflow at gas turbine conditions," Aerospace Science and Technology, Vol. 6, No. 7, 2002, pp. 495-506.

[4] Ragucci, R., Bellofiore, A., and Cavaliere, A., "Breakup and breakdown of bent kerosene jets in gas turbine conditions," Proceedings of the Combustion Institute, Vol. 31, No. 2, 2007, pp. 2231-2238.

[5] Ashgriz, N., Handbook of atomization and sprays, Springer Science Business Media LLC, 2011, (Chapter 19, pp. 383-424 and Chapter 29, pp. 657-683).

[6] Cotton, I., Hill, D. E., and McRae, R. P., "Study of liquid jet penetration in a hypersonic stream," AIAA Journal, Vol. 6, No. 11, 1968, pp. 2084-2089.

[7] Schetz, J. A., Kush, E. A. Jr., and Joshi, P. B., "Wave phenomena in liquid jet breakup in a supersonic crossflow," AIAA Journal, Vol. 18, No. 7, 1980, pp. 774-778.

[8] Nejad, A. S., and Schetz, J. A., "Effects of properties and location in the plume on droplet diameter for injection in a supersonic stream," AIAA Journal, Vol. 21, No. 7, 1983, pp. 956-961.

[9] Wu P. K., Kirkendall K. A., Fuller R. P., Gruber M. R., and A. S. Nejad, "Spray trajectories of liquid fuel jets in subsonic crossflows," International Journal of Fluid Mechanics Research, Vol. 24, Nos. 1-3, 1997, pp. 128-137.

[10] Lin K. C., Kennedy P. J., and Jackson T. A., "A review on penetration heights of transverse liquid jets in high-speed flows," 15th Annual Conference on Liquid Atomization and Spray systems, pp. 345-349, May 2002.

[11] Tambe S. B., and Jeng S. M., "Liquid jets in subsonic crossflow," 43rd AIAA Aerospace Sciences Meeting and Exhibit, AIAA Paper, 10-13 Jan. 2005.

[12] Brown C. T., and McDonell V. G., "Near field behavior of a liquid jet in a cross flow," ILASS Americas 19th Annual Conference on Liquid Atomization and Spray Systems, 23-26 May 2006.

[13] Ahn K., Kim J., and Yoon Y., "Effects of orifice internal flow on transverse injection into subsonic crossflows: cavitation and hydraulic flip," Atomization and Sprays, Vol. 16, No. 1, 2006, pp. 15-34.

[14] Iyogun C. O., Birouk M., and Popplewell N., "Trajectory of water jet exposed to low subsonic cross-flow," Atomization and Sprays, Vol. 16, No. 8, 2006, pp. 963-979.

[15] Birouk M., Iyogun C. O., and Popplewell N., "Role of viscosity on trajectory of liquid jets in a cross-airflow," Atomization and Sprays, Vol. 17, No. 3, 2007, pp. 267-287.

[16] Brown C. T., Mondragon U. M., and McDonell V. G., "Investigation of the effect of injector

discharge coefficient on penetration of a plain liquid jet into a subsonic crossflow," ILASS Americas 20th Annual Conference on Liquid Atomization and Spray Systems, 15-18 May 2007.

[17] Wang Q., Mondragon U. M., Brown C. T., and McDonell V. G., "Characterization of trajectory, break point, and break point dynamics of a plain liquid jet in a crossflow," Atomization and Sprays, Vol. 21, No. 3, pp. 203-219, 2011.

[18] Farvardin, E., Johnson, M., Alaee, H., Martinez, A., and Dolatabadi, A., "Comparative study of biodiesel and diesel jets in gaseous crossflow," Journal of Propulsion and Power, Vol. 29, No. 6, 2013, pp. 1292-1302.

[19] Bolszo C. D., McDonell V. G., Gomez G. A., and Samuelsen G. S., "Injection of water-in-oil emulsion jets into a subsonic crossflow: an experimental study," Atomization and Sprays, Vol. 24, No. 4, 2014, pp. 303-348.

[20] Stenzler J. N., Lee J. G., and Santavicca, D. A., "Penetration of liquid jets in a crossflow," 41st AIAA Aerospace Sciences Meeting and Exhibit, AIAA Paper, 6-9 Jan. 2003.

[21] Lakhamraju R. R., and Jeng S. M., "Liquid jets in subsonic airstream at elevated temperatures," ILASS Americas 18th Annual Conference on Liquid Atomization and Spray Systems, May 2005.

[22] Stenzler J. N., Lee J. G., Santavicca D. A., and Lee W., "Penetration of liquid jets in a crossflow," Atomization and Sprays, Vol. 16, No. 8, 2006, pp. 887-906.

[23] Yoon H. J., Hong J. G., and Lee C. W., "Correlations for penetration height of single and double liquid jets in cross flow under high-temperature conditions," Atomization and Sprays, Vol. 21, No. 8, 2011, pp. 673-686.

[24] Becker J., and Hassa C., "Breakup and atomization of a kerosene jet in crossflow at elevated pressure," Atomization and Sprays, Vol. 12, Nos. 1-3, 2002, pp. 49-67.

[25] Elshamy O. M. and Jeng S. M., "Study of liquid jet in crossflow at elevated ambient pressures," ILASS Americas 18th Annual Conference on Liquid Atomization and Spray Systems, May 2005.

[26] Freitag S., and Hassa C., "Spray characterization of a kerosene jet in cross flow of air at elevated pressure," ILASS, 2008, Cologne, Germany.

[27] Lubarsky E., Shcherbik D., Bibik O., Gopala Y., Bennewitz J. W., and Zinn B. T., "Fuel jet in cross flow- experimental study of spray characteristics," 23rd Annual Conference on Liquid Atomization and Spray Systems, May 2011, Ventura, Canada.

[28] Song J., Cain C. C., and Lee J. G., "Liquid jets in subsonic air crossflow at elevated pressure," Journal of Engineering for Gas Turbines and Power, Vol. 137, No. 4, Oct 28, 2014.

[29] Masuda B. J., and McDonell V. G., "Penetration of a recessed distillate liquid jet into a crossflow at elevated Pressure and Temperature," ICLASS, 2006, Kyto, Japan.

[30] Bellofiore A., Cavaliere A., and Ragucci R., "Air density effect on the atomization of liquid jets in crossflow," Combustion Science and Technology, 2007, pp. 319-342.

[31] Ragucci R., Alessandro B., and Cavaliere A., "Breakup and breakdown of bent kerosene jets in gas turbine conditions," Proceedings of the Combustion Institute, pp. 2231-2238, 2007.

[32] Ragucci R., Bellofiore A., and Antonio C., "Trajectory and momentum coherence breakdown

of a liquid jet in high-density air cross-flow," Atomization and Sprays, Vol. 17, No. 1, 2007, pp. 47-70.

[33] Gopala Y., Lubarsky E., and Zinn B. T., "Liquid jet in crossflow: a novel method to locate the column breakup point," 46st AIAA Aerospace Sciences Meeting and Exhibit, AIAA Paper, Reno, NV 2008.

[34] Amighi A., Eslamian M., and Ashgriz N., "Trajectory of a liquid jet in high pressure and high temperature subsonic air crossflow," ICLASS Paper 2009-225, July 2009.

[35] Li L., Lin Y., and Xue X., "Injection of liquid kerosene into a high-pressure subsonic air crossflow from normal temperature to elevated temperature," Proceedings of ASME Turbo Expo, 2012, Ventura,Canada.

[36] Eslamian M., Amighi A., and Ashgriz N., "Atomization of liquid jet in high-pressure and high-temperature subsonic crossflow," AIAA Journal, Vol. 52, No. 7, 2014, pp. 1374-1385.

[37] Chen T. H., Smith C. R., Schommer D. G., and Nejad A. S., "Multi-zone behavior of transverse liquid jet in high-speed flow," AIAA-93-0453, Jan 1993. Dayton, USA.

[38] Birouk M., and Lekic N., "Liquid jet breakup in quiescent atmosphere: a review", Atomization and Sprays, Vol. 19, No. 6, 2009, pp. 501–528.

[39] Fuller, R. P., Wu, P.K., Kirkendall, K. A., and Nejad, A. S., "Effects of injection angle on atomization of liquid jets in transverse airflow," AIAA Journal, Vol. 38, No. 1, 2000, pp. 64-72.

[40] Mashayek A., Jafari A., and Ashgriz N., "Improved model for the penetration of liquid jets in subsonic crossflows," AIAA Journal, Vol. 46, No. 11, 2008, pp. 2674-2686.

[41] Marzbali S. N., and Dolatabadi A., "Near-field trajectory of circular liquid jets injected into subsonic gaseous crossflow," 49th AIAA Aerospace Sciences Meeting including the New Horizons Forum and Aerospace Exposition, AIAA Paper, Orlando, Florida, January 2011.

[42] Ranger A. A., and Nicholls J. A., "Aerodynamic shattering of liquid drops," AIAA Journal, Vol. 7, No. 2, 1969, pp. 285–290.

[43] Chryssakis C. A., and Assanis D. N., "A secondary atomization model for liquid droplet deformation and breakup under high weber number conditions," 18th Annual Conference on Liquid and Atomization and Spray Systems, 2005.

[44] Khosla S., and Crocker D. S., "CFD modeling of the atomization of plain liquid jet in crossflow for gas turbine applications," American Society of Mechanical Engineers Turbo Expo, Paper GT2004-54269, June 2004.

[45] Mashayek A., Behzad M., and Ashgriz N., "Multiple injector model for primary breakup of a liquid jet in crossflow," AIAA Journal, Vol. 49, No. 11, 2011, pp. 2407-2420.

[46] Sallam K.A., Aalburg C., and Faeth G.M., "Breakup of round nonturbulent liquid jets in gaseous crossflow," AIAA Journal, Vol. 42, 2004, pp. 2529-2540.

[47] Nguyen T. T., and Karagozian A. R., "Liquid fuel jet in subsonic crossflow," Journal of Propulsion and Power, Vol. 8, No. 1, 1992, pp. 21–29.

[48] Baranovsky S. I., and Schetz J. A., "Effect of injection angle on liquid injection in supersonic flow," AIAA Journal, Vol.18, No. 6, 1980, pp. 625-629.

[49] Madabhushi R. K., Leong M. Y., and Hautman D. J. "Simulation of the breakup of a liquid jet in crossflow at atmospheric conditions," Proceedings of the ASME Turbo Expo 2004, ASME, Vienna.

[50] Mazallon J., Dai Z., and Faeth G.M., "Primary breakup of nonturbulent round liquid jets in gas crossflows," Atomization and Sprays, Vol. 9, 1999, pp. 291-311.

[51] White, F. M., Fluid mechanics, Forth Edition, Mcgraw-Hill Series in Mechanical Engineering, 1998, (Chapter 7, pp. 427-492).

[52] Costa M., Melo M. J., Sousa J. M. M., and Levy Y., "Spray characteristics of angled liquid injection into subsonic crossflows," AIAA Journal, Vol. 44, No. 3, 2006, pp. 646-653.

[53] Almeida H., Sousa J. M. M., and Costa M., "Effect of the liquid injection angle on the atomization of liquid jets in subsonic crossflows", Atomization and Sprays, Vol. 24, No. 1, 2014, pp. 81-96.

[54] Broumand M., and Birouk M., "A model for predicting the trajectory of a liquid jet in a subsonic gaseous crossflow," Atomization and Sprays, 2014 (in press).

[55] Brown C. T., Mondragon U. M., and McDonell V. G., "Liquid jet in crossflow: consideration of injector geometry and liquid physical properties," ILASS Americas 25th Annual Conference on Liquid Atomization and Spray Systems, Pittsburgh, PA, May 2013.

[56] Lee K., Aalburg C., Diez F. J., Faeth G. M., and Sallam K. A., "Primary breakup of turbulent round liquid jets in uniform crossflows", AIAA Journal, Vol. 45, No. 8, 2007, pp. 1907–16.

[57] Lefebvre, A.H., Atomization and sprays, Hemisphere Publishing Corporation, Chapter 5, 1989.

[58] Scharfman B. E., Bush J. W. M., and Techet A. H., "Hydrodynamic instabilities in round liquid jets in gaseous crossow," ILASS Americas 25th Annual Conference on Liquid Atomization and Spray Systems, Pittsburgh, PA, May 2013.

Chapter 5

Effect of Nozzle Exit Turbulence on the Column Trajectory and Breakup Location of a Transverse Liquid Jet in a Gaseous Flow

5.1. Abstract

This study examines the effect of fully developed turbulent flow at the exit of nozzle/injector on the trajectory and column breakup location of a liquid jet injected transverly into a gaseous crossflow. Liquid jet trajectory and column breakup for different nozzle geometries at different velocities of liquid jet and crossflow are analytically and experimentally investigated. Shadowgraph imaging technique is used to determine the jet trajectory and breakup location of a transverse liquid jet in a uniform airflow. Particle image velocimetry (PIV) is used to measure the near-field velocity profile of a liquid jet discgarged into a quiescent atmosphere. The experimental results show a higher penetration and breakup height for the liquid jet ensuing from a nozzle with a smaller length to diameter ratio. This is due to the surface irregularities of the liquid column of a turbulent jet, which breaks up and consequently follows the cross airflow sooner. In order to capture the effect of turbulence, the analytical trajectory correlation developed in our previous studies is modified to account for the discharge coefficient of a nozzle. The discharge coefficient is estimated indirectly by comparing the liquid column trajectory predicted by the modified

analytical correlation with that determined experimentally. The indirectly determined discharge coefficient is then used in the analytical correlation for predicting the breakup height of a transverse liquid jet. The results predicted using this approach are in good agreement with the experimental data of the present study at standard temperature and pressure (STP) test conditions.

Nomenclature

A_o	nozzle exit area, m^2
Bo	Bond number, $\rho_l g d_j^2/\sigma$
C_D	liquid column average drag coefficient
C_d	discharge coefficient of nozzle
d_j	liquid jet diameter at the nozzle exit, m
L	exit length of nozzle, m
$\dot{m}_f$	nozzle mass flowrate, kg/s
q	jet momentum flux ratio, $\rho_l v_j^2/\rho_g u_g^2$
Re_j	jet Reynolds number, $\rho_l v_j d_j/\mu_l$
t_b	column breakup time, s
t_i	onset of surface breakup time, s
t_s	characteristic liquid-phase time, $(\rho_l/\rho_g)^{\frac{1}{2}} d_j/u_g$
t_v^*	characteristics viscous time, $d_j^2/(\mu_l/\rho_l)$
u_g	crossflow velocity, m/s
v_j	liquid velocity at the nozzle exit, m/s
We_g	gas phase Weber number, $\rho_g u_g^2 d_j/\sigma$
We_j	jet Weber number, $\rho_l v_j^2 d_j/\sigma$
x	coordinate in gas crossflow (horizontal) direction,m
z	coordinate in liquid injection (vertical) direction, m

Greek symbol

μ	viscosity, kg/(m.s)
ρ	density, kg/m^3
σ	liquid surface tension, N/m
ψ_o	injection angle

Subscripts

b	column breakup
g	gas
j	jet
l	liquid
w	water

5.2. Introduction

The flowfield associated with a liquid jet injected transversely into a subsonic gaseous crossflow, known as a transverse liquid jet, has superior mixing properties compared to a jet in quiescent surroundings, which makes this flowfield layout appealing especially for engineering applications when rapid mixing is desired [1], [2]. This flowfield has various applications in power generation systems from stationary to avionic combustion engines, such as low NOx gas turbines, lean

premixed prevaporized (LPP) combustors, high speed direct injection (HSDI) diesel engines and aircraft engine afterburner sections. The application of this flowfield configuration in these power systems is advantageous as it enhances liquid fuel-air mixture, which in turn improves flame stabilization, fuel conversion efficiency, and accordingly emissions reduction [3], [4]. Another application of transverse liquid jet is the injection of lubricating oil into a rotating annular airflow in the cavity of aero-engine bearing chamber [5], [6]. The injection of suspension/liquid radially into a jet flame during thermal spray processes is also another example of the application of this flowfield configuration [7].

When a liquid jet is injected transversely into a subsonic gaseous crossflow, it leaves the injector/nozzle as an unbroken column, begins to ruffle as a result of axial instabilities which develop along the liquid column, and finally breaks up into ligaments and droplets. This process is named as the column breakup process [8]–[10]. As liquid begins to disintegrate from the surface of the liquid column (as a result of hydrodynamic instabilities on the jet lateral surface), the surface breakup process becomes dominant [8]–[10]. In the breakup process of a transverse liquid jet, both column and surface breakup mechanisms coexist but with the predominance of one over the other depending on flow conditions. Liquid fragments (i.e., ligaments and droplets) shedding from a jet along its trajectory undergo subsequent secondary breakup process leading to smaller droplets, and consequently the formation of a spray. As is illustrated in Fig. 5-1, the core of a transverse liquid jet (i.e., liquid column) forms a continuous stream between the jet exit and the location of its complete fracture, and it is referred to as the column breakup location. Data describing the column trajectory and breakup location of a transverse liquid jet is important for the design of the aforementioned power systems. For instance, this information is needed to prevent liquid impingement onto a combustor's wall. More importantly, these features are necessary for

predicting liquid distribution which directly affects droplets primary and secondary breakup, droplets collision, evaporation and vapor mixing rate with the gaseous phase, and thereby affects the overall efficiency of a system. Nonetheless, accurate acquisition of these features is difficult experimentally because of droplets density around the near-field liquid column [11], [12].

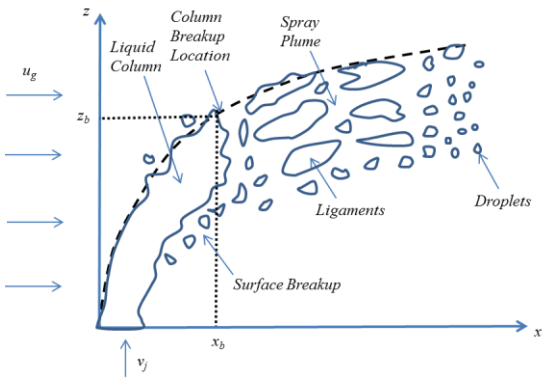

Figure 5-1: Schematic diagram of a liquid jet injected perpendicularly into a gaseous crossflow. Reprinted from Ref. [13] with permission from Begell House.

Numerous studies examined the role of different parameters which include liquid properties, test conditions, and liquid injector/nozzle geometry on the column trajectory and breakup location of a transverse liquid jet (e.g., [14] and references cited therein). Generally, it is revealed that jet momentum flux ratio, $q = \rho_l v_j^2 / \rho_g u_g^2$, plays the most important parameter for predicting the column trajectory and breakup height, z_b/d_j, of a transverse liquid jet. Conversely, the column breakup distance, x_b/d_j, is found to be a constant value. However, there exist differences in the predictions of these jet features between different published correlations, even at constant q. The reason for these discrepencies can be attributed to different factors such as the variation in liquid properties, test conditions and nozzle internal geometries, as well as errors associated with measurement and numerical uncertainties [13], [14]. For instance, q appears and plays a key role

in all publsihed correlations for predicting a liquid jet's trajectory and breakup location. However, this parameter depends on the value of liquid jet velocity, v_j. Thus the reliability of q strongly depends on that of v_j. It appeared that in most published correlations, v_j is calculated based on the volumetric flow rate divided by the injector (or nozzle) orifice cross sectional area, which implies a unity value of the discharge coefficient [15]. The actual jet velocity is inversely proportional to the discharge coefficient of an injector/nozzle, C_d. This coefficient, C_d, is a function of several factors such as nozzle (or injector) internal geometry, liquid injection pressure, jet Reynolds number (Re_j), turbulence, cavitation and hydraulic flip, ambient pressure, etc. [16]. Consequently, each of these parameters can affect the actual value of v_j and hence q, which in turn can result in different predictions of the column trajectory and its breakup location.

Brown et al. [15], [17], [18] reported that the value of C_d depends on both the internal geometry and diameter of a nozzle which can change the value of the momentum flux ratio, q, up to 50% for a nozzle with a length to diameter ratio of $L/d_j = 4$. To address this issue, they considered a non-unity C_d of a nozzle by taking into account the nozzle's injection pressure instead of v_j, and proposed a trajectory correlation with different set of coefficients for each specific nozzle [17]. Ahn et al. [19], [20] investigated the effect of cavitation and hydraulic flip on C_d and reported that the liquid column trajectory of non-cavitating and cavitating jets have a similar trend, but were different than that of jets which experience hydraulic flip as this causes liquid jet flow to detach from the inner wall of the orifice. They also asserted that the liquid breakup height and distance of a cavitating flow is smaller in comparison with that of a non-cavitating jet. Lubarsky et al. [21] investigated the trajectory of Jet-A fuel injected into a cross airflow using different injector geometries (i.e., sharp edge with $L/d_j = 10$, and round edge with $L/d_j \sim 1$). They reported that,

within their tested range of Re_j, the discharge coefficient of a sharp edge orifice is relatively constant, C_d~0.75; while the discharge coefficient of a round edge orifice is C_d~0.96 for Reynolds numbers exceeding $Re_j = 10{,}000$. They indicated a greater spray penetration into a cross airflow (~12%) for a sharp edge orifice compared to a round edged orifice.

Lee et al. [22] investigated the deformation and breakup properties of a turbulent liquid jet in a gaseous crossflow. They asserted that the presence of turbulence in a liquid jet has little effect on liquid column trajectory but exerted an apparent impact on the column breakup loction; that is, $x_b/d_j = 5.20$ and $x_b/d_j = 8.64$ for turbulent and nonturbulent liquid jet in a crossflow, respectively. Osta et al. [23] measured the column breakup distance of a turbulent liquid jet issuing from nozzles with different length/diameter ratios. They showed that the column breakup distance of a turbulent liquid jet with different length/diameter ratios ranged between the two constant values in agreement with the findings of Lee et al. [22] for turbulent liquid jet, and Sallam et al. [24] for nonturbulent liquid jets; i.e., $x_b/d_j = 5.20 - 8$. Osta et al. [23] also measured the column breakup height of a turbulent liquid jet by testing nozzles with different length/diameter ratios, and proposed an empirical correlation for each specific length/diameter ratio, which is expressed as follows: $z_b/d_j = 3.3q^{0.5}$ for a length/diameter ratio of 10 and $d_j = 4$ mm, $z_b/d_j = 3.1q^{0.5}$ for a length/diameter ratio of 20 and $d_j = 2$ mm, $z_b/d_j = 2.7q^{0.5}$ for a length/diameter ratio of 40 and $d_j = 4$ mm.

To examine the effect of jet exit turbulence on the column trajectory and breakup location of a transverse liquid jet, the spray regime map provided by Wu et al. [25] for round liquid jets injected into a quiescent gaseous environment (see Fig. 5-2) is utilized. According to this map, liquid jet has a smooth surface with no reattachment (i.e., implying a non-turbulent flow) for a nozzle's

length/diameter ratio less than $4-6$ at high Re_j. On the other hand, a nozzle with a larger length/diameter ratio generates a fully developed turbulent flow at the jet exit for sufficiently high Re_j.

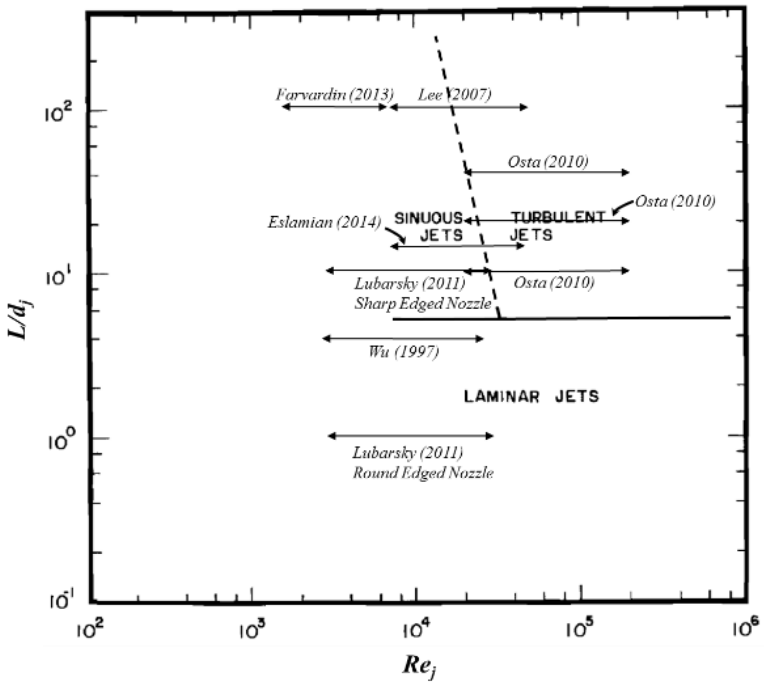

Figure 5-2: Primary breakup regime map for round liquid jets injected into quiescent gases Adapted by the present authors from Ref. [25] with permission from Begell House.

Furthermore, in order to assess the impact of jet exit turbulence conditions on the characteristics of a liquid jet injected into a gaseous crossflow, details of the geometries and the range of Re_j associated with different studies (e.g., references [9], [21]–[23], [26], [27]) on the transverse liquid jets are added in Fig. 5-2. As it is shown in this figure, the type of nozzles used in different experiments is either under the range of $L/d_j = 4-6$ or above this line, and there exists no study that examined the rang of nozzles on both (i.e., lower and upper) side of this line except Lubarsky

et al. [21]. In their study [21], however, the shape of nozzles are different, and they focused on a comparison between the trajectory of a transverse liquid jet injected from a sharp edge orifice versus a round edged orifice. This indicates that the effect of jet exit conditions has not yet been examined. In fact, the impact of nozzle exit conditions, particularly that of turbulence which could be one of the probable reasons of the discrepancies between the correlations proposed for liquid column trajectory and its breakup location, seems to be ignored.

The present study, therefore, aims at examining the role of fully developed turbulent flow conditions at the nozzle exit on the predictions of the trajectory and column breakup location of a transverse liquid jet when q and other controlling nondimensional parameters are kept unchanged. To do so, three round edged nozzles with a diameter of $d_j = 2$ mm and $L/d_j = 4, 20$ and 40 are used at a sufficiently high range of $Re_j = 17 \times 10^3 - 57 \times 10^3$ (in order to examine the effect of fully developed turbulent exit conditions). The mean axial velocity profiles and axial turbulence intensity at a region very close to (near-field) the nozzle exit are obtained using a PIV, and the column trajectory and its breakup location are extracted from shadowgraphy images. The correlation for predicting liquid jet column trajectory, which was developed in our previous studies [28], [29], with unknown discharge coefficient, C_d, is compared with the present experimental data in order to estimate the value of C_d for each specific nozzle geometry at different test conditions. Based on the obtained values of C_d, the analytical correlation for predicting the column breakup height is used to predict these jet characteristics for both non-turbulent and turbulent liquid jet at standard temperature and pressure (STP) test conditions.

5.3. Methodology

Both analytical and experimental approaches, which will be described in the following subsections, are employed to examine the nozzle exit turbulence on the prediction of the trajectory of a liquid jet and its breakup length.

5.3.1. Analytical Method

For predicting the trajectory of a liquid jet injected perpendicularly into a subsonic cross airflow, the sinusoidal-exponential correlation proposed by Broumand and Birouk [29] has the following form:

$$\frac{z}{d_j} = \frac{\beta}{\alpha}\left(sin^{-1}\left[sin\,\psi_o . exp\left(\left(\frac{\alpha}{\beta}\right)\frac{x}{d_j} \right) \right] - \psi_o \right) \tag{5-1}$$

where $\psi_o = \pi/2$ is the injection angle, and d_j is the liquid jet diameter at the nozzle exit. β, α and γ are the coefficients which are dependent on different non-dimensional numbers and their modified forms are presented below. In the present study, two modifications are performed to estimate the coefficients in Eq. (5-1). In order to make the liquid injection velocity independent of the nozzle's internal geometry and Re_j (i.e., nozzle exit conditions) and deteremine the actual jet velocity needed for calculating q, Re_j, and We_j, the nominal jet velocity, $v_{j,nom}$, which is calculated based on the metered liquid flowrate divided by the nozzle exit area (i.e., $C_d = 1$), is instead normalized by the actual nozzle's discharge coefficient (non-inity discharge coefficient; i.e., $C_d \neq 1$). The discharge coefficient of a plain-orifice atomizer/nozzle can be expressed as follows [16]:

$$v_{j,act} = \frac{\dot{m}_f}{\rho_l A_o C_d} = \frac{v_{j,nom}}{C_d} \tag{5-2}$$

Equation (5-1) uses an average value of the discharge coefficient suggested by Brown et al. [15] with some degree of uncertainty. Thus, in order to improve the reliability of Eq. (5-1), a more accurate value of the discharge coefficient of each specific nozzle must be determined. In doing so, the ligaments and droplets formed by the surface breakup mechanism are assumed to leave the liquid column from its downstream half [22], [24], as opposed to droplets formation over the entire periphery of a liquid jet in a quiescent gaseous environment [30]. Hence, the mass ratio used for calculating the rate of mass shedding from the liquid column in Eq. (5-1) is halved (as indicated in the second term of Eq. (5-5)). Given the two afornmentioned assumptions, the coefficients of Eq. (5-1) can be rewritten explicitly as a function of C_d.They are expressed as follows:

$$\beta = \frac{2{C_d}^2}{We_j} - 1 \tag{5-3}$$

$$\alpha = \gamma + \left(\frac{Bo.{C_d}^2}{We_j}\right)^2 \frac{1}{\gamma} \tag{5-4}$$

$$\gamma = \frac{2C_D.{C_d}^2}{\pi q} + \frac{1}{2}\left[\left(\frac{410{C_d}^2}{q}\right)^{\frac{3}{4}} \left(\frac{\rho_g}{\rho_l}\right)^{-\frac{1}{12}} \left(\frac{\mu_g}{\mu_l}\right)^{\frac{1}{6}} \left(\frac{Re_j}{C_d}\right)^{-\frac{1}{2}} \left(\frac{t_b - t_i}{t_b}\right)\right] \tag{5-5}$$

where $q = \rho_l v_j^2/\rho_g u_g^2$, $Re_j = \rho_l v_j d_j/\mu_l$, and $We_j = \rho_l v_j^2 d_j/\sigma$ are simply calculated based on the nominal jet velocity, $v_{j,nom}$, and the Bond number is defined as $Bo = \rho_l g d_j^2/\sigma$. An average value of the drag coefficient, C_D, along the entire length of the liquid column for different liquids is adopted from the correlation proposed by Wu et al. [9] as $C_D/C_{Dw} = 0.984(\mu_l/\mu_w)^{0.364}$, where $C_{Dw} = 1.51$ and μ_w are the water drag coefficient and viscosity, respectively. The column breakup

time, t_b, is adopted from Sallam et al. [24] for $We_g < 300$ as $t_b = 2.5t_s$, where $t_s = (\rho_l/\rho_g)^{\frac{1}{2}} d_j/u_g$ is the characteristic liquid-phase time, and the time of the onset of surface breakup, t_i, is defined as $t_i = 0.0004\left[(\mu_l/\mu_g)/\, We_g\right] t_v^*$, where $t_v^* = d_j^2/(\mu_l/\rho_l)$ is the characteristic viscous time.

The column breakup height, z_b/d_j (i.e., liquid jet streamwise direction), is predicted following the approach of Wu et al. [9], who assumed that the time required for the column to breakup is a fixed portion of the characteristic liquid-phase time, $t_b = C_z t_s$. Assuming a constant liquid jet velocity, v_j, up to the column breakup location, the column breakup height, z_b, can be obtained by multipliying t_b by v_j. Then, using $t_b = C_z t_s$ and the definition of $t_s = (\rho_l/\rho_g)^{\frac{1}{2}} d_j/u_g$, and also employing Eq. (5-2), the correlation for prediciting the column breakup height can be expressed as follows:

$$\frac{z_b}{d_j} = C_z \left[\frac{q}{{C_d}^2}\right]^{\frac{1}{2}} \tag{5-6}$$

where q is calculated based on the nominal jet velocity , $v_{j,nom}$, and C_z was adopted from Sallam et al. [24] as $C_z = 2.5$ for $We_g < 300$. The column breakup distance, x_b/d_j (i.e., cross airflow streamwise direction), as discussed by Wu et al. [9], should be relatively independent of q due to the cancellation of aerodynamic effect on the liquid acceleration and on the column breakup time scale. Hence, it can be represented by a constant as $x_b/d_j = C_x$.

Exploiting these two modified correlations for the column trajectory, Eq. (5-1), and its breakup location, Eq. (5-6), which are explicitly expressed as a function of C_d, the impact of nozzle exit turbulence can be captured and predicted quantitatively.

5.3.2. Experimental Method

5.3.2.1. Apparatus and Conditions

The experimental apparatus is an open wind tunnel which operates at atmospheric conditions and generates a uniform crosswind (crossflow) in a transparent test section made of acrylic. Several honeycomb and screens are utilized immediately before the test section to remove lateral and swirl velocity components in the test section. The test section has a square cross-section of $305\ mm \times 305\ mm$ and a length of $600\ mm$. The blower generating the wind/flow in the tunnel is controlled by a frequency drive, and the full characterization of flow in the test section versus different blower's speed has been performed using laser Doppler velocimetry (LDV) and reported in our previous publications (e.g., Iyogun et al. [31], Birouk et al. [32], [33]). The wind tunnel is capable of generating a uniform flow in the test section with a velocity ranging between $7.5\ m/s$ and $70.7\ m/s$ [31]–[33]. The nozzle is setup flush with the inner surface of the test section.

An injection system is used to deliver the liquid fluid into the test section through a nozzle which is located 200 mm downstream of the inlet of the test section. It consists of a compressed nitrogen tank which supplies high pressure nitrogen into a sealed chamber which contains the working fluid. The working fluid is introduced to the sealed chamber via either a liquid storage tank in the case of water or via a handheld funnel for other liquids. The liquid in the chamber is pressurized to cause liquid to flow out of the bottom of the chamber into a supply tubing and finally discharges through a nozzle into the test section. The pressure in the chamber is controlled by a typical mechanical pressure regulator attached to the nitrogen tank. The pressure in the chamber is measured using a digital pressure gauge having an output reading in $psig$ with

a single decimal digit on a refresh rate of approximately 1 Hz. The pressure gauge assembly includes a manually opened release valve to lower the chamber pressure, as well as a safety release valve which opens automatically at a chamber pressure of approximately 140 $psig$. More detail about the setup can be found in [34], [35].

Three different nozzle geometries with two different types of contraction profiles are used in the experiment (see Fig. 5-3). The two different contractions have a conical section with 60° where there is no gradual change in the cross-section, and a rounded one which has a 2 mm radius edge fillet around the exit diameter. All of these nozzles are manufactured out of stainless steel rods with an outer diameter of 9.5 mm. The internal cross-section of all nozzles is circular with a diameter of $d_j = 2$ mm. The nozzle specifications are tabulated in Table 5-1.

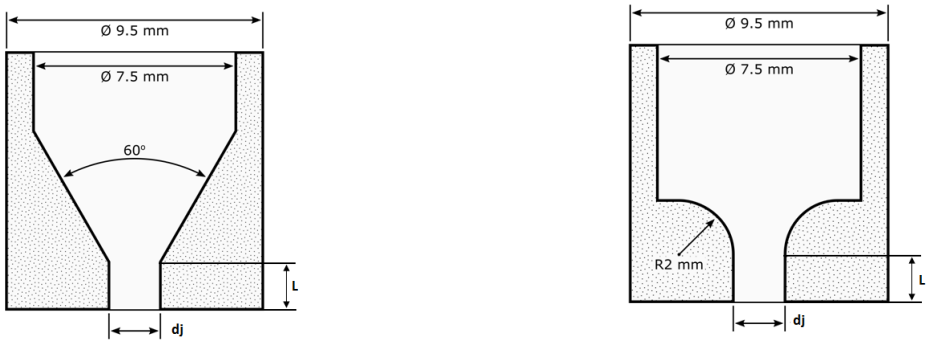

Figure 5-3: Schematic of the different nozzles: a) Nozzle N (i-iii) with 60° contraction, and (b) N (4) and N (2) with rounded contraction.

Table 5-1: Geometric parameters of the nozzles used in the experiment

Nozzle Name	Contraction Type	L (mm)	d_j (mm)	L/d_j
N(i-iii)	60° (small L/d_j)	8	2	4
N4	Round (large L/d_j)	40	2	20
N2	Round (large L/d_j)	80	2	40

Each nozzle has been calibrated to determine the relationship between chamber pressure and nozzle exit velocity. The liquid jet nominal velocity is calculated based on the volume flow rate divided by the nozzle's cross sectional area.

5.3.2.2. Imaging Setup

Shadography technique is employed to image the jet trajectory and its breakup location, while particle image velocimetry (PIV) is used to measure the liquid jet axial mean velocity and its corresponding axial turbulence intensity at distances very close to the nozzle exit.

Imaging of a liquid jet in the a crossflow is performed in the near- and far-field. In the near-field imaging, the camera is setup close to the test section to reveal details when the liquid jet first comes into contact with the crossflow. These images divulge the interaction between the jet's surface and crossflow at distances very close to the nozzle exit which would influence the overall jet trajectory and breakup location.

The imaging of the far-field seeks to determine the overall trajectory of the injected liquid jet and the column breakup location. For both the near- and far-field imaging of the liquid jet in the crossflow, 75 images are collected using a high-speed camera with an exposure time of 5 μs and a frame rate of 30 fps with a resolution of 1280×1024 pixels. However, for the far-field, the camera is setup much farther back from the test section in order to image a much larger area. In order to improve the uniformity of the light source, the light is reflected off a spherical concave mirror which has a focal point on the camera's sensor. This setup is schematically illustrated in Fig. 5-4.

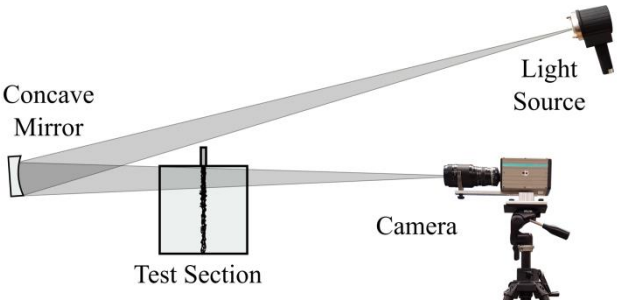

Figure 5-4: Schematic of the imaging system of the nozzle jet ejecting into a cross-flow in the far-field.

The liquid jet upwind boundary is used to determine the column trajectory in the crossflow. The jet's trajectory is determined by averaging 75 images using an in-house developed MATLAB code. A threshold has been applied to these images to identify the jet/spray boundary [17], [36]. Following the method of Thawley et al. [37], the breakup length of the liquid jet is defined as the point where the liquid column first separates. For each test conditions, the breakup location of 10 successive images is first identified manually, and an average value is used to define the breakup location in the crossflow and liquid jet streamwise direction. The uncertainty in the average for the breakup hight is found less than $1 \times d_j$.

A Dantec Dynamics Particle Image Velocimetry (PIV) is used to measure the axial mean velocity and its corresponding turbulence intensity of liquid jet in a quiescent atmosphere (without crossflow). The PIV setup consists of a Nd:YAG laser with a pulse energy of 135 mJ and a repetition rate of 10 Hz, a double-frame FlowSense EO 4M CCD camera with 20.4 fps at 2048×2048 pixel^2 sensor resolution, and Dynamic Studio Software. Silver-coated hollow glass spheres of 10 μm are used as seeding particles for the liquid jet. The duration between the two pulses is adjusted according to the jet velocity which ranges between 2-4 μs. Twelve hundred

image pairs are acquired in a field of view of 24×24 mm^2. An interrogation area of 32×32 with 50% overlap in addition to range validation for spurious vectors elimination are applied in post processing. An average filter of 3×3 vectors is used for flow field smoothing.

5.4. Results and Discussion

5.4.1. Liquid jet visualization and measurements

To investigate the effect of the presence of turbulence at the nozzle exit on the trajectory and breakup location of a transverse liquid jet, several experiments were carried out using different nozzle geometries and test conditions. Conditions for the appearance of non-turbulent and turbulent round liquid jet were obtained from the primary breakup regime map proposed by Wu et al. [25], as indicated in Fig. 5-2. Two different sets of nozzles (small: $L/d_j = 4$, and large: $L/d_j = 20$ and 40 to reach a fully developed turbulent flow) with similar nozzle exit diameter, $d_j = 2\ mm$, were employed.

As is qualitatively illustrated in Fig. 5-5, the shadowgraph images show that, in the near-field region (up to $z_b/d_j \approx 12$), the column surface of the liquid jet issuing from a larger length/diameter ratio (Fig. 5-5b) exhibits more surface irregularities and produces more ligaments particularly at the upwind side of the column (i.e., where crossflow is from right to left) than its counterpart's smaller length/diameter ratio nozzle (Fig. 5-5a). The relatively long ligaments observed in the jet isused from larger length/diameter ratio nozzle are an indication of a significant interaction with the ambient (cross airflow). These observations imply that the liquid jet is turbulent. The influence of the exit conditions of a fully developed turbulent flow on the liquid jet trajectory in the far-field region (up to $z_b/d_j \approx 80$) for both small and large length/diameter ratio nozzles is qualitatively

shown in Figs. 5-5c and 5d. As depicted in Fig. 5-5d, the turbulent jet exhibits an active and unsteady breakup process with a shorter breakup length, and it also bends into the crossflow slightly more than the nonturbulent jet (Fig. 5-5c). Hence, it appears that the disturbance of the jet, caused by turbulence, is an important factor for liquid column breakup in addition to the aerodynamic force of the crossflow. These qualitative observations will be quantified in the following sections.

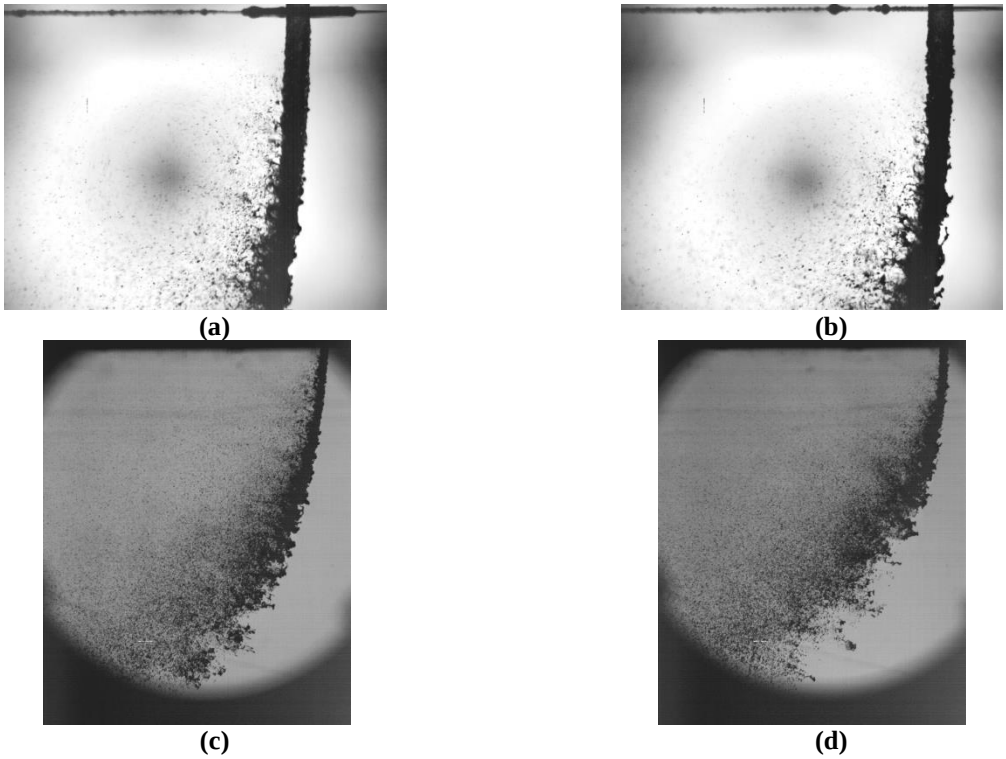

Figure 5-5: Flow visualization showing the effect of turbulent nozzle exit conditions on water jet for v_j=21 m/s, Re_j=39965, q=87, and We_g=134; where (a) $L/d_j = 4$ (up to $z_b/d_j \approx 12$), (b) $L/d_j = 40$ (up to $z_b/d_j \approx 12$), (c) $L/d_j = 4$ (up to $z_b/d_j \approx 80$), (d) $L/d_j = 40$ (up to $z_b/d_j \approx 80$)

In order to support the aforementioned observations, PIV velocity measurements in the near-field region of the liquid jet injected into a quiescent atmosphere are acquired at several axial planes; i.e., z = 2 mm, 10 mm and 20 mm. Figure 5-6 shows the radial profiles of the liquid jet axial mean velocity and its corresponding turbulence intensity for different nozzles at three axial planes. It is observed that the axial mean velocity increases in the flow directions farther away from the nozzle exit (from the plane z = 2 mm to z = 20 mm), as shown in Figs. 5-6a, 5-6c, and 5-6e. These figures also show that the nozzles with the larger length/diameter ratio (N (4) and N (2)) tend to produce flatter velocity profiles indicating that the issuing liquid jet is turbulent. In addition, the higher turbulence intensity of the nozzles with the larger length/diameter ratio (Figs. 5-6a, 5-6c and 5-6e), along with a lower mean velocity profiles (Figs. 5-6b, 5-6d and 5-6f), suggest a faster disruption of the liquid column surface and consequently a shorter column breakup length (see Fig. 5-5d).

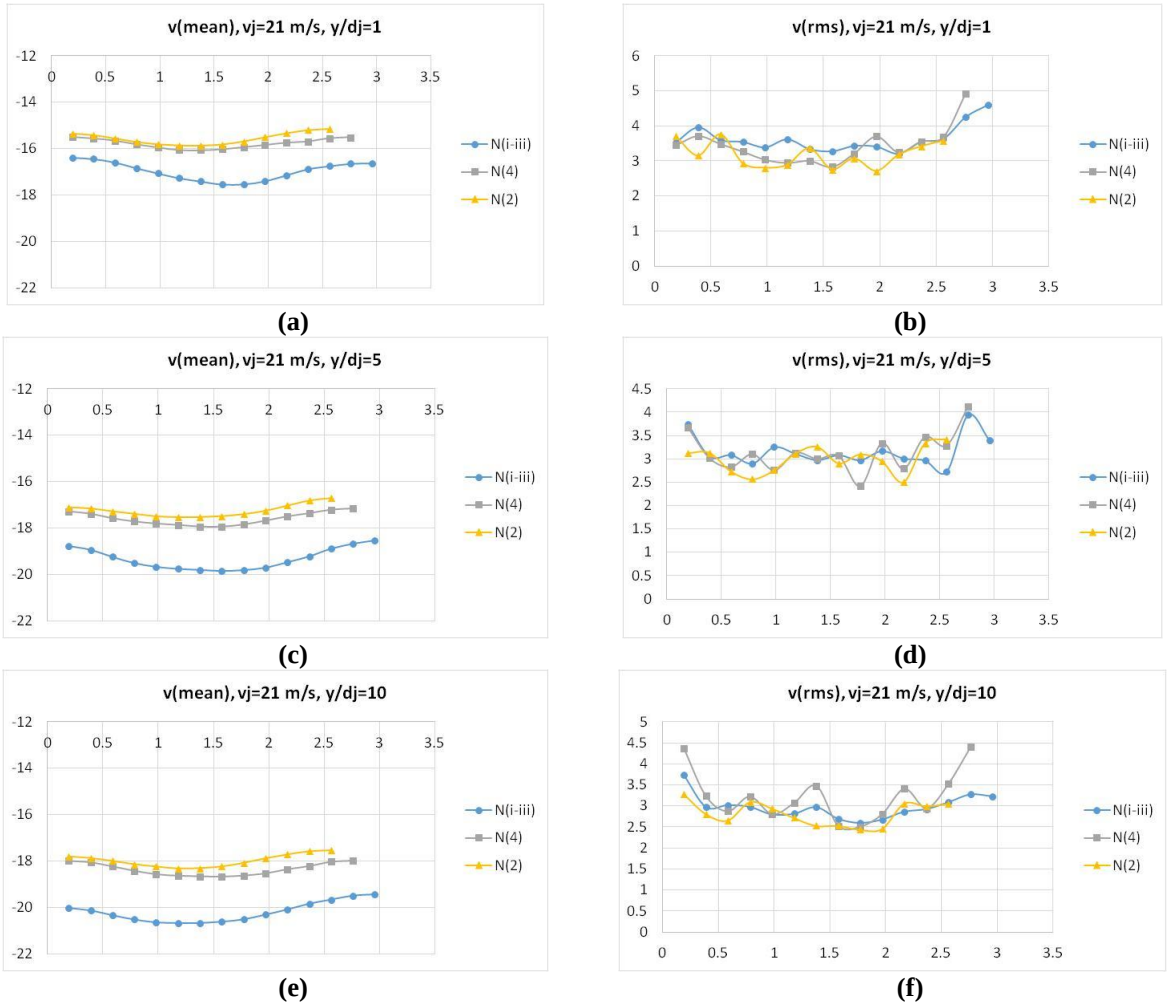

Figure 5-6: Radial profiles of a water jet injected into a quiescent atmosphere for v_j=21 m/s at z/d_j= 1, 5 and 10. (a, c and e) axial mean velocity, and (b, d and f) axial turbulence intensity.

In order to quantitatively assess the effect of nozzle exit turbulence on the liquid jet trajectory and its breakup location, the effect nozzle geometry was first investigated by determining the discharge coefficients of each set of nozzles using Eq. (5-1). Based on the obtained values of C_d at different range of q, Eq. (5-6) is then used to find the column breakup height of the transverse jet for different nozzle geometries.

5.4.2. Liquid Jet Trajectory

The main focus of this section is to examine the effect of nozzle's turbulent exit conditions on the trajectory of a transverse water jet. This is achieved using small and large L/d_j nozzles when keeping all other non-dimensional controlling parameters constant (e.g., q and We_g). The predicted liquid jet trajectory using Eq. (5-1) with an unknown discharge coefficient, C_d, is compared with their counterpart's experimental data in order to find the C_d of each nozzle over the tested range of water jet velocity (between 9 and 30 m/s) and two cross airflow velocities (47 and 65 m/s) at standard temperature and pressure (STP) test conditions.

Figure 5-7 depicts the near-field experimental data of water jet trajectory for different nozzle geometries; namely N (i-iii), N (4) and N (2), under shear breakup regime conditions (We_g=134). The other test conditions consists of $u_g = 65$ m/s, and $v_j = 12, 21$ and 30 m/s. As is expected, the jet penetrates farther with increasing q (see Figs. 5-7a to Fig. 5-7c). Furthermore, the trend exihibited in these figures reveals that the jet injected from small L/d_j nozzle (N (i-iii)) penetrates farther than that from large L/d_j nozzles (N (4) and N (2)), particularly when the jet velocity increases (Fig. 5-7c). This is an indication of the fact that the jet with turbulent exit conditions bends slightly more than the nonturbulent one.

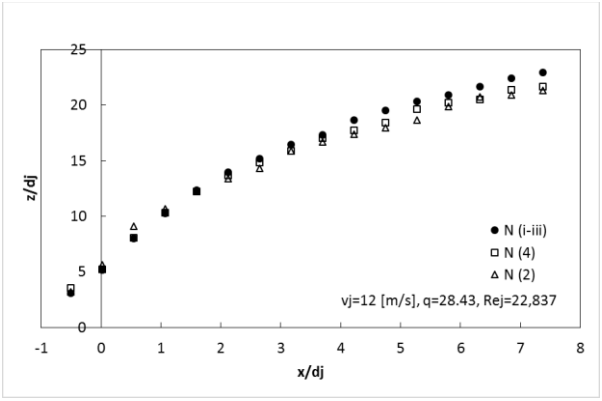

(a)

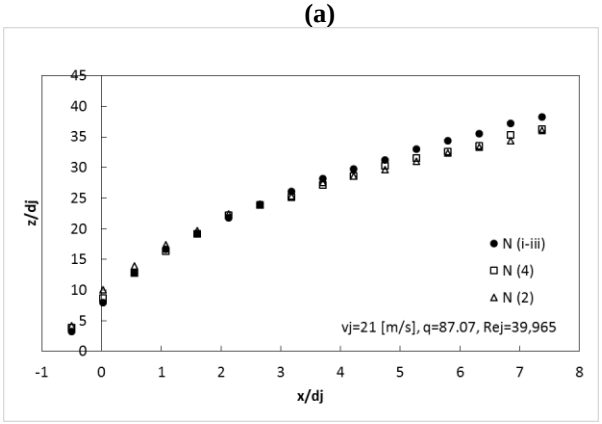

(b)

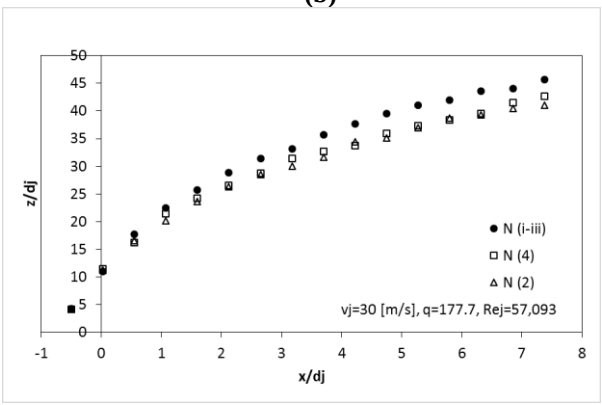

(c)

Figure 5-7: Water jet trajectory injected from various nozzles in a subsonic crossflow for We_g=134; (a) v_j=12, q=28, Re_j=22837, (b) v_j=21, q=87, Re_j=39965, and (c) v_j=30, q=178, Re_j=57093.

Figure 5-8 depicts the near-field experimental data of water jet trajectory for nozzles N (i-iii), N (4) and N (2) under multi-mode breakup regime conditions ($We_g = 70$). The test conditions

consists of $u_g = 47$ m/s, and $v_j = 12$ (Fig. 5-8a), 21 (Fig. 5-8b), and 30 m/s (Fig. 5-8c). Similar to the shear breakup regime conditions (Fig. 5-7), the nonturbulent liquid jet (nozzle N (i-iii)) in multi-mode breakup regime conditions (Figs. 5-8 a-c) penetrates farther than the turbulent jet.

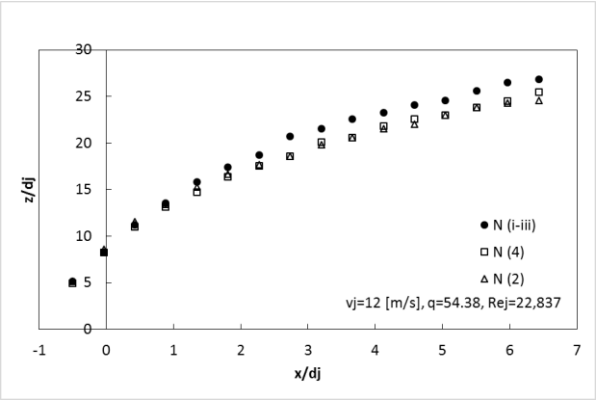

(a)

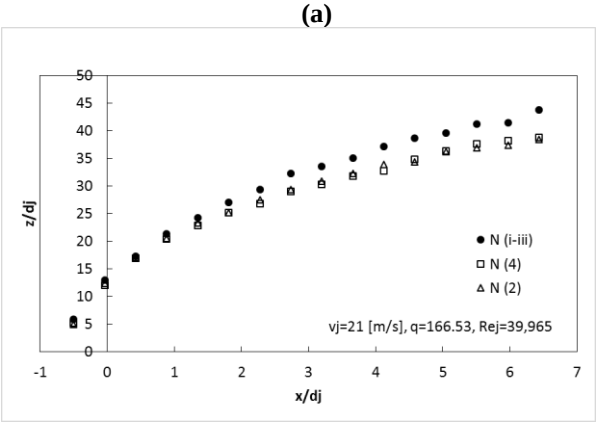

(b)

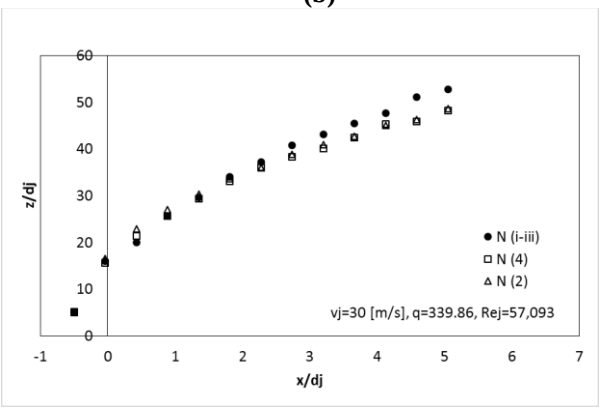

(c)

Figure 5-8: Trajectory of water jet of different nozzles for We_g=70; (a) v_j=12, q=54, Re_j=22837, (b) v_j=21, q=166, Re_j=39965, and (c) v_j=30, q=340, Re_j=57093.

Jet trajectory predicted by Eq. (5-1), with unknown C_d, is used to estimate the value of C_d that is capable of reproducing the experimental data. As is shown in Fig. 5-9, different ranges of C_d are calculated for different L/d_j and q. In essence, the discharge coefficient of a plain-orifice nozzle/injector is influenced by different factors such as the nozzle/injector internal geometry, liquid injection pressure, Re_j, turbulence, cavitation and hydraulic flip, and ambient pressure [16]. In this study, as the liquid jet is injected into a cross airflow, instead of a quiescent atmosphere, and in order to take into account the local pressure at the nozzle's outlet, as well as considering the thickness of the thin non-uniform boundary layer near the wall of the test section, q (i.e., which is a ratio of liquid inertia to gas inertia) is used to plot C_d in Fig. 5-9. As is illustrated in this figure, while the value of C_d shows nearly the same increasing trend with q for all examined nozzle geometries at different We_g, C_d is larger for the large L/d_j nozzles (N (4) and N (2)) compared with that of the small L/d_j nozzle (N(i-iii)). This demonstrates the importance of considering the influence of turbulent liquid jet exit conditions (i.e., which can be represented by nozzle's discharge coefficient, C_d) on the liquid jet trajectory.

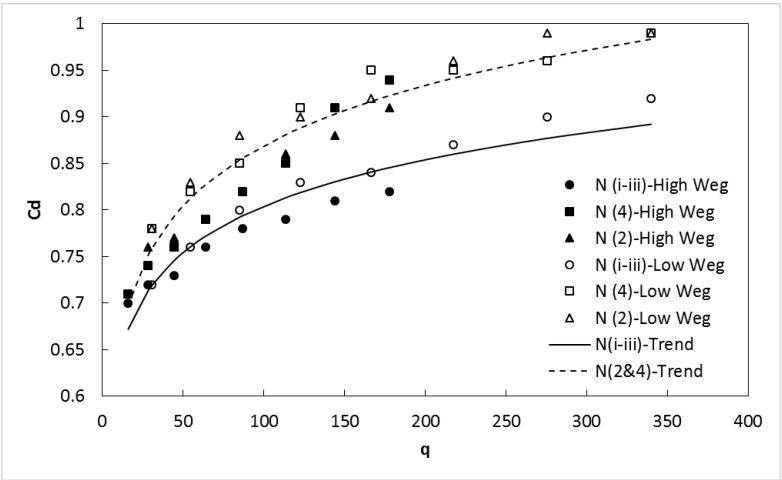

Figure 5-9: Discharge coefficient for various nozzles at different We_g as a function of q.

5.4.3. Liquid Jet Breakup Length

To show the effect of turbulence at the nozzle exit, which is represented by the nozzle's discharge coefficient, on the column breakup height of a transverse liquid jet, the breakup location is calculated using Eq. (5-6) while taking into account the discharge coefficient of each nozzle for each corresponding q and We_g from Fig. 5-9. The computed breakup location is compared with its counterparts' experimental data obtained in the present study. The column breakup height obtained from the present correlation and that from the experiments are also compared with published correlations (Thawley et al. [37]). As is shown in Fig. 5-10, the calculated height (using Eq. (5-6)) shows a good agreement with the present experimental data, while the correlation from Thawley et al. [37] with a constant coefficient $\left(z_b/d_j = 2.5q^{0.53}\right)$ overestimates the present experimental results at high values of q. This is again an illustration of the importance of considering the nozzle's turbulent exit conditions; that is, the nozzle's discharge coefficient, in determining the column breakup height.

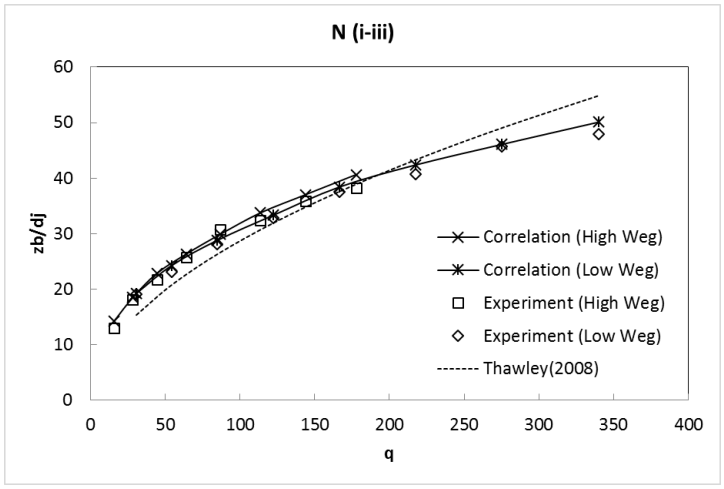

(a)

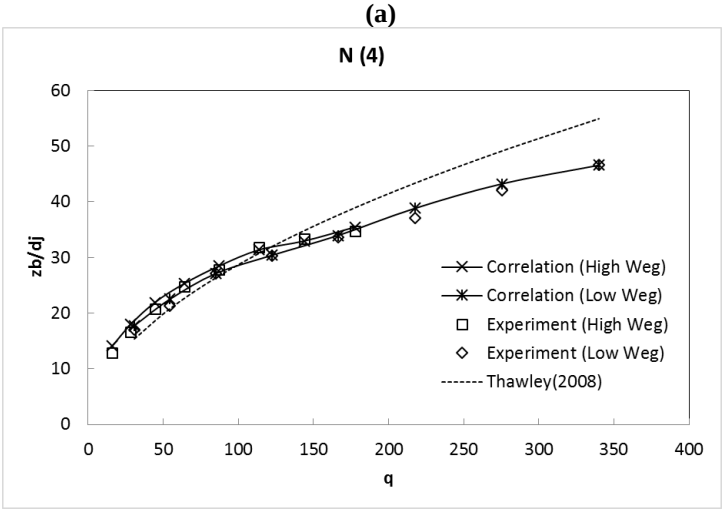

(b)

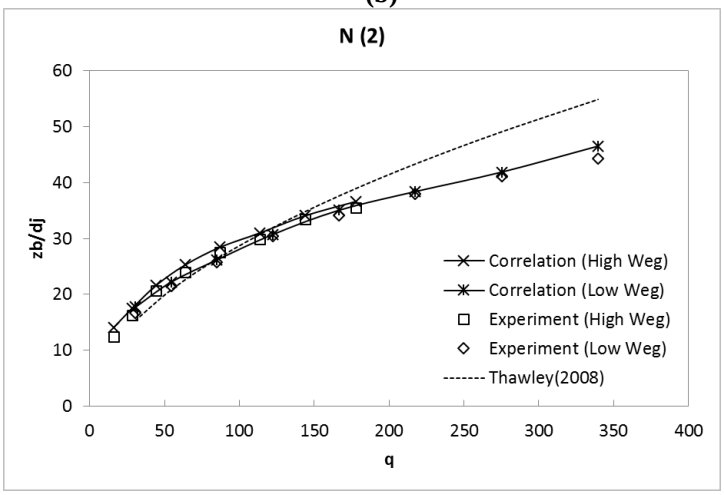

(c)

Figure 5-10: Water column's breakup height in a subsonic crossflow for various values of We_g as a function of q for (a) nozzle N (i-iii), (b) nozzle N (4), and (c) nozzle N (2)

Figure 5-11 presents a comparison of the water column's breakup height, z_b/d_j, for different nozzle geometries obtained from Eq. (5-6). It is evident that the column breakup height of the water jet injected from a shorter L/d_j nozzle (N (i-iii)) is higher than the breakup height of the larger L/d_j. This is in agreement with the literature where, for instance, Ahn et al. [20], Lee et al. [22], and Osta et al. [23], stated that the presence of turbulence enhances the process of liquid column breakup as a whole, and consequently shortens the column breakup time and length of a turbulent liquid jet in a crossflow when compared with a nonturbulent liquid jet. In essence, according to Lefebvre [16], for a fully turbulent jet, the radial velocity component soon causes disruption of the surface film, and consequently the precipitation of the disintegration of the jet.

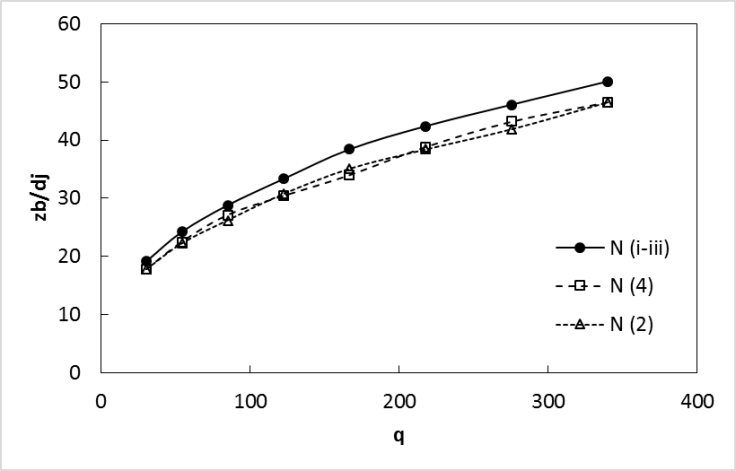

Figure 5-11: Comparison of water column's breakup height of different nozzle geometries

The measurements suggest that the column breakup distance, x_b/d_j, overall remaines constant for different nozzle internal geometry, and q. In the present study, the column breakup distance occurs in the range of $C_x = 5.69$ to 7.01 jet diameters downstream of the nozzle, which is in the range

that Osta et al. [23] reported for the column breakup distance using different nozzle geometries, that is $x_b/d_j = 5.20$ to 8.

5.5. Conclusion

The effect of nozzle internal geometry on the ensuing liquid jet turbulence at the nozzle exit, as well as its impact on the trajectory and column breakup location of a transverse liquid jet, are investigated at different test conditions. The results show a higher penetration and breakup height for a nonturbulent liquid jet compared to a turbulent jet. This is attributed to the surface irregularities produced by turbulent structures along a liquid column of a turbulent liquid jet which causes the jet to break up and follow the cross airflow sooner. It is shown that since both the jet trajectory and column breakup height are directly proportional to q, accounting for C_d in determining v_j is critical. In this regard, two modified correlations for predicting a tranverse liquid jet trajectory and its breakup height are proposed which take into account the discharge coefficient. The discharge coefficient is first found through a comparison of the analytically predicted trajectory with its experimental counterpart, and the estimated coefficients are employed in the analytical correlation in order to render it possible to prectict the breakup characteristics of both turbulent and non-turbulent transverse liquid jet. Overall, it is concluded that to reach a more comprehensive correlations for predicting a transverse liquid jet's trajectory and column breakup location, the effect of nozzle length to diameter ratio on jet's exit turbulence conditions should be taken into account via, for example, the discharge coefficient of a nozzle. Therefore, in order to expand the validity of the proposed correlation, the effect of the discharge coefficient of other types of nozzles (such as sharp-edge nozzle) should be determined. The generalization of these

correlations requires further testing to include elevated temperature and pressure (HTP) test conditions.

5.6. References

[1] N. Ashgriz, Handbook of Atomization and Sprays, Springer Science Business Media LLC, pp. 657-683, 2011.

[2] A. R. Karagozian, "Transverse jets and their control," Prog. Energy Combust. Sci., vol. 36, no. 5, pp. 531–553, Oct. 2010.

[3] J. M. Desantes, J. Arrègle, J. J. López, and J. M. García, "Turbulent gas jets and diesel-like sprays in a crossflow: A study on axis deflection and air entrainment," Fuel, vol. 85, no. 14–15, pp. 2120–2132, Oct. 2006.

[4] S. Padala, M. K. Le, S. Kook, and E. R. Hawkes, "Imaging diagnostics of ethanol port fuel injection sprays for automobile engine applications," Appl. Therm. Eng., vol. 52, no. 1, pp. 24–37, Apr. 2013.

[5] M. Birouk, B. J. Azzopardi, and T. Stäbler, "Primary Break-up of a Viscous Liquid Jet in a Cross Airflow," Part. Part. Syst. Charact., vol. 20, no. 4, pp. 283–289, Sep. 2003.

[6] M. Birouk, T. Stäbler, and B. J. Azzopardi, "An Experimental Study of Liquid Jets Interacting with Cross Airflows," Part. Part. Syst. Charact., vol. 20, pp. 39–46, 2003.

[7] M. Jadidi, S. Moghtadernejad, and A. Dolatabadi, "Penetration and breakup of liquid jet in transverse free air jet with application in suspension-solution thermal sprays," Mater. Des., vol. 110, pp. 425–435, Nov. 2016.

[8] J. A. Schetz and A. Padhye, "Penetration and Breakup of Liquids in Subsonic Airstreams," AIAA J., vol. 15, no. 10, pp. 1385–1390, Oct. 1977.

[9] P.-K. Wu, K. A. Kirkendall, R. P. Fuller, and A. S. Nejad, "Breakup Processes of Liquid Jets in Subsonic Crossflows," J. Propuls. Power, vol. 13, no. 1, pp. 64–73, Jan. 1997.

[10] M. Behzad, N. Ashgriz, and A. Mashayek, "Azimuthal shear instability of a liquid jet injected into a gaseous cross-flow," J. Fluid Mech., vol. 767, pp. 146–172, Feb. 2015.

[11] M. Linne, "Imaging in the optically dense regions of a spray: A review of developing techniques," Prog. Energy Combust. Sci., vol. 39, no. 5, pp. 403–440, Oct. 2013.

[12] D. Sedarsky, M. Paciaroni, J. Zelina, and M. Linne, "Near Field Fluid Structure Analysis for Jets in Crossflow with Ballistic Imaging," in ILASS Americas, 20th Annual Conference on Liquid Atomization and Spray Systems, 2007.

[13] M. Wang, M. Broumand, and M. Birouk, "Liquid Jet Trajectory in a Subsonic Gaseous Cross-flow: an Analysis of Published Correlations," At. Sprays, vol. 26, no. 11, pp. 1083–1110, 2016.

[14] M. Broumand and M. Birouk, "Liquid jet in a subsonic gaseous crossflow: Recent progress and remaining challenges," Prog. Energy Combust. Sci., vol. 57, pp. 1–29, Nov. 2016.

[15] C. Brown and V. McDonell, "Near field behavior of a Liquid Jet in a Crossflow," in ILASS Americas, 2006.

[16] A. H. Lefebvre, Atomization and Sprays. Hemisphere, New York, 1989.

[17] Brown C. T., M. U. Mondragon, and G. V. McDonell, "Investigation of the Effect of Injector Discharge Coefficient on Penetration of a Plain Liquid Jet into a Subsonic

Crossflow," in ILASS Americas 20th Annual Conference on Liquid Atomization and Spray Systems, 2007, pp. 15–18.

[18] C. T. Brown, U. M. Mondragon, and V. G. McDonell, "Liquid Jet in Crossflow: Consideration of Injector Geometry and Liquid Physical Properties," in ILASS Americas, 25th Annual Conference on Liquid Atomization and Spray Systems, 2013.

[19] K. Ahn, J. Kim, and Y. Yoon, "Effect of Cavitation on Transverse Injection into Subsonic Crossflows," in 39th AIAA/ASME/SAE/ASEE Joint Propulsion Conference and Exhibit, American Institute of Aeronautics and Astronautics, 2003.

[20] K. Ahn, J. Kim, and Y. Yoon, "Effects of Orifice Internal Flow on Transverse Injection into Subsonic Crossflows: Cavitation and Hydraulic Flip," At. Sprays, vol. 16, no. 1, pp. 15–34, 2006.

[21] E. Lubarsky, D. Shcherbik, O. Bibik, Y. Gopala, J. W. Bennewitz, and B. T. Zinn, "Fuel Jet in Cross Flow- Experimental Study of Spray Characteristics," in 23rd Annual Conference on Liquid Atomization and Spray Systems, 2011.

[22] K. Lee, C. Aalburg, F. J. Diez, G. M. Faeth, and K. A. Sallam, "Primary Breakup of Turbulent Round Liquid Jets in Uniform Crossflows," AIAA J., vol. 45, no. 8, pp. 1907–1916, Aug. 2007.

[23] A. R. Osta and K. A. Sallam, "Nozzle-Geometry Effects on Upwind-Surface Properties of Turbulent Liquid Jets in Gaseous Crossflow," J. Propuls. Power, vol. 26, no. 5, pp. 936–946, Sep. 2010.

[24] K. A. Sallam, C. Aalburg, and G. M. Faeth, "Breakup of Round Nonturbulent Liquid Jets in Gaseous Crossflow," AIAA J., vol. 42, no. 12, pp. 2529–2540, Dec. 2004.

[25] P.-K. Wu, R. F. Miranda, and G. M. Faeth, "Effects of Initial Flow Conditions on Primary Breakup of Nonturbulent and Turbulent Round Liquid Jets," At. Sprays, vol. 5, no. 2, pp. 175–196, 1995.

[26] E. Farvardin, M. Johnson, H. Alaee, A. Martinez, and A. Dolatabadi, "Comparative Study of Biodiesel and Diesel Jets in Gaseous Crossflow," J. Propuls. Power, vol. 29, no. 6, pp. 1292–1302, Aug. 2013.

[27] M. Eslamian, A. Amighi, and N. Ashgriz, "Atomization of Liquid Jet in High-Pressure and High-Temperature Subsonic Crossflow," AIAA J., vol. 52, no. 7, pp. 1374–1385, Jul. 2014.

[28] M. Broumand and M. Birouk, "A Model for Predicting the Trajectory of a Liquid Jet in a Subsonic Gaseous Crossflow," At. Sprays, vol. 25, no. 10, pp. 871–893, 2015.

[29] M. Broumand and M. Birouk, "Two-Zone Model for Predicting the Trajectory of Liquid Jet in Gaseous Crossflow," AIAA J., vol. 54, no. 5, pp. 1499–1511, Jan. 2016.

[30] K. A. Sallam, Z. Dai, and G. M. Faeth, "Liquid breakup at the surface of turbulent round liquid jets in still gases," Int. J. Multiph. Flow, vol. 28, no. 3, pp. 427–449, Mar. 2002.

[31] C. O. Iyogun, M. Birouk, and N. Popplewell, "Trajectory of Water Jet Exposed to Low Subsonic Cross-Flow," At. Sprays, vol. 16, no. 8, pp. 963–980, 2006.

[32] M. Birouk, C. O. Iyogun, and N. Popplewell, "Role of Viscosity on Trajectory of Liquid Jets in a Cross-Airflow," At. Sprays, vol. 17, no. 3, pp. 267–287, 2007.

[33] M. Birouk, N.-K. Baafour, and N. Popplewell, "Effect of Nozzle Geometry on Breakup

Length and Trajectory of Liquid Jet in Subsonic Crossflow," At. Sprays, vol. 21, no. 10, pp. 847–865, 2011.

[34] C. O. Iyogun, "Trajectory of Liquid Jets Exposed to a Low Subsonic Cross Airflow," M.Sc.Thesis, University of Manitoba, 2005.

[35] N.-K. Baafour, "Experimental Examination of Nozzle Geometry on Water Jet in a Subsonic Crossflow," M.Sc.Thesis, University of Manitoba, 2011.

[36] J. N. Stenzler, J. G. Lee, D. A. Santavicca, and W. Lee, "Penetration of Liquid Jets in a Cross-Flow," At. Sprays, vol. 16, no. 8, pp. 887–906, 2006.

[37] S. M. Thawley, U. M. Mondragon, C. T. Brown, and V. G. Mcdonell, "Evaluation of Column Breakpoint and Trajectory for a Plain Liquid Jet Injected into a Crossflow," 2008, no. May, pp. 1–11.

Chapter 6

Conclusions & Future Research

A summary of the findings of the research presented in this thesis is given below. In addition, the major contributions of this research are highlighted along with some suggested future research directions.

6.1. Research Summary

In the last decades, numerous correlations have been proposed to predict the trajectory and breakup length of a liquid jet injected into a subsonic gaseous crossflow. However, there is still a lack of universal correlations that are capable of predicting the main features (i.e., trajectory) of a liquid jet in a gaseous crossflow over a wide range of test conditions. One of the main reasons is that the transverse liquid jet's features depend on a number of variables such as liquid properties (e.g., density, viscosity, and surface tension), flow operating/test conditions (e.g., temperature and pressure), and liquid injector/nozzle internal geometry. In addition, these parameters may also have some level of interdependency. For instance, changing temperature would change air crossflow properties, which in turn could affect liquid jet trajectory in a gaseous crossflow.

Therefore, in order to develop more reliable correlations for predicting a liquid jet's trajectory and its breakup length in a gaseous crossflow, a mathematical approach was adopted and parameters that could have an impact were accounted for. In fact, this is the main objective of the present thesis where a number of gaps were identified in the open literature (Chapter 2) and several novel approaches were proposed to bridge these gaps (Chapter 3 and 4). Afterwards, the developed correlations were modified to extend their range of application, which was achieved by experimentally examining the effect of different influential parameters related to injector/nozzle internal geometry (Chapter 5).

A summary of the accomplished research and its contributions are summarized as follows:

- Mathematical modeling provides a valuable tool to derive more reliable and comprehensive correlations for predicting the mean features (e.g., trajectory and breakup length) of a transverse liquid jet with minimal experimental and computational costs. For instance, as is depicted in Fig. 4.3, for the mentioned test conditions, the predictions of the present mathematical model is compared with published experimental data and some correlations. It is found that the experimental data is best predicted by the present correlation with a standard deviation of 0.33 and a maximum error of 4.68%. The second and third best correlations to reproduce the experimental data were those of Elshamy and Jeng (2005) and Farvardin et al. (2013) with standard deviations of 0.45 and 0.70, and maximum errors of 8.44% and 12.80%. Finally, the correlation proposed by Stenzler et al. (2006) predicts the experimental data with a standard deviation of 1.50 and maximum error of 19.80%.

- Although the momentum flux ratio, q, plays a predominant role in the prediction of a transverse liquid jet's trajectory, other test/operating conditions (changing cross airflow's temperature and pressure (Chapter 4) or changing nozzle internal geometry (Chapter 5))

still important. The present mathematical model is capable of capturing the effect of these test conditions even when keeping constant q and $v_{j.}$

- Increasing the temperature or decreasing the pressure of a cross airflow causes a decrease in the density ratio $\left(\frac{\rho_g}{\rho_l}\right)$ and an increase in the viscosity ratio $\left(\frac{\mu_g}{\mu_l}\right)$, and hence a greater mass shedding from the liquid column, which in turn causes the liquid jet to bend more.
- The effect of temperature and pressure of the cross airflow on the jet trajectory can be accurately captured by the present mathematical model when using the density $\left(\frac{\rho_g}{\rho_l}\right)$ and viscosity $\left(\frac{\mu_g}{\mu_l}\right)$ ratio instead of the temperature $\left(\frac{T}{T_o}\right)$ and pressure $\left(\frac{p}{p_o}\right)$ ratio.
- At constant q, T and P, an increase in the liquid jet injection velocity leads to an increase in both Re_j and We_j, leading to a decrease in the mass shedding from the liquid column, which in turn causes the liquid jet to bend less.
- The influence of nozzle exit conditions (fully developed turbulent flow) on the trajectory and breakup length of a transverse liquid jet in a crossflow is an important factor in addition to the aerodynamic force of the cross airflow.
- Turbulent flow exit conditions cause the liquid column to breakup and follow the crossflow sooner compared to a non-turbulent jet, leading to a smaller penetration and breakup height. This effect of jet exit conditions can be accounted for in the mathematical correlations for predicting the trajectory and breakup length of a transverse liquid jet by considering the relationship between the discharge coefficient and a nozzle internal geometry.

6.2. Recommendations for Future Research

There are still many open-ended questions related to a transverse liquid jet's characteristics, which requires further research. Several possible research directions can be highlighted as follows:

1. There is still no consensus about the criterion concerning the breakup classification of non-turbulent liquid jet (i.e., transition from column to surface breakup regime) [1–3]. More studies are required to evaluate the suggestion that $We_j \cong 1000 - 5000$ (with an average $We_j \cong 3000$) is an appropriate region to describe the column/surface breakup transition region (instead of using $We_g - q$ map) for a liquid jet in a subsonic gaseous crossflow at standard (STP) and elevated (HTP) test conditions.

2. As for the transition criterion for turbulent breakup of a liquid jet in a gaseous crossflow, the relationship $We_{L\Lambda}q^{1/3}$ = 17,000 represents the transition borderline between the aerodynamic/turbulent primary breakup regimes [4,5]. However, further studies should be carried out to assess the suggestion that (instead of using $We_{L\Lambda}q^{1/3}$) $We_j \cong 22{,}000 - 50{,}000$ (with an average value of $We_j \cong 35{,}000$) is an appropriate boundary to predict the aerodynamic/turbulent breakup transition region for a liquid jet in a subsonic gaseous crossflow at both standard (STP) and elevated (HTP) test conditions.

3. Further studies are required on the effect of various parameters, such as We_j/Re_j, We_g/Re_g and nozzle geometry (round/sharp edged) on liquid jet instabilities and surface waves along a liquid column, as they play a key role on the primary breakup and the size

of ligaments and drops [6,7]. There is still a controversy amongst published experimental results and the data of high fidelity simulations [8].

4. Published transverse liquid jet trajectory correlations exhibit discrepancies in their prediction of the trajectory and penetration of a liquid jet in a crossflow [9–11]. Several parameters such as liquid and gas properties, STP and HTP test conditions, as well as liquid properties such as density, viscosity and surface tension and nozzle geometry (i.e., discharge coefficient) are key parameters for describing the trajectory, penetration and breakup length of a liquid jet in a crossflow. While, the influence of these parameters was studied in the present thesis at STP test conditions, their effect at HTP conditions (e.g., approaching real gas turbine conditions) requires further investigations. For instance, the effect of crossflow airflow density ratio (via changing the pressure) on the primary breakup and near nozzle disturbances of a transverse liquid jet while varying nozzle internal geometry has not been yet completely established. Also, the effect the temperature of a crossflow, which results in the evaporation of liquid, on the trajectory and breakup of a transverse liquid jet still requires further research, especially when varying nozzle internal geometry. In essence, since different nozzle internal geometry produces different sizes of ligaments and droplets, their evaporation rates are different for different nozzles, which in turn affects liquid jet characteristics in the far-field region.

5. The effect of a turbulent cross airflow (turbulence intensity and the length scales of turbulent structures embedded in the cross airflow) on the trajectory, penetration and

breakup length of a liquid jet in a crossflow at standard (STP) and elevated (HTP) test conditions [12,13] requires further studies.

6. According to the study of Osta et al. [5], when a liquid is injected into a wind tunnel's crossflow, the liquid jet must cross the wall boundary layer. This consequently causes a delay in its breakup time, and hence yields a shorter liquid column in comparison with that of a jet injected into a shock-tube test facility which has a much thinner boundary layer. Thus, the effect of the gas phase boundary layer (the boundary layer thickness) approaching the liquid jet injection point (for a flush, recessed and projected jet) on the breakup length of a transverse jet and its near-nozzle instabilities still needs further research to account for such effect the prediction of the breakup location of a transverse liquid jet [14,15].

7. The effect of viscous forces on the characteristics of a transverse liquid jet and the role of Ohnesorge number and/or jet Reynold number of viscous fluids on the primary breakup regime, turbulent structures, and jet trajectories all still require further investigations [16-18]. Investigating viscous liquids is of great importance, as liquid biofuels, which have relatively high viscosity, are gaining more ground as an important source of energy for power generation.

8. For injectors generating a plain liquid jet, high fluid viscosity suppresses the atomization capability of the fuel atomizers, such as air blast nozzles, and hence results in the formation of large fuel droplets and consequently inefficient combustion with undesired high emissions. Therefore, viscous biofuels (such as vegetable oil or glycerol) are usually

preheated to decrease the viscosity before atomization in order to generate fine spray and thus, achieve clean and efficient combustion. Atomization technology is developed to enhance spray fineness using different atomization mechanisms. For instance, pressure swirl atomizers, effervescent atomizers and flow-blurring injectors or electrostatic charge injection systems. Since the development of this technology was based on the injection of a liquid jet (i.e., including the high viscous liquids) in a quiescent atmosphere [19-21], the contribution of the aerodynamic effect of a cross airflow on the breakup characteristics of a liquid jet requires investigation. For instance, how the trajectory of a liquid column or its breakup location would change, while varying the electrical field in the presence of aerodynamic forces of a crossflow on a liquid jet, is still unknown.

9. The effect of the shape of a nozzle (e.g., elliptic or square nozzles instead of round plain orifice) on the characteristics of the liquid jet such as jet trajectory and penetration, breakup regimes, column breakup location, and size and velocity of droplets have been examined. However, most of these studies were carried out in a quiescent atmosphere [22,23]. Thus, the effect of aerodynamic forces associated with a cross airflow and axis-switching phenomenon of a non-circular nozzle on the breakup length and trajectory of a transverse liquid jet requires further investigations.

10. The near-field characteristics of a liquid jet such as near-nozzle hydrodynamics instabilities and jet's primary breakup mechanisms play a key role in defining its far field features such as jet penetration and droplets size. However, investigating the liquid jet near-field region is experimentally challenging due to high drops density around the jet column [24,25].

High-speed imaging systems have limited spatial resolution particularly in optically dense regions due to noise from multiply-scattered light. Thus, high-fidelity computer simulations [26,27] are still required to help understand the underlying physics of the near-nozzle region atomization of a transverse liquid jet in a cross airflow. Furthermore, using pulsed holography [7] and ballistic imaging [25] techniques to acquire more details of the evolution of liquid column surface and droplets formation, as a result of surface breakup in the primary breakup region (dense region), is highly required.

6.3. References

[1] Wu P-K, Kirkendall KA, Fuller RP, Nejad AS. Breakup Processes of Liquid Jets in Subsonic Crossflows. J Propuls Power 1997;13:64–73.

[2] Madabhushi RK, Leong MY, Arienti M, Brown CT, McDonell VG. On the breakup regime map of liquid jet in crossflow. ILASS Am. 19th Annu. Conf. Liq. At. Spray Syst., Toronto, Canada: 2006.

[3] Song J, Cary Cain C, Guen Lee J. Liquid Jets in Subsonic Air Crossflow at Elevated Pressure. J Eng Gas Turbines Power 2014;137:041502.

[4] Sallam K, Ng C, Sankarakrishnan R, Aalburg C, Lee K. Breakup of Turbulent and Non-Turbulent Liquid jets in Gaseous Crossflows. 44th AIAA Aerosp. Sci. Meet. Exhib., American Institute of Aeronautics and Astronautics; 2006.

[5] Osta AR, Sallam KA. Nozzle-Geometry Effects on Upwind-Surface Properties of Turbulent Liquid Jets in Gaseous Crossflow. J Propuls Power 2010;26:936–46.

[6] Mazallon J, Dai Z, Faeth GM. Primary breakup of nonturbulent round liquid jets in gas crossflows. At Sprays 1999;9:291–312.

[7] Sallam KA, Aalburg C, Faeth GM. Breakup of Round Nonturbulent Liquid Jets in Gaseous Crossflow. AIAA J 2004;42:2529–40.

[8] Pai MG, Pitsch H, Desjardins O. Detailed Numerical Simulations of Primary Atomization of Liquid Jets in Crossflow. 47th AIAA Aerosp. Sci. Meet. Incl. New Horizons Forum Aerosp. Expo., Orlando, Florida: 2009.

[9] Brown C, McDonell V. Near field behavior of a Liquid Jet in a Crossflow. ILASS Am., Toronto, Canada: 2006.

[10] Broumand M, Birouk M. A model for predicting the trajectory of a liquid jet in a subsonic gaseous crossflow. At Sprays 2015;25:871–93.

[11] Wang M, Broumand M, Birouk M. Liquid Jet Trajectory in a Subsonic Gaseous Cross-flow: an Analysis of Published Correlations. At Sprays 2016; 26,1083–1110.

[12] Masuda BJ, McDonell VG, Oskam GW. Mixing of a Plain Jet into a Swirling Crossflow. ILASS Am. 21st Annu. Conf. Liq. At. Spray Syst., Orlando, Florida: 2008.

[13] Tambe SB, Jeng S-M. A Study of Liquid Jets Injected Transversely into a Swirling Crossflow. ILASS Am. 21st Annu. Conf. Liq. At. Spray Syst., Orlando, Florida: 2008.

[14] Masuda BJ, Mcdonell VG. Paper ID ICLASS06-275 Penetration of a recessed distilate liquid jet into a crossflow at elevated pressure and temperature. Test, Kyto, Japan: 2006.

[15] Zheng Y, Marshall AW. Characterization of the initial spray from low-Weber-number jets in crossflow. At Sprays 2011;21:575–89.

[16] Birouk M, Azzopardi BJ, Stäbler T. Primary Break-up of a Viscous Liquid Jet in a Cross Airflow. Part Part Syst Charact 2003;20:283–9.

[17] Birouk M, Stäbler T, Azzopardi BJ. An Experimental Study of Liquid Jets Interacting with Cross Airflows. Part Part Syst Charact 2003;20:39–46.

[18] Farvardin E, Johnson M, Alaee H, Martinez A, Dolatabadi A. Comparative Study of

Biodiesel and Diesel Jets in Gaseous Crossflow. J Propuls Power 2013;29:1292–302.

[19] Malkawi G, Yarin AL, Mashayek F. Breakup mechanisms of electrostatic atomization of corn oil and diesel fuel. J Appl Phys 2010;108.

[20] Surya Prakash R, Gadgil H, Raghunandan BN. Breakup processes of pressure swirl spray in gaseous cross-flow. Int J Multiph Flow 2014;66:79–91.

[21] Jiang L, Agrawal AK. Investigation of Glycerol Atomization in the Near-Field of a Flow-Blurring Injector using Time-Resolved PIV and High-Speed Visualization. Flow, Turbul Combust 2015;94:323–38.

[22] G. Amini and A. Dolatabadi, "Axis-switching and breakup of low-speed elliptic liquid jets," Int. J. Multip. Flow 42, 96 (2012).

[23] Sharma, P., Fang, T.. Breakup of liquid jets from non-circular orifices. Exp. Fluids 55, 1–17 (2014).

[24] Sedarsky D, Paciaroni M, Zelina J, Linne M. Near Field Fluid Structure Analysis for Jets in Crossflow with Ballistic Imaging. ILASS Am. 20th Annu. Conf. Liq. At. Spray Syst., Chicago, IL: 2007.

[25] Linne M. Imaging in the optically dense regions of a spray: A review of developing techniques. Prog Energy Combust Sci 2013;39:403–40.

[26] Herrmann M, Arienti M, Soteriou M. The Impact of Density Ratio on the Liquid Core Dynamics of a Turbulent Liquid Jet Injected Into a Crossflow. J Eng Gas Turbines Power 2011;133:061501.

[27] Li X, Soteriou MC. High-fidelity Simulation of High Density-Ratio Liquid Jet Atomization in Crossflow with Experimental Validation. ILASS Am. 26th Annu. Conf. Liq. At. Spray Syst., Portland, OR: 2014.

Appendix

A.1. MATLAB Code for Determining Liquid Jet's Characteristics

The in-house MATLAB codes developed in Chapter 5 for determining the jet trajectory and breakup location of a transverse liquid jet are presented below.

A.1.1. Liquid Jet's Trajectory

An in-house developed MATLAB code was used to determine the mean column trajectory/penetration into the cross airflow. The code requires the following parameters as input: liquid jet velocity (denoted as `vt`), nozzle diameter (denoted as `D`), and the breakup length in the crossflow stream-wise direction (denoted as `xb`) in order to plot the data points up to the breakup point. The jet's trajectory is determined by averaging (`numFiles` = 75) the side view of shadowgraphy images of the liquid jet. These images are then thresholded vertically by scanning the average image from the bottom (where the liquid jet is injected from top) in order to identify the jet/spray windward boundary. The obtained results are then plotted along an x-y diagram. A description of how this code works is given in the following flow chart.

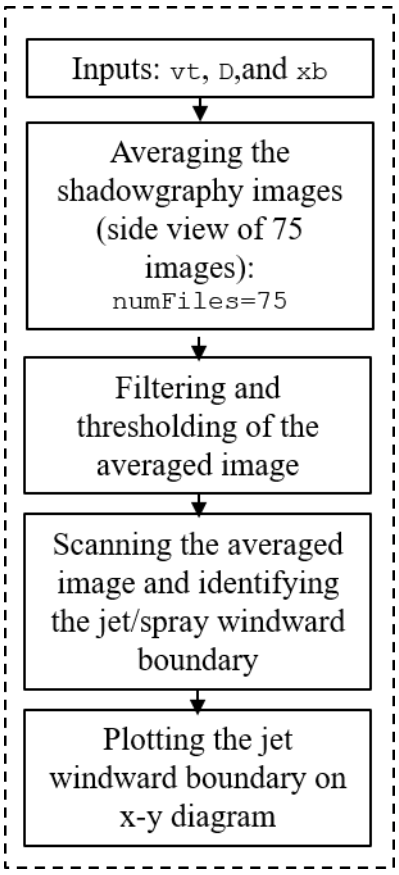


```
clear
clc
close all
% ---------------------- Nozzle  i-iii (round/D=2 mm)-----------------------
vt = 30;            % Theoetical veloocity % (8.9-38.5)m/s

D = 2.*10^-3;       % (0.5, 1.0, 2.0)mm
xb = 8;             % breakup length
A = imread('C:\Users\broumanm\Documents\00 Graham_Mohsen\Cross Flow - Far
Field\Nozzle i-iii\Ni-iii_30 m_s_001\Ni-iii_30 m_s_000000.bmp');
% IF AVERAGING IS DESIRED UNCOMMENT THIS SECTION
[M N] = size(A);
A = zeros(M,N);
numFiles = 75;

for i = 1:numFiles
    if (i <= 10)
        filename = ['C:\Users\broumanm\Documents\00 Graham_Mohsen\Cross Flow
- Far Field\Nozzle i-iii\Ni-iii_30 m_s_001\Ni-iii_30 m_s_00000' num2str(i-1)
'.bmp'];
    end
    if (i > 10 & i <= 100)
```

```
        filename = ['C:\Users\broumanm\Documents\00 Graham_Mohsen\Cross Flow
- Far Field\Nozzle i-iii\Ni-iii_30 m_s_001\Ni-iii_30 m_s_0000' num2str(i-1)
'.bmp'];
    end
    B = double(imread(filename));
    A = A+B;
end
A = A/numFiles;
A = A/max(max(A));
A = A*255;

imagesc(A);            %Orginal Single or Averaged image
title('Orginal Single or Averaged image');
colorbar      % image 1

A = fliplr(A);         %Flip for positioning of origin in imagesc

% Image filtering%
threshold = 102;
A(A>threshold) = 255;            %"darken" the stream
A(A<=threshold) = 0;             %may need adjustment on >, <=

figure,imshow(A) % image 3

A(1:10,1:end)=255;
A(1000:end,1:end)=255;
A(1:end,1:60)=255;
A(1:end,800:end)=255;

figure;imshow(A) % image 4
Original = A;

A = bwareaopen(A,50);          %remove "islands"
figure, imshow(A) % image 5

% f=imread('D:\FIG_5.bmp');
g=A(:,:,1);
% figure;imshow(g)
e=size(g(1,:))
d=e(2)
size(g)

for i=1:d
    s=g(:,i);
    ind=find(s==0);
    if isempty(ind)==1
        ind=0;
    end
A=ind;
C(i)=A(end);
end

pixel=0.088050314*10^-3;           % meter
ys=84;                %y start
ye=ys+xb*(D)/pixel;           %y end
yy=ys:ye;
figure;plot(C,1:d)
```

```
figure;imshow(g);hold on; plot(yy,C(yy),'ro')
xfinal=((yy(1:10:end)*pixel)-ys*pixel)/(D)-0.5;
yfinal=((C(yy(1:10:end))*pixel)-10*pixel)/(D);
figure;plot (xfinal,yfinal,'ro')

%************************************************************************
```

A.1.2. Liquid Jet's Breakup Length

The breakup length of the liquid jet is defined as the point where the liquid column first separates, and is determined using the following MATLAB code. This code uses liquid jet velocity (denoted as `vt`), and nozzle diameter (denoted as `D`) as an input. The single side view shadowgraph image of the jet (`numFiles` = 1) is then thresholded. For each test conditions, the breakup location of each of the 10 successive images is first identified manually, and an average value is used to define the mean breakup height. A description of how this code works is given in the flow chart below.

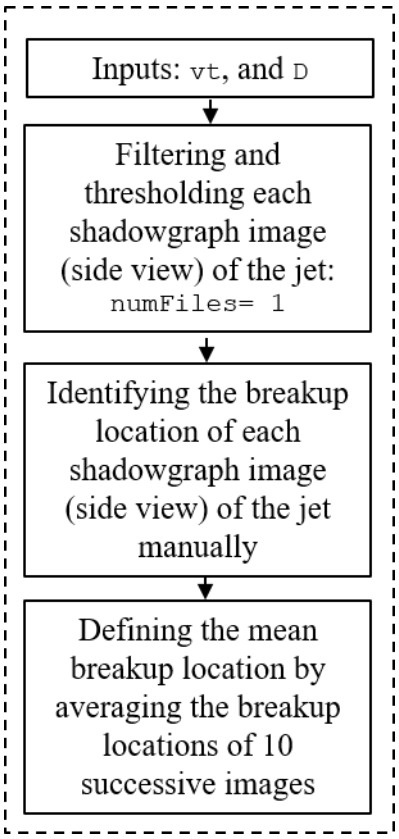

```
clear
clc
close all
% ------------------- Nozzle  i-iii (round/D= 2 mm)-----------------------
vt = 30;           % Theoetical veloocity % (8.9-38.5)m/s

D = 2.*10^-3;      % (0.5, 1.0, 2.0)mm
A = imread('C:\Users\broumanm\Documents\00 Graham_Mohsen\Cross Flow - Far
Field\Nozzle i-iii\Ni-iii_30 m_s_001\Ni-iii_30 m_s_000000.bmp');
% IF AVERAGING IS DESIRED UNCOMMENT THIS SECTION
[M N] = size(A);
A = zeros(M,N);
numFiles = 1;

for i =10
    if (i <= 10)
        filename = ['C:\Users\broumanm\Documents\00 Graham_Mohsen\Cross Flow
- Far Field\Nozzle i-iii\Ni-iii_30 m_s_001\Ni-iii_30 m_s_00000' num2str(i-1)
'.bmp'];
    end
    if (i > 10 & i <= 100)
        filename = ['C:\Users\broumanm\Documents\00 Graham_Mohsen\Cross Flow
- Far Field\Nozzle i-iii\Ni-iii_30 m_s_001\Ni-iii_30 m_s_0000' num2str(i-1)
'.bmp'];
    end
    B = double(imread(filename));
    A = A+B;
end
A = A/numFiles;
A = A/max(max(A));
A = A*255;

imagesc(A);           %Orginal Single or Averaged image
title('Orginal Single or Averaged image');
colorbar      % image 1

A = fliplr(A);        %Flip for positioning of origin in imagesc

% Image filtering%
threshold = 60;
A(A>threshold) = 255;           %"darken" the stream
A(A<=threshold) = 0;            %may need adjustment on >, <=

A(1:10,1:end)=255;
A(1000:end,1:end)=255;
A(1:end,1:73)=255;
A(1:end,800:end)=255;
figure;imshow(A) % image 2
[M,N]=size(A);
i=2:M;
j=2:N;
A(M+1,j)=A(M,j);
A(i,N+1)=A(i,N);
A(i,j)=(A(i-1,j-1)-A(i+1,j+1)).^2+(A(i,j+1)-A(i,j-1)).^2+(A(i-1,j)-
A(i+1,j)).^2+(A(i-1,j+1)-A(i+1,j-1)).^2;
figure,imshow(A) % image 3
%************************************************************************
```

A.2. Thresholding of shadowgraph images

From a gray scale image in which the value of each pixel carries the light intensity information, thresholding is used to create binary an image which has only two possible values 0 and 1 (or two colors, black and white) based on the contrast between the liquid jet and its gaseous background.

A.2.1. Liquid jet's trajectory

For finding the mean liquid's jet trajectory, after averaging 75 images, the light intensity of the pixels attributed to the gaseous background is identified manually. Then, the threshold is set in a way to subtract the background. To do so, the light intensity of each individual pixel of the recorded image is compared to the intensity of the background. If the intensity is more than that of the background, the pixel is assumed to be part of the background (white color); otherwise, it is considered as part of liquid jet (black color). The trajectory is then measured by scanning the black and white binary image.

In order to examine how the threshold may affect the final result and to check whether the intensity of light decreases gradually or abruptly, the chosen threshold is changed by 5% in either direction and the results are compared with the original threshold. In essence, if the light decreases gradually, it implies gradual loss of light due to light scattering; otherwise, a sharp (abrupt) change in light intensity is attributable to a sharp change in the light intensity (density jump) across the liquid/gas interface. The following figure shows, as example, the mean liquid jet trajectory for a liquid jet injected from nozzle (i-iii) at v_j = 9 m/s and u_g = 65 m/s when applying three different values of threshold $T = 127.5 \pm 5\%$. It is obvious that the windward trajectory of the jet (the measured value in the present study) is less affected by the thresholding in comparison with the leeward of the jet.

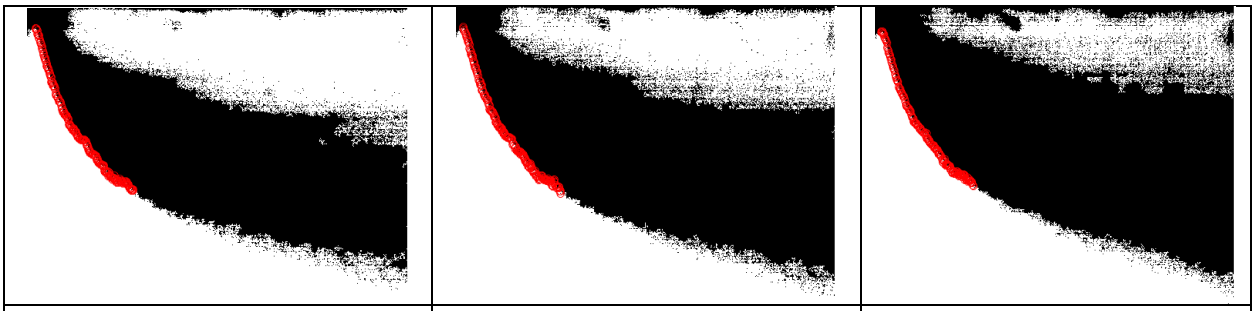

T=121.125	T=127.5	T=133.875

Figure A.2.1. Effect of the change of threshold value on the averaged binary images

The following figure shows the measured values of the liquid jet's trajectory associated with the three threshold values mentioned above. It is found that the variation in the values of *T* by 5% did not significantly change the results, indicating an abrupt change in the light intensity due to the liquid/gas interfacial boundary.

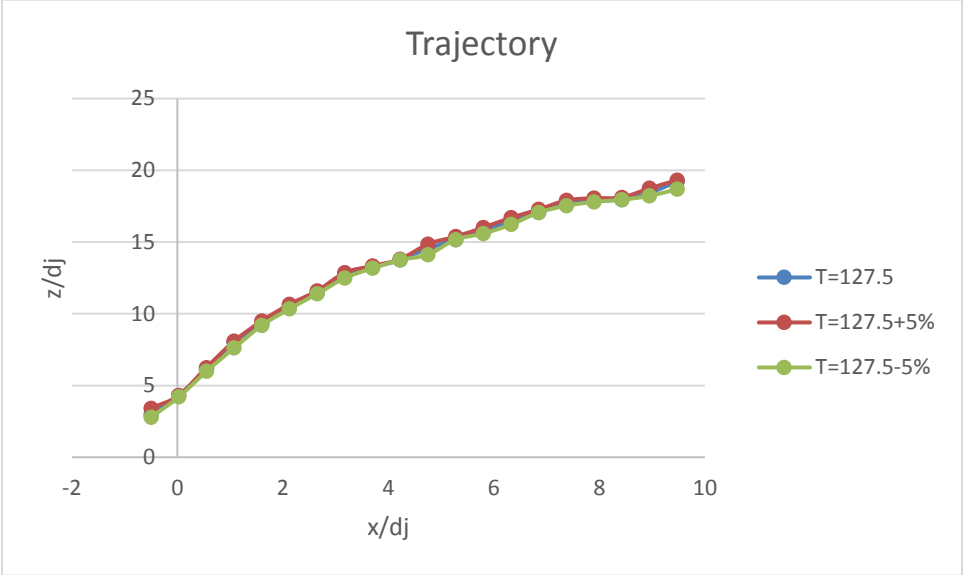

Figure A.2.2 Effect of the change of threshold value on the mean liquid jet's trajectory for a liquid jet injected from nozzle (i-iii) at *vj*=9 m/s and *ug*=65 m/s

A.2.2. Column breakup location

In order to determine the column breakup location, the threshold is set in a way to allow subtracting the gaseous phase background and render the liquid column region (near-nozzle) recognizable. To

do so, the light intensity of the pixels attributed to the liquid column region is first identified manually, and then the light intensity of each individual pixel of the recorded image is compared to it. If the intensity is more than that of the liquid column, the pixel is assumed to be part of the background; otherwise, it is considered as part of the liquid column. Then, following the approach of Thawley et al. [37], the edge of the liquid column is obtained, and finally the breakup location is identified visually as the point where the liquid column first separates.

The following figure (Fig. A.2.3) shows, as example, a single image of a liquid jet injected from nozzle (i-iii) at v_j=9 m/s and u_g=65 m/s with three different values of threshold $= 60 \pm 5\%$. This figure showed that no significant deference is observed by changing the threshold value by 5%.

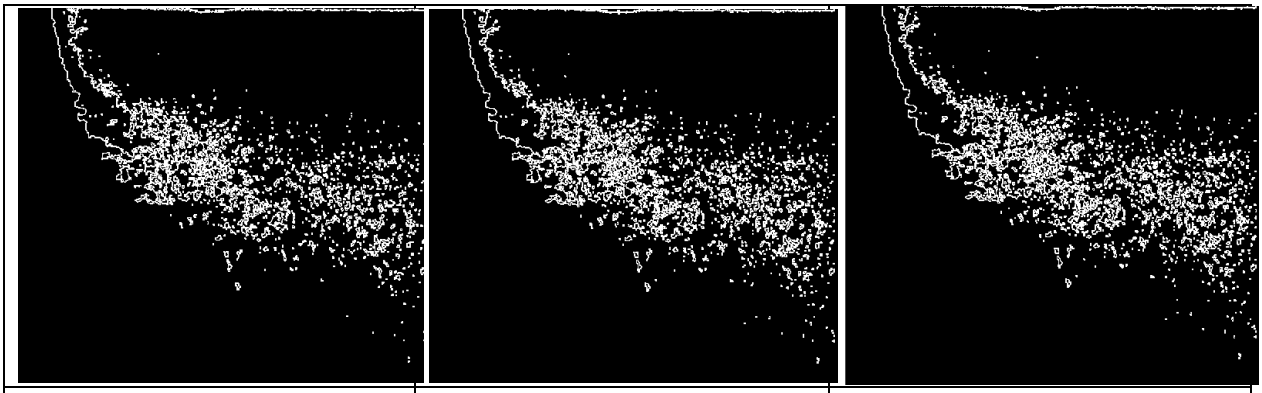

Figure A.2.3. Effect of the change of threshold value on a single binary image

The following table presents the measured values of the mean column breakup location associated with the aforementioned three values of threshold. It is found that this change in the values of T did not significantly change the results, about 1%.

Table A.2.1. Effect of the change of threshold value on the mean column breakup location of a liquid jet injected from nozzle (i-iii) at *vj*=9 m/s and *ug*=65 m/s

T	x_b	z_b
60-5%	6.982	13.963
60	7.297	13.805
60+5%	7.244	13.910

A.3. Uncertainty Analysis

Uncertainty analysis quantifies the difference between an experimentally measured value and its true value which is most often unknown. The total uncertainty, $E_V = \left({B_V}^2 + {P_V}^2\right)^{1/2}$, of a measured variable, $V(x_1, x_2, \dots, x_i, \dots, x_n)$, is the summation of the bias component (fixed or systematic errors), B_V, and a precision component (random error), P_V, where the dependent variable, V, is expressed as a function of the independent variable, x_i.

A.3.1. Shadowgraph technique

The primary sources of the bias uncertainties attributed to the shadowgraph technique employed in the present study are errors due to:

- instrumentation and measurements of fundamental quantities,
- camera's resolution and its field of view calibration,
- analysis code and thresholding,
- design and manufacturing of nozzles and wind tunnel, their calibrations, and etc.

The uncertainty associated with these possible sources of errors cannot be precisely determined because several factors are involved in the technique, each with some degree of uncertainty. The precision errors arise as a result of a spray's unsteadiness. They are reduced by increasing the number of measurement samples. The precision component, $P_V = \frac{t\sigma}{\sqrt{n}}$, of the uncertainties is determined by their standard deviation, $\sigma = \sqrt{\frac{\sum_{i=1}^{n}(x_i - \bar{x})^2}{n-1}}$, as well as the mean of the data, $\bar{x} = \frac{\sum_{i=1}^{n} x_i}{n}$, where x_i is the independent variable in the measurement and n is the number of data samples. The parameter t is the confidence coefficient which is 2 at 95% confidence level [1,2]. For example, the estimated precision errors of the water jet's trajectory for 75 samples at v_j=9 m/s and u_g=65 m/s for nozzle (i-iii) are found as follows (Table A.3.1):

Table A.3.1. Precision error for liquid jet's trajectory at x/d_j=4.2

n	z/d_j (ave)	P_V	Error (%)
75	13.75	0.19	1.38

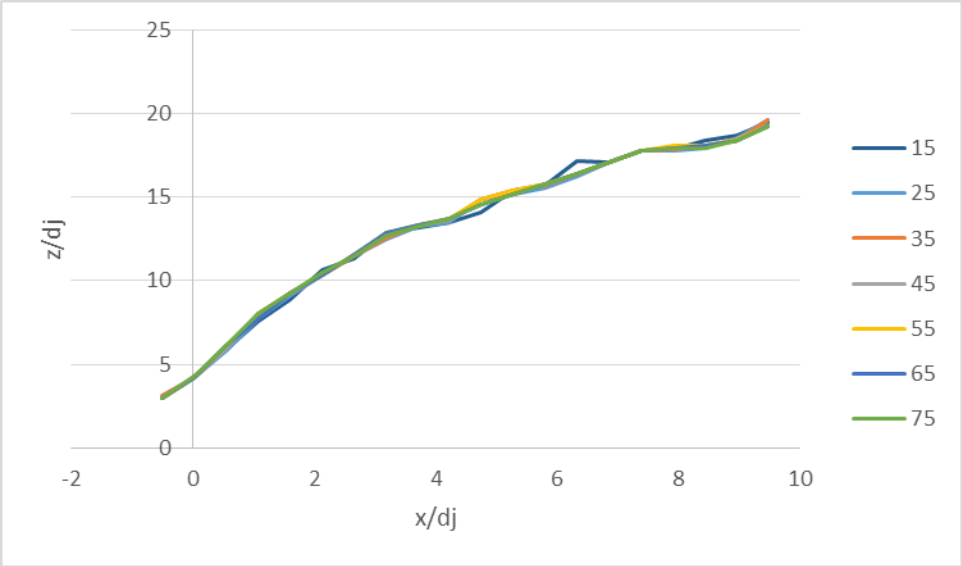

Figure A.3.1. Effect of the increasing of number of data samples (from 15 to 75) on the mean liquid jet's trajectory for nozzle (i-iii) at *vj*=9 m/s and *ug*=65 m/s

As it is shown in Figure A.3.1, the prediction of the mean liquid jet's trajectory did not change significantly with increasing the number of data samples from 15 to 75, and accordingly 75 data samples are enough to achieve the prediction with a precession error of 0.19 or 1.38%. Therefore, 75 data samples are used in the present study to find the average value of the trajectory.

The precision errors of the liquid jet's column breakup location at, for example, v_j=9 m/s and u_g=65 m/s for nozzle (i-iii) are calculated for three different number of data samples (n=5, 10 and 15) and found as in Table A.3.2.:

Table A.3.2. Precision error for column breakup location

n	z_b/d_j (ave)	P_V	Error (%)
5	12.840	0.599	4.66
10	13.034	0.586	4.49
15	13.071	0.586	4.48

As is shown in Table A.3.2, by increasing the number of data samples from 10 to 15, the averaged z_b/d_j did not change significantly with a precession error of 0.586. Therefore, 10 data samples are used in the present study to determine the average value of z_b/d_j.

A.3.2. Particle image velocimetry (PIV) technique

The primary sources of the bias uncertainties attributed to PIV technique employed in the present study are errors due to the

- selection of time between image pairs and light pulse timing,
- light sheet positioning,
- tracing quality (i.e., particles response time and settling velocity),
- non-homogeneous distribution of tracing particles, and etc.

For instance, the bias error, B_V, associated with measuring the axial mean-velocity, V_{mean}, can be estimated as , $B_V^2 = \sum \eta_{x_i}^2 B_{x_i}^2$ [1,2]. The sensitivity coefficient is defined as, $\eta_{x_i} = \frac{\partial V_{mean}}{\partial x_i}$, and the biased uncertainties of independent variables B_{x_i} are obtained from the manufacturer's specifications catalogue [3].

In each interrogation area, the axial mean velocity is obtained using the following equation, $V_{mean} = \Delta s/M\Delta t$, where $x_1 = \Delta s$ is the streamwise component of the particles displacement in the interrogation area, $x_2 = M$ is the magnification factor, and $x_3 = \Delta t$ is the time interval between the two laser pulses. Hence, the sensitivity coefficients are as follows, $\eta_{\Delta s} = \frac{1}{M\Delta t}$, $\eta_M = -\frac{\Delta s}{M^2\Delta t}$, and $\eta_{\Delta t} = -\frac{\Delta s}{\mathrm{M}\Delta t^2}$. The estimated bias error of the axial mean-velocity, V_{mean}, on the centerline of, for example, nozzle (i-iii) at y/dj = 5 and nominal jet velocity of v_j = 12 m/s is reported in Table A.3.3.

Table A.3.3. Bias error of the axial mean-velocity on the centerline of nozzle (i-iii) at *y/dj*= 5 and *vj*=12 m/s

Variable (x_i)	**Magnitude**	η_{x_i}	B_{x_i}	$\left(\eta_{x_i} B_{x_i}\right)^2$
Δs (pix)	8.00E+00	1.50E+00	1.27E-02	3.64E-04

Δt (s)	7.80E-06	-1.54E+06	1.00E-07	2.38E-02
M (pix/m)	8.53E+04	-1.41E-04	2.00E-01	7.95E-10

Hence, the bias error is estimated as B_V=0.155, or in other words an error of 1.29%.

The average value of V_{mean} and its standard deviation on the centerline velocity of nozzle (i-iii) at *y/dj*= 5 and nominal jet velocity of v_j=12 m/s are estimated for three different samples, namely n=300, 600 and 1200.

Table A.3.4. Precision error of the axial mean-velocity on the centerline of nozzle (i-iii) at *y/dj*= 5 and *vj*=12 m/s

n	V_{mean}	V_{rms}	P_V	Error (%)
300	11.71	2.15	0.25	2.12
600	12.00	1.66	0.14	1.13
1200	11.85	1.87	0.11	0.91

The precision error of V_{mean} estimated by $P_V = \frac{t\sigma}{\sqrt{n}}$ for n=1200 captured instantaneous pair images resulted in the least precision error of about P_V = 0.11, or in other words an error of 0.91% with a 95% confidence level. Therefore, 1200 data samples are adopted for each test condition. As a result, the total error and uncertainties of the axial mean-velocity measured by PIV technique is $E_V = \left({B_V}^2 + {P_V}^2\right)^{1/2} = 0.19$, which is equal to 1.58%.

A.4. References

[1] Rabinowicz, E.: An introduction to experimentation. Addison-Wesley Publishing Company (1970).
[2] Holman, J., Gajda, W.: Experimental methods for engineers. McGraw Hill Inc., New York. (1994).
[3] DynamicStudio 4.1." Dantec Dynamics, Skovlunde, Denmark, 2014.